Low Noise Techniques Applied to a Piezoceramic Receiver for Gas Coupled Ultrasonic Flaw Detection

ROGER FARLOW

Submitted in April 1998,
for the degree of
Doctor of Philosophy,

in the
Department of Electronic and Electrical Engineering
of the
University of Strathclyde, Glasgow.

Department of Electronic and Electrical Engineering, University of Strathclyde, Royal College Building, 204 George Street, Glasgow, Scotland, UK, G1 1XW

Abstract

Piezoelectric plate transducers are commonly used for the generation and detection of ultrasonic signals and have applications in, for example, non-destructive testing and medical imaging. A rigorous theoretical investigation of thermal noise in plate transducers has been undertaken with the aim of establishing the absolute limits of receiver sensitivity in terms of both Minimum Detectable Power (MDP) and Minimum Detectable Force (MDF). The central feature of the work has been the development of two independent theories which provide identical results. One theory is based on an electrical approach which makes use of an extensively modified version of Hayward's linear systems model of the piezoelectric plate transducer, along with the well known work of Johnson and Nyquist. The other theory is based on a mechanical approach which makes use of the less well known work of Callen and Welton. Both theories indicate that only two parameters are required in order to determine the MDP and MDF of an open circuit transducer. These parameters are the transducer's characteristic acoustic impedance and its mechanical quality factor. Significantly, the thermally limited sensitivity of an open circuit receiving transducer has been shown not to be related to its electromechanical coupling efficiency or any of its electrical properties. By applying the new theories it has been possible to design an ultra low noise ultrasonic receiver with wide ranging applications. Among other things, this receiver has been used to demonstrate the viability of a robust and truly practical air-coupled Lamb wave scanner suitable for detecting defects in thin plates which can be made from almost any type of material. The complete system has sufficient sensitivity to allow rapid scanning without the requirement for transducer matching layers or electronic signal averaging.

Dedicated to Annie and George Farlow

Acknowledgements

This PhD Thesis and the research upon which it is based would not have been possible without the contributions which were made by a large number of individuals and organisations. The author wishes to express his gratitude to all who contributed.

Within the University of Strathclyde, special thanks are due to the following. *Gordon Hayward* for supervision of the PhD. *Walter Galbraith* for his assistance with many aspects of the work but especially for his time and effort on the high pressure investigation. *Anthony Gachagan*, *Stephen Kelly* and *Jamie Hyslop* for the design, construction and repair of the ultrasonic transducers. *David Powell* and *Paul Reynolds* for their assistance with computer hardware and software problems. *Robert Banks* for contributing noise measurement data. *Tommy McCunnie* and *George Brown* for the manufacture of the transducers and many other components. *John Dickson* and his team in the *Mechanical Workshop* for the design and manufacture of the mechanical components used in the imaging systems, and for organising the temporary installation of a high pressure vessel in the Royal College building. *David Skillen* for his highly competent assistance with all aspects of the electronics.

Special thanks are also due to the following individuals and organisations. *The Electronics and Physical Sciences Research Council (EPSRC)* for providing most of the research funding. *Rolls Royce Mateval* and the *Ford Motor Company* for additional funding and support. *Paul Mundel* and his colleagues at *British Gas* for funding the high pressure study and for providing the high pressure vessel. *Peter Cawley* and his colleagues at *Imperial College* for assistance with all aspects of the Lamb wave work. *Kevin Taylor* and *John Smith* at *British Aerospace* for their interest and support, and for providing carbon fibre test samples.

Contents

List of Symbols

The following is a list of the more important symbols to be found in this Thesis. Less significant symbols are defined within the text as required. In a few cases different parameters are indicated by the same symbol. For example, k has been used to indicate wave number in Chapter 2 but in the remainder of the Thesis it is used to indicate electromechanical coupling efficiency. By keeping the original symbols it has been possible to use terminology which is consistent with a number of important references. The terminology which has been used in the development of the *Absolute Sensitivity Theory* (Chapters 4,5 and 6) is largely consistent with that which was used by Hayward in the development of the *Linear Systems Model.* All parameters are expressed in SI units except where a note has been added to indicate the use of special units.

CHAPTER 1

c Propagation velocity of a wave

f Frequency

θ Angle of incidence relative to normal incidence

λ Wavelength

CHAPTER 2

C_T Total coupling loss

C_{TR} Combined transmit/receive coupling efficiency

E Echo transmission coefficient

L Insertion loss expressed as a ratio

R Reflection coefficient in terms of acoustic pressure

T Transmission coefficient in terms of acoustic pressure

Z Acoustic impedance

b Propagation velocity - transverse wave

c Propagation velocity - longitudinal wave

θ_{LC} Critical angle for longitudinal waves

θ_{TC} Critical angle for transverse waves

k Wave number - longitudinal wave

α Attenuation coefficient (dB cm^{-1})

κ Wave number - transverse wave

ρ Material density

ϕ Acoustic field potential - longitudinal wave

ψ Acoustic field potential - longitudinal wave

ω Angular frequency

CHAPTER 3

D Dielectric displacement

E Electric field

X Stress - force per unit area

Y Young's modulus

c Material stiffness - stress per unit strain

d One of four piezoelectric coefficients (d,e,g,h)

e One of four piezoelectric coefficients (d,e,g,h)

f Frequency

g One of four piezoelectric coefficients (d,e,g,h)

h One of four piezoelectric coefficients (d,e,g,h)

s Material compliance - strain per unit stress

x Strain - change in length per unit length

ε Material permittivity

ρ Material density

CHAPTERS 4,5,6 AND 7

A Transducer front face area (πr^2)

B Bandwidth

C_0 Static capacitance of a transducer

F Force

F_0 Amplitude of an applied sinusoidal force

F_1 Signal force in the coupling medium - F_{SM} also used

F_N Transducer force fluctuations

F_{NM} Force fluctuations in the coupling medium

F_{SM} Signal force in the coupling medium - F_1 also used

G Voltage gain of transmitter amplifier

$G(R)$ Relative particle displacement - any transducer

$G_0(R)$ Relative particle displacement - open circuit transducer

I_{AN} Amplifier noise current

I_C Transistor collector current

K_{33} Relative dielectric constant

K_B Transducer back face reverberation factor

K_F Transducer front face reverberation factor

MDD Minimum detectable displacement

MDF Minimum detectable force on the fluid side of a fluid/transducer boundary

MDF_0 Best possible minimum detectable force in the coupling medium

MDF_T Minimum detectable force on the transducer side of a fluid/transducer boundary

MDP Minimum detectable power in the coupling medium

MDP_0 Best possible minimum detectable power in the coupling medium

MDP_T Minimum detectable power within the transducer material

$M(R)$ Transducer electrical impedance modification factor (unpoled to poled)

P_N Noise power

P_{SM} Signal power within the coupling medium

P_{ST} Signal power within the transducer material

P_T Transmitter power

Q_E Electrical quality factor ($1/tan\delta$)

Q_{EFF} Effective mechanical quality factor (Q_M reduced by electrical loading)

Q_M Transducer intrinsic mechanical quality factor

Q_T Transducer mechanical quality factor due to transmission loss only

R Relative frequency ($R=f/f_n$)

R_2 For a transducer and a resistive electrical load this has been defined as $2\pi f_n R_L C_0$

R_B Transducer back face reflection coefficient (from inside to outside) - force

R_E Electrical resistance - real

Re The real part of a complex value (e.g. $Re(Z_E)$ is the real part of Z_E)

R_F Transducer front face reflection coefficient (from inside to outside) - force

R_L Transducer resistive load (c.f. Z_L)

R_P Power reflection coefficient

R_S Pre-amplifier source impedance (resistive)

SNR Signal to noise ratio

T Time taken for a sound wave to cross a transducer ($T=1/2f_n$)

T_A Absolute temperature (K)

T_B Transducer back face force transmission coefficient (from outside to inside)

T_F Transducer front face force transmission coefficient (from outside to inside)

T_P Power transmission coefficient

T_S Stress or pressure - force per unit area

U Transducer forward loop attenuation factor

V_{AN} Amplifier noise voltage

V_0 Transducer signal voltage corresponding to a signal force, F_1 or F_{SM}

$V_{EN}(R)$ Transducer noise voltage due to force fluctuations in the coupling medium

$V_{JN}(R)$ Transducer Johnson noise (v_{JN} is also used)

V_S Amplitude of transmitter source voltage

$V_S(R)$ Transducer signal voltage as a function of relative frequency, R

X Imaginary part of Z_M

Z_0 Output impedance of transmitter electronics

Z_1 Acoustic impedance of the coupling medium

Z_2 Acoustic impedance of a transducer - real part of the mechanical impedance, Z_M

Z_C For a transducer this is defined as AZ_{CHA} (c.f. Linear Systems Model)

Z_{CHA} Characteristic acoustic impedance ($Z_{CHA}=\rho c$)

Z_E Electrical impedance of a transducer - complex

Z_{ES} Electrical impedance associated with a transducer's static capacitance, C_0

Z_F Transducer feedback factor

Z_L Lumped electrical impedance - transducer's electrical load

Z_M Mechanical impedance - complex

Z_S Specific acoustic impedance (T_S/v)

c Propagation velocity of a wave (as in $c=f\lambda$)

c_c Damping constant for critical damping - as in a damped mechanical oscillator

c_d Damping constant - as in a damped mechanical oscillator ($Q_M=c_c/2c_d$)

f Signal frequency

f_n Transducer fundamental thickness mode resonance frequency

g_m Transconductance of a field effect transistor (FET)

h Piezoelectric charge constant

j	Square root of -1
k	Electromechanical coupling coefficient
k_B	Boltzmann's constant (1.38×10^{-23} J K^{-1})
k_h	Spring constant - as in Hook's law
m	Mass of a particle
q	Charge on an electron (1.6×10^{-19} C)
r	Transducer radius
r_{bb}	Transistor base spreading resistance
$tan\delta$	Loss tangent
v	Particle velocity - also used to identify Lamb wave phase velocity
v_L	Longitudinal velocity
v_S	Shear wave velocity
v_g	Lamb wave group velocity
v_n	Noise voltage
x	Particle displacement
x_0	Amplitude of particle displacement
x_S	Static particle displacement (F_0/k_h)
Γ_T	Material factor for a field effect transistor
δ	$\lvert 90° - \phi_{MAX} \rvert$
ε	Permittivity of transducer material
ε_0	Permittivity of free space
ρ	Material density
τ	Transducer thickness
ϕ	Current-voltage phase angle
ϕ_{MAX}	Largest possible negative value of ϕ ($\lvert \phi_{MAX} \rvert < 90°$ for all real materials)
ω	Angular frequency ($\omega = 2\pi f$)
ω_n	Transducer fundamental angular frequency ($\omega_n = 2\pi f_n$)

CHAPTER 8

S_1, S_2, S_3	Tensional strains in the x,y and z directions respectively
V_L, V_S, V, V_g	Longitudinal, shear, Lamb wave phase and Lamb wave group velocities
u, v, w	Displacements in the x,y and z directions respectively
μ, λ	Shear modulus and Lamé's constant respectively

Chapter 1

INTRODUCTION

1.1 Background

1.1.1 Support and Collaboration

A large proportion of the research which is described in this PhD Thesis was undertaken in collaboration with Imperial College, London and was funded by EPSRC[1]/industry[2] through a research contract which was given the name *Ultrasonic Testing Without Coupling Fluids*. The title was chosen with the aim of providing both research teams (Strathclyde and Imperial) with the widest possible remit to investigate a range of novel ultrasonic testing techniques which would not depend on the use of a liquid coupling agent for their success. Although the fact is not reflected in the project title, air and other gases are fluids and can be used as coupling media in the same way as liquids. Gas coupled testing at normal atmospheric pressure was to have been the exclusive theme of this PhD Thesis, however, because some of the original findings were published [1] at an early stage, a number of additional commercial organisations expressed interest. Among these organisations was British Gas[3] who later funded an extension of the work which involved investigating the possible advantages of using gas coupled piezocomposite transducers in a high pressure environment. Continued interest from academic and industrial organisations resulted from a number of further publications [2 to 11] which were prepared during the course of the work.

1.1.2 Feasibility

The feasibility of air coupled ultrasonic testing was first reported by Luukkala *et al.* [12,13] in the early 1970's. The transducers used in this work were of the capacitive type consisting of a gold coated Melinex membrane stretched over a roughened rectangular back plate. It has also been demonstrated that low bandwidth air coupled ultrasonic test systems are feasible using piezoceramic plate transducers. One of the first practical demonstrations of this was reported by Rogovsky in 1991 [14]. Rogovsky found that, in order to be able to use piezoceramic plate transducers for air coupled inspection, it was necessary to provide both of the transducers with acoustic matching layers. Even with the aid of signal processing, Rogovsky found that his system could only be used to inspect certain materials which have a low characteristic impedance

1 Engineering and Physical Sciences Research Council

2 Rolls Royce Mateval and the Ford Motor Company

3 British Gas On Line Inspection Centre (Cramlington)

resulting in a low level of acoustic coupling loss. As a consequence of research by Rogovsky and others (e.g. Reilly [15]) working in the same field, transducers based on piezoceramic technology have been considered by many not to be the most appropriate choice for practical air coupled flaw detection. Despite this, QMI have based their commercial *Airscan* systems on focused piezoceramic plate transducers.

1.1.3 The Central Feature of this Research

The central feature of the research described in this PhD Thesis is a rigorous theoretical investigation of the factors which limit the performance of piezoelectric plate transducers when used as part of an ultra low noise receiver system. By taking advantage of the knowledge gained during this investigation it has been possible to design an ultra low noise ultrasonic receiver. The sensitivity of this receiver is limited only by the acoustic coupling coefficient of the receiving transducer. Among other things, this receiver has been used to demonstrate the viability of a robust and truly practical air coupled Lamb wave scanner suitable for detecting defects in thin plates made from almost any type of material. The complete system has sufficient sensitivity to allow rapid scanning without the requirement for transducer matching layers or electronic signal averaging.

1.2 Ultrasound

As previously mentioned, part of this Thesis is concerned with the fundamental physical limitations which nature imposes on the design of ultrasonic measurement systems. With this in mind it is worth considering what is meant by the term *ultrasound*.

1.2.1 A Definition of Ultrasound

The range of frequencies with which ultrasonic engineering is concerned is not definite. In general the term *ultrasonic* refers to those sounds which are too high in frequency to be heard by the human ear. The practical upper limit of frequency, as far as ultrasonic wave theory is concerned, is that frequency which gives a wavelength which is comparable to the atomic spacing. This frequency is reached at about 10^{13} Hz in liquids and solids. In ultrasonic test applications involving liquid or solid coupling it is common to select the operating frequency such that the wavelength of the sound in the test sample is comparable with the size of the expected defect.

1.2.2 *The History of Ultrasonic Technology*

The first efforts to produce ultrasonic vibrations were made over a hundred years ago by Rudolph Koenig [16], one of the pioneers in acoustical research. Ultrasonics as a technology can probably be said to have had its birth during World War I in a laboratory in Toulon, France. There Professor P. Langevin [16] was conducting research which was aimed at developing methods of detecting submarines. In the course of his investigations he designed and built a high power transmitter which used quartz crystals to produce ultrasonic waves in water. In this system Langevin was making use of the piezoelectric effect in the naturally occurring quartz crystals. This effect had been discovered some 35 years earlier but no practical use had been found for it. Langevin developed several techniques to enhance the effect and one of these was to vibrate the quartz at its resonant frequency.

1.2.3 *Ultrasound in Air*

A unique experiment for detecting and measuring ultrasonic waves in air was carried out by Altberg in 1907 [17]. His sound source was the spark discharge of a condenser, which is oscillatory instead of being a single unidirectional surge of current. Detecting and analysing the ultrasonic signal involved using a diffraction grating consisting of parallel glass rods and a microphone made from a light vane of mica supported on a quartz fibre. With this set-up he was able to detect and measure ultrasonic waves in air at frequencies of up to 300 kHz. This is a particularly interesting piece of history since most of the research discussed in this Thesis was conducted at frequencies close to 600 kHz.

1.3 The Early History of Ultrasonic Flaw Detection

Ultrasonic waves are useful in flaw detection because they can be easily aimed in one direction and can penetrate much deeper into many solid materials than is possible with, for example, X-rays. Also, ultrasonic techniques are fast, safe and inexpensive. The literature indicates that the possibility of using ultrasonic waves for flaw detection was first suggested by Sokolov [18] in 1929. Development of ultrasonic flaw detection during the following decade depended on three main factors. Firstly, methods of generating and detecting electrical signals whose frequencies were in the region of 1 MHz were at hand. Secondly, piezoelectric crystals were available for converting

electrical energy into sound waves, and vice versa. Thirdly, the flaws that were being sought were ideal in size for detection because of the short wavelength of the ultrasonic waves. The first experiments used continuous waves of sound rather than pulses with a typical test configuration consisting of a test sample placed between a transmitting transducer and a receiving transducer. As the test sample was moved the amplitude of the received signal remained constant unless a defect in the sample came between the two transducers. Hence, a reduction in signal strength indicated the presence of a flaw. The more useful echo systems made their appearance in the early 1940's [16,19,20,21,22]. In addition to the basic through transmission and echo methods there are a number of more sophisticated ultrasonic techniques which can be used for flaw detection. In order to discuss all of the possible ultrasonic flaw detection techniques it will be necessary to review some basic principles.

1.4 Basic Principles

Sound travels from one place to another in the form of waves. Material in some form or other is always required for the transmission of these waves. What is actually transmitted is a disturbance in the equilibrium arrangement of the atoms of the material. Under most circumstances the material itself does not go anywhere and only the disturbance is propagated. Sound waves act like light waves in many respects, in that they undergo interference, diffraction, reflection and refraction; it is even possible to have polarised sound waves in solids. In addition to these properties a sound wave has an attenuation coefficient and a velocity that are dependent on the type of wave and the medium in which it is travelling. This Section provides a very brief description of the different ways in which sound can propagate in various types of media. Mode conversion is also discussed along with methods of generating and detecting sound waves in solids.

1.4.1 Longitudinal Waves

The longitudinal wave illustrated in Figure 1.1 is encountered in all branches of ultrasonics and can be produced in solids, liquids and gasses. It is called a longitudinal wave because the particle motion is along the direction of propagation of the wave. The dots represent particles of the material that move back and forth under the action of the sound wave. The term *particle* is to be understood as meaning a volume element large

enough to contain millions of molecules, so that it may be thought of as a continuous material, but yet small enough so that the commonly used acoustic variables such as pressure, density and velocity are constant throughout the element. The regions labelled 'A' are regions of rarefaction and as a consequence the density of the material is slightly lower there. The parts of the figure indicated by 'B' are regions of compression and they represent areas of increased density. At any given instant the particles will have a displacement to the left or to the right. The wavelength is the distance between adjacent regions of maximum compression or rarefaction and the frequency is the number of waves that pass a particular point per second.

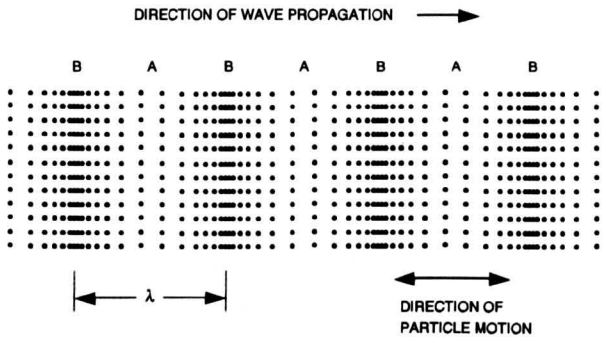

FIGURE 1.1 LONGITUDINAL WAVE

1.4.2 Shear Waves

In solids it is possible for sound waves to have all or part of their vibrational amplitude perpendicular to the direction in which they are travelling. In an infinite medium these waves are called transverse waves and there is no longitudinal motion of the particles of the medium. In the field of non-destructive testing it is more common to refer to transverse waves as shear waves and this convention will be adopted throughout the remainder of this PhD Thesis. A schematic diagram of this type of wave is shown in Figure 1.2. A unique characteristic of these waves is the absence of regions of compression and rarefaction. In other words, there are no localised fluctuations in density such as occur with other wave types.

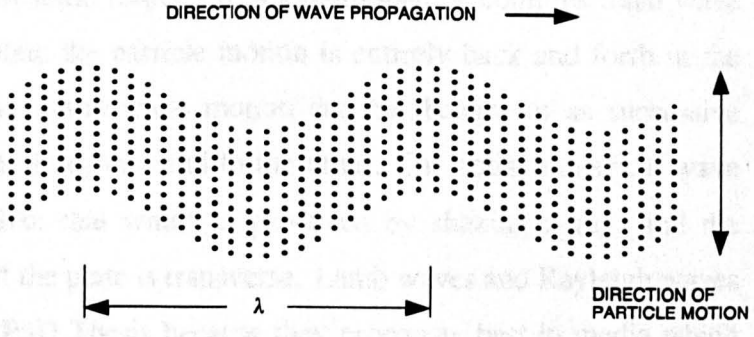

FIGURE 1.2 TRANSVERSE OR SHEAR WAVE

1.4.3 Surface Waves

There are several different wave types that can exist at the boundary between a fluid and a solid. In 1885 Lord Rayleigh demonstrated theoretically that waves can be propagated over the plane boundary between an elastic half-space and a vacuum or a sufficiently rarefied medium, for example, air. As shown in Figure 1.3, Rayleigh waves, as they came to be known, produce an elliptical motion of the particles close to the surface of the solid. The amplitude of the motion decreases exponentially as the depth below the surface increases. At a distance of one wavelength below the surface the amplitude of vibration is less than 10% of that at the surface.

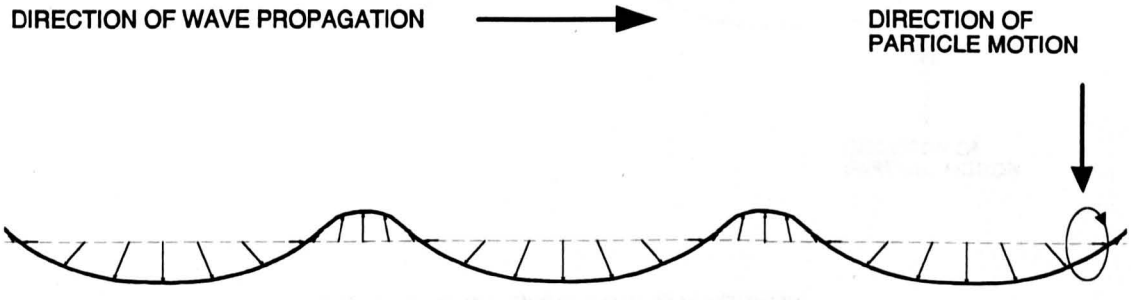

FIGURE 1.3 RAYLEIGH WAVE PROPAGATING ALONG THE SURFACE OF A SOLID

1.4.4 Lamb Waves

Waves produced in a plate whose thickness is comparable to the wavelength are referred to as plate waves or Lamb waves after H. Lamb who first described them in 1917 [23]. The two basic types of particle motion that are possible in a plate are shown in Figures 1.4 and 1.5. The waves that produce these are called symmetrical and antisymmetrical waves and in both cases particle motion at the surface is elliptical. The symmetrical wave is similar in some respects to a longitudinal or compressional wave and along the centre of the plate the particle motion is entirely back and forth in the direction of propagation. The symmetrical motion can be thought of as successive "bulges" travel along the plate from one end to the other. The antisymmetrical wave is a flexural type of wave (like that which is produced by shaking a rug) and the particle motion at the centre of the plate is transverse. Lamb waves and Rayleigh waves are of special interest in this PhD Thesis because they propagate best in media which is bounded by a vacuum or a sufficiently rarefied medium such as air. The theory of Lamb waves is considered in detail in Chapter 8 of the Thesis.

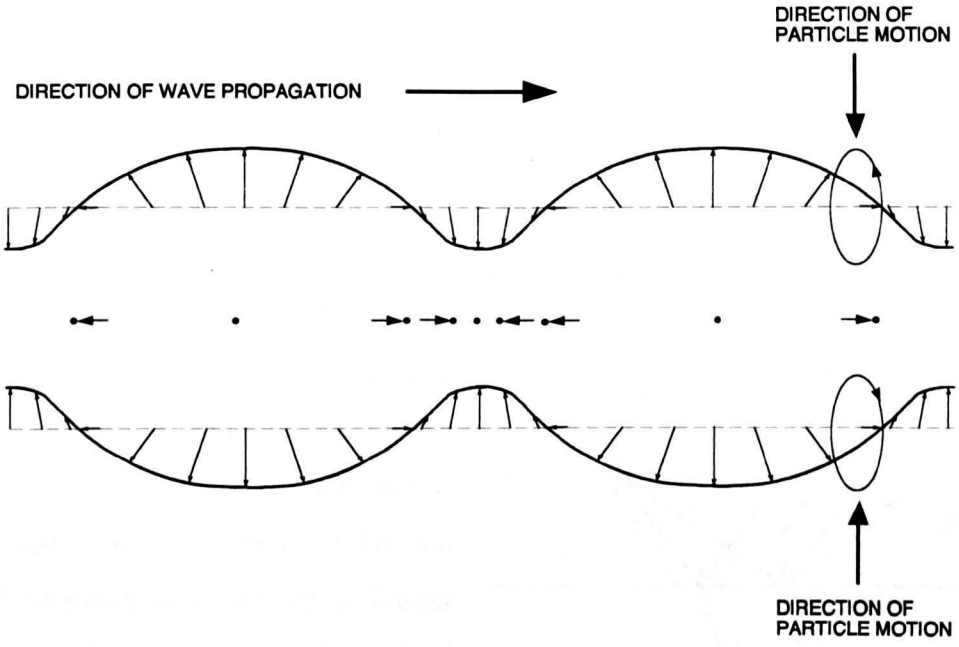

FIGURE 1.4 SYMMETRICAL LAMB OR PLATE WAVE

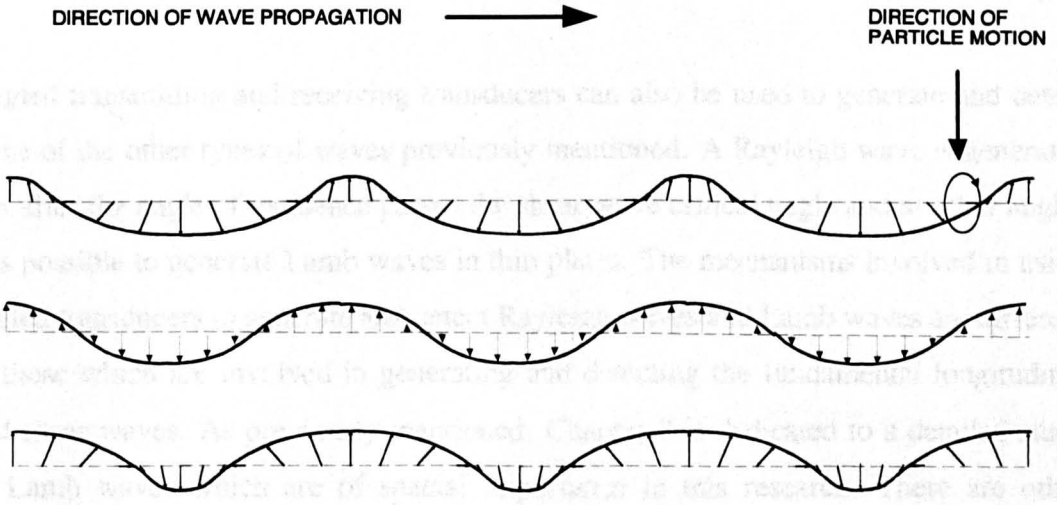

FIGURE 1.5 ASYMMETRICAL LAMB OR PLATE WAVE

1.4.5 Mode Conversion

It is possible to convert one type of sound wave into another and this is an important concept with regard to the present work. For example, when sound waves in a fluid are directed towards the surface of a bulk solid all of the waves generated in the solid are longitudinal provided that the surface of the solid is flat and the waves in the fluid are parallel to this surface. However, when the waves in the fluid are incident at an angle various modes are generated in the solid. For example, as illustrated in Figure 1.6, a pressure wave incident at an angle on the surface of a solid will generate shear waves as well as longitudinal waves. However, as the angle of incidence is increased a point is reached beyond which longitudinal waves are no longer produced. This is known as the critical angle for longitudinal waves. As the angle of incidence is increased further another critical angle is reached beyond which neither longitudinal nor shear waves can exist in the solid. This is known as the critical angle for shear waves. Techniques which involve directing sound waves in a fluid towards the surface of a solid provide an efficient means of producing longitudinal waves and shear waves in a solid. In each case the process can be reversed so that it is possible to detect a particular mode with a transducer placed at the appropriate angle.

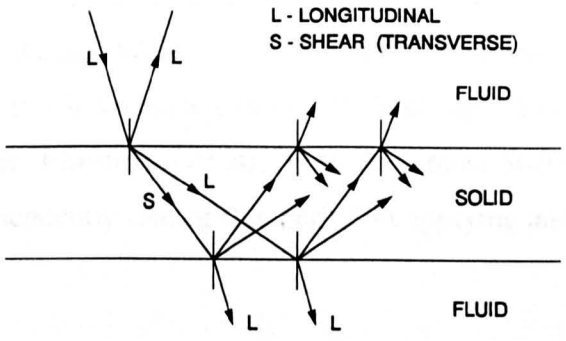

FIGURE 1.6 GENERATION OF L AND S WAVES IN A SOLID

Angled transmitting and receiving transducers can also be used to generate and detect some of the other types of waves previously mentioned. A Rayleigh wave is generated just after the angle of incidence passes the shear wave critical angle and at other angles it is possible to generate Lamb waves in thin plates. The mechanisms involved in using angled transducers to generate and detect Rayleigh waves and Lamb waves are different to those which are involved in generating and detecting the fundamental longitudinal and shear waves. As previously mentioned, Chapter 8 is dedicated to a detailed study of Lamb waves which are of special importance in this research. There are other methods of generating and detecting the various types of mechanical vibration that are possible in a solid but most of them require direct contact and are not relevant here.

1.5 Direct Ultrasonic Flaw Detection Techniques

As mentioned previously, the use of ultrasound for flaw detection was first suggested by Sokolov [18] in 1929. Developments in the next decade centred around finding ways and means to use sound as a supplement to X-rays in the inspection of materials. Efforts were confined to using continuous waves, to learning about transmission of sound waves across interfaces and through structures, and to developing satisfactory display systems. Progress was relatively slow and the number of reports that appeared in the literature was less than 1 per cent of the number reported in other areas of ultrasonics [16]. The situation changed during World War II with the practical development of what has proved to be a much superior method of detecting flaws, namely, the use of the pulse-echo technique. Firestone [19,20,21] in the United States and Sproule [22] in England worked independently during this period in applying and evaluating this new method.

1.5.1 Pulse-Echo Flaw Detection

Figure 1.7 shows a block diagram of the apparatus needed for flaw detection using the pulse-echo technique. A short pulse of electrical energy about 1 or 2 microseconds long is produced by the pulse generator and applied many times per second to an ultrasonic transducer which is attached to the material being tested. Dry contact, as indicated in the diagram, is possible but it is more common to place a thin layer of liquid between the transducer and the sample in order to achieve good coupling. The electrical pulse is converted to an ultrasonic pulse and travels into the block of material as shown. Two echoes come back. One is from the far end of the block and the other is from the flaw. When these echoes reach the transducer they generate an electrical signal which goes into an amplifier. Sufficient amplification is applied so that the position of the echoes in time can be displayed on an oscilloscope as illustrated in Figure 1.7.

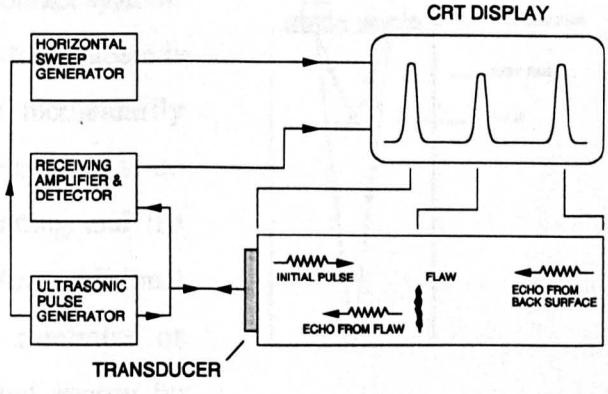

FIGURE 1.7 A SIMPLE PULSE-ECHO FLAW DETECTION SYSTEM

1.5.2 *Immersion Testing*

A version of immersion testing based on the pulse-echo technique is illustrated in Figure 1.8. The sound waves leave the transducer, travel through the liquid (water) and into the test sample. Echoes are returned from the top surface of the sample, the flaw and the back surface of the sample. The advantages of this type of testing are that the top surface of the test sample does not have to be as smooth as with the contact method, flaws near the surface can be more readily detected, the speed of testing is greater, higher test frequencies can be used and tests on more complex shapes are possible. Clearly there are circumstances where this type of testing is not feasible. For example, the test sample may be too large or it may be unacceptable to immerse it in water.

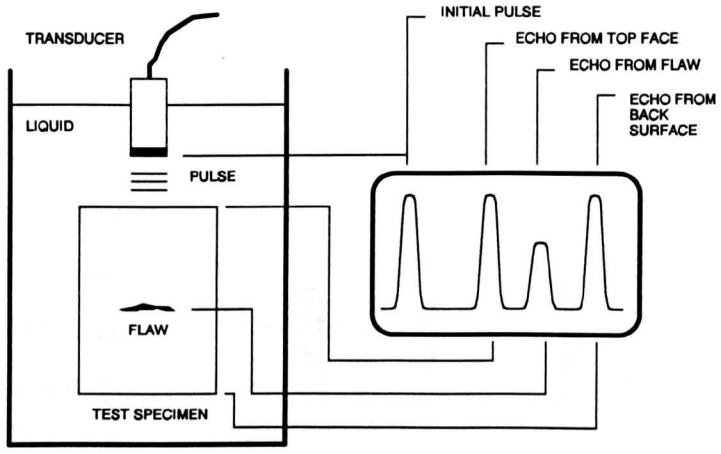

FIGURE 1.8 BASIC IMMERSION TESTING SYSTEM

1.5.3 *Two Transducer Testing*

Two ultrasonic transducers may be used in either contact or immersion testing. Figure 1.9 shows one possible version of a two transducer contact system. The principal advantage of using two transducers is that the transmitted pulse does not momentarily blank out the receiving amplifier since there is no electrical connection between the sending and the receiving parts of the system. An additional advantage is that it is possible to minimize or eliminate unwanted echoes or scattered energy by aligning the receiving transducer in a favourable direction for detecting echoes from the flaw.

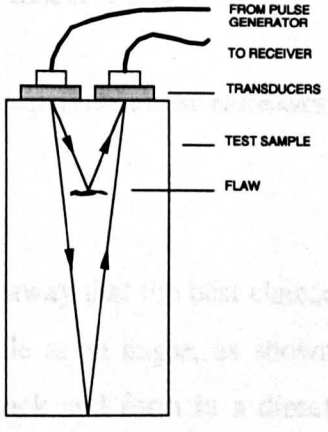

FIGURE 1.9 A TWO TRANSDUCER TESTING SYSTEM

1.5.4 *Through Transmission Testing*

The through transmission mode of testing is illustrated in Figure 1.10. Unlike the early experiments with through transmission which used continuous waves it is now more common to use ultrasonic pulses. When the flaw gets between the transmitting transducer and the receiving transducer, the signal level is reduced or it may go to zero depending on the relative sizes of the defect and the ultrasonic beam.

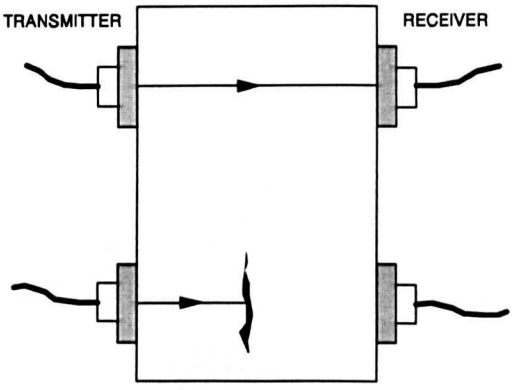

FIGURE 1.10 BASIC THROUGH TRANSMISSION TEST

1.5.5 *The Resonance Method*

Continuous waves are used in the resonance method. As shown in Figure 1.11, a single transducer placed on the surface of a part suspected of having a flaw is used to produce a standing-wave pattern of an integral number of wavelengths. One value for the thickness is obtained in the region where there is no flaw and another when the flaw is under the transducer.

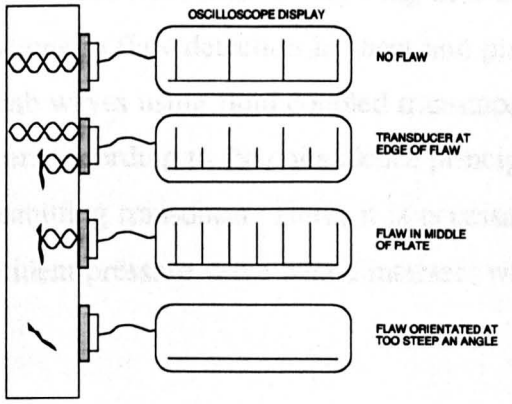

FIGURE 1.11 DETECTING FLAWS USING RESONANCE

1.5.6 *Shear Wave Testing*

There are many types of defect that are orientated in such away that the best chance of getting a good echo is to send a pulse into the test sample at an angle, as shown in Figure 1.12 for a butt weld. The probe can be moved back and forth in a direction perpendicular to the weld and thus scan the region of the flaw. The ultrasonic transducer normally produces shear waves in the test sample when it is used in this way.

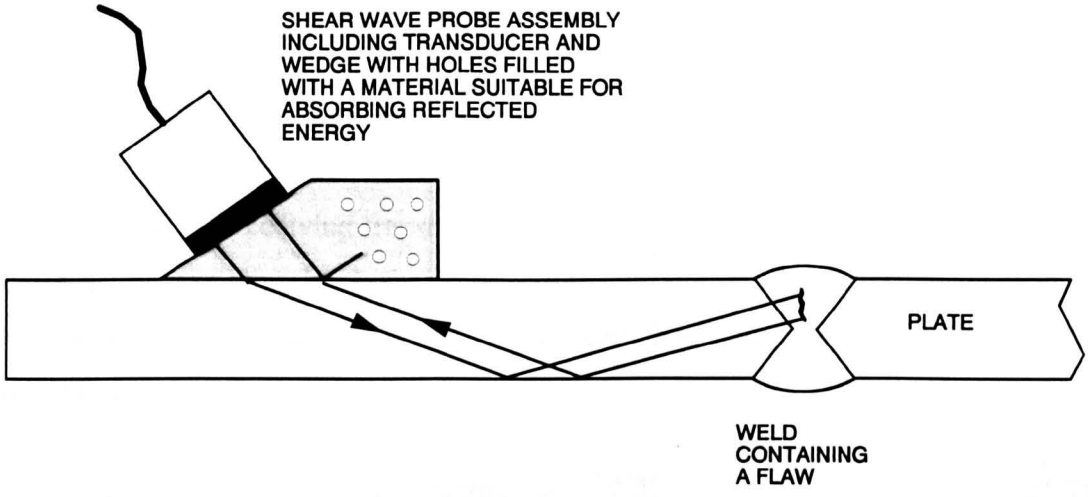

FIGURE 1.12 AN ANGLED TRANSDUCER IS USED TO PRODUCE SHEAR WAVES AND DETECT A FLAW IN A BUTT WELD

1.5.7 Lamb Wave Testing

The general characteristics of Lamb (plate) waves were presented in Section 1.4.4 and they are considered in depth in Chapter 8. It has been known for a very long time that these waves have important potential applications in flaw detection in sheet and plate materials. In order to generate and detect Lamb waves using fluid coupled transducers it is necessary to set the angle of the transducers according to the coincidence principle which is illustrated in Figure 1.13 for a transmitting transducer. Here, it is necessary to match up the points in the crests of the incident pressure wave which intersect with

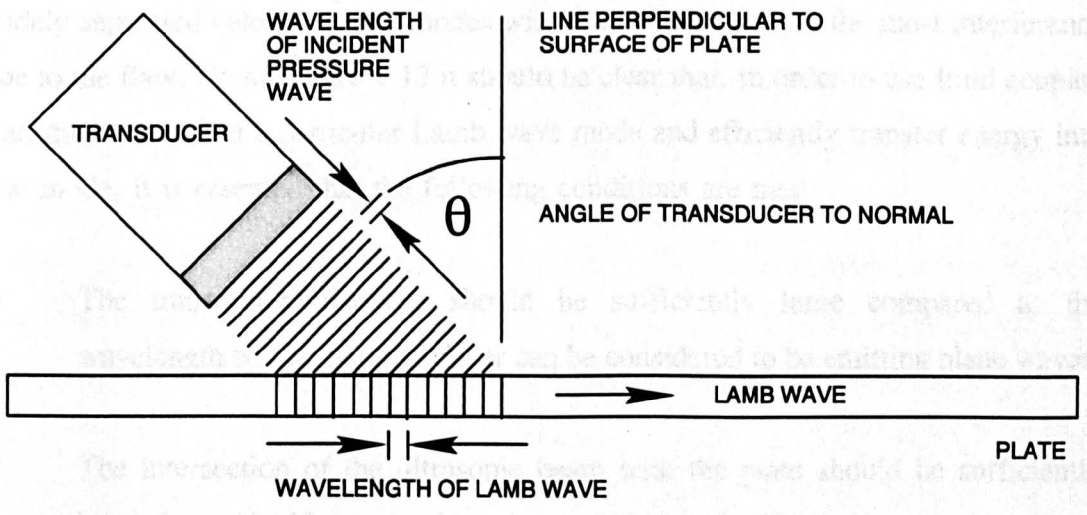

FIGURE 1.13 USING AN ANGLED TRANSDUCER TO PRODUCE LAMB WAVES IN A THIN PLATE

the surface of the plate, with points on the surface of the plate which are separated by intervals of length which are equal to the wavelength of the required Lamb wave mode. The coincidence principle also works in reverse so that the receiving transducer should be set at the same angle as the transmitting transducer. From Figures 1.14 it can be seen that, since $c=f\lambda$, the coincidence principle requires that:

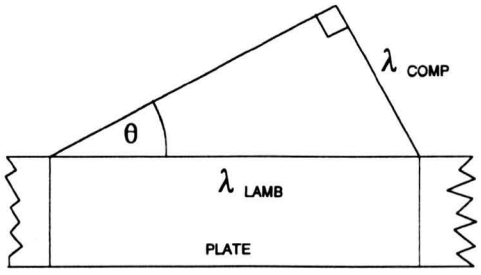

FIGURE 1.14 ANGLE-WAVELENGTH RELATIONSHIP

$$\sin(\theta) = \frac{c_{COMP}}{c_{LAMB}} \tag{1.1}$$

where c_{COMP} is the propagation velocity of the incident compressional wave and c_{LAMB} is the phase velocity of the required Lamb wave mode. From Figure 1.13 it can be seen that θ is the angle of the transducer relative to the normal. It should be noted that, because Lamb waves result from the superposition of longitudinal and shear waves, they also have associated with them a group velocity. Group velocity and phase velocity will be discussed in Chapter 8.

Lamb wave testing is often much more complicated than with other types of waves because of the many possible modes of vibration. Conventional Lamb wave testing (dry or liquid coupling) can only be carried out provided that care is taken to work with as simple a set of conditions as possible; this means as few modes as possible, modes with widely separated velocities, and modes with which there will be the most interference due to the flaw. From Figure 1.13 it should be clear that, in order to use fluid coupled transducers to select a particular Lamb wave mode and efficiently transfer energy into that mode, it is essential that the following conditions are met:

- The transmitter diameter should be sufficiently large compared to the wavelength so that the transducer can be considered to be emitting plane waves.

- The intersection of the ultrasonic beam with the plate should be sufficiently large that a significant number of wave crests coincide.

An ideal but obviously impractical configuration would be one where both the transducer diameter and the intersection area are infinite. Clearly the use of focused transducers is not consistent with the coincidence principle. A focused beam of ultrasound may produce Lamb waves in a plate but this does not provide a means of efficiently transferring energy into the required mode.

Viktorov has published extensively on the use of Lamb waves in non-destructive testing and monitoring applications and his book [23] has become a standard text in the field. However, it was probably Worlton [24,25] who first recognized the advantages of using Lamb waves to nondestructively test plates. Since then there has been a very great interest in these and other guided waves for flaw detection. For example, Mansfield [26] and Ball and Schewring [27] describe using Lamb waves to carry out coarse, quick inspection on a variety of different strips and plates. Silk and Bainton [28] investigated the use of guided waves to locate defects in boiler and heat exchanger piping and Rokhlin [29] has reported several studies on the sensitivities of Lamb waves to elongated delaminations. Rokhlin and Bendec [30] have also studied the interaction of Lamb waves with spot welds. Rose *et al.* [31] have reported investigations using Lamb waves to globally inspect K-joints in off-shore structures and the Welding Institute in the United Kingdom (see for example, Bartle [32]) have developed an acoustic pulsing technique to monitor crack growth in large plate-like structures. The preceding summary was reproduced from a paper [33] by Alleyne and Cawley. Prof. Peter Cawley and his team at Imperial College have conducted some of the most detailed research into the use of Lamb waves for flaw detection. Some of their work is discussed briefly in the next paragraph.

In 1991 Alleyne and Cawley published a paper which describes a technique for the analyses of propagating multimode signals [34]. The method involves a two-dimensional Fourier transformation of the time history of the waves received at a series of equally spaced positions along the propagation path. In 1992 Alleyne and Cawley published a paper [33] which describes a theoretical and experimental investigation of the interaction of Lamb waves with defects. Here, a technique based on the finite element method was used to make theoretical predictions. A series of experiments indicated that the technique was capable of accurately predicting a wide variety of situations. Alleyne

and Cawley also describe methods for the optimisation of Lamb wave inspection techniques [35]. In another important paper Guo and Cawley discuss the interaction of Lamb waves with delaminations in composite laminates [36].

Conventional ultrasonic inspection (pulse-echo etc.) of large structures is very time consuming because the transducer(s) need to be scanned over each point of the structure that must be tested. The use of Lamb waves is potentially a very attractive solution to this problem since they can be excited at one point on the structure and can be propagated over considerable distances. If a receiving transducer is positioned at a remote point on the structure, the received signal contains information about the integrity of the line between the transmitting and receiving transducers. The test therefore monitors a line rather than a point and considerable savings in test time may be obtained. Since Lamb waves produce stresses throughout the plate thickness the entire thickness of the plate is interrogated, which means that it is possible to find defects initiating at either surface, and also to detect internal defects. The sensitivity of Lamb wave testing with regard to the size of crack that can be detected is comparable with other types of ultrasonic flaw detection. For example, cracks .001 inches deep that are favourably orientated can readily be detected [16]. An example of Lamb wave testing is illustrated in Figure 1.15. Here, liquid coupled transducers are being used to test for flaws in a length of thin-wall tubing. Testing thin-wall tubing would be very difficult if not impossible using some of the previously mentioned ultrasonic test configurations. The use of Lamb and torsional waves for detecting flaws in tubes has been investigated by, for example, Lockett [37].

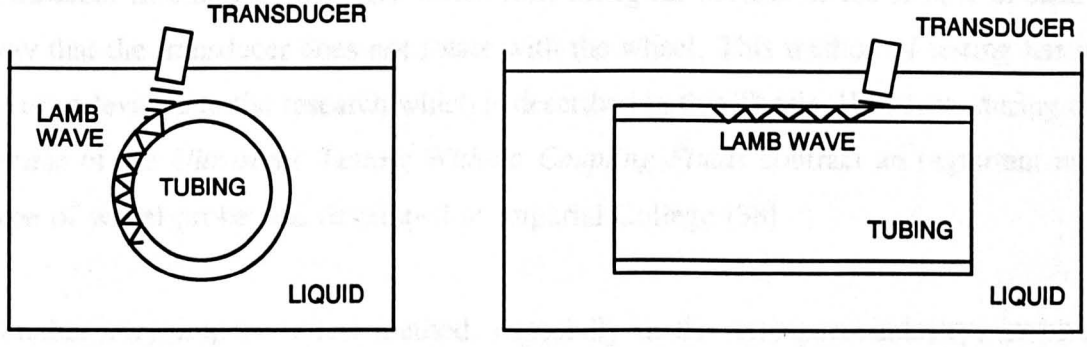

FIGURE 1.15 LAMB WAVES USED TO DETECT FLAWS IN THIN-WALL TUBING

Most of the work which has been referenced in this Section on Lamb waves involves the remote detection of defects. Later it will be shown that it is also possible to use Lamb waves in localised nondestructive testing as an alternative to conventional ultrasonic testing using bulk waves. Here, the dispersive nature (see Chapter 8) of Lamb waves is not so problematic, as the propagation distances are relatively small.

1.5.8 Summary

Section 1.5 provided a brief description of seven of the most common flaw detection techniques which involve the direct use of ultrasound. Many of the examples indicate dry coupling but in every case liquid coupling is also possible and probably preferable. This liquid coupling can be provided either by immersing the transducer(s) and the sample in a bath of liquid, as illustrated in Figure 1.8 for the pulse echo technique, or by placing a small amount of liquid between the front face of the transducer(s) and the sample. Although there are of course other flaw detection techniques which involve either the direct or indirect use of ultrasound, these particular methods have been grouped together in one Section because, as will become clear later, it is now possible to envisage implementing each of them using air coupled rather than liquid or dry coupled transducers. It will be evident that attention has been focused on the use of Lamb waves. The reasons for this will also become clear at a later stage.

One important ultrasonic device which requires coupling media and which has not previously been mentioned is the wheel probe. With this device, smooth continuous acoustical contact between a transducer and a test sample is achieved by immersing the transducer in a liquid filled tyre which rolls along the surface of the sample in such a way that the transducer does not rotate with the wheel. This method of testing has no direct relevance to the research which is described in this Thesis. However, during the course of the *Ultrasonic Testing Without Coupling Fluids* contract an important new type of wheel probe was developed at Imperial College [38].

Another very important test method, especially in the aerospace industry, involves using water jets to couple ultrasound from a transmitting transducer into a sample and from the sample into a receiving transducer [39]. This technique provides a means of rapidly scanning large structures but the use of water jets is clearly inconvenient and

their use may be completely unacceptable with some modern non-metallic materials. A considerable proportion of the air coupled research which is currently being undertaken at the University of Strathclyde and else where is aimed at replacing these system with non-contact through transmission systems [4].

1.6 Indirect Ultrasonic Flaw Detection Techniques

In Section 1.5 the term *direct* was used to identify ultrasonic test systems which require an external coupling medium. Here, the term *indirect* is used to identify test systems which involve generating ultrasound in a sample but which do not require an external coupling medium.

One of the most impressive examples of an indirect ultrasonic test system is LUIS[1], the Laser Ultrasonic Inspection System [40]. With this system, complex composite parts and structures can be inspected by pulse-echo at a distance of up to 2.4 m without the use of a couplant. Defect mapping of contoured parts can be easily and rapidly performed by scanning laser beams over the surface of the part to be inspected. Two laser beams are used - one to generate and one to detect ultrasonic waves at the surface of the component. With this technology, not only is there no need for a couplant, but several other limitations of conventional ultrasonic testing are overcome. For example, there is no critical orientation requirement of the optical beams with respect to the inspected component's surface. Very complex geometrical shapes can thus be inspected and access is only needed from one side. An inspection rate of 5.5 m^2/h is achievable and the system can be used with many different types of materials, including polymer-matrix composites (graphite, Kevlar and glass epoxy), thermoplastics and painted metal. With LUIS, complete aircraft inspection has become a reality and a system has been purchased by the United States Air Force for the inspection of components up to 12 x 4.8 m in size. The ultrasound generator in the LUIS system is a 150 mJ CO_2 laser which can produce spot sizes of either 2.5 or 5 mm diameter. The ultrasound detection system is based on a YAG laser which produces a 55μs pulse. Both lasers operate in the infra-red part of the spectrum and eye protection is required.

1 Developed by UltraOptec Inc. of Boucherville, near Montreal, Canada

Other types of non-contact testing which use ultrasound have been investigated. For example, a hybrid system has been constructed and evaluated by Hutchins, Wright, Hayward and Gachagan [41]. Here, a laser was used to generate ultrasound in a test sample and a piezocomposite transducer was used as an air coupled detector. Further examples of non-contact testing which involve the generation and detection of ultrasound include, for example, the use of electromagnetic acoustic transducers (EMAT's) and capacitance devices, however, a major limitation with these devices is that they are only suitable for testing electrically conductive materials.

A vast number of papers have been written on indirect and hybrid non-contact test systems which involve using lasers and EMAT's to generate and/or detect ultrasound in a test sample. A detailed discussion of these systems is not relevant to this PhD Thesis, however, it should be noted that for an air coupled flaw detector to be of value it must be capable of competing with these systems in terms of effectiveness, convenience, cost and safety.

1.7 Transducer Developments

Having discussed the ultrasonic techniques which are available for conversion from liquid coupling to air coupling it is now appropriate to consider the available transducer technology. Transducers for the generation and detection of sound are without doubt the most critical components of an air coupled ultrasonic test system. Six classes of electro-acoustic air transducer are potentially of interest: electrostatic, variable reluctance, moving coil, piezoelectric, electrostrictive and magnetostrictive. It has been found by many researchers that, in order to simultaneously obtain the high levels of sensitivity and bandwidth required for air coupled testing, it is necessary to use devices which fall into either the electrostatic class or the piezoelectric class. The electrostatic class of devices includes the condenser microphone, the solid dielectric microphone and the relatively new capacitive transducer which is made using silicon micro-machining techniques. There are also many different types of piezoelectric transducers which can be considered along with the conventional and composite thickness mode devices.

Piezoelectric transducer technology is now very mature and it is reasonable to say that transmitting transducers based on this technology can be operated at the physical limits

of the available materials. For example, assuming a 2 kV/mm dielectric breakdown strength, a 25 mm diameter PZT-5A disc should be capable of handling approximately 15 kW of peak electrical power but in practice this is not achievable because strains larger than 10^{-4} (ratio of displacement to total thickness) cannot be sustained for extended periods. These figures were obtained from a recent paper by Grandia and Fortunko [42] where the authors also claim that, at the present time, 10 kW is the maximum electrical power that can be delivered by practical ultrasonic pulsers or gated amplifiers. A major problem with using piezoelectric transducers in air coupled applications is that, because they provide a very inefficient acoustic impedance match with air, most of the available transmitter power is converted into heat in the transducer or returned to the pulser unit. The transduction efficiency can, in principle, be improved by using an impedance matching layer, or by reducing the specific acoustic impedance of the transducer material. Materials with the properties required for producing efficient mechanical matching layers include, for example, cork, balsa wood and silicon rubber. Unfortunately, there are practical problems associated with all of these materials and many researchers are attempting to engineer more suitable ones. There is also a very great interest in developing new types of ultrasonic transducers and a considerable amount of research effort is being devoted to the development of both piezoceramic and electrostatic devices.

At low frequencies, below 100 kHz, condenser microphones can be used to generate and receive ultrasonic signals in air [43]. In the condenser microphone the restoring force is provided by the tension in the membrane, which is typically made of high strength steel. One of the problems associated with this technology is that the operating frequency of conventional designs is too low for most air coupled defect detection applications. The reason for this is that the resonant frequency of the membrane is physically limited by the properties of the material.

Another type of electrostatic transducer is the solid dielectric microphone which can operate at frequencies well above 100 kHz. This device does not use applied tensile force to restore the position of the membrane which typically has a thickness of between 2.5 μm and 10 μm. Instead, the restoring forces are due principally to the presence of air pockets between the membrane and the back plate [44]. With this type

of device, which is illustrated in Figure 1.16, it is possible to achieve a much better acoustic match with air than is possible with piezoelectric thickness mode devices. Until relatively recently the performance of these devices has been unpredictable and inconsistent. However, as a result of advances in micro-machining technologies [45] new construction techniques have become available and there is now the potential to design devices with predictable performance.

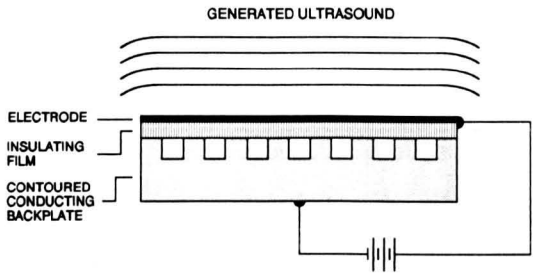

FIGURE 1.16 SOLID DIELECTRIC TRANSDUCER

Figure 1.17 illustrates a relatively new type of micromachined capacitive air transducer which typically employs a 0.5 μm thick membrane which is much thinner than that which is used with the previously mentioned solid dielectric devices. This type of transducer appears to embody the most desirable features of the condenser and solid dielectric microphones [46]. It uses the residual stresses in the membrane to provide the restoring forces but has a sensitivity and a dynamic range significantly greater than that of the solid dielectric microphone. In the transmission mode, front face displacements as high as 0.3 μm at 2 MHz have been reported. This type of transducer is very efficient and fractional bandwidths range from 5% to 20%.

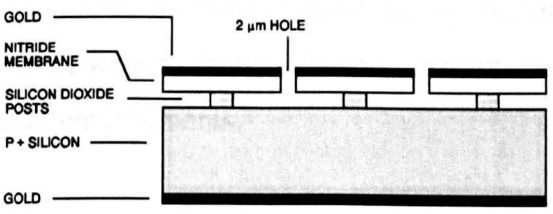

FIGURE 1.17 MICROMACHINED TRANSDUCER

1.8 Aims of this Thesis

As previously mentioned, a large proportion of the research which is described in this PhD Thesis was funded by EPSRC, Rolls Royce and Ford through a research contract which was given the name *Ultrasonic Testing Without Coupling Fluids*. The fundamental aim of the research was to investigate the feasibility of developing robust and truly practical ultrasonic test systems which do not require liquid coupling. Air coupled transducer technology was to be investigated at the University of Strathclyde while researchers at Imperial College would work mainly on the development of a new type of wheel probe. At Strathclyde, the original intention was to concentrate on air

coupled systems suitable for operation at normal atmospheric pressure, however, early publication of the initial results attracted interest from British Gas who provided additional funds to support a high pressure study.

Even before the EPSRC contract had been awarded it was realised that the ultrasonic transducer technologies that had been used by researchers such as Luukkala *et al.* and Rogovsky would not be suitable for the development of a system capable of rapidly scanning a test sample in an industrial or high pressure environment. The electrostatic devices used by Luukkala *et al.* were known to be fragile and unreliable and although the piezoceramic devices used by Rogovsky were robust they were known not to have sufficient air coupled sensitivity. It was known that the air coupled performance of piezoceramic devices could be improved by applying mechanical matching layers but the materials which provided the best performance were recognised by most researchers to be unsuitable for use in, for example, damp environments.

An alternative transducer technology which had not previously been used for air coupled ultrasonic inspection was the ceramic-polymer composite. This type of ultrasonic transducer had originally been developed for SONAR systems and had also found applications in medical imaging systems. A new generation of piezocomposite transducers was under development within the Ultrasonics Research Group at the University of Strathclyde [47], and it had been demonstrated that, by using advanced linear systems [48] and finite element [49] modelling techniques, the properties of these devices could be optimised for use in air. A major aim of this research was to demonstrate that these new piezocomposite transducers were sufficiently sensitive and sufficiently robust to be considered for industrial air coupled testing at both normal atmospheric pressure and at higher pressures. It was recognised that, although the piezocomposite transducers could provide an improvement in air coupled sensitivity compared to piezoceramic devices, the research would also involve investigating techniques capable of providing further substantial improvements in sensitivity. In particular, integration of the receiving transducer with an ultra low noise pre-amplifier would be a key feature of the research and modelling of the transducer/pre-amplifier combination would be of fundamental importance to the overall system design. It was intended that the research would lead to the development of a complete imaging system

capable of producing rapid single sided scans without the requirement for either fragile transducer matching layers or signal averaging techniques. The new air coupled system was to be simple, robust, inexpensive and safe. Further, it was to be as easy to use as a liquid coupled test system.

Although the new piezocomposite transducers had obvious potential for air coupled testing it was recognised that there were other ways in which piezoelectric materials could be employed to produce sensitive air coupled transducers. An additional aim of this research was to thoroughly investigate these alternatives. As mentioned in Section 1.7, exciting new types of electrostatic devices were under development while this research was in progress. Although good air coupled sensitivity was being reported by a number of researchers, and it appeared that it was possible to obtain consistent results from some of these devices, there was nothing in the literature to indicate that any of these transducers would be sufficiently robust for use in an industrial environment. Also, experiments at the University of Strathclyde indicated that solid dielectric transducers could not function at the level of pressure that might be found, for example, in a gas pipe line. Based on these observations it was decided that the EPSRC funded research effort should be focused on the use of piezoceramic transducer technology and in particular the new piezocomposite technology which was already under development at the University of Strathclyde.

1.9 Contributions of this Thesis

In addition to achieving all of the original project aims, this research has resulted in many additional contributions to the field of ultrasonics and non-destructive testing. A major contribution to the field of ultrasonics has been the development of a new theory which can be used to predict the absolute sensitivity of a piezoelectric receiver. This research also provides an improved understanding of how gas coupled transducers can be used to generate and detect longitudinal waves, shear waves, Rayleigh waves and Lamb waves. The work on Lamb waves is of particular significance and this has led to the development of a complete scanner which is capable of producing *single-sided*[1] scans without the need to employ signal averaging techniques. As a consequence of the

1 The technique involves using two transducers which are both placed on one side of the test sample.

interest shown by British Gas it has been possible to show that piezocomposite based receiver systems are ideally suited to operation at pressures of up to 1000 psi. One very exciting aspect of the work is that it indicates the feasibility of using gas coupled piezocomposite transducers for pulse-echo inspection at high pressure.

This work has already contributed to other research programs within the University of Strathclyde and at Imperial College. For example, the ultra low noise receiver system has been used to demonstrate the feasibility of through transmission defect testing using piezocomposite transducers. An eight channel version of the receiver has been constructed and is being used as part of a rapid scanning system which will replace water jet systems in the aircraft industry [50]. A complete Lamb wave system has been supplied to Imperial College where it has been used to confirm theoretical results obtained using a finite element model [8,9]. Knowledge gained during the Lamb wave investigation has been used to assist the Optoelectronics Group at Strathclyde in experiments involving the generation of Lamb waves using a laser source [5]. This aspect of the work has also been of value during the development of a membrane hydrophone which will be used for the calibration of air coupled transducers [51]. Outside Strathclyde and Imperial, the work has been referenced by, for example, Grandia and Fortunko [42]. The work also features in a recent book entitled *Ultrasonic Methods of Non-destructive Testing* by Jock Smith (Brunel University) and Geoff Simpson [52].

In 1997 there were almost 300 applicants for the *John Logie Baird Awards*. In recognition of the work on air-coupled ultrasonic testing, Strathclyde University was joint winner in the Glasgow Regional Awards and runner-up in the Scottish National Awards for University Spin-Out Companies.

A list of the eleven publications arising from this Thesis can be found at the end of the Reference Section. The paper entitled *A frequency-agile ultrasonic Lamb wave scanner for NDE systems* has been judged by the British Institute of Non-Destructive Testing to be the best paper to appear in *Insight* in 1997. As will be reported in the August 1998 issue of *Insight*, the *John Grimwade Medal* is to be awarded in recognition of this achievement.

Chapter 2

Air as a Coupling Medium

2.1 Introduction

As with an ordinary mirror which reflects almost all of the light which is incident upon it, a gas/solid interface is normally thought of as a 100% reflector of sound waves. However, in reality, it is possible for a very small percentage of a sound wave's energy to cross a solid/air boundary and vice versa. This is what makes gas coupled ultrasonic testing possible. A mathematical analysis of the problems is presented in this Chapter.

All of the techniques which were discussed in Section 1.5, and which are normally implemented using liquid coupled transducers, can be considered for use with gas coupled transducers operating either at normal atmospheric pressure or at some higher pressure. For the purpose of analysis these techniques can be placed into one of the following three basic categories:

1) Pulse-echo
2) Through transmission
3) Pitch-catch

Modern ultrasonic test systems which employ liquid coupling are, almost without exception, based on robust piezoceramic plate transducers. In this Chapter it will be assumed that the proposed air coupled systems will also employ piezoceramic plate transducers. In this way it is possible to make a direct comparison between liquid coupled and air coupled systems based on each of the three available techniques. The theoretical performance of systems based on piezoceramic plate transducers also provides a reference against which alternative transducer designs can be judged. A large portion of Chapter 3 is dedicated to a discussion of alternative piezoceramic transducer designs.

It is widely believed that atmospheric absorption is the major obstacle to the use of air coupled ultrasonic inspection. This is not so. In this Chapter it will be shown that, in the frequency range of interest, the limitations are almost entirely due to the very large specific acoustic impedance differences between typical solids and gases. In a system which uses air coupled transducers for both generation and detection, the received signal amplitude is principally determined by the transmission losses at the four air/solid interfaces. Additional, but significantly smaller, losses can also be expected due to diffraction, loss of phase front coherence, and finite amplitude saturation effects

which are sometimes experienced at very high drive levels [42]. Most of this Chapter is dedicated to an investigation of coupling losses at the media boundaries.

2.2 Reflection and Transmission of Sound Waves at Media Boundaries

It is clear that the main difference between using a gas and a liquid as a coupling medium is that the values of the reflection and transmission coefficients at the media boundaries are such that it is difficult for sound to penetrate a solid and then escape again. In order to quantify the differences between gas coupling and liquid coupling it is necessary to obtain accurate mathematical expressions for the reflection and transmission coefficients of sound at the media boundaries.

2.2.1 Mathematical Analysis

A large number of publications are available which present the equations for the reflection and transmission coefficients of sound waves at media boundaries. While researching this subject it was often found that a publication would be biased towards a particular field of study (e.g. seismology), the notation would be appropriate to that field and only the necessary equations would be provided. For this reason it was difficult to check that an equation appearing in one publication was exactly equivalent to one appearing in another and that no application specific approximations had been made. For example, all of the reviewed literature assumed 100% reflection at an air/solid boundary and disregarded the possibility of transmission across such a boundary. For this work it was necessary to obtain all of the nine equations which apply at fluid/solid/fluid boundaries. Further, it was necessary to ensure that the notation was appropriate to this application, that it was consistent across all of the equations and that no application specific approximations had been used in the derivations. Unfortunately, most published sources were either found to be incomplete or could be shown to be inaccurate. The unreliability of published theory on the reflection and transmission of sound at media boundaries had previously been recognised by Pearson [53] who has derived all of the necessary reflection and transmission coefficients from first principles. Unfortunately, Pearson did not use the concept of acoustic impedance in his work and the result is a set of equations which are cumbersome and not well suited to modern computational techniques. Pearson's work is unpublished, however, it provided the means by which it was possible to check for

errors in the published sources.

Accurate versions of the nine equations for the reflection and transmission coefficients at fluid/solid/fluid boundaries are presented here. These are modified versions of those derived by Brekhovskikh in his impressive and highly regarded book [54]. For convenience, Brekhovskikh has derived an expression for each coefficient in terms of the ratio of the amplitudes of the acoustic field potentials ϕ, ϕ_1 and ψ_1. In order to express the coefficients in terms of acoustic pressure it is necessary to multiply each expression by the ratio of the material densities. Following Brekhovskikh's terminology, let the density in the upper medium (fluid) be ρ and that in the lower medium (solid) be ρ_1. Clearly the conversion factor is unity (ρ/ρ or ρ_1/ρ_1) for reflection of a wave in either the upper or the lower medium. For transmission from the upper medium to the lower medium the conversion factor is ρ_1/ρ and for transmission from the lower medium to the upper medium it is ρ/ρ_1. Each of the nine equations presented here has been modified accordingly.

Case 1

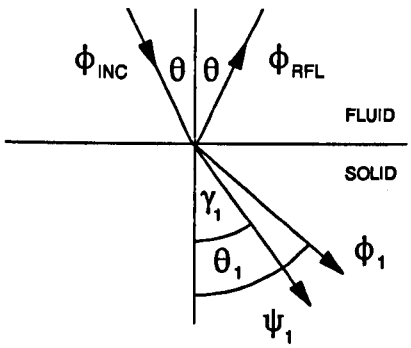

FIGURE 2.1 WAVE INCIDENT FROM FLUID

Consider, as illustrated in Figure 2.1, a plane sound wave incident from a fluid on a fluid-solid boundary. This can be represented by:

$$\phi_{inc} = A e^{jk(x\sin\theta - z\cos\theta)} \qquad (2.1)$$

where θ is the angle of incidence and A is the amplitude of the wave. The reflected wave may be written in the form:

$$\phi_{rfl} = A_r e^{jk(x\sin\theta + z\cos\theta)} \qquad (2.2)$$

Thus the total sound field in the fluid will be:

$$\phi = [A e^{-jkz\cos\theta} + A_r e^{jkz\cos\theta}] e^{jkx\sin\theta} \qquad (2.3)$$

A longitudinal and a transverse wave will be excited in the solid. These waves can be written in the form:

$$\phi_1 = B_l T_L e^{jk_1(x\sin\theta_1 - z\cos\theta_1)} \tag{2.4}$$

$$\psi_1 = B_t T_T e^{j\kappa_1(x\sin\gamma_1 - z\cos\gamma_1)} \tag{2.5}$$

Where B_l is the amplitude of the longitudinal wave and B_t is the amplitude of the transverse wave. The subscript 1 in all of these equations indicates the lower medium i.e. the solid. Here, R, T_T and T_L are the required coefficients. The wave numbers are defined as follows:

$$k = \frac{\omega}{c}, \quad k_1 = \frac{\omega}{c_1}, \quad \kappa_1 = \frac{\omega}{b_1} \tag{2.6}$$

where c is the velocity of sound in the fluid, c_l is the longitudinal velocity of sound in the solid and b_l is the transverse velocity of sound in the solid. For the case of an incident longitudinal wave in the fluid, solving the above equations and applying appropriate boundary conditions leads to the following three equations for the reflection and transmission coefficients. The coefficient, in terms of acoustic pressure, for the longitudinal wave reflected back into the fluid is:

$$R = \frac{A_r}{A} = \frac{Z_1\cos^2 2\gamma_1 + Z_t\sin^2 2\gamma_1 - Z}{Z_1\cos^2 2\gamma_1 + Z_t\sin^2 2\gamma_1 + Z} \tag{2.7}$$

The transmission coefficient, in terms of acoustic pressure, for the refracted longitudinal wave in the solid is:

$$T_L = \left(\frac{\rho_1}{\rho}\right)\frac{B_l}{A} = \frac{2Z_1\cos 2\gamma_1}{Z_1\cos^2 2\gamma_1 + Z_t\sin^2 2\gamma_1 + Z} \tag{2.8}$$

Finally, the transmission coefficient, in terms of acoustic pressure, for the transverse wave in the solid is:

$$T_T = \left(\frac{\rho_1}{\rho}\right)\frac{B_t}{A} = -\frac{2Z_t\sin 2\gamma_1}{Z_1\cos^2 2\gamma_1 + Z_t\sin^2 2\gamma_1 + Z} \tag{2.9}$$

In the above equations Z, Z_l and Z_t denote respectively the impedances of sound waves in the liquid, longitudinal waves in the solid and transverse waves in the solid. Each

of these impedances is a function of the angle of propagation of the wave relative to the normal:

$$Z = \frac{\rho c}{\cos\theta}, \quad Z_1 = \frac{\rho_1 c_1}{\cos\theta_1}, \quad Z_t = \frac{\rho_1 b_1}{\cos\gamma_1} \tag{2.10}$$

Here, θ_l and γ_l are the propagation angles of the longitudinal wave and the transverse wave respectively in the solid. At normal incidence of the sound wave on the boundary $\theta=\theta_l$ and $\gamma_l=0$. Under this condition it is clear from Equation (2.9) that $T_T=0$ (i.e. transverse waves are not excited) and from Equations (2.7) and (2.8) we obtain the following familiar equations for the longitudinal reflection and transmission coefficients:

$$R = \frac{Z_1 - Z}{Z_1 + Z} \tag{2.11}$$

$$T_L = \frac{2Z_1}{Z_1 + Z} \tag{2.12}$$

The transmission of sound from a transducer into a coupling fluid is a special case since pressure waves are emitted from both faces of the device. Provided that the coupling medium is the same on both sides of the transducer it can be shown [55] that:

$$T_{TC} = \frac{Z_A}{Z_C + Z_A} \tag{2.13}$$

where Z_C is the characteristic acoustic impedance of the transducer and Z_A is the acoustic impedance of the coupling fluid.

Case 2

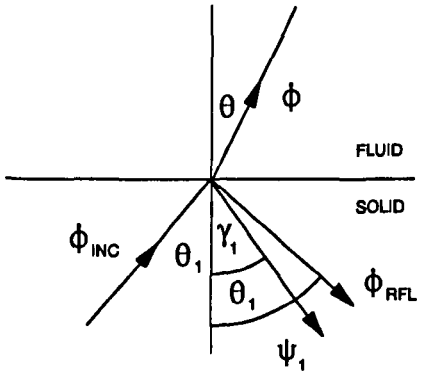

FIGURE 2.2 LONGITUDINAL WAVE INCIDENT FROM A SOLID

Now consider, as shown in Figure 2.2, a longitudinal wave of amplitude A_l incident from a solid on a solid/fluid boundary. This wave will excite a reflected longitudinal wave of amplitude B_l, a reflected transverse wave of amplitude B_t and a pressure wave of amplitude D in the fluid. The sound wave in the fluid can be written:

$$\phi = De^{jk(x\sin\theta + z\cos\theta)} \tag{2.14}$$

For the incident and longitudinal waves we have:

$$\phi_1 = A_l e^{jk_1(x\sin\theta_1 + z\cos\theta_1)} + B_l e^{jk_1(x\sin\theta_1 - z\cos\theta_1)} \tag{2.15}$$

Finally, for the reflected transverse wave:

$$\psi_1 = B_t e^{j\kappa_1(x\sin\gamma_1 - z\cos\gamma_1)} \tag{2.16}$$

By solving these equations and applying appropriate boundary conditions we obtain the required reflection and transmission coefficients. The reflection coefficient, in terms of acoustic pressure, for the longitudinal wave in the solid is:

$$R_{L\text{-}L} = \frac{B_l}{A_l} = \frac{Z + Z_t \sin^2 2\gamma_1 - Z_1 \cos^2 2\gamma_1}{Z + Z_t \sin^2 2\gamma_1 + Z_1 \cos^2 2\gamma_1} \tag{2.17}$$

The transmission coefficient, in terms of acoustic pressure, for the longitudinal wave generated in the fluid is:

$$T_{L\text{-}L} = \left(\frac{\rho}{\rho_1}\right)\frac{D}{A_l} = \left(\frac{\rho}{\rho_1}\right)\frac{c\cos\theta_1}{c_1 \cos\theta \cos^2 2\gamma_1}\left(1 - \frac{B_l}{A_l}\right) \tag{2.18}$$

The reflection coefficient, in terms of acoustic pressure, for the transverse wave generated in the solid is:

$$R_{L\text{-}T} = \frac{B_t}{A_l} = \left(\frac{b_1}{c_1}\right)^2 \frac{\sin 2\theta_1}{\cos 2\gamma_1}\left(1 - \frac{B_l}{A_t}\right) \tag{2.19}$$

Case 3

Consider, as shown in Figure 2.3, a transverse wave of amplitude A_t incident from a solid onto a fluid/solid boundary where the system of waves can be written as follows. For the sound wave in the fluid we have:

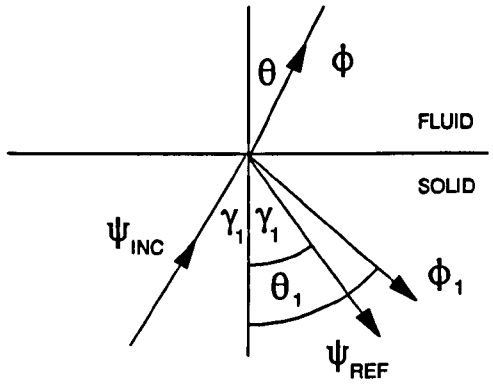

FIGURE 2.3 TRANSVERSE WAVE INCIDENT FROM A FLUID

$$\phi = De^{jk(x\sin\theta + z\cos\theta)} \quad (2.20)$$

For the reflected longitudinal wave in the solid:

$$\phi_1 = B_l e^{jk(x\sin\theta_1 - z\cos\theta_1)} \quad (2.21)$$

Finally, for the incident and reflected transverse waves we have:

$$\psi_1 = A_t e^{j\kappa_1(x\sin\gamma_1 + z\cos\gamma_1)} + B_t e^{jk_1(x\sin\gamma_1 - z\cos\gamma_1)} \quad (2.22)$$

Solving these equations and applying the appropriate boundary conditions we obtain the following reflection and transmission coefficients for the case of an incident transverse wave on a solid-fluid boundary. The coefficient, in terms of acoustic pressure, for the reflected transverse wave in the solid is:

$$R_{T\text{-}T} = \frac{B_t}{A_t} = -\frac{Z + Z_1\cos^2 2\gamma_1 - Z_t\sin^2 2\gamma_1}{Z + Z_1\cos^2 2\gamma_1 + Z_t\sin^2 2\gamma_1} \quad (2.23)$$

The coefficient, in terms of acoustic pressure, for the transmitted longitudinal wave in the fluid is:

$$T_{T\text{-}L} = \left(\frac{\rho}{\rho_1}\right)\frac{D}{A_t} = \left(\frac{\rho}{\rho_1}\right)\frac{\tan\theta}{2\sin^2\gamma_1}\left(1 + \frac{B_t}{A_t}\right) \quad (2.24)$$

Finally, the coefficient, in terms of acoustic pressure, for the reflected transverse wave in the solid is:

$$R_{T\text{-}L} = \frac{B_l}{A_t} = -\left(\frac{c_1}{b_1}\right)^2 \frac{\cos 2\gamma_1}{\sin 2\theta_1}\left(1 + \frac{B_t}{A_t}\right) \quad (2.25)$$

Echo Transmission Coefficients and Insertion Loss

In addition to the nine basic coefficients which have been described previously it is also possible, in the case of a thick plate immersed in either a liquid or a gas, to define two echo coefficients. The longitudinal echo coefficient is defined as:

$$E_L = T_L R_{L\text{-}L} T_{L\text{-}L} \tag{2.26}$$

The transverse echo coefficient is defined as:

$$E_T = T_T R_{T\text{-}T} T_{T\text{-}L} \tag{2.27}$$

Now, using either the longitudinal or the transverse echo coefficient, the total acoustic insertion loss for an ultrasonic testing system can be calculated using the following equation:

$$L_{dB} = 20\log(L) \quad where \quad L = T_{T\text{-}F} E T_{F\text{-}T} \tag{2.28}$$

Here, $T_{T\text{-}F}$ is the coupling loss associated with the transmitting transducer, E is an echo transmission coefficient associated with the test sample and $T_{F\text{-}T}$ is the coupling loss associated with the receiving transducer. An alternative way of writing Equation (2.28) is:

$$L_{dB} = 20\log(L) \quad where \quad L = C_{TR} E \tag{2.29}$$

Here, C_{TR} will be referred to as the combined transmit/receive coupling efficiency. Depending on the test configuration this may be either a property of one transducer or two transducers.

2.2.2 *A Computer Program for Reflection, Transmission and Echo Coefficients*

The theoretical analysis presented in the previous Section has been used as the basis of a computer program which will run on any IBM compatible PC. The program includes a user interface which allows the various coefficients to be plotted and viewed directly on the computer screen. Also included in the program is a means of creating data files which can be read by any suitable graph drawing package. Each of the coefficients can be plotted either as a function of angle of incidence or as a function of one of the angles in the solid. Another feature is a library of materials data which can be read directly into the main program. This means that reflection and transmission coefficients for most fluid/solid/fluid combinations can be plotted without the need for locating and typing in data.

2.2.3 *Validation*

In order to validate the theory presented here, parameters appropriate to water/aluminium/water boundaries have been used in the previously mentioned computer program. The results for shear waves in aluminium are illustrated in Figures 2.4, 2.5, 2.6 and 2.7. These results are in good agreement with a comprehensive set of graphical data for water/aluminium/water boundaries which has been published by Krautkramer [39].

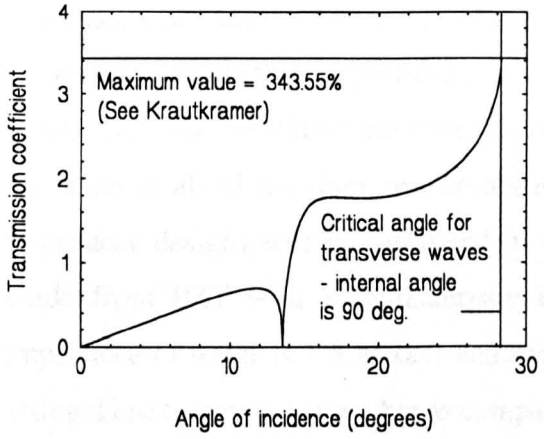

FIGURE 2.4 TRANSMISSION COEFFICIENT (WATER TO ALUMINIUM)

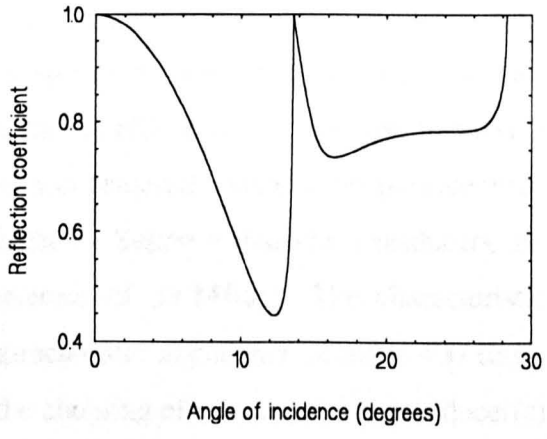

FIGURE 2.5 REFLECTION COEFFICIENT (ALUMINIUM TO ALUMINIUM)

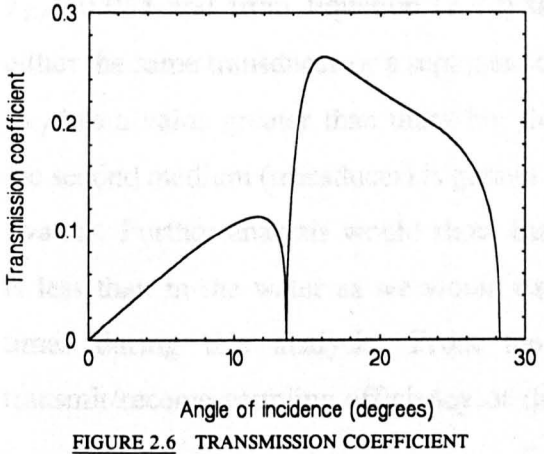

FIGURE 2.6 TRANSMISSION COEFFICIENT (ALUMINIUM TO WATER)

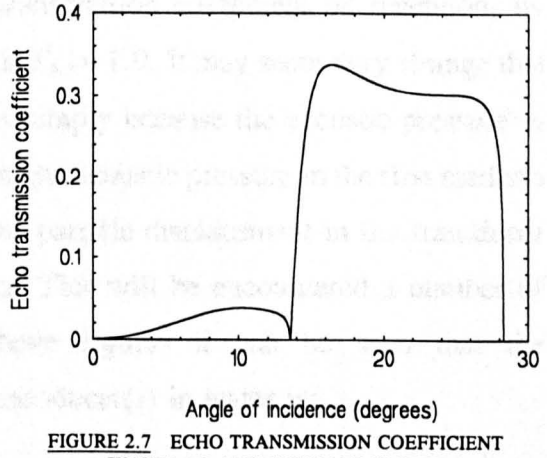

FIGURE 2.7 ECHO TRANSMISSION COEFFICIENT (WATER TO ALUMINIUM TO WATER)

2.3 *An Analysis of the Three Possible Test Configurations*

As mentioned at the start of this Chapter, the three basic techniques available for ultrasonic testing are pulse-echo, through transmission and pitch-catch. The feasibility of adapting these techniques so that it is possible to use air coupling rather than liquid

coupling will now be assessed using the previously discussed theory. For the moment the effects of absorption in the coupling media will be ignored but this subject will be revisited at the end of the Chapter.

2.3.1 Transducer Coupling

In the following analysis it will be assumed that, for the three test configurations considered, the ultrasonic transducers are simple piezoceramic plate devices. The piezoceramic material is assumed to be the same in each configuration and the transducers are identical in every other respect. Making this assumption means that, regardless of whether a particular test configuration uses one transducer or two transducers, the combined transmit/receive coupling efficiency for the transducer(s) is the same in all of the three test configurations considered. Alternative piezoceramic transducer designs will be discussed in Chapter 3. Suppose that the transducers are made from PZT with a characteristic impedance of 33 MRayl. The characteristic impedance of water is 1.5 MRayl and the characteristic impedance of air is 400 Rayl. Using these figures it is possible to compare the coupling efficiency of the transducer(s) when operated in water and then in air. Consider water first. From Equation (2.13) the transmission coefficient for sound launched from a PZT transducer into water is $T_{T\text{-}F}$=0.044 and from Equation (2.12) the transmission coefficient on reception, by either the same transducer or a separate one, is $T_{F\text{-}T}$=1.9. It may seem very strange that $T_{F\text{-}T}$ has a value greater than unity but this is simply because the acoustic pressure in the second medium (transducer) is greater than the acoustic pressure in the first medium (water). Further analysis would show that the particle displacement in the transducer is less than in the water as we would expect. This will be encountered a number of times during this analysis. From the above figures it can be seen that the transmit/receive coupling efficiency of the transducer(s) in water is:

$$C_{TR} = 0.044 \times 1.9 = 0.084 \quad (-22\ dB)$$

Now consider what happens in air. Using Equation (2.13) again, $T_{T\text{-}F}$=1.2 x 10^{-5} and using Equation (2.12) again, $T_{F\text{-}T}$=1.9. Combining these the transmit/receive coupling efficiency of the transducer(s) in air is found to be:

$$C_{TR} = 2.4 \times 10^{-5} \quad (-92\ dB)$$

Comparing the transmit/receive coupling efficiencies for air and water it can be seen that, in order to compensate for the loss in transducer performance alone, it would be necessary to improve the sensitivity of the test system by 70 dB. In Chapter 3 it will be shown that there are a number of ways in which the transmit/receive coupling efficiency of the transducer(s) can be improved. However, as will now be shown, each of the possible configurations has associated with it losses which are determined by the properties of the test sample and which cannot be reduced other than by altering the properties of the coupling fluid.

2.3.2 *Pulse-Echo Analysis*

As illustrated in Figure 2.8, one version of the conventional pulse-echo test method involves placing a single ultrasonic transducer and a test sample in a tank containing water which acts as the coupling medium. Suppose that the test sample is made of aluminium with a characteristic impedance of 17 MRayl. The reflection and transmission coefficients associated with the test sample are as follows. Using Equation (2.11) the reflection coefficient at the front face of the test sample is R_F=0.64 and from Equation (2.12) the transmission coefficient for a sound wave entering through the front face of the solid is T_F=1.84. From Equation (2.11) the reflection coefficient at the back face of the test sample is R_B=-0.84. Here, R_B is negative because there has been a phase change on reflection relative to the incident wave. From Equation (2.12) the transmission coefficient for a sound wave leaving the solid through the front face is T_{F2}=0.16. For normal incidence the echo transmission coefficient as:

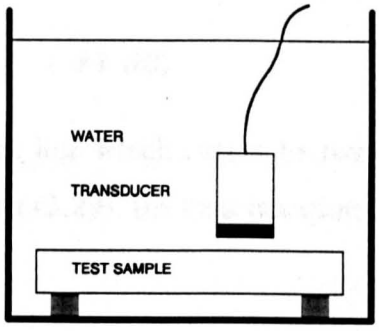

FIGURE 2.8 PULSE ECHO TEST CONFIGURATION

$$E_N = T_F R_B T_{F2} \qquad (2.30)$$

Thus, on inserting the above values the magnitude of E_N is found to be 0.25 (-12 dB). This is a fixed loss which cannot be reduced by altering the design of the test system. From Equation (2.29) the total acoustic insertion loss is:

$$L_N = 0.021 \ (-34 \ dB)$$

As will be seen later when considering air coupling, it is instructive to calculate the ratio of the signal amplitudes from the front and back faces of the test sample. For water coupling the ratio is:

$$R_{FB} = \frac{R_F}{|E_N|} = \frac{0.84}{0.25} = 3.36$$

Now consider what happens if the coupling fluid is changed from water to air. Since Z_1 (test sample) is very much larger than Z (air) it is immediately obvious from Equations (2.11) and (2.12) that, to a very good approximation, R_F=1, T_F=2 and R_B=-1. Also T_B=4.7 x 10^{-5}. From Equation (2.30) the echo transmission coefficient associated with the test sample is:

$$|E_N| = T_F R_B T_{F2} = 9.4 \times 10^{-5} \ \ (-81 \ dB)$$

As was the case with water coupling, this is a fixed loss which cannot be reduced by altering the design of the test system. From Equation (2.29), the total insertion loss for the air coupled pulse-echo configuration is:

$$L_N = 2.3 \times 10^{-9} \ \ (-173 \ dB)$$

With the water coupled system the ratio of the amplitudes of the reflections from the front and back faces of the sample was 3.36 but with air coupling it is much greater:

$$R_{FB} = \frac{R_F}{|E_N|} = 1.1 \times 10^4$$

Comparing the insertion loss figures for air coupling with those obtained for water coupling it can be seen that it would be necessary to improve the system sensitivity by 139 dB (173 dB - 34 dB). Unfortunately, with the pulse-echo technique this is only part of the problem. Because of the massive front face reflection it would be difficult, if not impossible, to design a transducer/pre-amplifier combination which has sufficient dynamic range to allow accurate distance measurements to be made. The main problem associated with designing a suitable receiver front end is saturation of the pre-amplifier, however, a limited transducer operating frequency presents another major problem. Later in this Chapter it will be shown that, because of attenuation in air, the operating

frequency should not be greater than approximately 1.3 MHz. As will be discussed later, although air coupled pulse-echo testing at normal atmospheric pressure is probably impossible with a single transducer, the technique may be useful in a high pressure gas environment.

2.3.3 Through Transmission Analysis

The through transmission technique, which employs two transducers rather than one, offers a way of avoiding the problems associated with the front face echo encountered in the pulse-echo configuration. As illustrated in Figure 2.9, the transducers are placed either side of the test sample and on a common axis. This technique can be analyzed in exactly the same way as with the pulse-echo configuration and as mentioned previously it will be assumed that each transducer has exactly the same properties as the single transducer used in the pitch-catch configuration. This means that, as before, the transmit/receive coupling efficiency of the transducers for water is:

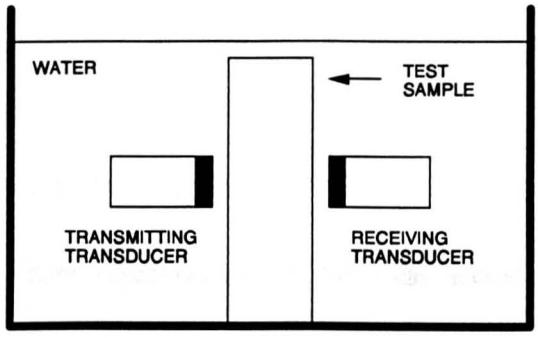

FIGURE 2.9 THROUGH TRANSMISSION CONFIGURATION

$$C_{TR} = 0.084 \quad (-22\ dB)$$

and for air it is:

$$C_{TR} = 2.5 \times 10^{-5} \quad (-92\ dB)$$

For water coupling the relevant reflection and transmission coefficients associated with the test sample are as follows. From Equation (2.12) the transmission coefficient for sound entering the test sample through its front face is $T_F = 1.84$ and the transmission coefficient for sound leaving the test sample at the back face is $T_B = 0.16$. Thus the total coupling loss associated with the test sample is:

$$C_T = 1.84 \times 0.16 = 0.29 \quad (-11\ dB)$$

This is slightly better than for pulse-echo (c.f. E_N=-12 dB) because one internal

reflection (R_B=-0.84) has been avoided. As in the pulse-echo configuration this is an unavoidable loss. From Equation (2.29) the total acoustic insertion loss is:

$$L_T = C_{TR}C_T = 0.084 \times 0.29 = 0.024 \quad (-32\ dB)$$

For air coupling the relevant reflection and transmission coefficients associated with the test sample are as follows. From Equation (2.12) the transmission coefficient for sound entering the test sample through its front face is T_F=2 and the transmission coefficient for sound leaving the test sample at its back face is T_B=4.7 x 10^{-5}. Thus the total coupling loss associated with the test sample is:

$$C_T = 2 \times 4.7 \times 10^{-5} = 9.4 \times 10^{-5} \quad (-81\ dB)$$

As previously this is an unavoidable loss. From Equation (2.29) the total acoustic insertion loss is:

$$L_T = C_{TR}C_T = 2.3 \times 10^{-5} \quad (-173\ dB)$$

Comparing the figures for air coupling with those for water coupling it can be seen that it would be necessary to improve the sensitivity of a through transmission system by 141 dB (173 dB - 32 dB) in order to obtain exactly the same performance from both systems. Here the required improvement factor is slightly greater than with the pulse-echo system but with through transmission there are no problems associated with a large front face echo. The obvious disadvantage with the through transmission technique is that, under most circumstances, it is unsuitable for testing structures which have already been assembled. For example it could not be used for in service inspection of an aircraft wing.

2.3.4 Pitch-Catch Analysis

The pitch-catch inspection technique will now be analyzed. This technique avoids the problems associated with the pulse-echo technique. It also involves using two transducers rather than one but, unlike through transmission, single sided inspection is possible. A basic pitch-catch configuration is illustrated in Figure 2.10. Here, the angle at which both transducers are set is greater than the critical angle for longitudinal waves and less than the critical angle for shear waves. This means that only shear waves are generated and detected in the test sample and no other modes are produced. If the

transducer angles were set below the critical angle for longitudinal waves then both longitudinal waves and shear waves would propagate together in the test sample. This would mean that under typical test conditions two echoes would be obtained from a single defect and it would be almost impossible to interpret the results. Also, the process would be very inefficient since the energy from the transducer would be split between two modes.

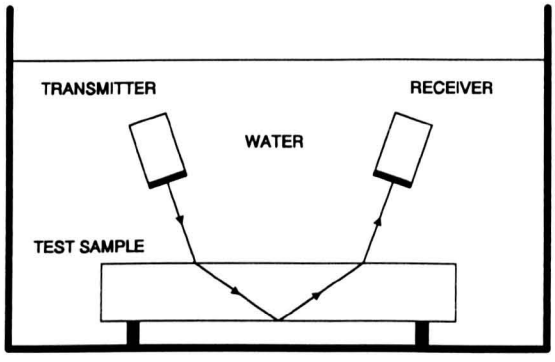

FIGURE 2.10 PITCH-CATCH CONFIGURATION

Transverse wave coefficients for water/aluminium/water boundaries are illustrated in Figures 2.4, 2.5, 2.6 and 2.7. All of the coefficients are plotted as a function of the angle of incidence of the sound wave in the coupling fluid. The data from which the curves were plotted was obtained using the previously mentioned computer program. Results for air/aluminium/air boundaries are illustrated in Figures 2.11, 2.12, 2.13 and 2.14. Data from the two sets of curves will now be used to analyze the pitch-catch configuration illustrated in Figure 2.10. The values for the transducer transmit/receive coupling efficiencies (air and water) are exactly the same as for the previous configurations. From the first set of curves it can be seen that, for water/aluminium/water boundaries, the longitudinal and transverse critical angles are $\theta_{LC}=13.6°$ and $\theta_{TC}=28.3°$ respectively and the peak in the transverse echo transmission curve is $E_T=0.34$ at 16.4°. As with the previous configurations this is a fixed loss. From Equation (2.29) the total insertion loss is:

$$L_{PC} = 0.028 \quad (-31\ dB)$$

From the second set of curves it can be seen that the longitudinal and transverse critical angles are $\theta_{LC}=3°$ and $\theta_{TC}=6.1°$ respectively and the peak in the transverse echo transmission curve is $E_T=1.57 \times 10^{-4}$ at 3.6°. Again, this is a fixed loss and from Equation (2.29) the total insertion loss is:

$$L_{PC} = 3.77 \times 10^{-9} \quad (-168\ dB)$$

Comparing the two sets of results it can be seen that to achieve the same performance with air coupling as with water coupling will require the system sensitivity of the pitch-catch configuration to be improved by 137 dB (168 dB - 31 dB).

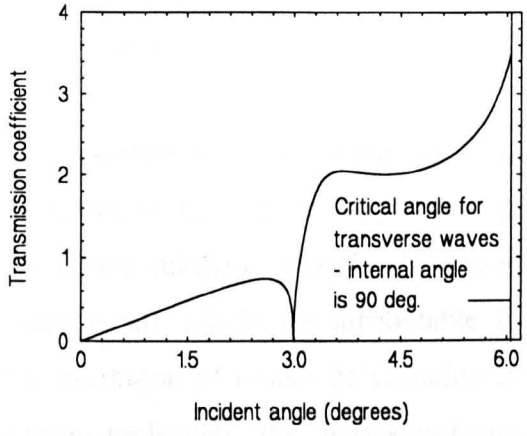

FIGURE 2.11 TRANSMISSION COEFFICIENT (AIR TO ALUMINIUM)

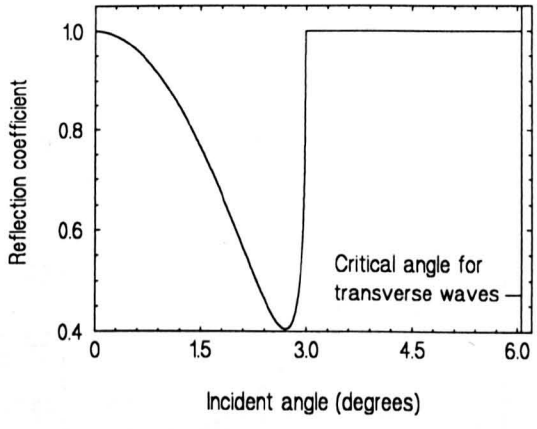

FIGURE 2.12 REFLECTION COEFFICIENT (ALUMINIUM TO ALUMINIUM)

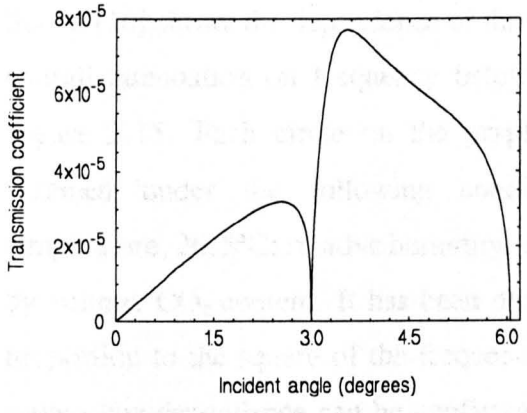

FIGURE 2.13 TRANSMISSION COEFFICIENT (ALUMINIUM TO AIR)

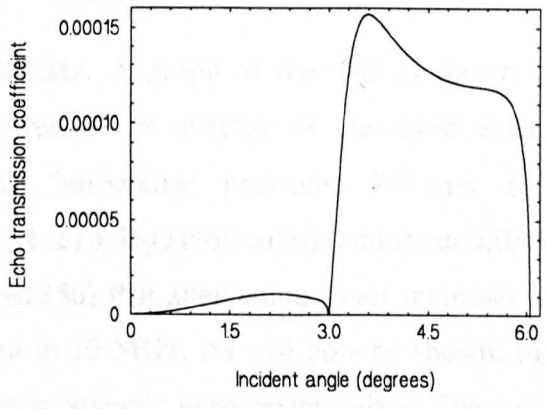

FIGURE 2.14 ECHO TRANSMISSION COEFFICIENT (AIR TO ALUMINIUM TO AIR)

2.4 Attenuation in the Coupling Medium

The previously discussed losses take no account of attenuation in the coupling medium and in the test sample. In solids and liquids the attenuation of sound is mainly due to absorption and for many metallic test samples this will be almost insignificant. For example, at an operating frequency of 1 MHz the absorption coefficient in aluminium is 0.018 dB cm^{-1} and has been shown to be a linear function of frequency out to

10 MHz [56]. In many non-metallic materials (e.g. carbon fibre) absorption will be significant, however, since this loss is always present regardless of whether a system is water coupled or air coupled it will, for now, be ignored in this comparative analysis. Absorption in the coupling fluid cannot be ignored since it depends on the nature of the coupling medium and on the operating frequency of the testing system. Water has an absorption coefficient of 0.0022 dB cm^{-1} at 1 MHz and it has been shown, in measurements extending out to 10 MHz, to increase in proportion to the square of the frequency [56].

The attenuation of ultrasonic waves in air is due to three factors: (1) viscosity, (2) heat conduction and (3) absorption mechanisms which are attributable to the excitation of modes of vibration in certain molecules, the most significant of which are those of water vapour [16]. Experimental data obtained by Sivian [16] shows the dependence of the overall attenuation on frequency below 600 kHz. A graph of the data is shown in Figure 2.15. Each circle on the graph represents an average of measured values obtained under the following conditions: barometric pressure, 760 mm Hg; temperature, 26.5°C; relative humidity, 37% (1.26% H_2O molecules); and about 0.03% by volume CO_2 content. It has been observed [56] that attenuation in air increases in proportion to the square of the frequency out to 10 MHz. As will now be shown, the square law dependence can be confirmed using Sivian's experimental data. The solid line in Figure 2.15 was produced using the following equation:

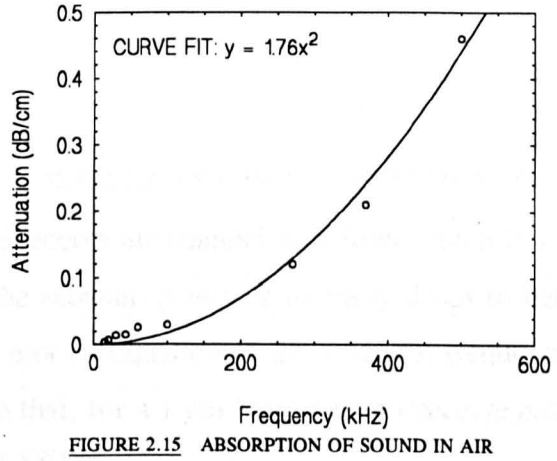

FIGURE 2.15 ABSORPTION OF SOUND IN AIR

$$\alpha = \beta f^2 \tag{2.31}$$

where α is the attenuation coefficient in dB cm^{-1} and f is the frequency in MHz. With β set equal to 1.76 an excellent fit with the data was obtained using the least squares method. This exercise indicates that, at a frequency of 1 MHz, the attenuation coefficient for sound in air is approximately 1.8 dB cm^{-1} which is slightly higher than the value of 1.2 dB cm^{-1} quoted by Wells [56] for the same frequency. However, which

ever value is used, it is clear that at any given frequency the attenuation coefficient for sound in air is much higher than that for sound in water.

It has been shown that the coupling losses in air (168 dB to 173 dB) are much greater than those in water (31 dB to 34 dB). This means that it is essential, when designing a practical air coupled test system, to ensure that losses due to attenuation in the transmit/receive air channel are insignificant compared to the coupling losses at the various boundaries. A useful approach is to think of the transmit/receive air channel as a filter which has a bandwidth defined by the point at which the acoustic power or intensity drops to half (3 dB) of its peak value. Figure 2.16 is a plot of Equation (2.31) over the frequency range 0 to 2 MHz. From this it can be seen that, for a 1 cm long transmit/receive path in air, the bandwidth of the channel is 1.3 MHz.

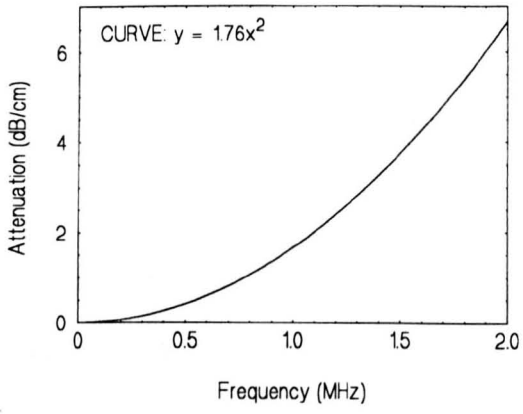

FIGURE 2.16 EXTRAPOLATED ABSORPTION IN AIR

2.5 *Conclusions*

The combined effect of attenuation and the limited bandwidth of the air channel mean that any practical air coupled test system must be designed to operate at frequencies which are at least an order of magnitude less than is usual with water coupled systems. This results in a very significant loss in resolution which, apart from the previously mentioned problems, would make it almost impossible to implement a viable pulse-echo system using a single transducer. The coupling losses associated with each test configuration are summarised in Tables 2.1, 2.2 and 2.3. These values do not take account of attenuation, however, it has been shown that this will not be significant provided that, for example, the total length of the air channel is not greater than 1 cm and the operating frequency of the system is not greater than 1.3 MHz. As will become apparent in Chapter 3, the operating frequency of an air coupled test system will be limited not only by attenuation in the air channel but also by the available transducer technology. A final important aspect is as follows. Here, all of the media involved have

been treated as semi-infinite half spaces. Doing this excludes the possibility of interference between incident and reflected waves. A more comprehensive analysis, which accounts for finite dimensions and hence interference, would involve describing the behaviour of the transducer(s) and the test sample using the concept of complex mechanical impedance. In this way it is possible to predict the effect of resonances both within the transducer(s) and the test sample. These are particularly important when the thickness of either the transducer(s) or the test sample are comparable to the wavelength. In Chapters 4,5,6 and 7, accurate models will be used to account for transducer resonances and in Chapter 8 Lamb wave theory will be used to model test samples which take the form of thin plates. As will become evident later, the transducer coupling losses quoted in Tables 2.1, 2.2 and 2.3 are only meaningful for *non-resonant* transducers (see Appendix II).

TABLE 2.1

SUMMARY OF COUPLING LOSSES IN WATER

	TRANSDUCER (PZT)	SAMPLE (ALUMINIUM)	TOTAL
PULSE-ECHO	-22 dB	-12 dB	-34 dB
THROUGH TRANSMISSION	-22 dB	-11 dB	-33 dB
PITCH-CATCH	-22 dB	-9 dB	-31 dB

TABLE 2.2

SUMMARY OF COUPLING LOSSES IN AIR

	TRANSDUCER (PZT)	SAMPLE (ALUMINIUM)	TOTAL
PULSE-ECHO	-92 dB	-81 dB	-173 dB
THROUGH TRANSMISSION	-92 dB	-81 dB	-173 dB
PITCH-CATCH	-92 dB	-76 dB	-168 dB

TABLE 2.3

COMPARISON OF TOTAL COUPLING LOSSES IN AIR AND WATER

	AIR	WATER	DIFFERENCE
PULSE-ECHO	-173 dB	-34 dB	-139 dB
THROUGH TRANSMISSION	-173 dB	-33 dB	-140 dB
PITCH-CATCH	-168 dB	-31 dB	-137 dB

Chapter 3

PIEZOELECTRIC TRANSDUCER TECHNOLOGY

3.1 Introduction

As mentioned at the start of this PhD Thesis, the feasibility of air coupled ultrasonic testing was first reported by Luukkala *et al.* [12,13] in the early 1970's. The transducers used in this work were of the capacitive type, consisting of a gold coated Melinex membrane stretched over a roughened rectangular back plate. Since then, new types of air coupled capacitive and electrostatic transducers have been developed. Examples [42 to 46] of each new type were discussed in Chapter 1. For many different air coupled applications including the non-destructive testing which is of interest here, electrostatic devices have been used in preference to the conventional piezoceramic plates which were discussed in Chapter 2. The main justification for using these devices is based on claims that they all provide a better acoustic impedance match with air, however, a recent comparative evaluation of different air coupled transducer technologies performed at the University of Strathclyde [57], indicates that the actual performance of many electrostatic devices may not be as good as the claims suggest. In fact, this evaluation [57] indicates that a new generation of piezocomposite plate transducers can provide better air coupled sensitivity than many of the electrostatic designs which are currently available. It is claimed that, relative to the electrostatic devices which were used in the Strathclyde tests, each new piezocomposite transducer can provide an improvement in air coupled sensitivity of at least 20 dB when used with a new type of matching layer [58] which has also been developed at Strathclyde. In addition to their impressive air coupled sensitivity these new piezocomposite transducers provide a consistent level of performance which is independent of environmental conditions and aging. They have also proved to be highly reliable, robust and easy to manufacture to a consistent specification. These features make air coupled piezocomposite transducers particularly attractive for use in a variety of industrial and high pressure environments. As discussed in Chapter 1, one of the main goals of the EPSRC funded *Ultrasonic Testing Without Coupling Fluids* project was to demonstrate that the new air coupled piezocomposite transducers could be used to construct a practical air coupled scanner capable of producing *real-time* images of defects in a wide range of materials. However, the present Chapter is not concerned specifically with piezocomposite transducers but rather provides a comprehensive review of all of the ways in which piezoelectric technology might be used to construct transducers which are suitable for air coupled testing applications. The review concludes that, in the near

term, piezocomposites provide the most effective method of constructing air coupled transducers using piezoelectric materials. However, it is proposed that the availability of micromachining techniques could provide a way of, for example, constructing an array of miniature bimorph elements which would be made to vibrate in phase at frequencies suitable for air coupled testing. This is one of the many interesting possibilities which is discussed in this Chapter.

A practical demonstration of the use of piezoelectric transducers for air coupled testing was reported by Rogovsky in 1991 [14]. Rogovsky found that, in order to be able to use piezoceramic plate transducers for air coupled inspection, it was necessary to provide both of the transducers with acoustic matching layers. He also found that it was necessary to use a *high intensity* tone burst and a sophisticated signal processing system manufactured by TestPro [14]. Even with the aid of signal processing, Rogovsky found that his system could only be used to inspect certain materials which have a low acoustic impedance resulting in a low level of acoustic coupling loss. In order to construct a truly practical air coupled test system using piezoceramic transducers it is necessary to improve the system sensitivity while maintaining an adequate system bandwidth and a good directivity pattern. For a given transducer bandwidth, there are three possible ways in which receiver sensitivity can be improved. These are:

- Reduce the acoustic impedance of the piezoceramic transducer to provide improved coupling into air. This is by far the most effective option and is the one with which the present Chapter is concerned. If a reduction in system bandwidth is acceptable then increasing the mechanical quality factor of the transducer has a similar effect.

- Improve the transducers electromechanical coupling efficiency. Here, there is very little room for improvement since it is relatively easy to achieve a conversion efficiency of better than 50% with standard piezoelectric plates.

- Reduce the electronic noise generated in the receiving system. In Chapters 4,5, and 6 it will be shown that it is impossible to reduce transducer noise, however, as will be discussed in Chapter 7 it is possible to reduce pre-amplifier noise.

3.2 Theory of Piezoelectric Materials

Certain crystalline solids become electrically polarized when they are elastically strained and this is known as the direct piezoelectric effect. These same solids become strained when exposed to an external electric field applied in certain directions and this is known as the converse piezoelectric effect. The first practical use of the piezoelectric effect was in a sonar system developed during World War I. Since then the technology has developed to a state where piezoelectric devices can be found in anything from gas lighters to print heads in ink jet printers and servo mechanisms for fine tracking of the heads in video recorders. There are many less obvious applications such as SAW (surface acoustic wave) devices which have been used widely in military electronic systems and which now appear in domestic electronic systems such as televisions. As a consequence of commercial exploitation, piezoelectric materials research and development has been extensive and there is now a wide range of materials to choose from. Also, the mature nature of the technology has ensured that the theory of piezoelectric materials is well understood and documented. In the context of this PhD Thesis, it is the ability of piezoceramic devices to generate high frequency (up to about 1.3 MHz) sound waves that is of interest.

3.2.1 Piezoelectric Crystals

Piezoelectricity is a property which is possible only for ionic solids which crystallize in structures lacking a centre of inversion. Of the 32 point groups which can be envisaged in three dimensions, 21 lack a centre of inversion symmetry. One of these has so high a degree of symmetry in other respects that piezoelectricity is excluded, which leaves 20 types of point group symmetry which are compatible with piezoelectric behaviour. Only for a relatively small fraction of the solids utilizing these 20 point groups is the piezoelectric effect large enough to be measurable. To a first approximation, the deformation of a piezoelectric solid is linear in the applied electric field and the polarization induced by stress is proportional to the strain achieved. For any ionic solid, piezoelectric or not, there is a much smaller contraction in an applied electric field, which varies as the square of the field. This more universal phenomenon of electrostriction arises from the failure of Hook's law to describe the changes of inter-ionic distances with the applied electric field.

3.2.2 *The Constitutive Equations*

The piezoelectric constitutive equations are as follows. For the direct effect:

$$D = dX + \varepsilon^X E \tag{3.1}$$

and for the converse effect:

$$x = s^E X + dE \tag{3.2}$$

There are other forms of the constitutive equations but these are the most appropriate versions for the moment. The terms that appear in these equations are as follows:

E	Electric field
D	Dielectric displacement
X	Stress - force per unit area
x	Strain - change in length per unit length
d	Piezoelectric coefficient
s	Compliance of the material - strain per unit stress
ε	Material permittivity

The superscript X in Equation (3.1) indicates that the material permittivity value used is that for a condition of constant stress. The superscript E in Equation (3.2) indicates that the value of material compliance used is that for a condition of constant electric field. The properties of crystalline materials are different in different directions i.e. they are anisotropic. A convenient way of representing each array of values for d, s and ε is to use tensor notation. Many references on piezoelectric materials show the constitutive equations written using conventional tensor notation or a modified version of tensor notation which has a less cluttered appearance. As will be mentioned again later, a compact matrix notation can also be used. Not all of the tensor components are independent. Between Equations (3.1) and (3.2) there are 45 independent tensor components as follows:

Elastic compliances (s^E):	21
Permittivity (ε^X):	6
Piezoelectric coefficients:	18

Crystal symmetry and the choice of reference axes reduce this number further.

3.2.3 *Piezoceramics*

Polycrystalline materials in which the crystal axes of the grains are randomly orientated all behave electrostrictively irrespective of the structural class of the constituent crystallites. If the crystals belong to a piezoelectric class and their crystal axes can be suitably aligned, then a piezoelectric polycrystalline ceramic becomes possible. A polar direction can be developed in a ferroelectric ceramic by applying a static field; the process is known as poling. The remainder of this discussion is restricted to poled polycrystalline ceramics, which have ∞-fold symmetry in a plane perpendicular to the poling direction. The symmetry of a poled ceramic is therefore described as ∞mm and this is equivalent to 6mm in the hexagonal symmetry system. Taking note of the anisotropic nature of the properties of piezoelectric materials, the linear constitutive equations can be written in compact matrix notation [59] and the coefficients can then be written as:

$$[s^E] = \begin{bmatrix} s_{11} & s_{12} & s_{13} & 0 & 0 & 0 \\ s_{12} & s_{11} & s_{13} & 0 & 0 & 0 \\ s_{13} & s_{13} & s_{33} & 0 & 0 & 0 \\ 0 & 0 & 0 & s_{44} & 0 & 0 \\ 0 & 0 & 0 & 0 & s_{44} & 0 \\ 0 & 0 & 0 & 0 & 0 & (s_{11}-s_{12})/2 \end{bmatrix} \tag{3.3}$$

$$[d^E] = \begin{bmatrix} 0 & 0 & d_{31} \\ 0 & 0 & d_{31} \\ 0 & 0 & d_{33} \\ 0 & d_{15} & 0 \\ d_{15} & 0 & 0 \\ 0 & 0 & 0 \end{bmatrix} \tag{3.4}$$

$$[\varepsilon^X] = \begin{bmatrix} \varepsilon_{11} & 0 & 0 \\ 0 & \varepsilon_{11} & 0 \\ 0 & 0 & \varepsilon_{33} \end{bmatrix} \tag{3.5}$$

The physical significance of the subscript notation can be understood by referring to Figure 3.1. Here, the convention is to refer to the poling direction in the material as the 3 axis. The shear planes are indicated by the subscripts 4, 5 and 6 and are perpendicular to the directions 1, 2 and 3 respectively. In Equation (3.4) the coefficient d_{31} relates the field E_3 along the polar axis to the strain perpendicular to it and the coefficient d_{33} relates the field E_3 along the polar axis to the parallel strain. Shear can only occur when a field is applied at right angles to the polar axis so there is only one coefficient, d_{15}. Using Equations (3.4) and (3.5), Equation (3.1) can be expanded into the a set of three equations for the direct effect. Using Equations (3.3) and (3.5), Equation (3.2) for the converse effect can be expanded into a set of 5 equations. Following Hook's law and using Equation (3.3), it is possible to obtain a set of 6 equations relating the material strains to the material stresses in terms of the compliances. In all of these piezoelectric equations each of the compliances s_{ij} can have one of two possible values corresponding to either short-circuit or open-circuit conditions depending on the application. It is common practice to indicate the short-circuit and open-circuit compliances using the superscripts E and D respectively. Converting the various short-circuit compliance values to the corresponding open-circuit values and vice versa is a straightforward matter [59]. An alternative to expressing the elastic behaviour of a piezoelectric material in terms of the compliances or elastic constants s_{ij} is to use the stiffness constants c_{ij}. Stiffness is expressed as stress per unit strain. As with the compliance coefficients each of the stiffness coefficients c_{ij} can have one of two possible values corresponding to either short-circuit or open circuit conditions i.e. the stiffness coefficients can also have either a D or an E superscript. Equations are available which allow conversion from the compliance coefficients to the stiffness coefficients and vice versa [59]. The coefficients d_{ij} are the most commonly quoted for piezoelectric ceramics, however, the coefficients e_{ij}, h_{ij} and g_{ij} are also important. For example the electrical response due to the direct effect can be expressed in terms of strain (x) by:

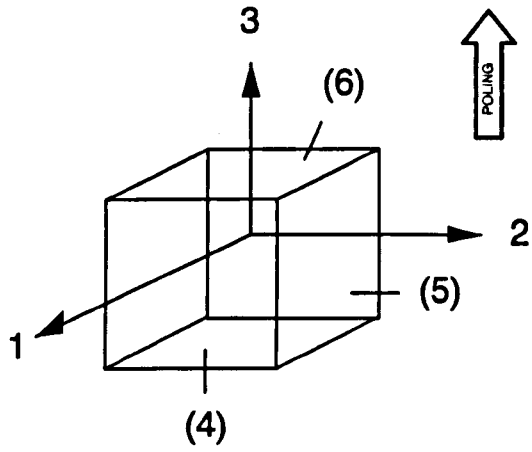

FIGURE 3.1 LABELLING OF REFERENCE AXES AND PLANES FOR PIEZOCERAMICS

$$D = eX \tag{3.6}$$

or:

$$E = hc \tag{3.7}$$

The converse effect can be represented by:

$$x = gD \tag{3.8}$$

or:

$$x = dE \tag{3.9}$$

Converting between the different types of piezoelectric coefficients is not difficult [59]. It should be noted that both ε^X and ε^x may appear in the various equations and should not be confused. These are the clamped and free permittivities respectively. Another set of important terms are denoted k_{jk} and are known as the electromechanical coupling coefficients. Each coupling coefficient is a measure of the efficiency of a device when converting electrical energy into a particular mode of vibration and vice versa.

3.2.4 Piezoceramic Materials

Piezoceramic compositions have been developed for a variety of applications including the generation of high voltages, the generation of acoustic/ultrasonic vibrations, the control of frequency in electronic circuits and for mechanical actuators. Some of the most common piezoceramics in current use are listed in Table 3.1. The properties of these materials are well documented and will not be discussed in detail in this PhD Thesis. Barium titanate was the first material to be developed as a piezoceramic and was used on a wide scale for the generation and detection of acoustic/ultrasonic vibrations. For most commercial purposes it has been superseded by PZT. The structure of all of the materials in Table 3.1 can be tailored to suit particular applications. Also, the properties of some of these materials can be modified by the addition of various dopants. In this PhD Thesis frequent reference is made to PZT-5A and PZT-5H. Comprehensive data for $BaTiO_3$, PZT-5A, PZT-5H, PZT-7A and PZT-8 can be found in Appendix I.

TABLE 3.1

SOME COMMON PIEZOCERAMIC MATERIALS

Barium titanate	$BaTiO_3$
Lead zirconate	$PbZrO_3$
Lead titanate	$PbTiO_3$
Lead niobate	$PbNb_2O_6$
Lithium niobate	$LiNbO_3$
Lithium tantalate	$LiTaO_3$
PZT	$Pb(Ti,Zr)_3$

3.3 Piezoceramic Transducers

3.3.1 The Ideal Piezoceramic Transducer

In order to design an ultrasonic transducer capable of operating efficiently in air it is necessary for it to have the highest possible electromechanical coupling efficiency and the lowest possible value of characteristic acoustic impedance. The transducer should be capable of producing the largest possible displacement at the surface which forms the transducer/air interface and all parts of this surface should move in phase. Under most circumstances surface displacement should be uniform across the entire front face of the transducer.

3.3.2 Available Stress and Strain

Some of the problems associated with using solid piezoceramic plates as ultrasonic transducers can be understood by performing a simple static analysis. Consider a uniform rectangular plate of piezoceramic material as illustrated in Figure 3.2. Here, the plate dimensions are

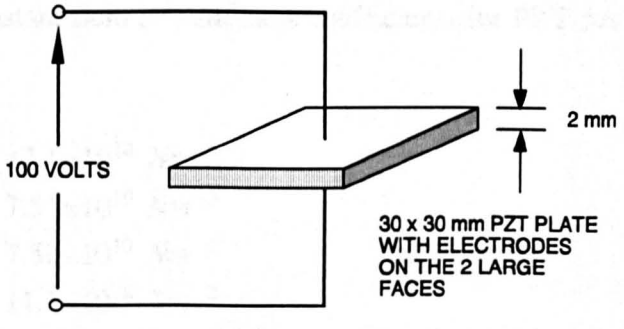

FIGURE 3.2 100 VOLTS APPLIED TO PZT-5A PLATE

30 x 30 x 2 mm and electrodes have been placed over the two 30 x 30 mm faces. It will be assumed that the sample is poled in a direction perpendicular to these faces. From Appendix I, the values of the piezoelectric coefficients for PZT-5A are:

$$\begin{aligned} d_{31} &= -171\times10^{-12}\ CN^{-1} \\ d_{33} &= +374\times10^{-12}\ CN^{-1} \\ d_{15} &= +584\times10^{-12}\ CN^{-1} \end{aligned}$$

If we want to find the various strains in the sample when a voltage is applied across the electroded faces then the piezoelectric coefficients of interest are d_{33} and d_{31} since a field is being applied parallel to the direction of poling (i.e. the 3 axis). Now, if the applied voltage is, for example, 100 volts then the applied electric field is E=50 V/m. Using Equation (3.9), the changes in length in each direction are:

$$\begin{aligned} \delta L_3 &= d_{33}\cdot L_3\cdot E = +0.037\mu m \\ \delta L_2 &= d_{31}\cdot L_2\cdot E = -0.257\mu m \\ \delta L_1 &= d_{31}\cdot L_1\cdot E = -0.257\mu m \end{aligned}$$

The dimensionless changes in length per unit length, i.e. the strains, are:

$$\begin{aligned} x_3 &= \delta L_3/L_3 = +1.87\times10^{-5} \\ x_2 &= \delta L_2/L_2 = -8.55\times10^{-6} \\ x_1 &= \delta L_1/L_1 = -8.55\times10^{-6} \end{aligned}$$

The force per unit area, i.e. the stress, in each direction in the sample can be found using the following equations [59]:

$$\begin{aligned} X_3 &= c_{13}\cdot x_1 + c_{13}\cdot x_2 + c_{33}\cdot x_3 \\ X_2 &= c_{12}\cdot x_1 + c_{11}\cdot x_2 + c_{13}\cdot x_3 \\ X_1 &= c_{11}\cdot x_1 + c_{12}\cdot x_2 + c_{13}\cdot x_3 \end{aligned}$$

From Appendix I, the values of the constant field (c^E) stiffness coefficients for PZT-5A are:

$$\begin{aligned} c_{11} &= 12.1\times10^{10}\ Nm^{-2} \\ c_{12} &= 7.51\times10^{10}\ Nm^{-2} \\ c_{13} &= 7.52\times10^{10}\ Nm^{-2} \\ c_{33} &= 11.1\times10^{10}\ Nm^{-2} \end{aligned}$$

Using these values the stress in each direction is found to be:

$$X_3 = 7.9\times10^5\ Nm^{-2}$$
$$X_2 = 2.7\times10^5\ Nm^{-2}$$
$$X_1 = 2.7\times10^5\ Nm^{-2}$$

The corresponding force in each direction is:

$$F_3 = X_3 \cdot L_1 \cdot L_2 = 710.8\ N$$
$$F_2 = X_2 \cdot L_2 \cdot L_3 = 16.23\ N$$
$$F_1 = X_1 \cdot L_1 \cdot L_3 = 16.23\ N$$

From the above figures it can be seen that the displacement of the front face of the plate relative to the back face is only 0.037 μm. For the moment this is the only relevant displacement but later it will be shown that it is possible to make use of the larger displacements which take place along the two perpendicular axes. In this example the applied field was 50 V/mm. For materials such as PZT the maximum field that can be applied is between 1 kV/mm and 2 kV/mm. Clearly it would be possible to obtain a larger displacement by applying a higher voltage but in most applications very high voltages are undesirable. Another way to achieve a larger displacement along the 3 axis would be to increase the value of L_3 but this is not consistent with the requirement for resonant operation at ultrasonic frequencies close to 1 MHz. Although the material strains are small the stresses are very large and consequently there is considerable potential for devising a transducer which is capable of converting these very large values of stress into large values of strain in an appropriate direction. A large number of piezoceramic transducer designs have been proposed in an attempt to do this and many of these are discussed here.

3.3.3 Plate Transducers

In Chapter 2 it was shown that coupling losses of -22 dB and -92 dB are encountered when a pair of typical piezoceramic plates are used as ultrasonic transducers in water and air respectively. As will be discussed in Chapter 7, these losses can be greatly reduced by operating the transducers at resonance. For high power applications such as ultrasonic cleaning and sonar, it is relatively easy to manufacture resonant discs for operation in the frequency range 20 kHz to 100 kHz. The thickness of the disc is a half wavelength, which for 100 kHz would be approximately 15 mm. Much thinner devices which operate at higher frequencies are commonly used in liquid coupled non-

destructive testing (NDT) systems. This type of device, with an electromechanical coupling coefficient which may exceed 50%, provides a very efficient method of converting electrical energy into mechanical energy and vice versa. However, even when operated at resonance, the simple piezoceramic plate transducer fails to provide the sensitivity which is required for air coupled testing. Although piezoceramics provide poor air coupling, the simple disc structure is very attractive for the NDT applications under consideration. The main advantage is that, unlike some of the structures which are discussed later, discs can provide relatively good directivity.

3.4 Composite Transducers

An enormous variety of ultrasonic transducer designs are based on the concept of combining piezoceramic and passive elements in a composite structure. Here, it will only be possible to look at a few of the most interesting ideas. Many of these designs have been known about for a long time but currently there is a renewed interest brought about by the availability of new materials and sophisticated modelling techniques such as the finite element method which can now be implemented using relatively inexpensive computer systems.

3.4.1 Bimorphs

It has been shown that piezoceramics have high Young's moduli so that large forces are required to generate strains that produce easily measured electrical responses from solid blocks of material. For the same reason it is possible to produce large forces by generating high electric fields within a block of material. Compliance can be greatly increased by making long thin strips or plates of material and mounting them as cantilevers or diaphragms. Bending of a plate causes one half to stretch and the other half to compress so that, to a first approximation, there can be no electrical output from a homogeneous body by bending. Also, there can be no bending of a homogeneous plate by generating an electric field in the plate. This is

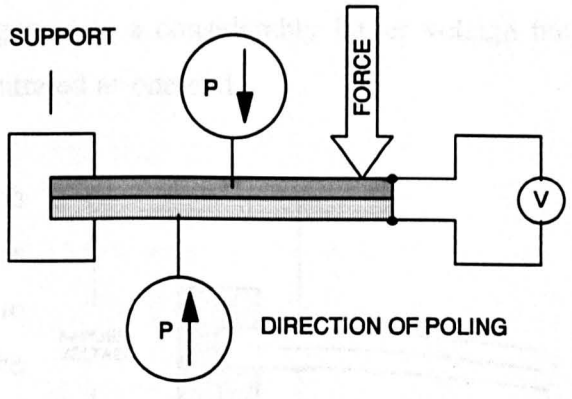

FIGURE 3.3 A FORCE APPLIED TO A CANTILEVER BIMORPH PRODUCES A VOLTAGE

overcome in the bimorph by making the two halves of separate beams with an intervening electrode as well as electrodes on the outer surfaces. If, as illustrated in Figure 3.3, the beams are poled from the outer electrodes towards the centre, the resulting polarities will be in opposite directions and the voltages generated on the outer electrodes will be additive. Alternatively, if the beams are poled in the same direction, output from bending can be obtained between the outer electrodes, connected together, and the centre electrode. It can be shown that the voltage generated between the outer electrodes of a bimorph under stress is [59]:

$$V = \frac{3}{8}\left[\frac{H}{L}\right]^2 h_{31}\delta z \qquad (3.10)$$

where, h_{31} is the piezoelectric charge constant, H is the thickness of the bimorph, L is the length and δz is the deflection at the free end. Consider a cantilever bimorph which is made from PZT-5A and which has dimensions which are similar to those of the simple plate considered earlier. From Appendix I, h_{31} = -7.3 x 10^8 V/m. Using Equation (3.10) it can be shown that for L = 30 mm, H = 2 mm and δz = 1 x 10^{-9} m, the potential difference between the outer electrodes is 62 volts. It is interesting to compare this with the voltage that would be generated by the previously considered plate for a 1 x 10^{-9} m displacement in the thickness direction. From Appendix I, h_{33} = 21.5 x 10^8 V/m hence the voltage generated between the two large faces of the plate is 2.2 volts. Clearly the bimorph generates a considerably larger voltage but, unlike the plate, the force must be concentrated at one end.

Although, by the converse effect, a bimorph will bend (see Figure 3.4) when a voltage is applied to it, this will not be according to the inverse of Equation (3.10) because the deformation due to an applied field is governed by a different piezoelectric constant d_{ij} which is not the inverse of h_{ij}. Furthermore, the applied field will produce uniform strains along the length of the bimorph so that it will bend in the form of a circular arc. This is not the case for a

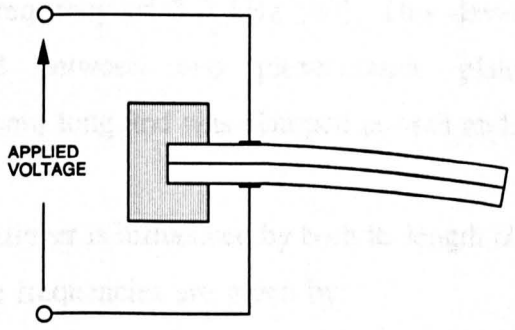

FIGURE 3.4 FREE END OF CANTILEVER BIMORPH IS DEFLECTED WHEN VOLTAGE IS APPLIED

cantilever beam clamped at one end, as was considered previously for a bimorph used to generate a voltage. Deriving an equation which describes how a bimorph will bend when a voltage is applied is in fact very simple and the analysis is similar to that for a bimetallic strip which bends when heated. The result is [59]:

$$\delta z = \frac{3}{2}\left[\frac{L}{H}\right]^2 d_{31} V \qquad (3.11)$$

Consider again a bimorph made from PZT-5A with L = 30 mm and H = 2 mm. From Appendix I, d_{33} = -171 x 10^{-12} C/N. For a potential difference of 100 volts, Equation (3.11) indicates that the free end of the bimorph will be deflected by 5.8 μm. By comparison, the magnitude of the change in thickness (δL_3) of the previously considered plate was 0.037 μm, however, the length and width changed by 0.257 μm. Clearly the cantilever bimorph can produce a considerably greater (5.8/0.037=157) displacement than the plate but only at its free end. Obviously there are limits to how much mechanical movement can be achieved with a simple structure such as a bimorph. If the aspect ratio (length/thickness) becomes too large then the structure will become too fragile to be of any use and it will be unable to exert any useful force. Also, as mentioned previously, the maximum field that can be generated in a slice of piezoelectric material such as PZT is between 1 kV/mm and 2 kV/mm.

Optical beam deflectors provide a good example of how piezoelectric bimorphs can be used to produce high frequency vibrations. For example, in 1990 a researcher at the Toshiba Research and Development Centre reported a device which could produce a 20 x 10^{-3} radian deflection at a resonant frequency of 3.0 kHz [60]. This device consisted of a brass plate sandwiched between two piezoceramic plates (d_{31}=-196 x 10^{-12} m/V). The device was 11 mm long and was clamped at both ends.

The mechanical resonance frequency of a cantilever is influenced by both its length (L) and its thickness (H). The possible resonance frequencies are given by:

$$f_i = \left(\frac{Y}{12\rho}\right)^{1/2} \frac{H}{L^2} M_i^2 \qquad (3.12)$$

where Y is Young's modulus and ρ is the density of the material from which the cantilever is constructed. The coefficients M_i (M_1=1.875, M_2=4.694, M_3=7.855)

correspond to the vibrational modes. Clearly the frequency of the fundamental mode (one node) can be found by using M_1 in Equation (3.12). For PZT-5A piezoceramic with ρ=7750 kg/m^3 and Y=11.1 x 10^{10} N/m^2, the fundamental frequency of the previously considered bimorph (L=30 mm and H=2 mm) is 8.54 kHz. From this calculation it can be seen that, in order to fabricate a device capable of working at ultrasonic frequencies, it would be necessary to significantly scale down the dimensions. For example, if the aspect ratio is kept the same and the dimensions are reduced by a factor of 100 then L=300 μm and H=20 μm. For these dimensions Equation (3.12) indicates that the fundamental resonance would be at a frequency of 854 kHz.

Although a bimorph offers an attractive way of producing a piezoceramic transducer with reduced stiffness, the preceding analysis indicates that it would be difficult to produce a device suitable for operation at sufficiently high frequencies. Also, because a bimorph does not produce a uniform displacement across its surface, it is not possible to fabricate a source of ultrasound with a good directivity pattern using a single device. In order to produce a high frequency source with a good directivity pattern using the bimorph concept it would be necessary to construct quite complex piezoceramic structures on a very small scale and then arrange these devices in the form of a large two dimensional array. For best performance each bimorph element would be operated at its resonance frequency. A possible configuration is illustrated in Figure 3.5. Building an ultrasonic transducer of this type would involve using micromachining technology similar to that used for constructing small silicon components.

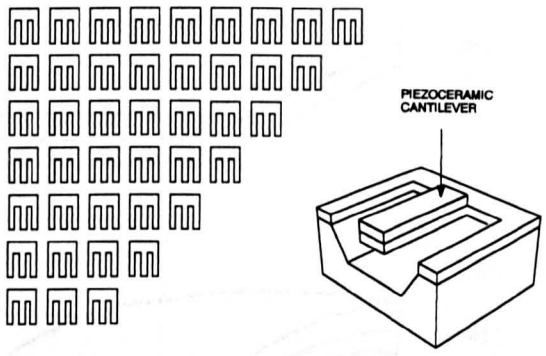

FIGURE 3.5 POSSIBLE CONFIGURATION FOR AN ULTRASONIC TRANSDUCER CONSISTING OF AN ARRAY OF CANTILEVER BIMORPHS

In order to get some idea of the problems involved in fabricating a bimorph array suitable for operation at frequencies between about 100 kHz and 1 MHz it is worth looking at what can currently be achieved using micromachining techniques. Currently there are a number of techniques available for the fabrication of metallic

microstructures. These include photoresist and stencil based technologies, and photoelectroforming technologies [61]. In 1994 Hoffmann *et al.* reported the fabrication of micromechanical cantilever resonators with integrated optical interrogation [62]. Although this work does not involve the use of piezoceramic materials it is of considerable interest because of the operating frequencies involved. The research involved constructing a cantilever resonator using a $SiO_2/SiON/SiO_2$ sandwich which also acted as an optical waveguide. By transmitting light across a 2 μm gap from the free end of the cantilever to the end of a fixed wave guide, it was possible to produce a vibration detector capable of operating in the 80 kHz to 120 kHz frequency range. The corresponding cantilever lengths are in the range 170 μm to 140 μm.

Earlier, the cantilever bimorph was used as an example to indicate the advantages that can be gained by constructing devices with reduced stiffness. As shown in Figure 3.6, plate and disc bimorph structures are also possible. These devices bend in two directions and are the more common choice for high frequency sound generation. Unfortunately, the possible modes of vibration are not easy to predict and it is difficult to arrange that all parts of the emitting surface move in phase. Phase differences across the emitting surface result in reduced efficiency and poor directivity. A good example of how this type of device can be used to produce high audio frequency sound is the high fidelity *tweeter*. Here, the active element is a lightly supported circular bimorph. An alternating voltage causes the disc to flex which, in turn, drives a light-weight cone. This type of device has a frequency response which is almost flat from about 4 kHz to 30 kHz [59].

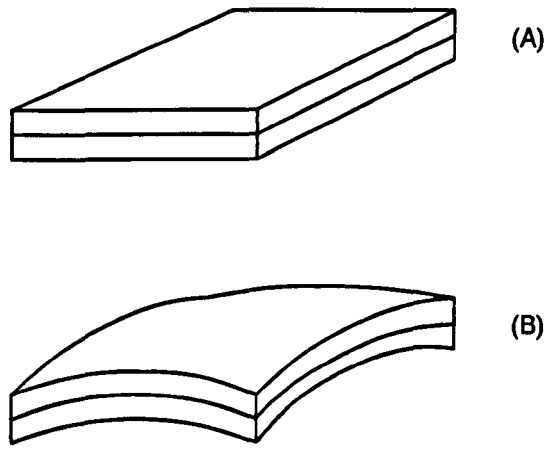

FIGURE 3.6 PLATE BIMORPH (A) BEFORE AND (B) AFTER VOLTAGE IS APPLIED

A transducer which is similar to the previously mentioned disc bimorph can be made by bonding a single disc of piezoceramic material to a metal plate or diaphragm. This

type of device is sometimes referred to as unimorph. Here, the bending depends on the relative lateral expansion between the piezoceramic plate and the metal plate. For this type of transducer the frequency of operation is directly proportional to the plate thickness and inversely proportional to the square of its diameter [63,64]. A transducer which will resonate at about 30 kHz can be made by bonding a 1 mm thick, 10 mm diameter piezoceramic disc to a 1 mm thick, 15 mm diameter aluminium diaphragm.

3.4.2 Radiating Membranes

One of the most interesting radiating membrane designs was reported by Babic [65] in 1991. A significant feature of this device, which is illustrated in Figure 3.7, is that it is capable of operating at frequencies close to 200 kHz. The device consists of an axially symmetric aluminium housing and an axially polarized piezoceramic disc. The housing has the form of a hollow cylinder, closed at one end, with an inner diameter of 10 mm and an outer diameter of 12 mm. The overall length of the housing depends on the thickness of the front closing plate (membrane) and is typically 5 mm. The piezoceramic disc has a diameter of 10 mm and a thickness of 1 mm. It is bonded to the inner wall of the housing with Araldite bonding epoxy. The piezoceramic disc is driven by an external electric source and radial vibrations of the disc are converted into transverse vibrations of the front membrane. This device has been analyzed in considerable detail using the finite element method. At the time of publication, several transducers had been fabricated using ordinary aluminium and PZT-5A piezoceramic discs. The input electrical admittance of each device was measured with a standard HP 4195A impedance analyzer. Series resonant frequencies obtained from the admittance plots showed good agreement with theory. A major problem with the basic device is that it exhibits a very inconvenient directivity characteristic with strong side lobes. The poor performance of the basic device is due to parts of the membrane moving in counter phase to one another. According to Babic, *a remarkable improvement in performance* can be achieved by bonding a disc made from an acrylic plastic to the middle of the membrane. The thickness of the acrylic disc equals half the

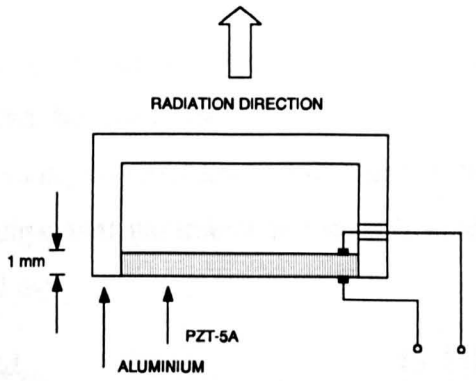

FIGURE 3.7 RADIATING MEMBRANE TRANSDUCER

wavelength of the radiated ultrasound and the diameter corresponds to the nodal circle diameter. The plastic disc causes all particles of the air near the membrane to vibrate in phase. The directivity pattern of the modified device, as measured with a Bruel & Kjaer 4138 microphone, indicates that the main lobe has a -3 dB beamwidth of 12°. Compared to the unmodified device, the acrylic disc had the effect of suppressing the side lobes by -12 dB. However, the poor beamwidths available from these devices makes them unlikely candidates for air coupled testing.

3.4.3 Ceramic-Metal Composites

This type of transducer has been developed mainly for use as a hydrophone. A good example of what can be achieved was reported by Xu *et al.* [66] in 1991. The importance of the piezoceramic coefficients d_{33} and d_{31} was explained at the start of this Chapter. For hydrophone applications another important parameter is the hydrostatic piezoelectric charge coefficient which is defined as:

$$d_h = d_{33} + 2d_{31} \tag{3.13}$$

From some of the previous examples it is clear that PZT ceramics have high values of both d_{33} and d_{31}. However, because these coefficients have opposite signs, the value of d_h may be quite low. For example, for PZT-5A, d_h=357-2 x 171 = 32 pC/N. In order to enhance the value of d_h, Yoshikawa *et al.* have developed a PZT/metal composite with, as illustrated in Figure 3.8, very shallow cavities between the PZT ceramic and the thick metal electrodes. The effect of this is to convert a portion of the z-direction stress into large radial stresses of opposite signs. As a result the d_{33} and d_{31} contributions to d_h are caused to add rather than subtract leading to a high d_h. A theoretical analysis of the PZT/ brass composite transducer was performed using the

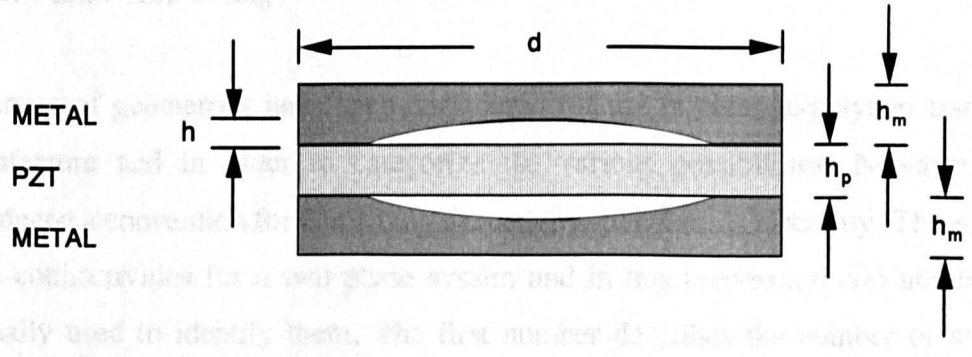

FIGURE 3.8 CERAMIC-METAL COMPOSITE TRANSDUCER

ANSYS finite element program and it was shown that the lowest vibrational mode of the transducer is a flextensional mode. This flextensional mode determines the operating frequency of the device and is controlled by the cavity diameter d_c, the height of the cavity h, the thickness of the metal h_m and the stiffness of the ceramic in the planar mode. Devices were constructed with overall diameter d = 11 mm, metal thickness h_m =1.2 mm, ceramic thickness h_p = 1.1 mm and cavity height h = 100 - 150 μm. Four versions were evaluated with cavity diameters (d_c) of 7.6 mm, 5.8 mm, 4.1 mm and 2.5 mm. Constructing these devices involved using a silver paste which was fired at 600°C for 10 min. After an intermediate process the device was then poled in oil at 150°C with a 2.5 kV electric field for about 15 min. Experiments performed with these devices indicated that a large cavity size results in large values of d_h and g_h. Conductance measurements performed in both air and water indicated that the lowest flextensional mode was close to 30 kHz.

3.4.4 Ceramic-Polymer Composites

Ceramic-polymer composites were initially developed for use in low frequency hydrophones. As explained previously, the hydrostatic charge coefficient, d_h, for a solid piezoceramic sample can be very low because d_{33} and d_{31} have opposite signs. The original aim of fabricating a hydrophone from a ceramic-polymer composite was to decouple laterally applied energy from the ceramic by embedding it in a soft polymer matrix. Transducers made from ceramic-polymer composites are now used in a wide variety of applications including medical ultrasonic imaging where the devices used have been designed to have a close impedance match with human tissue. It is the possibility of obtaining a substantially reduced characteristic impedance without sacrificing electromechanical coupling efficiency which is of special interest for air coupled ultrasonic testing.

A variety of geometries have been considered for use in ceramic-polymer transducer manufacture and in order to categorize the various possibilities, Newman *et al.* introduced a convention for describing the ceramic-polymer connectivity. There are ten basic connectivities for a two phase system and in this convention two numbers are normally used to identify them. The first number describes the number of mutually perpendicular directions in which the ceramic phase is continuous and the second

number describes the number of directions in which the polymer phase is continuous. Four examples are as follows. Devices based on the 3-1 structure can be fabricated by drilling holes in solid piezoceramic plates and then filling them with polymer. Transducers based on the 2-2 structure can be formed by laminating alternate plates of PZT and polymer side by side. The 0-3 structure involves mixing a piezoceramic powder in a fully connected polymer matrix. As will become evident, the 1-3 structure is of special importance. One of the best available methods for fabricating 1-3 connectivity transducers was developed by Savakus [67]. The technique involves taking a prepolarised ceramic disc, as supplied by the manufacturer, and using a diamond saw to dice the material so as to obtain a regular array of piezoceramic pillars. As illustrated in Figure 3.9, the spaces between the pillars are then filled with a suitable polymer and the device is lapped to the required thickness before placing electrodes on the two parallel faces.

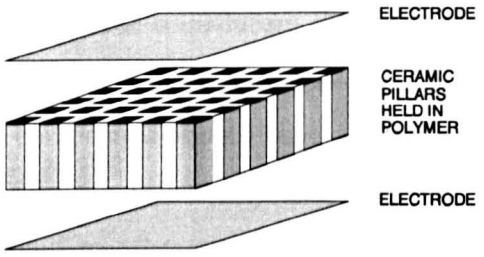

FIGURE 3.9 EXPANDED VIEW OF 1-3 CONNECTIVITY COMPOSITE TRANSDUCER.

During the development of ceramic-polymer composite transducers for hydrophone applications it was recognised that similar high efficiency devices could be used for wideband biomedical applications. Biomedical transducers normally have a centre frequency of between 1 MHz and 3 MHz and are commonly used in electronically steered arrays to produce images of human internal organs. The excellent matching to low impedance media and the low Q of ceramic-polymer composite transducers offered the prospect of excellent imaging performance. Gururaja *et al.* [68] investigated the high frequency performance of ceramic-polymer materials on a purely experimental basis using Erickson's standard tone burst pulse-echo method. This method involves exciting the transducer with a sinusoidal voltage, of approximately twenty cycles duration, and measuring the echo response from a large, thick planar reflector. Gururaja investigated transducers made from 1-3, 3-3, 3-1 and 2-2 ceramic-polymer composite materials. The 0-3 structure was not investigated since the technology for manufacturing such devices was not available at that time. The conclusion of this work was that only the 1-3 ceramic-polymer composite structure was worth serious consideration.

Following their initial investigation of ceramic-polymer composites, Gururaja *et al.* [69] conducted a more extensive investigation of 1-3 composite transducers. In this further work the significance of device thickness, ceramic volume fraction and pillar shape were each investigated. It was found that active composites should have a fine lateral scale so that the ceramic and the polymer phases are effectively tied resulting in uniform vibration. Otherwise, the pillars will tend to vibrate independently of the polymer phase. The investigation also showed that, if the lateral shear wavelength in the polymer is similar to the inter element spacing, then parasitic modes are set up and net performance is degraded. This implies that for optimal reception performance a fine lateral pillar spacing is required. Gururaja found that transmission efficiency was proportional to ceramic volume fraction. The acoustic impedance of the transducers was investigated theoretically and also experimentally using the transmission, reflection and resonance techniques. Only in the case of composites possessing a fine lateral scale at moderate frequencies (i.e. less than 1 MHz) could consistent results, in agreement with theory, be obtained. For composites with a coarse lateral scale operated at higher frequencies, the ceramic pillars vibrated independently and exhibited a higher velocity resulting in a higher than expected acoustic impedance.

3.5 Mechanical Matching Layers

An alternative to the composite transducer concept is to use a piezoceramic plate transducer with a mechanical matching layer applied to its front face. As mentioned earlier, this was the approach used by Rogovsky [14]. This has the advantage that the operating frequency of the transducer is determined by the thickness of the piezoceramic plate but the coupling efficiency is determined by the acoustic impedance of the matching layer. Also, the application of a mechanical matching layer to a piezoceramic plate should not significantly alter its directivity characteristics.

3.5.1 Theory

Many liquid coupled ultrasonic NDT systems use matching layers with a high degree of success but, as will now be discussed, it is not easy to make an effective matching layer for use in air because of the extreme impedance mismatch. In his PhD Thesis, Jackson has thoroughly investigated the use of both single and multiple matching layers [70]. It is not difficult to show that the coupling efficiency of a simple piezoceramic

plate can be greatly improved by applying to its front face a quarter wavelength layer of a material which has a characteristic acoustic impedance given by [70]:

$$Z_M = (Z_T \times Z_F)^{1/2} \tag{3.14}$$

where Z_T and Z_F are the characteristic impedances of the transducer and the coupling fluid respectively. The expected gain in emitted ultrasonic pressure that can be expected by employing a single mechanical matching layer can be calculated using:

$$g \approx \frac{Z_T}{Z_M} \tag{3.15}$$

The detailed analysis conducted by Jackson [70] indicates that it is possible to improve on the performance of a single matching layer by using a multiple layer system. However, the addition of more matching layers does not have such a significant effect, with the percentage increase in transmission gradually reducing per layer, for each additional layer added. Consider a typical PZT transducer with $Z_T = 33 \times 10^6$ $kgm^{-2}s^{-1}$. For air $Z_F = 418$ $kgm^{-2}s^{-1}$ and hence $Z_M = 0.12 \times 10^6$ $kgm^{-2}s^{-1}$. Based on these figures it can be seen that, by using a single optimised matching layer, it should be possible to increase the emitted pressure from a piezoceramic transducer by a factor of 275 or 49 dB. For reasons which are often not clear, many practical devices do not perform as well as would be expected, however, good results are possible.

3.5.2 Materials

A number of materials with sufficiently low acoustic impedances are available for the construction of mechanical matching layers. For example, in 1984 a research team at the University of Wurtzburg succeeded in transmitting ultrasonic signals through aerogel tiles [71]. Experiments indicated that the material had a density of 100 kg/m^3 and that sound was propagated in the tiles with a velocity of 100 m/s. Thus the characteristic acoustic impedance of the aerogel is 10^4 $kgm^{-2}s^{-1}$. In 1992 the same team reported [72] aerogels with densities in the range 300 to 2000 kgm^{-3}. The acoustic impedances of these aerogels make them ideal for mechanical impedance matching. With these devices the small thickness of the quarter wavelength layers leads to relatively low values of attenuation. Also, since SiO_2 aerogels are thermally stable up to several hundred degrees C, they are also attractive for high temperature applications.

Unfortunately, matching layers made from aerogels are not resistant to mechanical stress and moisture. Other materials which have been used to produce matching layers include balsa wood, cork, and RTV impregnated rubber with glass bubbles.

3.5.3 Engineered Matching Layers

Most of the materials which are suitable for producing mechanical matching layers exhibit either high attenuation, a high level of scattering, environmental instabilities, non-uniformities or are extremely difficult to shape. As a consequence of these problems, various attempts have been made to engineer alternative types of matching layer. For example, in 1992 researchers at Stanford University (M.I. Haller and B.T. Khuri-Yakub) reported a method of manufacturing low impedance materials using 1-3 air composites. The technique involved using a low pressure plasma to etch Kapton, a material similar to polyamide which is made by DuPont, into an array (20 μm pitch) of tall thin posts each of which had an aspect ratio of greater than 20:1. The minimum post width was 1 μm and the maximum post height was 125 μm. It was found that, with this technique, the volume fraction of the Kapton determines the acoustic impedance of the matching layer and the sound velocity within the layer. Theoretical predictions indicated that for values of Kapton volume fraction in the range 0.002 to 1, the corresponding acoustic impedance values were in the range 0.01 x 10^6 $kgm^{-2}s^{-1}$ to 2 x 10^6 $kgm^{-2}s^{-1}$. It was found that at low volume fractions the sound velocity in the material was approximately the shear velocity of the Kapton (850 ms^{-1}). One problem found with this technique was that, because air has a very low viscosity, it was possible for the air to remain stationary while the posts vibrated up and down. Calculations showed that at a frequency of 1 MHz there was a 1.5 μm region where the air followed the motion of the posts. In order to solve this problem and to protect the fragile posts from damage, it was found necessary to place a thin cap on the top of the posts. It was then found that due to the presence of the cap it was not possible to adopt the standard quarter wavelength ($\lambda/4$) matching technique described previously. This problem was solved by adopting a $\lambda/8$ design where, in effect, the cap becomes a second matching layer. For PZT-5A and at a frequency of 1 MHz, theory predicted that the performance that could be obtained with this design was almost identical to that which could be obtained using the standard $\lambda/4$ technique.

3.5.4 *The Multi-Horn Plate*

Another example of an engineered matching layer is the multi-horn plate described by Fletcher and Thwaites in a paper published in 1992 [73]. The bandwidth of a horn increases, for given throat and mouth diameters, as the length increases, but this clearly leads to dimensional difficulties if the device is to be used in a confined space. Consider for example a transducer diameter of 10 mm and a mouth diameter of 30 mm. In order to achieve a pressure gain of 10 dB at an operating frequency of 100 kHz it can be shown [73] that it would be necessary for the length of the horn to be greater than 100 mm. At an operating frequency of 200 kHz it would be necessary to double the length of the horn. In order to overcome the dimensional problems, Fletcher and Thwaites devised a plate which consists of an array of much smaller horns. Here, each horn serves only the small area of transducer surface located close to its open throat. An arrangement of this sort operating at 100 kHz requires a plate no more than 2 mm in thickness and can readily provide a pressure gain of 10 dB. It is possible to scale the design to produce plates which are suitable for operation at other frequencies but the theory of operation indicates that the performance of the multi-horn plate will deteriorate at frequencies greater than 100 kHz. Although the multi-horn plate is an interesting concept its performance does not match that which can be achieved using any of the previously discussed matching layer techniques.

3.6 Conclusions

All of the composite transducers described in this Chapter are capable of providing better coupling into air than is possible with a simple piezoceramic plate transducer. However, with the exception of the 1-3 ceramic-polymers, none of these devices is suitable for the non-destructive testing applications being considered in this PhD Thesis, either because they are not capable of operating at a sufficiently high frequency or because they exhibit poor directivity characteristics. The sensitivity of both piezoceramic and piezocomposite plate transducers can be significantly improved using mechanical matching layers. The importance of this technology is recognised and new matching layer technology is currently being investigated within the Ultrasonics Research Group at Strathclyde [58]. However, all of the experimental results which were obtained at normal atmospheric pressure and which are described in this Thesis were obtained using piezocomposite transducers which did not incorporate front face

matching layers. In addition to their excellent directivity characteristics and reduced acoustic impedance, these devices have the robust qualities required for a practical system which is suitable for use in an industrial environment. An attempt was made to use some of the new matching layers in the high pressure experiments described in Chapter 9 but it was impossible to prevent them from detaching from the transducers.

For convenience, the basic properties of the transducer technologies which were discussed both in Chapter 1 and the present Chapter are summarised in Table 3.1.

TABLE 3.1

COMPARISON OF AVAILABLE AIR COUPLED TRANSDUCER TECHNOLOGIES

TECHNOLOGY	Man.	Rob.	Rel.	B.P.	Freq.	Sens.	Rating	Ref.
Condenser mic.	High	Med.	Med.	High	Med.	High	Low	44
Solid dielectric mic.	High	Low	Low	High	High	High	Low	45
Electrostatic (M.M.)	Low.	Low	Med	High	High	High	High	46
Piezocomposite disc	High	High	High	High	High	Low	Low	59
Cantilever bimorph	Med.	Med.	High	Low	Low	Med.	Low	59
Disc or plate bimorph	Med.	Med.	High	Low	Low	Med.	Low	59
Bimorph array	Low	Med.	High	Med.	Med.	Med.	Med.	None
Unimorph	Med.	Med.	High	Low	Low	Med.	Low	63
Radiating membrane	Med.	High	High	Low	Med.	Med.	Low	65
Ceramic metal comp.	Med.	High	High	Med.	Low	Med.	Low	66
Ceramic poly. comp.	Med.	High	High	High	High	Med.	High	67
Piezoceramic (M.L.)	Med.	Med.	Med.	High	High	Med.	High	70
Piezocomposite (M.L.)	Med.	Med.	Med.	High	High	High	High	58

Man. - Ease of manufacture. **Rob.** - Robustness. **Rel.** - Reliability. **B.P.** - Beam profile. **Freq.** - Suitability of frequency range. **Sens.** - Relative sensitivity. **Rating** - Overall suitability for air coupled testing in an industrial environment. **Mic.** - Microphone. **M.M.** - Micromachined. **M.L.** - Device with mechanical matching layer. **Ref.** - Principle literature reference.

Chapter 4

The Absolute Sensitivity of a Piezoelectric Receiving Transducer

4.1 Introduction

It is natural to discuss sound waves either in terms of particle displacement or in terms of pressure variations within the medium involved. For example, in Chapter 1, diagrams showing particle displacement were used to illustrate a number of different wave types. In Chapter 2, the reflection and transmission of sound waves at media boundaries was described mathematically in terms of acoustic pressure. Although it is convenient to derive expressions for acoustic reflection and transmission coefficients in terms of pressure, the results obtained using these expressions can be difficult to interpret. To illustrate this, consider the following example.

The normal incidence pressure transmission Equation (2.12) indicates that when a piezoceramic transducer is used to detect sound waves in air, the acoustic pressure in the transducer is greater than the acoustic pressure in the surrounding air by a factor of two. Further inspection of Equation (2.12) indicates that the pressure transmission coefficient cannot be greater than two and that a massive reduction in transducer impedance would be required to significantly reduce its value. As a consequence, it could be concluded, incorrectly, that it is not possible to significantly improve the sensitivity of an air coupled receiving transducer by making small reductions in its acoustic impedance. However, from practical experience, it is known that as the acoustic impedance of a receiving transducer is reduced, in order to bring it closer to the impedance of the surrounding medium, its sensitivity improves. The reason that there appears to be a conflict is that the ratio of the acoustic signal pressures on either side of a media boundary is not a measure of the acoustic signal power which is transmitted across the boundary. In order to quantify the sensitivity of an ultrasonic receiving transducer it is the power transmission ratio which must be found. The signal power within the transducer must then be compared to the transducer's intrinsic acoustic noise power in order to quantify the minimum detectable power.

4.1.1 Minimum Detectable Power

The preceding example illustrates a general principle. When discussing the sensitivity of ultrasonic receiving transducers, it is easier and safer to perform the calculations in terms of acoustic power and then convert back into force, pressure or displacement as required. The power associated with a sound wave is the energy per unit time which

is transmitted from one part of the supporting medium to another. Here, the energy referred to is the sum of the potential and kinetic energies of the individual particles which make up the medium. At any instant the kinetic energy of a particular particle is determined by the particle velocity. The potential energy of the particle depends on the displacement of the particle from its undisturbed position. When a receiving transducer detects a signal, the wave energy associated with each particle has its origin in the transmitting transducer. However, it is important to realise that in the absence of a signal, the individual atoms, molecules, ions and free electrons within the receiver material are already in various forms of random motion. The kinetic energy associated with this random motion is related directly to the temperature of the receiving transducer, and the motion itself constitutes wideband acoustic noise. Clearly then, the power signal to noise ratio (SNR_T) within the receiving transducer is the ratio of the signal power to the mean noise power. This means that the minimum detectable power within the transducer material (MDP_T) is the signal power within the transducer for which $SNR_T=1$. Although MDP_T is a meaningful figure of merit for a receiving transducer, a much more useful version can be defined as follows. The MDP of a receiving transducer is the signal power within the coupling medium which results in a power signal to noise ratio of unity within the transducer. This version accounts for the transducer's front face power transmission coefficient, T_P. That is, MDP_T is MDP multiplied by T_P. Minimum detectable force (MDF) can also be used as a transducer figure of merit. Clearly, $MDF_T=(MDP_T\ Z_2)^{1/2}$ and $MDF=(MDP\ Z_1)^{1/2}$ where Z_1 and Z_2 are the acoustic impedances of the coupling medium and the transducer respectively. In Chapter 7 it will be shown that the MDP of a complete ultrasonic receiver is always worse than that of the receiving transducer which it employs. It is only by comparing the MDP of a receiver with the MDP of the transducer which it employs that it is possible to assess the effectiveness of the receiver electronics.

4.1.2 The Low Noise Concept

It is tempting to think that the voltage noise which appears across the terminals of an ultrasonic transducer is a function of the electrical properties of the materials from which it is made. This idea can be better understood by considering the performance of two hypothetical transducers. Suppose that these transducers are made from a different selection of materials but it is arranged that they have the same front face

transmission coefficient, that they are equally efficient in converting mechanical energy into electrical energy and that they have the same dimensions. It would seem reasonable to ask the following question. *Is it possible to select the transducer materials in such a way that one device is a low noise version of the other?* In this Chapter it will be shown that, although low noise design is possible for most purely electronic devices, it is not possible for an ultrasonic transducer. It will also be shown that, for any sound detection device, thermal noise is best regarded as a mechanical or acoustic phenomenon rather than an electrical phenomenon. In fact, as will be clear from remarks which have already been made, this is always the case since thermal noise originates from mechanical movement on a microscopic scale. Electrical noise results when this movement involves particles which have a net electrical charge. This electrical noise can be quantified using the well known Johnson noise equation.

4.1.3 Defining Receiver Sensitivity

From this discussion it will be clear that all ultrasonic receiving transducers have a noise limited sensitivity which can be quantified using, for example, the MDP figure of merit which has been introduced here. Obviously this is different from the transducer's conventional sensitivity which, for example, is quoted in terms of volts per newton. In this Thesis, a transducer's noise limited sensitivity will be referred to as its *absolute sensitivity* in order to avoid confusion with the conventional term. This concept is discussed in detail in Chapter 10.

Clearly, it should be possible to obtain mathematical expressions for a transducer's absolute sensitivity using either a mechanical analysis or an electrical analysis based on the Johnson noise equation. Using the material which is presented in this Chapter, and Chapters 5 and 6, it will be shown that all transducers which have the same dimensions and which have the same acoustic impedance, produce identical voltage noise spectra across their output terminals. The actual shape of the noise voltage spectrum is determined by the mechanical resonances of the transducer. However, because the signal voltage across a transducer's terminals is also determined by its resonant properties, the voltage signal to noise ratio of an open circuit device is found to be constant with respect to frequency. It follows from these observations that a transducer's absolute sensitivity is a function only of its mechanical properties.

4.2 Electrical Noise in Receiving Transducers

It would seem reasonable to suggest that the voltage noise which appears across the terminals of an ultrasonic transducer is a function of the electrical properties of the materials from which it is made. This possibility is explored in Sections 4.2.1 and 4.2.2 by adopting the same approach which is commonly used to determine the noise properties of electronic devices such as, transistors, diodes and capacitors. Section 4.4 is dedicated to the analysis of a mathematical model which is based on these ideas.

4.2.1 Noise in Electronic Devices

The main sources of random noise in electronic devices can be grouped into either of two types - *thermal noise*, which has a fundamental thermodynamic origin, and *shot noise* which is due to the average current flow in the device. Another source of noise in electronic devices is 1/f noise but this is only significant at low frequencies and can be neglected at the frequencies which are of interest in this Thesis.

Thermal Noise

Thermal noise is associated with the random motion of particles in a force-free environment. For example, the air pressure in a given room is due to the summed effect of countless air molecules moving chaotically in all directions. The molecules are in continuous turbulent motion, striking and rebounding from one to another. The pressure on any wall of the room is a consequence of the resultant force per unit area of all the molecules striking the wall. This force will fluctuate or vary in time as fewer or more molecules strike the wall from time to time. Because, under most circumstances, the number of molecules involved is very large, the average force in time will remain constant provided that the average molecular energy remains constant. However, the instantaneous force as a function of time will vary randomly about this average value. Increasing the temperature increases the molecular energy, and the average pressure goes up, as do the fluctuations about the average. Thermodynamics and the kinetic theory of heat applied to this problem indicate that, for an ideal gas, the average kinetic energy per molecule in any one direction is $k_B T_A/2$ where k_B is Boltzmann's constant and T_A is the absolute temperature in degrees Kelvin. As a consequence, the mean-squared thermal noise is proportional to $k_B T_A$. Brownian motion is a manifestation of this effect [74,75]. In the same way the small mirror which is part

of a sensitive ballistic galvanometer is seen to be subject to random deflections [75].

Fluctuations which are similar to those which have just been discussed are observed in electrical conductors. Such conductors are composed of ions which are strongly bound by molecular forces. Large numbers of free electrons are also present and these are continually colliding with the strongly bound ions. As a consequence, the ions vibrate randomly about their normal or average positions. There is a continuous transfer of energy between the electrons and the ions and this is the origin of the electrical resistance in the conductor. The freely moving electrons constitute a current, which over a long period of time averages to zero since, on average, as many electrons move in one direction as in the other. As with the previously discussed pressure variations, there are random current fluctuations about the average. Again, it is found that the mean-squared thermal noise current is proportional to $k_B T_A$.

Both of the examples described here (pressure fluctuations and current fluctuations) concern the chaotic motion of particles (molecules or electrons) possessing thermal energy. There are no forces present to organise the motion of the particles so that they have a preferred direction. Both cases may therefore be treated using equilibrium thermodynamics, with the mean-squared fluctuations found proportional to $k_B T_A$. This has a particular significance which will become clear later in this Chapter.

Thermal noise in electrical conductors was first studied experimentally by J. B. Johnson of the Bell Laboratories. The results of his work can be found in a paper entitled *Thermal Agitation of Electricity in Conductors* which was published in Physical Review in July 1928 [76]. An accompanying theoretical paper, by H. Nyquist of the American Telephone and Telegraph Company, was published simultaneously in the same journal. This second paper is entitled *Thermal Agitation of Electric Charge in Conductors* [77]. The work which is described in these two papers demonstrates that a metallic resistor can be considered the source of spontaneous fluctuation voltages with mean-square value:

$$v_n^2 = 4 k_B T_A R_E B \qquad (4.1)$$

where R_E is the electrical resistance in ohms, k_B is Boltzmann's constant, T_A is the

absolute temperature in degrees Kelvin and B is the electronic noise bandwidth. This equation is now commonly known as the Johnson noise equation. A more useful form of the equation, which can be applied to electronic devices which do not constitute a pure resistance, is:

$$v_n = (4 k_B T_A Re(Z_E) B)^{1/2} \quad (4.2)$$

Here, $Re(Z_E)$ is the real part of the complex electrical impedance of the device and v_n is the root mean square (r.m.s.) thermal noise voltage.

Shot Noise

An understanding of shot noise is not required in this Chapter. The reason for this is that the transducers which are to be discussed are all passive devices. In this context, *passive* should be read to mean that there is no requirement to connect any of the devices to a supply voltage which would produce a steady current and hence shot noise. However, shot noise in amplifier components is considered in Chapter 7 and here is a convenient place to introduce it. As with thermal noise, shot noise is due to the discrete nature of matter, however, here it is assumed that there is an average flow in some direction taking place: electrons and holes flowing in a semiconductor device, photons emitted in a laser system, fluid moving continuously under the action of a pressure gradient etc. In all these cases it is found that the mean-squared fluctuations about the average value are proportional to the average value itself. In an electrical conductor the mean value of the shot noise current generated by a direct current, I_D, is given by:

$$i_s = (2qI_D B)^{1/2} \quad (4.3)$$

where q is the electronic charge and B is the bandwidth [78].

Transducer Noise Spectrum

From Equation (4.2), it appears that it should be possible to obtain the voltage noise spectrum of a piezoelectric plate transducer simply by predicting $Re(Z_E)$. A very accurate way of doing this would be to use the Linear Systems Model developed by Hayward [55,79,80,81]. However, before investigating this possibility it will be found valuable to look at the more general problem of noise in electroceramic materials.

4.2.2 *Electroceramic Materials*

The thermal noise Equation (4.2) can be rewritten in the following form:

$$v_n = (4k_B T_A B|Z_E|\cos\phi)^{1/2} \tag{4.4}$$

Here, Z_E is the complex impedance of the device and ϕ is the current-voltage phase angle. The magnitude of, Z_E, and the phase angle, ϕ, for an unpoled sample of PZT-5A

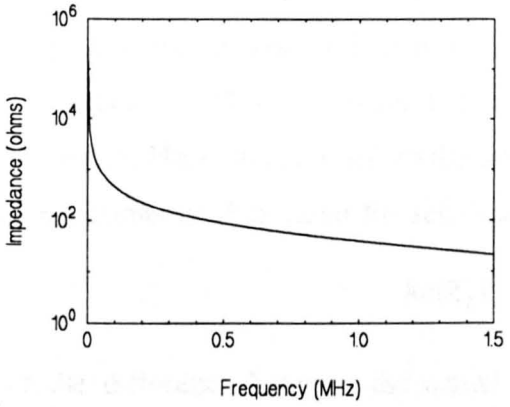

FIGURE 4.1 IMPEDANCE MAGNITUDE FOR UNPOLED PZT-5A PIEZOCERAMIC DISC

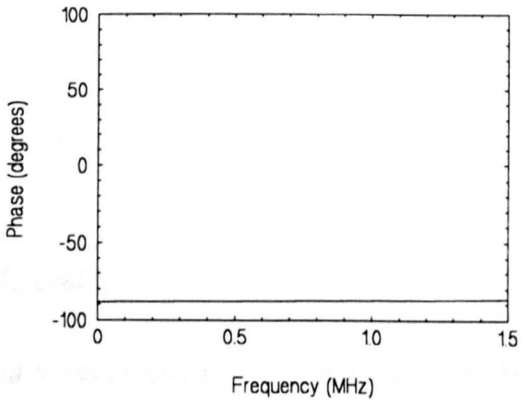

FIGURE 4.2 CURRENT-VOLTAGE PHASE FOR UNPOLED PZT-5A PIEZOCERAMIC DISC

piezoceramic material are illustrated in Figures 4.1 and 4.2. The experimental data used to produce these graphs was obtained using a Hewlett Packard 4194A impedance analyzer. From these curves it can be seen that the unpoled material behaves in exactly the same way as a capacitor. If an alternating voltage were applied to a perfect capacitor, the resulting current would lead the voltage by 90° and from Equation (4.4) it can be seen that no thermal noise would be generated by the capacitor. However, on close examination of Figure 4.2, it can be seen that, for the unpoled piezoceramic sample, the phase angle is always slightly less than 90°. Figure 4.3, which was produced using the same experimental data, provides a more detailed view of how the phase angle varies in the region close to -90°. From Figure 4.3 it can be seen that, over the frequency range 0 to 1.5 MHz, the phase

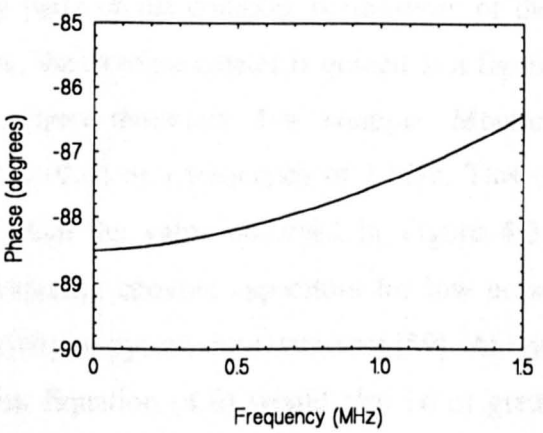

FIGURE 4.3 CURRENT-VOLTAGE PHASE FOR UNPOLED PZT-5A DISC IN THE REGION CLOSE TO -90 DEGREES

angle is in the range 88.5° to 86.5°. In all real capacitors the current leads the voltage by slightly less than 90°. This is a consequence of power dissipation in the dielectric material and from Equation (4.4) it is clear that a thermal noise voltage is generated as a result. However, unlike a pure resistance, the real part of the impedance is a function of frequency. This is illustrated in Figure 4.4. Here, the real part of the impedance of the ceramic disc was obtained from the experimental data using the relationship:

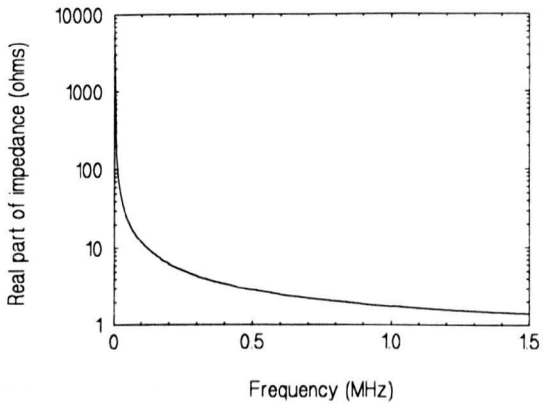

FIGURE 4.4 REAL PART OF THE ELECTRICAL IMPEDANCE FOR AN UNPOLED PZT-5A DISC

$$Re(Z_E) = |Z_E|\cos(\phi)$$

Let the difference between the actual current-voltage phase difference and 90° be denoted by δ. Equation (4.4) can now be rewritten as:

$$v_n = (4k_BT_AB|Z_E|\sin\delta)^{1/2} \qquad (4.5)$$

In most cases δ is small. For example, in the previously discussed experimental data it can be seen that δ is in the range 1.5° to 2.5°. Under these circumstances a very good approximation to the last equation is:

$$v_n = (4k_BT_AB|Z_E|\tan\delta)^{1/2} \qquad (4.6)$$

The advantage of writing the thermal noise equation in this way is that $tan\delta$ is exactly equal to the ratio of the real and imaginary parts of the complex permittivity of the dielectric material. Because of its importance, the $tan\delta$ parameter is quoted as a figure of merit by most manufactures of electroceramic materials. For example, Morgan Matroc quote the value of $tan\delta$ for PZT-5A as 0.02 at a frequency of 1 kHz. This is equivalent to 1.2° which is slightly better than the value observed in Figure 4.3. Equation (4.6) is of great importance in designing ceramic capacitors for low noise applications and also for predicting the sensitivity of pyroelectric detectors [59]. At one stage in this investigation it was thought that Equation (4.6) would also be of great significance in establishing the sensitivity of ultrasonic transducers constructed from

poled piezoceramic materials. It will now be shown that this is not the case.

4.2.3 Piezoceramic Materials

The impedance and phase characteristics illustrated in Figures 4.1 and 4.2 were obtained using a sample of PZT-5A which had been depoled by raising the temperature of the sample to above the Curie point (365°C) for the material. Similar measurements were made before depoling the material and these are illustrated in Figures 4.5 and 4.6. In Figure 4.5, one curve represents the magnitude of the impedance for the poled material and the other curve represents the magnitude of the impedance for the unpoled material. By comparing the two curves it can be seen that, at a number of frequencies, there are large variations in the magnitude of the impedance of the poled material compared to the magnitude of the impedance of the unpoled material. At these same frequencies large variations in current-voltage phase can be seen in Figure 4.6. Each deviation from the unpoled characteristic corresponds to a mechanical resonance in the piezoceramic disc. Most of the deviations in these graphs are due to radial vibrations in the disc but the one at 1 MHz corresponds to the main thickness mode vibration. As a consequence of poling there is now an interaction between the electrical and the mechanical properties of the material. Detailed inspection of Figure 4.6 indicates that, as in the case of the unpoled piezoceramic material, the largest negative value that the current-voltage phase angle, ϕ, can have is $-90° + \delta$. This happens at frequencies which are well removed from any mechanical resonances. It is interesting to note that $tan\delta = 1/Q_E$ where Q_E is the electrical damping factor [82]. A poled material also has associated with it a mechanical damping factor, Q_M [82]. As illustrated in Figure 4.6,

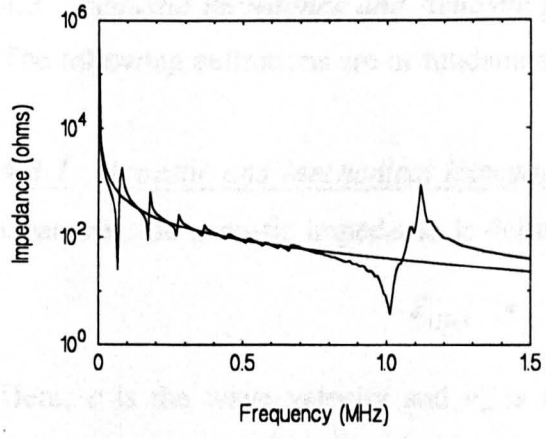

FIGURE 4.5 IMPEDANCE MAGNITUDE FOR POLED AND UNPOLED PZT-5A DISC

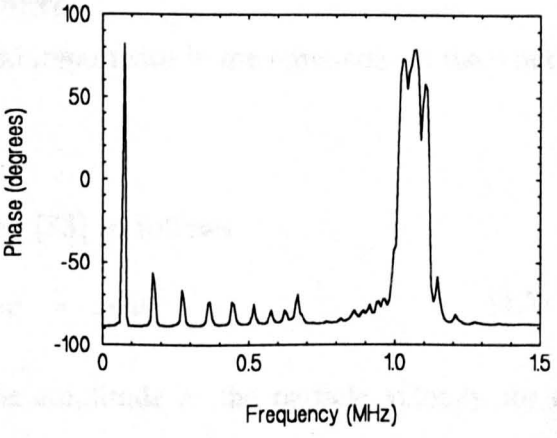

FIGURE 4.6 CURRENT-VOLTAGE PHASE FOR A POLED PZT-5A PIEZOCERAMIC DISC

mechanical damping ensures that the value of ϕ will always fall short of $+90°$. From the experimental results presented here, it can be seen that a poled piezoceramic material does not behave like a capacitor with the current leading the voltage by almost 90°. The current-voltage phase characteristic indicates that the material is behaving as if it were composed of capacitive, inductive and resistive elements. Early attempts to model the behaviour of piezoceramic transducers were based on this observation. More sophisticated modelling techniques are now available and one of these is discussed in Section 4.4. Before discussing this, it should be noted that, because of the large phase changes which take place in a poled piezoceramic material, it is no longer possible to use the $tan\delta$ parameter to calculate the thermal noise voltage. This means that it is not possible to use Equation (4.6) and instead it is necessary to use either Equation (4.2) or (4.4). Again, it is possible to obtain the real part of the electrical impedance from the experimental data for the poled ceramic material. The result of doing this is illustrated in Figure 4.7 from which it can be seen that the real part of the electrical impedance is a complicated function of frequency. It is possible to predict some of the features of this characteristic using the model which is described in the Section 4.4.

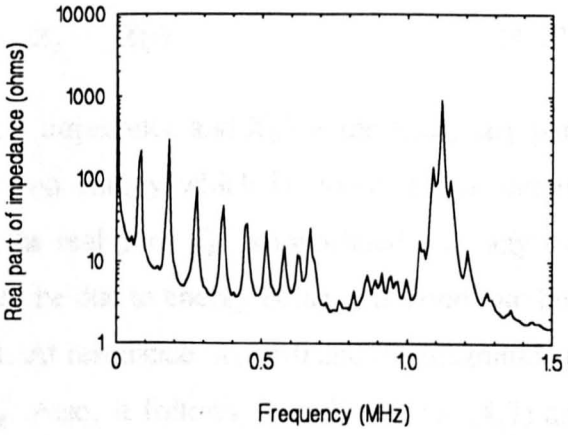

FIGURE 4.7 REAL PART OF ELECTRICAL IMPEDANCE FOR A POLED PZT-5A DISC

4.3 Acoustic Impedance and Acoustic Power

The following definitions are of fundamental importance in the remainder of the work.

4.3.1 Acoustic and Mechanical Impedance

Characteristic acoustic impedance is defined [83] as follows:

$$Z_{CHA} = \rho c = p/v_{\infty} \tag{4.7}$$

Here, c is the wave velocity and v_{∞} is the amplitude of the particle velocity for a sample which has infinite dimensions (no boundaries). Also, ρ is the material density

and p is the particle pressure. The *CHA* subscript has been used to avoid confusion with Z_C (see Section 4.4) which is defined as:

$$Z_C = AZ_{CHA} = A\rho c \tag{4.8}$$

where A is the area of the transducer. Mechanical impedance is a property of real structures such as plates, all of which have finite dimensions. It is defined [87] as the ratio of the total force required to move a particle to the velocity resulting, for a specified frequency of motion. Thus the magnitude of the mechanical impedance is:

$$|Z_M(f)| = F_0/v_0 \tag{4.9}$$

where f is the driving frequency, F_0 is the amplitude of the driving force and v_0 is the amplitude of the resulting particle velocity. Since mechanical impedance is a complex quantity the following equation also applies:

$$Z_M(f) = Z_R + jX(f) \tag{4.10}$$

Here, Z_R is the real part of the mechanical impedance and $X(f)$ is the imaginary part. The imaginary part, $X(f)$, is associated with energy which is stored in the reactive components of the vibrating system and the real part, Z_R, is associated with any loss of energy from the system. This loss could be due to energy being converted into heat or being transmitted into the environment. At resonance, $X(f)=0$ and the magnitude of the mechanical impedance is equal to Z_R. Also, it follows from Equations (4.7) and (4.8) that the magnitude of the mechanical impedance at resonance is $(v_\infty/v_R)Z_C$. Hence:

$$Z_R = (v_\infty/v_R)\,Z_C$$

where v_R is the resonant amplitude of the particle velocity in a structure such as a plate. The last equation leads directly to:

$$Z_R = (d_\infty/d_R)\,Z_C$$

where d_∞ and d_R are the displacements corresponding to v_∞ and v_R respectively. Hence:

$$Z_R = \frac{Z_C}{Q_\infty} = \frac{4}{\pi}\frac{Z_C}{Q_M} \tag{4.11}$$

where $Q_\infty=d_R/d_\infty$ and is a quality factor representing the resonant particle displacement

of a plate relative to the particle displacement in a medium with infinite dimensions. The alternative quality factor, Q_M, represents the resonant particle displacement of a plate relative to its zero frequency particle displacement (see Appendix II).

4.3.2 Acoustic Power

It is not difficult to show that the instantaneous power, P, in a sound wave is given by the following expression:

$$P = vF = v^2 |Z_M| \tag{4.12}$$

or:

$$P = \frac{F^2}{|Z_M|} \tag{4.13}$$

Since Z_M is complex this can also be written as:

$$P = \frac{F^2}{\sqrt{Z_R^2 + X^2}} \tag{4.14}$$

where, as mentioned previously, Z_R and X are the resistive and reactive components of the complex mechanical impedance, Z_M. Consider a longitudinal wave travelling in a medium which has an acoustic impedance Z_1. Further, suppose that the wave is incident on a plate for which the real part of the mechanical impedance is Z_R. It follows from Equations (2.11) that the power reflection coefficient is:

$$R_P = \left[\frac{Z_R - Z_1}{Z_R + Z_1}\right]^2 \tag{4.15}$$

and the power transmission coefficient is:

$$T_P = \frac{4Z_R Z_1}{(Z_R + Z_1)^2} \tag{4.16}$$

As will be discussed in Section 4.5.8, these important equations can be applied at the front face of a transducer. It should be noted that if the plate were to be replaced with a solid half-space (extends to infinity) then Z_R would be replaced by Z_C.

4.4 The Linear Systems Model

An accurate model for predicting the characteristics of thickness mode piezoelectric transducers is the Linear Systems Model (LSM) developed by Hayward [55,79,80,81]. This model has been used with a high degree of success to predict, for example, the wideband force to voltage transfer function of piezoelectric plate transducers with a variety of different compositions. With regard to this research, a key feature of the LSM is its ability to accurately predict the complex electrical impedance characteristic of thickness mode transducers. Recently, Hayward *et al.* [84,85] have modified the LSM to produce a Linear Systems Noise Model (LSNM). In order to do this it was necessary to apply Equation (4.2) to the theoretical complex impedance characteristic produced by the LSM. It had been hoped that it would be possible to use the LSNM to predict the nature of the voltage noise which appears across the output terminals of an open circuit piezoceramic transducer, and hence the signal to noise ratio (SNR). However, although results obtained for a complete receiver (a transducer connected to a pre-amplifier) appeared to be accurate [84,85], further work undertaken by the author of this Thesis lead to some apparently unusual and certainly unexpected results for open circuit transducers. These unusual results are only obtained when the LSNM is used to predict the SNR at the output terminals of a transducer which is not connected to an electrical load such as the input impedance of a pre-amplifier. In order to understand these results it will be necessary to describe the original noise model.

4.4.1 The Original Noise Model

In order to understand the original noise model (LSNM) it is necessary to understand the linear systems model (LSM). Consider the piezoelectric receiving configuration outlined in Figure 4.8, in which F_1 corresponds to the force incident on the front face of the transducer and V_0 is the voltage developed across the transducer electrodes. A lumped impedance, Z_L, is included to represent the electrical impedance of any load components. Such a configuration may be represented by the systems feedback model shown in Figure 4.9, in which the transducer is subject to the physical

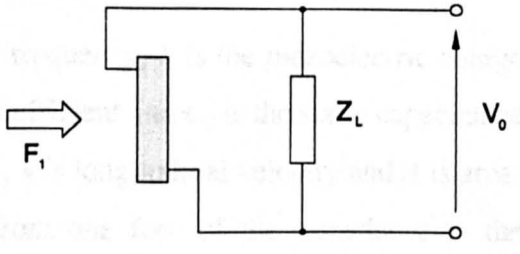

FIGURE 4.8 RECEIVER CONFIGURATION

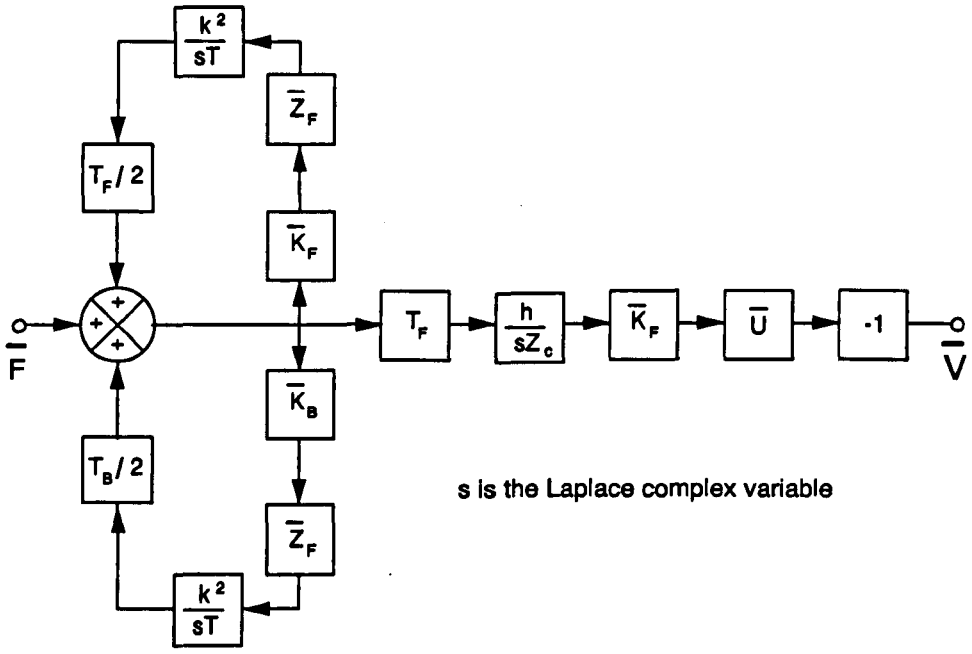

FIGURE 4.9 LINEAR SYSTEMS RECEIVER MODEL

constraints of linear, planar, lossless and unidirectional wave motion in the thickness direction. It is also assumed to radiate into semi-infinite, real media which are positioned at each face. For this configuration, it can be shown [55,79] that the transfer function relating output voltage to excitation force is given by:

$$\frac{V_0}{F_1} = \frac{-hT_F K_F U \,/\, j\omega Z_c}{1 - Z_F(\tfrac{1}{2}K_F T_F + \tfrac{1}{2}K_B T_B)k^2 \,/\, j\omega T} \tag{4.17}$$

and the electrical impedance is given by [55,80]:

$$Z_E = \frac{1}{j\omega C_0}\left[1 - \frac{k^2}{j\omega T}\left(\frac{K_F T_F}{2} + \frac{K_B T_B}{2}\right)\right] \tag{4.18}$$

Here, $j = \sqrt{-1}$, $\omega = 2\pi f$ where f is the signal frequency, h is the piezoelectric charge constant, k is the electromechanical coupling coefficient and C_0 is the static capacitance of the transducer. $Z_C = \rho v A$ where ρ is density, v is longitudinal velocity and A is area. The time taken for sound waves to travel from one face of the transducer to the opposite face is $T = 1/2f_n$ where f_n is the natural thickness mode resonant frequency. The front face reverberation factor is given by:

$$K_F = \frac{(1 - e^{-j\omega T})(1 - R_B e^{-j\omega T})}{(1 - R_F R_B e^{-j\omega T})} \tag{4.19}$$

and the rear face reverberation factor is given by:

$$K_B = \frac{(1 - e^{-j\omega T})(1 - R_F e^{-j\omega T})}{(1 - R_F R_B e^{-j\omega T})} \tag{4.20}$$

Using Equation (2.12), the front face transmission coefficient is:

$$T_F = \frac{2Z_C}{Z_C + Z_1} \tag{4.21}$$

and the rear face transmission coefficient is:

$$T_B = \frac{2Z_C}{Z_C + Z_2} \tag{4.22}$$

Using Equation (2.11), the front face reflection coefficients is :

$$R_F = \frac{Z_C - Z_1}{Z_C + Z_1} \tag{4.23}$$

and the rear face reflection coefficient is:

$$R_B = \frac{Z_C - Z_2}{Z_C + Z_2} \tag{4.24}$$

Here, Z_1 is the acoustic impedance of the front face medium and Z_2 is the acoustic impedance of the rear face medium. The forward loop attenuation factor is given by:

$$U = \frac{j\omega C_0 Z_L}{1 + j\omega C_0 Z_L} \tag{4.25}$$

and the feedback factor is given by:

$$Z_F = \frac{1}{1 + j\omega C_0 Z_L} \tag{4.26}$$

The basic description of the Linear Systems Model is now complete.

4.4.2 A Closed Form Solution for MDP

The remainder of this analysis is concerned with obtaining a closed form solution for the voltage signal to noise ratio across the terminals of a piezoceramic plate transducer used as an ultrasonic receiving device. This in turn will provide solutions for the minimum detectable force and the minimum detectable power. Some simplifying assumptions will be made. As a consequence of the way in which the Linear Systems Model has been constructed it has already been assumed that the transducer is lossless. Here, the term *lossless* should be read to mean that there is no attenuation of sound waves within the transducer material. This means that the mechanical Q of the transducer is a function of coupling losses at the transducer boundaries only. It will further be assumed that the backing medium is air i.e. it is the same as the front face medium. This is true for all of the transducers used in this research. In addition it will be assumed that the transducer is operated under open circuit conditions.

Under open circuit conditions $Z_L = \infty$ and $U = 1$. Also, $Z_F = 0$ which means that there is no secondary piezoelectric action and hence there is no feedback in the model. Let $Z_2 = Z_1$ which means that the transducer backing medium is the same as the front face coupling medium. It now follows that $K_B = K_F$, $T_B = T_F$, $R_B = R_F$ and Equation (4.18) becomes:

$$Z_E = \frac{1}{j\omega C_0}\left(1 - \frac{k^2 K_F T_F}{j\omega T}\right) \tag{4.27}$$

This is the open circuit electrical impedance where, from Equations (4.19) and (4.20):

$$K_F = K_B = \frac{1 - e^{-j\omega T}}{1 + R_F e^{-j\omega T}} \tag{4.28}$$

Equation (4.28) for the reverberation factor is easily expanded to give:

$$K_F = \frac{1 - [\cos(\omega T) - j\sin(\omega T)]}{1 + R_F[\cos(\omega T) - j\sin(\omega T)]} \tag{4.29}$$

Substituting Equation (4.29) into Equation (4.27) gives:

$$Z_E = \frac{1}{j\omega C_0}\left(1 - \frac{k^2T_F}{j\omega T}\left(\frac{1 - \cos(\omega T) + j\sin(\omega T)}{1 + R_F\cos(\omega T) - jR_F\sin(\omega T)]}\right)\right) \quad (4.30)$$

In order to obtain an expression for the transducer noise voltage it is necessary to find the real part of Z_E from Equation (4.30) and then substitute this into Equation (4.2). This can be done as follows. Within the inner brackets in Equation (4.30), the complex term can be removed from the bottom line by multiplying the top and bottom lines by the complex conjugate of the bottom line. Thus:

$$Z_E = \frac{1}{j\omega C_0}\left(1 - \frac{k^2T_F}{j\omega T}\frac{(1-\cos(\omega T)-j\sin(\omega T)) \times (1+R_F\cos(\omega T)+jR_F\sin(\omega T))}{1+2R_F\cos(\omega T)+R_F^2}\right)$$

Expanding this and collecting together the real and imaginary terms gives:

$$Z_E = \frac{k^2T_F}{\omega^2TC_0}\left(\frac{1+R_F\cos(\omega T)-\cos(\omega T)-R_F}{1+2R_F\cos(\omega T)+R_F^2}\right) - \frac{j}{\omega^2TC_0}\left(\frac{\omega T+2\omega TR_F\cos(\omega T)+\omega TR_F^2-k^2T_FR_F\sin(\omega T)-k^2T_F\sin(\omega T)}{1+2R_F\cos(\omega T)+R_F^2}\right)$$

From this it is clear that the real part of the complex electrical impedance is:

$$Re(Z_E) = \frac{k^2T_F}{\omega^2TC_0}\left(\frac{1+R_F\cos(\omega T)-\cos(\omega T)-R_F}{1+2R_F\cos(\omega T)+R_F^2}\right) \quad (4.31)$$

Hence the r.m.s. noise voltage across the terminals of the transducer is:

$$v_n = \sqrt{\frac{4k_BT_Ak^2T_F\,(1+R_F\cos(\omega T)-\cos(\omega T)-R_F)}{\omega^2TC_0(1+2R_F\cos(\omega T)+R_F^2)}} \quad (4.32)$$

From Equation (4.17), the signal voltage, v_S, across the transducer terminals is:

$$v_S = \frac{-hT_FK_FF_S}{j\omega Z_c} \quad (4.33)$$

where F_S is the signal force in the coupling medium. Substituting for K_F from

Equation (4.29) results in the following expression:

$$v_S = \frac{-hT_F F_S}{j\omega Z_c}\left(\frac{1 - \cos(\omega T) - j\sin(\omega T)}{1 + R_F(1 - \cos(\omega T) - j\sin(\omega T))}\right) \tag{4.34}$$

From this it is easily shown that the magnitude of v_S is:

$$|v_S| = \frac{hT_F F_S\sqrt{2(1 - \cos(\omega T)}}{\omega Z_C\sqrt{1 + 2R_F\cos(\omega T) + R_F^2}} \tag{4.35}$$

Equation (4.35) represents the magnitude of the signal voltage across the transducer terminals corresponding to a force F_S applied to the front face of the transducer. From Equations (4.32) and (4.35) it follows that the voltage signal to noise ratio is given by the following expression:

$$SNR = \frac{|v_S|}{v_n} = \frac{\dfrac{hT_F F_S\sqrt{2(1-\cos(\omega T)}}{\omega Z_C\sqrt{1+2R_F\cos(\omega T)+R_F^2}}}{\sqrt{\dfrac{4k_B T_A k^2 T_F\,(1+R_F\cos(\omega T)-\cos(\omega T)-R_F)}{\omega^2 C_0 T(1+2R_F\cos(\omega T)+R_F^2)}}} \tag{4.36}$$

This is easily simplified to give:

$$SNR = \frac{hF_S\sqrt{T_F C_0 T}}{Z_C k\sqrt{2k_B T_A(1-R_F)}} \tag{4.37}$$

Substituting for the reflection coefficient from Equation (4.23):

$$SNR = \frac{hF_S\sqrt{C_0 T}}{k\sqrt{2Z_C k_B T_A Z_1}} \tag{4.38}$$

It is not difficult to shown that [55]:

$$k = \sqrt{\frac{h^2 C_0 T}{Z_C}} \tag{4.39}$$

and by using this to substitute for k in Equation (4.38), the final expression for the

voltage signal to noise ratio is found to be:

$$SNR = \frac{F_S}{\sqrt{2k_B T_A Z_1}} \tag{4.40}$$

This is the required closed form solution for an intrinsically lossless open circuit piezoelectric plate transducer. Equation (4.40) has the following implications:

- The electrical SNR at the transducer output terminals depends purely on the acoustic impedance (Z_1) of the coupling medium.
- The electrical SNR at the transducer output terminals is completely independent of all of the transducer's mechanical and electrical properties.
- The electrical SNR at the transducer output terminals cannot be improved by reducing the transducer's acoustic impedance (Z_2).
- The electrical SNR is completely independent of the signal frequency.

Additional features of this analysis become apparent when Equation (4.40) is used to predict the transducer's MDP. By setting SNR=1 in Equation (4.40), it can be shown that the minimum detectable force per unit bandwidth in the coupling medium is:

$$MDF = \sqrt{2Z_1 k_B T_A} \tag{4.41}$$

Since power = force^2 / impedance:

$$MDP = \frac{MDF^2}{Z_1} \tag{4.42}$$

and the minimum detectable power per unit bandwidth in the coupling medium is:

$$MDP = 2k_B T_A \tag{4.43}$$

Equation (4.43) indicates that, for a lossless open circuit transducer, the MDP is independent of the front face transmission coefficient. It also indicates that the MDP per unit bandwidth is less than the noise power per unit bandwidth which is $4k_B T_A$. It would not be difficult to conclude from these results that an error has been made in the mathematical manipulation. For now, a numerical analysis will be used to show that this is unlikely. The full meaning of these results will be revealed in Chapter 6.

4.4.3 *Numerical Signal to Noise Ratio*

The accuracy of Equation (4.40) can be checked by running the LSNM in order to obtain some test results for SNR. Any significant difference between values obtained in this way and values obtained using Equation (4.40) would indicate that the derivation of Equation (4.40) was incorrect. Results obtained using a Mathcad version of the

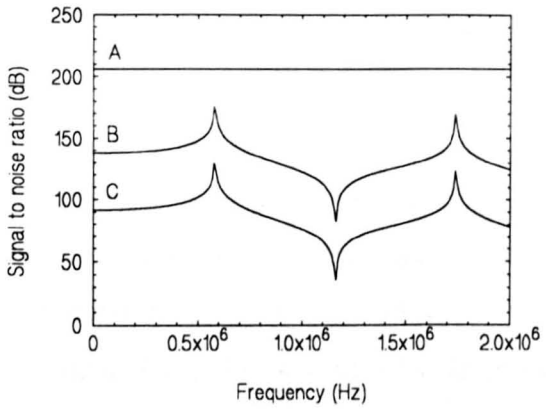

FIGURE 4.10 [A] SNR, [B] NOISE VOLTAGE (NOT TO SCALE) AND [C] TRANSFER FUNCTION (NOT TO SCALE) FOR AN OPEN CIRCUIT TRANSDUCER IN AIR

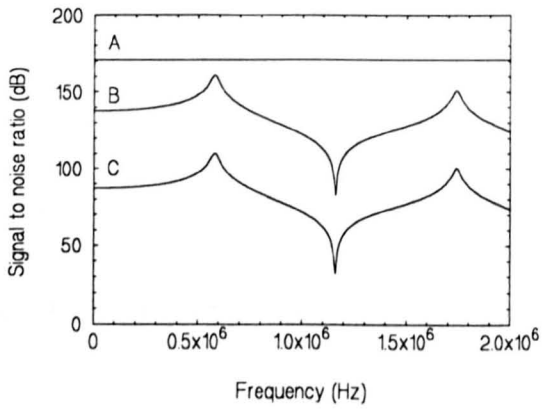

FIGURE 4.11 [A] SNR, [B] NOISE VOLTAGE (NOT TO SCALE) AND [C] TRANSFER FUNCTION (NOT TO SCALE) FOR AN OPEN CIRCUIT TRANSDUCER IN WATER

LSNM (see Appendix III) are illustrated in Figures 4.10 and 4.11. Here, the top line (A) in each graph represents the SNR at the output terminals of an open circuit transducer for an input force of 1 N. Also illustrated in each graph are the shapes (multiplying factors have been applied since the actual values are not important) of the force to voltage transfer function and the transducer's noise voltage spectrum. Both the air coupled results (Figure 4.10) and the water coupled results (Figure 4.11) show that, because the noise voltage tracks the transfer function, the signal to noise ratio is frequency independent. For air coupling the SNR is 206 dB and for water coupling it is 171 dB. Now, the acoustic impedance of air is 400 Rayl. So, for a transducer with a diameter of 30 mm, as was used in the Mathcad model, $Z_I = 400 \times 0.00071 = 0.28$. Using this in Equation (4.40) along with $F_S = 1$ N gives SNR = 206 dB which is identical to the result obtained using the Mathcad model. The acoustic impedance of water is 1.48 M Rayl. So, for a transducer with a diameter of 30 mm, as was used in the Mathcad model, $Z_I = 1480000 \times 0.00071 = 1051$. Using this in Equation (4.40) along with $F_S = 1$ N gives SNR = 171 dB which is again identical to the result obtained using the Mathcad model. These two examples confirm the accuracy of Equation (4.40). It should be noted that the SNR values quoted here are very large partly because they are based on unity bandwidth noise and partly because a 1 N input force is very unrealistic.

4.5 An Alternative Approach

As will be discussed in Chapter 6, the intriguing results which are presented in Section 4.4 are now known to be correct and meaningful, however, they only apply under very special circumstances. Although the type of approach used in Section 4.4 might have provided a reasonably accurate description of how dry and liquid coupled devices (these experience a relatively high degree of external damping) perform, it does not provide a way of obtaining accurate SNR, MDP and MDF values for air coupled devices, for which external damping is insignificant. What is required is a new closed form solution for the LSNM which is based on a more realistic transducer specification. At an early stage in the research it appeared that it would be impossible to obtain such a solution, however, as discussed in Chapters 5 and 6, a method was later found. An alternative method of calculating transducer SNR, MDP and MDF has also been investigated and this will now be described.

4.5.1 Acoustic Noise

As previously noted, a fundamental concept which can be explained using either classical or quantum physics [74,75] is that the mean kinetic energy per degree of freedom associated with the random motion of the molecules in an ideal gas is $k_B T_A/2$ where k_B is Boltzmann's constant and T_A is the absolute temperature in degrees Kelvin. It was also noted that the free electrons in a solid behave in the same way as the molecules in an ideal gas. This thermal energy limits the absolute sensitivity of all detection systems whether they are intended to detect radio waves, light waves, acoustic vibrations or some other quantity. As illustrated in Figure 4.12, thermal noise is

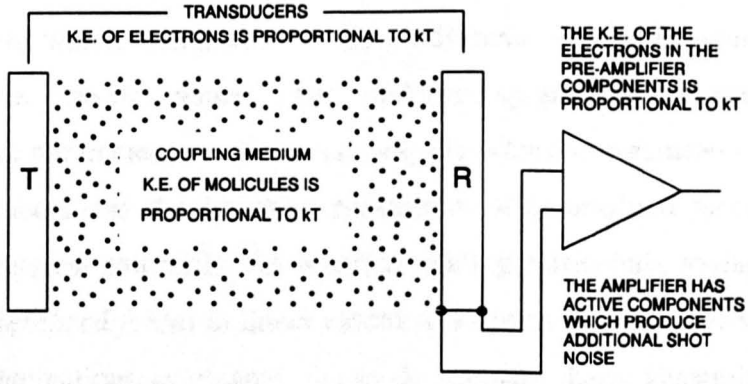

FIGURE 4.12 NOISE POWER IN THE VARIOUS ELEMENTS OF A RECEIVER SYSTEM

present in all of the elements of an ultrasonic test system and the noise power is proportional to $k_B T_A$. Nyquist, in his 1928 paper [77], showed that, in an electrical resistor, this results in a noise voltage which can be calculated using the Johnson noise equation. However, the random motion of the atoms, molecules, ions and free electrons in any material is fundamentally mechanical in nature and constitutes wideband acoustic noise. An ultrasonic transducer cannot distinguish between this acoustic noise and the acoustic signal which is transmitted through the boundary between the coupling medium and the transducer. Consequently, a transducer detects an acoustic signal in the presence of acoustic noise. In order to detect a signal, the acoustic signal power must exceed the mean acoustic noise power. It is obvious from the Johnson noise equation that the electrical noise power produced by a receiving transducer is:

$$P_N = 4k_B T_A B \tag{4.44}$$

where B is the bandwidth of the detection system. It may be less obvious that this equation also represents the acoustic noise power produced by the transducer. This can be explained using a generalized version of Nyquist's theorem.

4.5.2 *The Generalized Nyquist Theorem*

A generalized version of Nyquist's theorem is described by Callen and Welton in their paper entitled *Irreversibility and Generalized Noise* which was published in 1951 [86]. In this paper, Callen and Welton start by reviewing Nyquist's 1928 paper in which he derives what has become known as the Johnson noise equation. Their observations are summarised in the following paragraph.

The parameters which characterize a thermodynamic system in equilibrium do not generally have precise values, but undergo spontaneous fluctuations. These thermodynamic parameters are of two classes: the *extensive* parameters such as volume and mole numbers and the *intensive* parameters or *generalized forces*, such as the pressure or chemical potentials. An equation relating particularly to the fluctuations in voltage (a *generalized force*) in linear electrical systems has been derived by Nyquist. The voltage fluctuations are related, not to the standard thermodynamic parameters of a system, but to the electrical resistance. The Nyquist equation is thus a form unique in physics, correlating a property of a system in *equilibrium* (i.e., the voltage

fluctuations) with a parameter which characterizes an irreversible process (i.e., the electrical resistance). The equation, furthermore, gives not only the mean square fluctuating voltage, but provides, in addition, the frequency spectrum of the fluctuations. The proof of the relation is based on an ingenious union of the second law of thermodynamics and a direct calculation of a particularly simple system (an ideal transmission line).

Having made these observations, Callen and Welton proceed to show that the Nyquist relation can be extended to a general class of dissipative systems other than merely electrical systems. The general theorem, which is sometimes referred to as the *Fluctuation Dissipation Theorem*, thus establishes a relationship between the *impedance* in a general linear dissipative system and the fluctuations of appropriate generalized *forces*. In this context, a system may be said to be dissipative if it is capable of absorbing energy when subjected to a time-periodic perturbation. An electrical resistor absorbing energy from an impressed periodic voltage is the best known example. The system may be said to be linear if the power dissipation is quadratic in the magnitude of the perturbation. For a linear dissipative system, an impedance may be defined and the proportionality constant between the power and the square of the perturbation amplitude is simply related to the impedance.

Callen and Welton provide several fascinating illustrative applications of the theorem in their paper. For example, the viscous drag of a fluid on a moving body is shown to imply a fluctuating force, and application of the theorem immediately yields the fundamental results of the theory of Brownian motion. Application of the theorem also yields the Plank radiation law. Finally, the existence of an acoustic radiation impedance of a gaseous medium is shown to imply pressure fluctuations which may be related to the thermodynamic properties of the gas. The theorem thus correlates a number of known effects under one general principle and is able to predict a class of new relations. By applying the Callen and Welton theorem to a solid object, it follows that the mean square force fluctuations are given by:

$$F_N^2 = 4k_B T_A Re(Z_M) B \tag{4.45}$$

Here, $Re(Z_M)$ is the real part of the complex mechanical impedance, Z_M.

4.5.3 *Minimum Detectable Transducer Force*

Equation (4.45) can be applied to the piezoceramic transducers which are of interest in this Thesis. Thus:

$$MDF_T = (4k_B T_A Re(Z_M) B)^{1/2} \tag{4.46}$$

Here, the T subscript has been used to emphasise the fact that this is the minimum detectable force on the transducer side of the boundary with the coupling medium. In Section 4.3.1 it was shown that for a simple plate vibrating in the thickness mode, the real part of the mechanical impedance is given by Equation (4.11). That is:

$$Z_R = \frac{4}{\pi} \frac{Z_C}{Q_M} \tag{4.47}$$

Here, $Z_C = AZ_{CHA}$ where Z_{CHA} is the characteristic acoustic impedance of the plate and A is its area. Q_M is the plate's mechanical quality factor. Using Equation (4.47) to substitute for $Re(Z_M)$ is Equation (4.46) gives the following expression for the minimum detectable force on the transducer side of the boundary with the coupling medium:

$$MDF_T = \left(\frac{16 k_B T_A Z_C B}{\pi Q_M} \right)^{1/2} \tag{4.48}$$

4.5.4 *Minimum Detectable Power within a Transducer*

From Equation (4.45) it follows that the acoustic noise power is:

$$P_N = \frac{F^2}{Re(Z_M)} = 4k_B T_A B \tag{4.49}$$

So, by using the Callen and Welton theorem or, as will be shown later, by direct application of the laws of solid state physics, it is possible to show that Equation (4.44) represents the acoustic or mechanical noise power produced by a transducer as well as the electrical noise power. From this analysis it is clear that it is not really necessary to refer to the noise power as acoustical, mechanical or electrical, it is simply the noise power. Equation (4.49) also represents the MDP within the transducer. Thus:

$$MDP_T = 4k_B T_A B \tag{4.50}$$

Equation (4.50) is independent of structure and can be applied directly to a transducer. So, noting that k_B=1.38 x 10^{-23} and that, at normal room temperature, T_A=293 K:

$$MDP_T = 1.62\times10^{-20} \quad W/\sqrt{Hz} \tag{4.51}$$

This result can also be obtained directly using the laws of modern solid state physics.

4.5.5 Minimum Detectable Displacement

Some investigators who work with sound detection devices express absolute sensitivity in terms of minimum detectable surface displacement (MDD_T). This can be useful when, for example, comparing theoretical results with ones obtained by experiment. The MDD_T can be calculated as follows. When an ultrasonic transducer detects a signal, the particles of the transducer material are caused to vibrate such that their displacement is given by:

$$x = x_0 \sin(\omega t - \phi) \tag{4.52}$$

Here, x_0 is the amplitude of the particle displacement. The particle velocity is given by:

$$v = \frac{dx}{dt} = x_0 \omega \cos(\omega t - \phi) \tag{4.53}$$

From this it can be seen that the amplitude of the particle velocity is:

$$v_0 = x_0 \omega \tag{4.54}$$

For thermally generated fluctuations:

$$v_0 = \sqrt{\frac{P_N}{Re(Z_M)}} \tag{4.55}$$

where P_N is the thermal noise power within in the supporting medium. Combining Equations (4.54) and (4.55) gives:

$$x_0 = \frac{v_0}{\omega} = \frac{1}{\omega}\sqrt{\frac{P_N}{Re(Z_M)}} \tag{4.56}$$

As discussed previously, the noise power is given by $P_N = 4k_BT_AB$. Thus, noting that the minimum detectable displacement (MDD_T) is equal to the amplitude of the particle

displacement (x_0):

$$MDD_T = \frac{1}{\omega}\sqrt{\frac{4k_BT_AB}{Re(Z_M)}} = \frac{1}{\pi f}\sqrt{\frac{k_BT_AB}{Re(Z_M)}} \qquad (4.57)$$

Substituting for $Re(Z_M)$ from Equation (4.11) gives the following expression for a simple plate vibrating in the thickness mode:

$$MDD_T = \frac{1}{f}\sqrt{\frac{Q_Mk_BT_AB}{4\pi Z_C}} \qquad (4.58)$$

Now consider a typical piezoelectric plate transducer with a characteristic acoustic impedance (Z_{CHA}) of 34 M Rayl and a mechanical quality factor (Q_M) of 75. For a 30 mm diameter area, $Z_C=\rho cA=2.4 \times 10^4$. These figures have been used in Equation (4.58) to obtain a graph of the MDD_T per unit bandwidth. This graph, which is illustrated in Figure 4.13, indicates that for a centre frequency (f) of 600 kHz the MDD_T per unit bandwidth is 1.7×10^{-18} m/√Hz. For a bandwidth (B) of 10 kHz this corresponds to an MDD_T of 1.7×10^{-16} m. It is interesting to note that, from the rare gases to the alkali metals, atomic diameters are in the 0.6×10^{-10} to 5.5×10^{-10} m range [87]. So, the predicted displacements are insignificant compared to the atomic spacing.

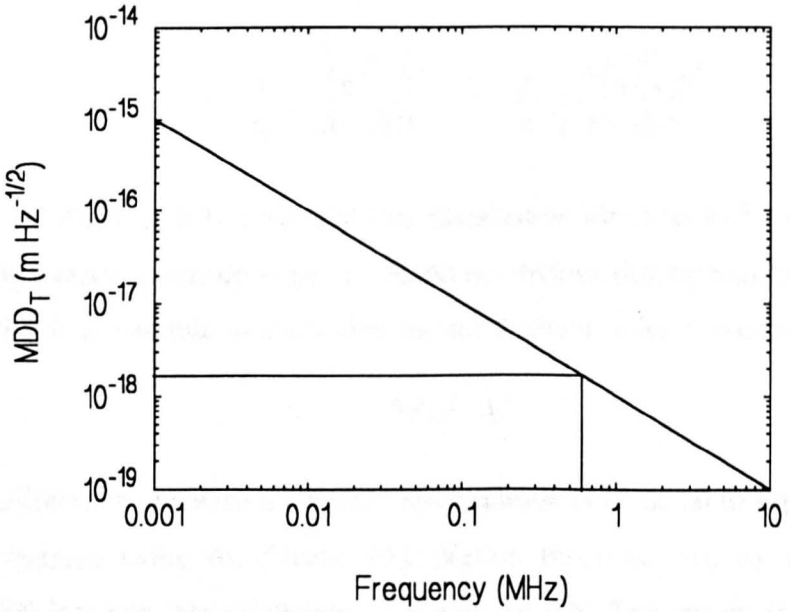

FIGURE 4.13 MINIMUM DETECTABLE DISPLACEMENT PER UNIT BANDWIDTH FOR A 30mm DIAMETER PLATE TRANSDUCER MADE FROM PZT-5A PIEZOCERAMIC MATERIAL

4.5.6 *Obtaining the Minimum Detectable Displacement Directly*

The theoretical result for MDD_T obtained in the previous Section is of particular significance because Equation (4.57) is identical to an equation which appears in a paper on absolute sensitivity limits which was recently published by Boltz *et al.* [88]. In this paper Equation (4.57) is obtained using a totally different approach to the one which has just been used here. According to Boltz *et al.*, the mean square displacement of the atoms in a cubic lattice was calculated by Debye [89] and Waller [90] using the laws of classical physics and by Ott [91] using a rigorous quantum mechanical approach. This thermal limit is given by Maradudin *et al.* [92] as:

$$\langle \delta_{\infty}^2 \rangle = \left(\frac{h}{4\pi M}\right)\frac{1}{3N}\sum_{kj}\frac{1}{\omega_j(k)}\coth\left(\frac{h\omega_j(k)}{4\pi k_B T_A}\right) \tag{4.59}$$

Here, δ is the displacement, h is Plank's constant, M is the atomic mass, k are the phonon wave vectors, ω is the phonon angular frequency, k_B is Boltzmann's constant, T_A is the absolute temperature in degrees Kelvin, N is the number of phonon modes and the subscript ∞ indicates that the equation is valid for an infinite solid. According to Boltz *et al.*, if the sum over k is replaced with integrals restricted to a corresponding real-space area on a half-space and only surface normal phonon components are considered, then, provided that $2\pi k_B T_A \gg h\omega$, this expression for the root mean square fluctuation reduces to:

$$\langle \delta_{min} \rangle = \frac{1}{\pi f}\sqrt{\frac{k_B T_A \Delta f}{Re(Z(f))}} = \frac{1}{\omega}\sqrt{\frac{4k_B T_A \Delta f}{Re(Z(f))}} \tag{4.60}$$

Since $\Delta f = B$ and $Z(f) = Z_M$ it is clear that this equation is identical to Equation (4.57), except for a difference in terminology. It should be obvious that by working back from Equation (4.60) it is possible to show that the mechanical noise power is given by:

$$P_N = 4k_B T_A \Delta f \tag{4.61}$$

Except for a difference in notation ($\Delta f = B$), this equation is identical to Equation (4.49) which was obtained using the Callen and Welton theorem. So, by starting with Equation (4.59) it is possible to confirm Equation (4.49). This means that one of the key results in this Thesis can also be arrived at using the laws of quantum mechanics. It is interesting to note from the paper by Maradudin *et al.* that Equation (4.59) was

derived in order to provide an explanation of effects which are observed in x-ray and neutron scattering experiments. For example, the scattering or reflection of waves by a perfectly periodic lattice gives rise to a sharp interference pattern when the wavelength of the incident radiation is of the order of the lattice spacing. Random vibrations in the separation distance between members of atomic pairs lead to more diffuse patterns and the broadening of x-ray lines. It was never anticipated that Equation (4.59) would also be used to solve problems in ultrasonics.

4.5.7 Summary

Equations (4.44) and (4.45) can be applied to any type of transducer. For example, Tarnow has used this approach to calculate the absolute sensitivity of a condenser microphone [93]. This work is described in his paper entitled *The Lower Limit of Detectable Sound Pressure* which was published in the Journal of the Acoustical Society of America in July 1987. It is now clear that the material parameters of a transducer are of no significance in calculating its minimum detectable power. For a given temperature, all transducers produce exactly the same thermal noise power. As illustrated in Figure 4.12, no matter what a transducer is made from or how it is structured, the noise power is the same and this is also true of the coupling medium which could be a solid, a liquid or a gas. Also, the electrical impedance characteristics of the transducer and the amplifier components have no bearing on this component of the noise power, however, as will be discussed in Chapter 7, the amplifier is constructed from active components which do produce additional noise.

4.5.8 Minimum Detectable Power in the Coupling Medium

Having found a way to calculate the minimum detectable power (MDP_T) within a transducer, the minimum detectable power (MDP) in the coupling medium can be found by taking into account the power transmission coefficient. Suppose that the mean signal power in the coupling medium is P_{SM}. Using Equation (4.16), the signal power transmitted into the transducer is:

$$P_{ST} = \left[\frac{4Z_R Z_1}{(Z_R + Z_1)^2}\right] P_{SM} \qquad (4.62)$$

Here, Z_1 is the acoustic impedance of the coupling medium and Z_R is the real part of

the transducer's mechanical impedance. It should be noted that $Z_I = Z_A A$ where, for air, $Z_A = 400$ Rayl. The power signal to noise ratio within the transducer is:

$$SNR = \frac{P_{ST}}{P_N} = \frac{1}{4k_B T_A B}\left[\frac{4Z_R Z_1}{(Z_R + Z_1)^2}\right] P_{SM} \tag{4.63}$$

It follows that the minimum detectable power in the coupling medium (SNR=1) is:

$$MDP = \frac{(Z_R + Z_1)^2 k_B T_A B}{Z_R Z_1} \tag{4.64}$$

For a simple plate vibrating in the thickness mode, the real part of the transducer's mechanical impedance (Z_R) can be found using Equation (4.11) i.e. $Z_R = 4Z_C/\pi Q_M$.

Best Possible MDP

If Z_R is matched to the acoustic impedance of the coupling medium then $Z_R = Z_I$ and:

$$MDP_0 = 4k_B T_A B \tag{4.65}$$

The value of Boltzmann's constant is 1.38×10^{-23} JK^{-1}. Hence at normal room temperature (293 K) the transducer's minimum detectable power, as would be measured in the coupling medium, is:

$$MDP_0 = 1.62 \times 10^{-20} \quad W/Hz \tag{4.66}$$

This represents the absolute limit of transducer MDP. If Z_R is either less than or greater than the acoustic impedance of the coupling medium then the MDP is impaired.

Air Coupled MDP

For air coupling and for the transducers which are of interest in this research, the real part of the transducer's mechanical impedance will always be significantly greater than the acoustic impedance of the coupling medium. This means that it is possible to make the following very accurate approximation:

$$MDP = \frac{Z_R k_B T_A B}{Z_1} \tag{4.67}$$

Combining this with Equation (4.11) gives:

$$MDP = \frac{4k_B T_A Z_C B}{\pi Q_M Z_1} \tag{4.68}$$

where Q_M is the transducer's mechanical quality factor. Equations (4.67) and (4.68) are apparently very different from Equation (4.43) which was obtained using the Linear Systems Noise Model. The new results indicate that the MDP of a typical air coupled piezoelectric transducer will be poor compared to the theoretical limit predicted by Equation (4.65). However, it can now be seen that, as would be expected, it is possible to improve the absolute sensitivity (MDP) of a transducer by arranging for Z_R/A, to be closer to the acoustic impedance of the coupling medium which surrounds it. The absolute sensitivity can also be improved by increasing Q_M.

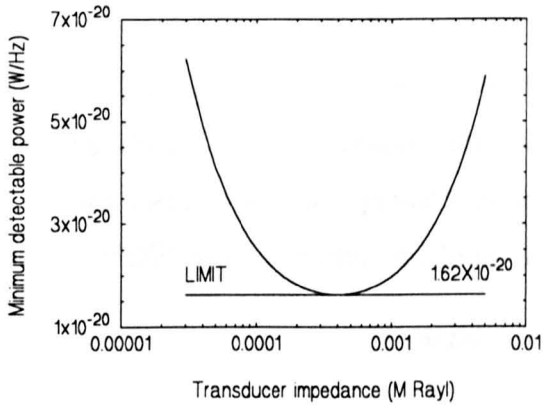

FIGURE 4.14 MDP OF A TRANSDUCER FOR WHICH Z_R/A IS CLOSE TO THE ACOUSTIC IMPEDANCE OF AIR

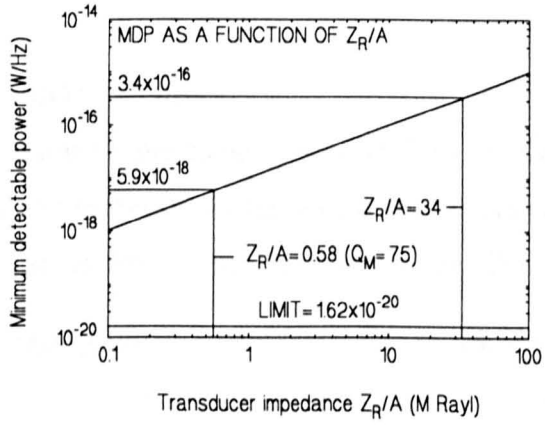

FIGURE 4.15 MDP OF A TRANSDUCER FOR WHICH Z_R/A IS CLOSE TO THAT OF A TYPICAL PIEZOELECTRIC DEVICE

As previously mentioned, the acoustic impedance of air (Z_A) is 400 Rayl. The graph which is shown in Figure 4.14 and which was produced using Equation (4.64), shows how the MDP of a transducer, for which Z_R/A is close to the acoustic impedance of air, varies as a function of Z_R/A. Obviously, values of Z_R/A which are less than 400 Rayl are completely hypothetical and the same is probably true for values which are not much greater than 400 Rayl. For most practical ultrasonic transducers Z_R/A is much greater than the acoustic impedance of air. The graph which is shown in Figure 4.15, which was also produced using Equation (4.64), shows how the MDP of a transducer varies as a function of Z_R/A for a range of values which might be possible for a practical piezoelectric plate transducer. Consider a typical piezoceramic plate transducer with a characteristic acoustic impedance (Z_{CHA}) of 34 M Rayl and a mechanical quality

factor (Q_M) of 75. For this transducer Equation (4.11) indicates that Z_R/A has a value of 0.58 M Rayl and by using this in Equation (4.64) the air coupled MDP is found to be 5.9 x 10^{-18} W/Hz. This value is represented by the middle horizontal line in Figure 4.15. It is a factor of 364 worse than the thermally limited sensitivity of a transducer which is impedance matched to the surrounding coupling medium. The bottom horizontal line in Figure 4.15 represents the MDP of an impedance matched transducer. If it were possible to leave the transducer's characteristic acoustic impedance (Z_{CHA}) unchanged at 34 M Rayl and reduce its Q_M to a value of $4/\pi$ then Z_R would also be 34 M Rayl and the transducer's MDP in air would be 3.4 x 10^{-16} W/Hz. This value is represented by the top horizontal line in Figure 4.15. It is a factor of 2.1 x 10^4 worse than the thermally limited sensitivity of a transducer which is impedance matched to the surrounding coupling medium.

4.5.9 Minimum Detectable Force in the Coupling Medium

Having obtained an expression for the minimum detectable power (MDP) in the coupling medium it is now possible to obtain an expression for the minimum detectable force (MDF) in the coupling medium. This can be done using Equation (4.13). Thus:

$$MDF = (MDP\, Z_1)^{1/2} \tag{4.69}$$

or from Equation (4.64):

$$MDF = \left[\frac{(Z_R+Z_1)^2\, k_B T_A B}{Z_R}\right]^{1/2} = (Z_R+Z_1)\left[\frac{k_B T_A B}{Z_R}\right]^{1/2} \tag{4.70}$$

For a simple plate transducer vibrating in the thickness mode, Z_R can be found using Equation (4.11) i.e. $Z_R=4Z_C/\pi Q_M$.

Best Possible MDF

From Equation (4.70) it can be seen that the best possible transducer MDF is achieved with $Z_R=Z_1$. Hence:

$$MDF_0 = \sqrt{4 k_B T_A Z_A A B} \tag{4.71}$$

As previously mentioned, the acoustic impedance of air (Z_A) is 400 Rayl. So, for a 30 mm diameter air coupled transducer the best possible minimum detectable force is:

$$MDF_0 = 6.8\times10^{-11} N/\sqrt{Hz} \tag{4.72}$$

Air Coupled MDF

Provided that $Z_R \gg Z_I$, Equation (4.70) approximates very accurately to:

$$MDF = \left[k_B T_A Z_R B\right]^{1/2} \tag{4.73}$$

This equation could have been obtained directly by noting that the force fluctuations within the transducer are given by $F_N=(4k_BT_AZ_R)^{1/2}$ and that for air coupling the force transmission coefficient is almost exactly 2. Using Equation (4.11) to substitute for Z_R in Equation (4.73) leads to the following expression for the minimum detectable force per unit bandwidth:

$$MDF = \sqrt{\frac{4k_B T_A Z_C}{\pi Q_M}} \tag{4.74}$$

This very important equation provides the means by which it is possible to predict the absolute sensitivity of an air coupled piezoelectric receiving transducer. In Chapter 6 it will be shown that it is possible to obtain an identical result using an extensively modified version of the Linear Systems Model.

A graph of MDF has been plotted using Equation (4.70) and this is illustrated in Figure 4.16. It shows how the MDF per unit bandwidth varies as a function of Z_R/A for a 30 mm diameter transducer. Consider a typical transducer with a characteristic acoustic impedance (Z_{CHA}) of 34 M Rayl, a diameter of 30 mm and a mechanical quality factor (Q_M) of 75. It follows from Equation (4.70) that for this transducer the MDF in air is 1.3 x 10^{-9} N/√Hz. This value is

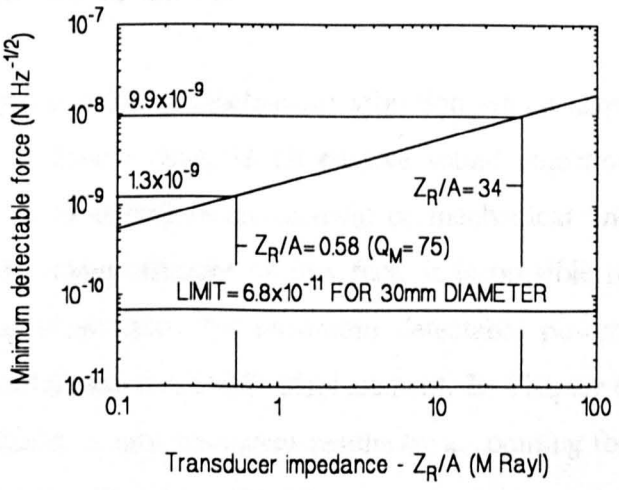

FIGURE 4.16 MDF PER UNIT BANDWIDTH AS A FUNCTION OF Z_R/A FOR A 30mm DIAMETER TRANSDUCER

represented by the middle horizontal line in Figure 4.16. This value is a factor of 19 worse than the thermally limited sensitivity of a transducer which is impedance matched to the surrounding coupling medium. If it were possible to leave the transducer's characteristic acoustic impedance (Z_{CHA}) unchanged at 34 M Rayl and reduce its Q_M to a value of $4/\pi$ then Z_R would also be 34 M Rayl and the transducer's MDF in air would be 9.9×10^{-9} N/$\sqrt{\text{Hz}}$. This value is represented by the top horizontal line in Figure 4.16. It is a factor of 146 worse than the thermally limited sensitivity of a transducer which is impedance matched to the surrounding coupling medium.

4.6 Conclusions

4.6.1 The Goal

The single goal of this part of the research was to investigate thermal noise in an open circuit piezoelectric transducer with a view to establishing a theory which would allow the prediction of signal to noise ratio (SNR), minimum detectable power (MDP), minimum detectable force (MDF) and minimum detectable displacement (MDD). Mathematical relationships for SNR, MDP, MDF and MDD have been obtained using a mechanical approach but, as yet, these have not been shown to be consistent with corresponding relationships obtained using the Linear Systems Model (LSM). In Chapter 5 an extensively modified version of the LSM is developed and in Chapter 6 this is used to show that the LSM results are consistent with those presented here.

4.6.2 Principal Findings and Achievements

The principal findings and achievements are as follows:

- The fundamental origin of thermal noise is mechanical vibration which takes place on a microscopic scale. It follows that, in all passive sound detection devices, the noise source can be modelled as an acoustic or mechanical one instead of an electrical one. By taking account of this fact, it is possible to arrive directly at mathematical expressions for minimum detectable power, minimum detectable force and minimum detectable displacement. In Chapter 6 it will be shown that it is possible to obtain consistent results by accounting for a transducer's *electrical* noise using Johnson's equation.

- Thermal noise is a property, not only of the receiving transducer, but also the surrounding medium and any amplifier components which are attached to the transducer. Thermal noise is even produced in the transmitting transducer along with the required signal vibrations.

- It is not possible to distinguish between signal vibrations and thermal vibrations in any part of a sound transmission system. As a consequence, the acoustic or mechanical signal to noise ratio is constant with respect to frequency in all parts of the system. This is true in the transmitting transducer, the coupling medium and the receiving transducer.

- Because a sound detection device cannot distinguish between particle vibrations which are of thermal origin and particle vibrations which are produced by any other sound generator, it is to be expected that the voltage signal to noise ratio across the terminals of a resonant open circuit receiving transducer will also be constant with respect to frequency. Mechanical resonances associated with the shape and size of the transducer will have the same influence on both the signal vibrations and the thermal vibrations. In Chapter 6, an extensively modified version of the LSM will be used to investigate this feature in detail.

- As a consequence of the above findings it is possible to state that the absolute sensitivity of an open circuit receiving transducer, expressed in terms of minimum detectable power (MDP) or minimum detectable force (MDF) is constant with respect to frequency. This will also be investigated in detail in Chapter 6 using the extensively modified version of the LSM.

- There is no such thing as low noise receiving transducer. For a given temperature, all receiving transducers produce the same noise power. Also, all transducers which have the same characteristic acoustic impedance produce the same r.m.s. force fluctuations. The voltage noise spectrum which is observed across the terminals of an open circuit receiving transducer is a function of the shape and size of the transducer. That is, the spectrum is a function of the transducers mechanical resonances.

- It is interesting to note that the thermally limited sensitivity of an open circuit receiving transducer does not depend on its electromechanical coupling coefficient. Again, this is because the transducer cannot distinguish between signal vibrations and thermal vibrations.

4.6.3 Concluding Summary

At the start of this investigation it was obvious that, as with all detection systems, the absolute sensitivity of an ultrasonic transducer would be limited by thermal noise. From a personal point of view, the best approach appeared to be to look at how the noise voltage generated by other electroceramic devices such as ceramic capacitors and pyroelectric detectors can be calculated. This approach supported the interests of colleagues within the Ultrasonics Research Group (URG) who believed that it might be possible to identify certain ceramic material parameters which could be selected or controlled in order to allow the design of *low noise ultrasonic transducers*. It soon became clear that the only ceramic parameter which influences the noise voltage produced by an electroceramic device is $tan\delta$. For the small values of δ which are typical of piezoelectric materials such as PZT-5A, the $tan\delta$ parameter provides a simple way of calculating the real part of the complex electrical impedance and hence the thermal noise voltage produced by a particular device. A low value of $tan\delta$ is the key to the successful design of, for example, low noise ceramic capacitors and sensitive pyroelectric detectors.

Because of electromechanical interaction in poled electroceramic materials, it is not possible to use the $tan\delta$ parameter to calculate the voltage noise spectral density of a transducer, however, it did appear that a perfectly reasonable approach would be to use the real part of the complex electrical impedance in the Johnson noise equation. This is the approach which is used in the design of low noise electronic devices such as transistors. An exciting feature of this approach was that the URG is in the fortunate position of having available to it a Linear Systems Model (LSM) which is capable of predicting the electrical impedance of thickness mode piezoelectric transducers. At this stage in the work other researchers in the URG had already modified the LSM in such a way that it was possible to obtain the real part of the complex electrical impedance. This was then used in the Johnson noise equation to simulate a transducer's voltage

noise generator. The Linear Systems Noise Model (LSNM), as it became known, was organised in such a way that it took account of, not only the transducers voltage noise generator, but also an amplifier voltage noise generator and an amplifier current noise generator. During the course of this investigation it became evident that the LSNM had never been tested with both of these noise generators set to zero in order to determine what the transducer was doing by itself. When the author of this Thesis set the amplifier noise sources to zero it was found that the LSNM was predicting that the voltage signal to noise ratio (SNR) at the transducer terminals would be constant with respect to frequency. It is now known that this is to be expected, however, there was another problem. On further inspection of the results for an open circuit transducer it was found that the LSNM was also predicting that the thermally limited sensitivity of the transducer was, not only constant with respect to frequency, but that the values of minimum detectable force (MDF) and minimum detectable power (MDP) in the coupling medium would be many orders of magnitude better than is possible. This was established by comparing the MDP results with a direct calculation of thermal noise power. The LSNM was tested further by using the equations from which it is constructed to obtain closed form solutions for the SNR, MDF and MDP. These solutions were found to give results which appeared not to be consistent with values obtained by other means. Chapter 6 is partly dedicated to explaining the initial LSNM results.

An alternative to the LSNM approach involved looking in detail at the thermodynamic origins of the Johnson noise equation. This involved reviewing Johnson's experimental work and Nyquist's theoretical work. While doing this it was discovered that Nyquist's theory is in fact only one example of a more general theory. This generalized theory, which dates back to before 1951, is the work of Callen and Welton. By using the principles discussed by Callen and Welton it was found that it is possible to immediately write down an expression for the root mean square force fluctuations per unit bandwidth produced by any sound detection device:

$$F_N^2 = 4k_B T_A Re(Z_M)$$

Here, k_B is Boltzmann's constant (1.38×10^{-23} J K^{-1}), T_A is the absolute temperature (normal room temperature is 293 K) and $Re(Z_M)$ is the real part of the devices

mechanical impedance. This equation is the mechanical equivalent of the Johnson noise equation. Clearly, since force is equivalent to voltage and mechanical impedance is equivalent to electrical impedance, the existence of such a relationship could have been postulated simply by drawing an analogy with the electrical version. However, the Callen and Welton treatment is a rigorous one which predicts not only this relationship but many others. Clearly, F_N also represents the minimum detectable force (MDF_T) on the transducer side of the fluid/transducer boundary. Also, it follows directly that the minimum detectable power per unit bandwidth within the transducer is:

$$MDP_T = 4k_B T_A$$

It is also possible to obtain this result directly from the laws of modern quantum physics. From this equation it can be seen that the absolute limit of minimum detectable power for any sound detection device is:

$$MDP_0 = 1.62 \times 10^{-20} \quad W/Hz$$

This limit is a property of a transducer's environment as well as of the transducer itself.

Chapter 5

AN AIR COUPLED TRANSDUCER MODEL

5.1 Introduction

This Chapter can be regarded as an essential prelude to the development of the Receiver Noise Model (RNM) which is described in Chapter 6. The Air Coupled Transducer Model (ACTM) described here has been developed for use with receiving transducers which are both air coupled and air backed. A major feature of this model is its ability to account for a transducer's mechanical quality factor, Q_M, which is one of the most important parameters associated with an air coupled receiver.

5.1.1 Background

A transducer's mechanical quality factor, Q_M, is a measure of its intrinsic mechanical damping and it is quoted by most manufacturers of piezoelectric materials as an important figure of merit. For example, Morgan Matroc quote the values of Q_M for PZT-5A and PZT-5H as 75 and 65 respectively. The significance of intrinsic mechanical damping was previously discussed in Section 4.2.3 along with the electrical quality factor, Q_E, which is equal to $1/tan\delta$. Unfortunately, the Linear Systems Model (LSM) does not account for the existence of either of these transducer quality factors. The reason for this is that the LSM was originally developed for use with liquid and dry coupled transducers. With these devices the main cause of mechanical damping is contact with the coupling medium itself, and in many cases intrinsic damping is found to be almost insignificant. However, with air coupled transducers the situation is reversed. In this case external mechanical damping is totally insignificant and intrinsic mechanical damping is of major importance. In this Chapter it will be shown that it is possible to define another quality factor, Q_T, which is a measure of mechanical damping due to the transmission of sound back into the coupling medium which surrounds a transducer. For a typical 34 MRayl transducer used to detect sound in air, the value of Q_T is 54,000. The fact that this value is almost three orders of magnitude greater than typical values of Q_M indicates that Q_M is much more important than Q_T when using a piezoceramic or piezocomposite transducer to detect ultrasound in air. Because of the importance of Q_M in this work it was found necessary to find a way of incorporating it into the LSM. In the process of doing this it became evident that it is possible to produce a version of the LSM which can be represented by a very neat and compact set of mathematical functions. As will be discussed in Chapter 6, this greatly simplifies the development of a Receiver Noise Model (RNM).

5.2 *Mechanical Resonance*

The fundamental properties of a damped mechanical oscillator can be explained using the simple model illustrated in Figure 5.1. Here, a mass m is being subjected to a

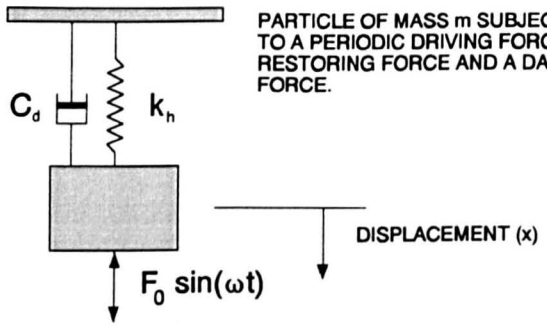

FIGURE 5.1 MODEL OF A DAMPED MECHANICAL OSCILLATOR

periodic driving force $F_0 sin(\omega t)$ and a restoring force $k_h x$, provided by a spring. It should be obvious that the restoring force obeys Hook's law. The model includes a velocity dependent damping force $c_d(dx/dt)$. Here, k_h is known as the spring constant and c_d is known as the damping constant. Applying Newton's second law, *force equals mass times acceleration*, leads to the following differential equation:

$$m\frac{d^2x}{dt^2} = -k_h x - c_d\frac{dx}{dt} + F_0 \sin\omega t \tag{5.1}$$

or:

$$m\frac{d^2x}{dt^2} + k_h x + c_d\frac{dx}{dt} = F_0 \sin\omega t \tag{5.2}$$

The solution to this differential equation is [94]:

$$x = x_0 \sin(\omega t - \phi) \tag{5.3}$$

where:

$$x_0 = \frac{F_0}{\sqrt{(c_d\omega)^2 + (k_h - m\omega^2)^2}} \tag{5.4}$$

and:

$$\phi = \tan^{-1}\left[\frac{2c_d\omega/c_c\omega_n}{1-\omega^2/\omega_n^2}\right] \tag{5.5}$$

Here, x_0 is the amplitude of the displacement and ϕ is the phase relative to the driving force. Also:

$$c_c = 2\sqrt{mk_h} = 2m\omega_n \tag{5.6}$$

where ω_n is the undamped natural frequency of the suspended mass. The constant c_c is the damping factor for critical damping.

5.2.1 *The Mechanical Quality Factor*

The result expressed by Equations (5.4) and (5.5) can also be written as follows:

$$x_0 = x_S\,|G(\omega)| \tag{5.7}$$

where:

$$|G(\omega)| = \left[\left(1-\frac{\omega^2}{\omega_n^2}\right)^2+\left(\frac{1}{Q_M}\cdot\frac{\omega}{\omega_n}\right)^2\right]^{-1/2} \tag{5.8}$$

and:

$$arg(G(\omega)) = \frac{\omega/Q_M\omega_n}{1-\omega/\omega_n} \tag{5.9}$$

It will also be found useful to note the following :

$$x_S = \frac{F_0}{k_h} \tag{5.10}$$

Here, x_S is the static displacement. This is the amount by which the mass would be displaced if a static force F_0 were to be applied to it. In the context of the current

investigation it is most important to note that:

$$Q_M = \frac{c_c}{2c_d} \tag{5.11}$$

Here, Q_M is known as the *mechanical quality factor* or the *mechanical damping factor*. This was mentioned previously in Section 4.2.3. Clearly Equation (5.8) represents the gain in displacement that is obtained at or close to resonance. Using Equations (5.8) and (5.9) it is not difficult to show that:

$$G(R) = \left[(1 - R^2) - j\left(\frac{R}{Q_M}\right)\right]^{-1} \tag{5.12}$$

where $R = \omega/\omega_n$ and $j = \sqrt{-1}$. Here, R is the signal frequency relative to the natural resonance frequency. The magnitude of $G(R)$ is plotted in Figure 5.2 for six values of Q_M. Corresponding curves for the argument of $G(R)$ are plotted in Figure 5.3. Equation (5.12) can be applied to many different types of resonator including the ultrasonic transducers which are of interest here. From Figure 5.2, or any similar set of gain curves, it can be seen that as the signal frequency approaches zero, the gain in particle displacement tends towards unity but as the signal frequency tends towards the thickness mode resonance frequency, the gain in particle displacement tends towards Q_M. In a piezoelectric transducer an increase in particle displacement corresponds to a proportional increase in signal voltage across the terminals of the device. As will be discussed in detail later, curves similar to those in Figure 5.2 can be used to find the

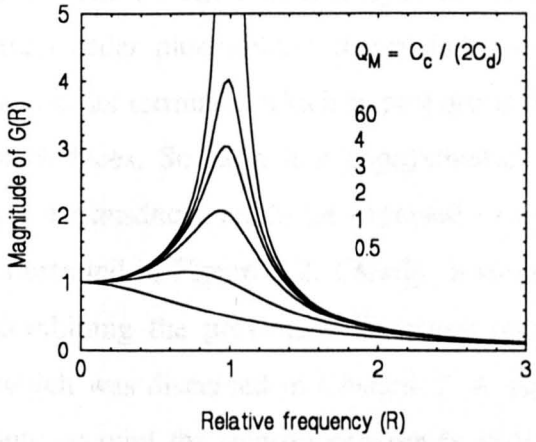

FIGURE 5.2 MAGNITUDE OF GAIN FACTOR AS A FUNCTION OF RELATIVE FREQUENCY

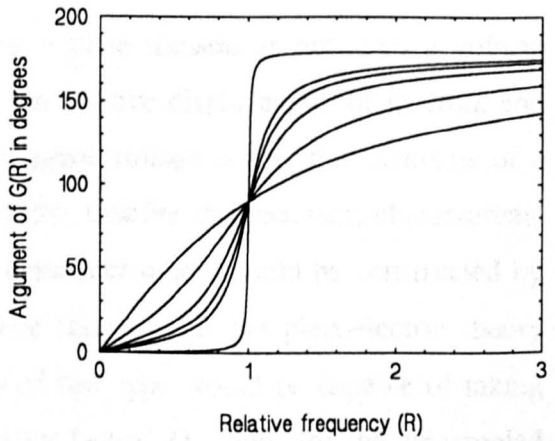

FIGURE 5.3 ARGUMENT OF GAIN FACTOR AS A FUNCTION OF RELATIVE FREQUENCY

relative sensitivity of a complete receiver system.

5.2.2 *Bandwidth*

An interesting property of Figure 5.2 is that the maxima of the various curves do not occur at $R = \omega/\omega_n = 1$ but at a lower frequency which depends on the amount of mechanical damping. In fact, in the case of damped vibrations in an ultrasonic transducer there are three different frequencies which are of interest. These are the undamped natural frequency, the damped natural frequency and the frequency of maximum forced vibration which will be referred to here as the resonant frequency. For small values of mechanical damping these three frequencies are very close together. This is a valid assumption for the air coupled transducers of interest here. The bandwidth of an ultrasonic transducer can be defined as [82,95]:

$$B_M = f_2 - f_1 \tag{5.13}$$

Here, f_1 and f_2 are those frequencies on either side of f_n for which the signal amplitude is $1/\sqrt{2}$ of its maximum value. It is not difficult to show that [82,95]:

$$B_M = \frac{f_n}{Q_M} \tag{5.14}$$

From this equation it can be seen that as Q_M tends towards zero, B_M tends towards infinity and the transducer becomes less resonant. For a typical air coupled PZT-5A transducer with a centre frequency of 600 kHz and a Q_M of 75, the bandwidth is 8 kHz.

5.3 The Modified Linear Systems Model

First order piezoelectric theory indicates that a plate transducer produces a voltage across its terminals which is proportional to the relative displacement of its front and back faces. So, to a first approximation the signal voltage across the terminals of a plate transducer might be expected to follow the relative displacement characteristic illustrated in Figure 5.2. Clearly, a simple transducer model could be constructed by combining the previously discussed resonance theory with the piezoelectric theory which was discussed in Chapter 3. A model of this type would be capable of taking into account the transducer's mechanical quality factor, Q_M, and, for the air coupled work of interest here, this would be a very attractive feature. Unfortunately, this simple

model would have many deficiencies. For example, by solving the equation of motion for the system illustrated in Figure 5.1 it is only possible to take account of one degree of freedom. In other words, the approach does not allow for the fact that a transducer vibrating in the thickness mode will also resonate, with reduced amplitude, at odd harmonics of the fundamental resonance frequency. Also, as will be discussed in detail later, it is of great importance to know how a transducer's mechanical resonances are affected by connecting it to an electrical load. With these problems in mind, it can be seen that it is worth looking at the Linear Systems Model (LSM) again to see how it can be modified to take into account Q_M.

5.3.1 Intrinsic Mechanical Damping

The LSM can be used to obtain the equivalent of the gain factor which is represented by Equation (5.12) and which is plotted for various values of Q_M in Figure 5.2. In the LSM, the force to voltage transfer function is represented by Equation (4.17). Using this equation it is not difficult to show that, for an open circuit transducer, there is a finite response at zero frequency which depends on the amount of external damping [79]. If the acoustic impedance of the front face medium is the same as that of the back face medium then this zero frequency response is given by:

$$\frac{V_0(0)}{F_1(0)} = \frac{-k^2}{hC_0} = \frac{-hT}{Z_C} \qquad (5.15)$$

The various terms are defined in Section 4.4.1. From Equations (4.17) and (5.15) it follows that:

$$G(\omega) = \frac{V_0(\omega)}{V_0(0)} = \frac{T_F K_F U \,/\, j\omega T}{1 - Z_F(\tfrac{1}{2}K_F T_F + \tfrac{1}{2}K_B T_B)k^2 \,/\, j\omega T} \qquad (5.16)$$

For the transducers which are of interest in this research the front face coupling medium is air and the backing medium is also air. This means that $K_B = K_F$ and $T_B = T_F$. Hence:

$$G(\omega) = \frac{T_F K_F U \,/\, j\omega T}{1 - Z_F K_F T_F k^2 \,/\, j\omega T} \qquad (5.17)$$

As was the case in the simple resonance analysis, this new gain equation represents the

relative sensitivity of a plate transducer as a function of frequency. Unlike Equation (5.12), the new version takes account of both external mechanical damping and external electrical loading, however, it does not take account of intrinsic mechanical damping. In the case of an air coupled transducer, intrinsic mechanical damping is much more significant than external mechanical damping and a way must be found to account for it. One possible approach is as follows. If the transducer is operated under open circuit conditions then $Z_F=0$ and $U=1$. Hence:

$$G_0(\omega) = \frac{T_F K_F}{j\omega T} \tag{5.18}$$

Here, the *0* subscript is used to indicate the open circuit condition. Substituting from Equation (4.28) for the reverberation factor (version for $Z_1=Z_2$) gives:

$$G_0(\omega) = \frac{T_F}{j\omega T}\left[\frac{1 - e^{-j\omega T}}{1 + R_F e^{-j\omega T}}\right] \tag{5.19}$$

From Equations (4.21) and (4.23):

$$T_F = R_F + 1 \tag{5.20}$$

For convenience let:

$$R = \frac{f}{f_n} = \frac{\omega}{2\pi}\frac{1}{f_n} = \frac{\omega T}{\pi} \tag{5.21}$$

where f is the signal frequency, f_n is the fundamental thickness mode resonance frequency of the transducer and T is the time taken for a sound wave to travel from one face of the transducer to the opposite face. Substituting Equations (5.20) and (5.21) into Equation (5.19) gives:

$$G_0(R) = \frac{R_F+1}{j\pi R}\left[\frac{1 - e^{-j\pi R}}{1 + R_F e^{-j\pi R}}\right] \tag{5.22}$$

Equation (5.22) represents one way of expressing the relative sensitivity of a transducer as a function of the relative frequency R. Clearly the relative sensitivity at any given value of R depends entirely on the value of the reflection coefficient R_F. If R_F is less than unity then mechanical energy is transmitted into the surrounding medium, resulting

in damping of the transducer vibrations. At this stage it will be found useful to introduce a quality factor Q_T which performs a similar function to the quality factor Q_M which was discussed earlier. This factor will be used to quantify transducer damping due to transmission loss. The M subscript used previously indicates that Q_M is used to quantify intrinsic mechanical damping where energy is lost as heat. If the relative frequency, R, is 1 (i.e. $f=f_n$) then $G_O(R)=Q_T$ and it follows from Equation (5.22) that:

$$Q_T = \frac{2}{\pi}\left[\frac{1+R_F}{1-R_F}\right] \tag{5.23}$$

Substituting for R_F from Equation (4.23) reveals the following interesting relationship:

$$Q_T = \frac{2Z_C}{\pi Z_1} \tag{5.24}$$

where, Z_1 is the acoustic impedance of the coupling medium. Also, $Z_C=Z_{CHA}A$ where Z_{CHA} is the characteristic acoustic impedance of the transducer and A is its area. Equation (5.24) is in itself is a very useful and previously unknown relationship.

Consider a typical PZT-5A transducer with a characteristic acoustic impedance of 34 MRayl. When this transducer is used in an air coupled application it follows from Equation (5.24) that, since the acoustic impedance of air is 400 Rayl, Q_T=54,000. This exceptionally high figure indicates that the transducer would be very sharply resonant. For example, from Equation (5.14) it can be seen that, for a typical 600 kHz air coupled transducer, the transducer would have a very narrow bandwidth of 11 Hz. As previously noted, the actual bandwidth of a typical 600 kHz, PZT-5A, air coupled transducer is 8 kHz. This much wider bandwidth is a consequence of the fact that, for this typical device, Q_M=75.

The analysis which has been presented here provides the justification for modifying the LSM to accurately account for a transducer's intrinsic mechanical damping. Previous attempts at doing this have been made. For example, the version of the LSM which is currently being run on a Sun workstation at Strathclyde takes account of intrinsic mechanical damping by introducing an attenuation factor into Equations (4.19) and (4.20). This technique is demonstrated in Appendix III. By contrast with this method,

the value of Q_M for any standard transducer material can be obtained from the manufacturers data. For composite materials the value of Q_M can be obtained by making simple bandwidth measurements using an impedance analyzer. It will now be shown that it is possible to modify the LSM to take account of Q_M. Rearranging Equation (5.23) gives:

$$R_F = \frac{Q_T\pi - 2}{Q_T\pi + 2} \tag{5.25}$$

Combining Equations (5.22) and (5.25) gives:

$$G_0(R) = \left[\frac{\left(\frac{Q_T\pi - 2}{Q_T\pi + 2}\right) + 1}{j\pi R}\right]\left[\frac{1 - e^{-j\pi R}}{1 + \left(\frac{Q_T\pi - 2}{Q_T\pi + 2}\right)e^{-j\pi R}}\right]$$

This can be simplified to:

$$G_0(R) = \frac{2j(-1 + e^{-j\pi R})}{R\pi + R\pi e^{-j\pi R} + \frac{2R}{Q_T} - \frac{2R}{Q_T}e^{-j\pi R}}$$

from which it follows that:

$$G_0(R) = \frac{1}{jR}\left[\frac{1}{Q_T} + \frac{\pi}{2}\frac{1 + e^{-j\pi R}}{1 - e^{-j\pi R}}\right]^{-1} \tag{5.26}$$

In deriving Equation (5.26) it has been assumed that transducer damping is entirely due to a loss of energy from the transducer into the surrounding medium. However, the effect on the transducer is the same regardless of how the energy is lost. The validity of Equation (5.26) is unaltered if Q_T is replaced by Q_M. It is therefore possible to write:

$$G_0(R) = \frac{1}{jR}\left[\frac{1}{Q_M} + \frac{\pi}{2}\frac{1 + e^{-j\pi R}}{1 - e^{-j\pi R}}\right]^{-1} \tag{5.27}$$

Equation (5.27) is more appropriate to an air coupled receiving transducer since, as previously discussed, intrinsic mechanical damping is much more significant than

damping due to energy lost through transmission into the surrounding medium. It is worth noting that Equation (5.27) is simply a more sophisticated version of Equation (5.12). To illustrate this both equations are plotted in Figure 5.4 for $Q_M=10$. From

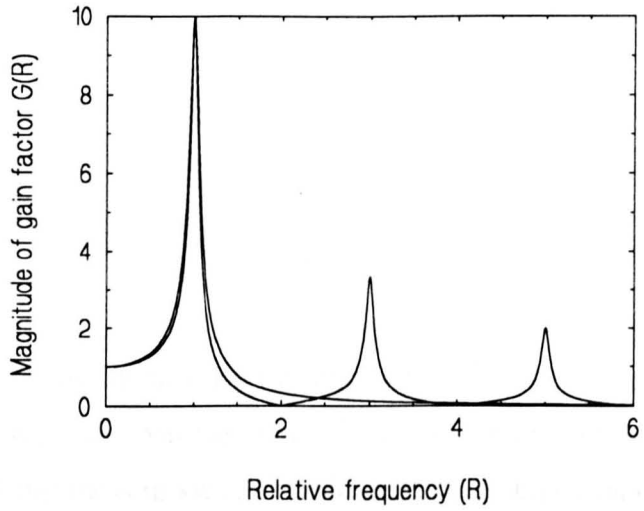

FIGURE 5.4 GAIN FACTOR PLOTTED USING BOTH EQUATIONS (5.27) AND (5.12) FOR $Q_M=10$

these curves it can be seen that Equation (5.12) is only suitable for predicting the relative sensitivity of a transducer close to its fundamental thickness mode resonance frequency. By contrast, Equation (5.27) is suitable for predicting the relative sensitivity of a transducer at any frequency. In Figure 5.4, the curve corresponding to Equation (5.27) indicates that there are peaks in the relative sensitivity, not only at the transducer's fundamental thickness mode resonance frequency, but also at frequencies close to the odd harmonics of this frequency. The magnitude and argument of Equation (5.27) are plotted in Figures 5.5 and 5.6 respectively. These curves are equivalent to those which were plotted in Figures 5.2 and 5.3 respectively.

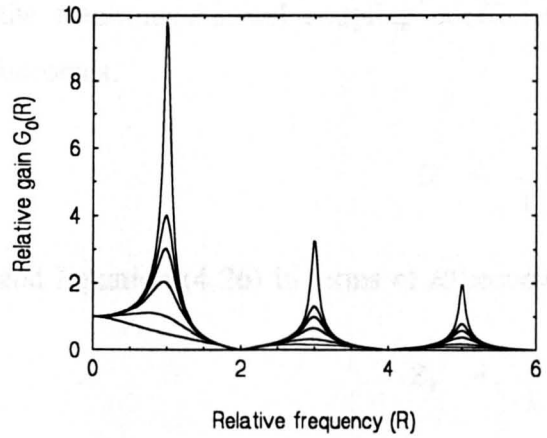

FIGURE 5.5 MECHANICAL GAIN OF A TRANSDUCER FOR MECHANICAL Q=10,4,3,2,1 AND 0.5

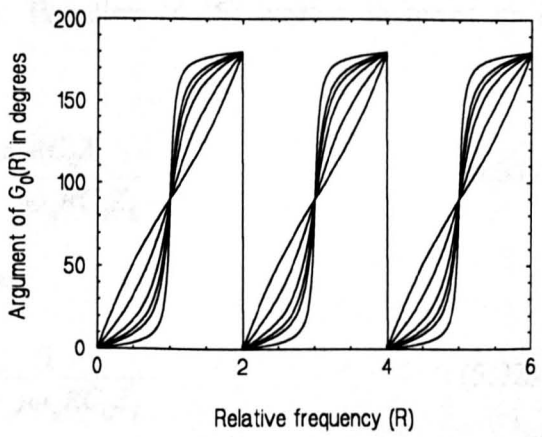

FIGURE 5.6 ARGUMENT OF THE GAIN FACTOR FOR MECHANICAL Q=10,4,3,2,1, AND 0.5

5.3.2 *The Relative Sensitivity of an Electrically Loaded Transducer*

At this stage in the development of the new transducer noise model, only open circuit transducers have been considered. As discussed previously, it is necessary to account for additional damping which takes place when a transducer is connected to an electrical load. This can be done as follows. Equation (5.17) for the mechanical gain can be written as follows:

$$G(R) = \frac{T_F K_F U}{j\pi R}\left[1-\frac{Z_F K_F T_F k^2}{j\pi R}\right]^{-1} \tag{5.28}$$

This version gives the mechanical gain of an electrically loaded transducer in terms of relative frequency R rather than the actual frequency. As previously, ω_n corresponds to the fundamental thickness mode resonance frequency. Equation (5.18) for the open circuit gain can also be written in terms of relative frequency:

$$G_0(R) = \frac{T_F K_F}{j\omega_n RT} \tag{5.29}$$

Combining Equations (5.28) and (5.29) gives:

$$G(R) = \frac{UG_0(R)}{1 - Z_F k^2 G_0(R)} \tag{5.30}$$

Equation (5.30) expresses the mechanical gain of an electrically loaded transducer in terms of the open circuit mechanical gain. Here, U is the forward path attenuation factor, Z_F is the feedback factor which controls secondary piezoelectric action and k is the electromechanical coupling coefficient. Equation (4.25) written in terms or R becomes:

$$U = \frac{j\omega_n RC_0 Z_L}{1 + j\omega_n RC_0 Z_L} \tag{5.31}$$

and Equation (4.26) in terms of R becomes:

$$Z_F = \frac{1}{1 + j\omega_n RC_0 Z_L} \tag{5.32}$$

Here, C_0 is the static capacitance of the transducer and Z_L is the electrical impedance

of the load. It will be found more convenient to write Equation (5.30) in the following way:

$$G(R) = \left[\frac{1}{U} \frac{1}{G_0(R)} - \frac{Z_F k^2}{U} \right]^{-1} \tag{5.33}$$

Substituting Equations (5.31) and (5.32) into Equation (5.33) gives:

$$G(R) = \left[\frac{1}{G_0(R)} \left(\frac{1}{j\omega_n R C_0 Z_L} + 1 \right) - \frac{k^2}{j\omega_n R C_0 Z_L} \right]^{-1} \tag{5.34}$$

This is the next important equation in the development of the new receiver noise model. It represents the mechanical gain of an electrically loaded transducer in terms of the mechanical gain of an open circuit transducer. The only restriction that applies to this equation is that the front and back face media are identical. Equation (5.34) is therefore valid for all of the transducers used in this research since they are all both air coupled and air backed. Let $Z_L = R_L$ where R_L is a pure resistance. It is then interesting to note that $R_L C_0$ is a time constant. So, it is possible to define another frequency:

$$f_L = \frac{1}{2\pi R_L C_0} \tag{5.35}$$

or:

$$\omega_L = \frac{1}{R_L C_0} \tag{5.36}$$

Using this definition it is possible to write Equation (5.34) in the following very simple form:

$$G(R) = \left[\frac{1}{G_0(R)} \left(\frac{1}{jRR_2} + 1 \right) - \frac{k^2}{jRR_2} \right]^{-1} \tag{5.37}$$

Here, R_2 is another relative frequency given by:

$$R_2 = \frac{\omega_n}{\omega_L} = \omega_n R_L C_0 \tag{5.38}$$

Remember, ω_n corresponds to the fundamental thickness mode resonance frequency and

ω_L is a function of the transducer's static capacitance, C_0, and its electrical load, R_L. From Equation (5.37) it can be seen that the additional damping which results from connecting a transducer to a resistive load depends only on R_2 and the electromechanical coupling coefficient, k. It is appropriate to use Equation (5.37) when, for example, the transducer is connected to a pre-amplifier which has a purely resistive input impedance. This is the case for the ZN460 pre-amplifier which was used in many of the experimental test systems which are described later in this Thesis. Figure 5.7 shows the relative sensitivity of an open circuit transducer with a Q_M of 10. The relative sensitivities of the same transducer when connected to 7000 Ω, 1000 Ω and 100 Ω loads are shown in Figures 5.8, 5.9 and 5.10 respectively. Here, 7000 Ω is the maximum input impedance of the ZN460 pre-amplifier. The curves illustrated here were obtained using Equations (5.27) and (5.37). The parameters used in Equation (5.37) to produce Figures 5.8, 5.9 and 5.10 are k=0.5, f_n=600 kHz and C_0=1x10^{-9} F. From these graphs it can be seen that by connecting the transducer to an electrical load its Q_M is effectively reduced. This can be explained as follows. As mentioned previously, Q_M is a measure of the energy which is lost by a transducer due to intrinsic mechanical damping. Figures 5.8, 5.9 and 5.10 illustrate that it is also possible for energy to be lost from a transducer by the generation of heat in an external electrical load. This can happen in a piezoelectric material because mechanical energy and electrical energy are continually being converted from one form to the other as the transducer vibrates.

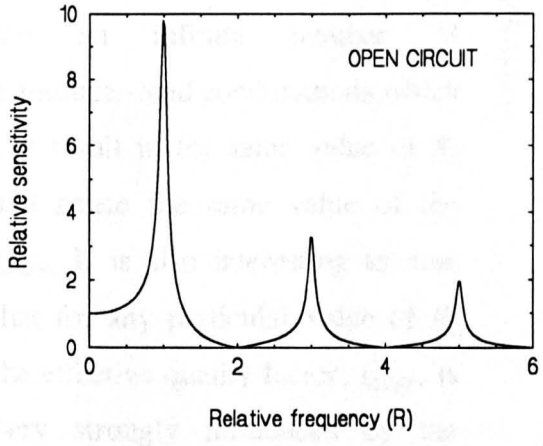

FIGURE 5.7 RELATIVE SENSITIVITY, G(R), AS A FUNCTION OF R FOR AN OPEN CIRCUIT TRANSDUCER WITH A MECHANICAL Q OF 10

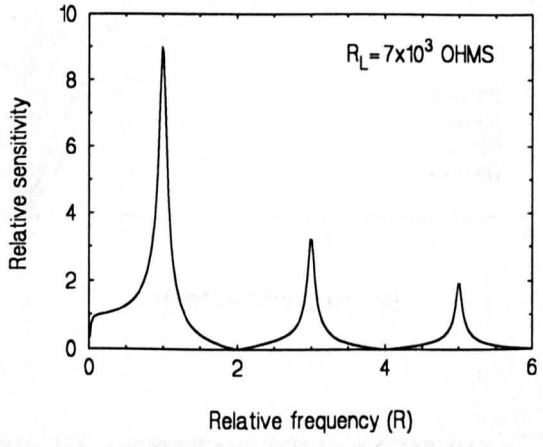

FIGURE 5.8 G(R), AS A FUNCTION OF R FOR A TRANSDUCER WITH A MECHANICAL Q OF 10 AND CONNECTED TO A 7000 Ω LOAD

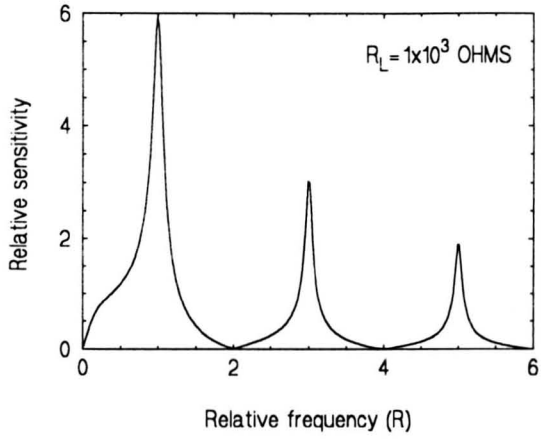

FIGURE 5.9 G(R) AS A FUNCTION OF R FOR A TRANSDUCER WITH A MECHANICAL Q OF 10 AND CONNECTED TO A 1000 Ω LOAD

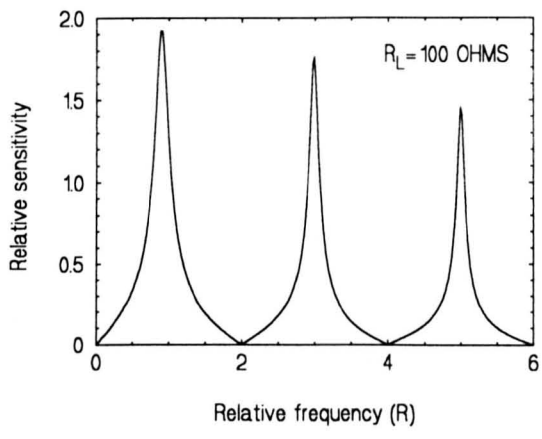

FIGURE 5.10 G(R), AS A FUNCTION OF R FOR A TRANSDUCER WITH A MECHANICAL Q OF 10 AND CONNECTED TO A 100 Ω LOAD

5.3.3 *The Effective Q of an Electrically Loaded Transducer*

An effective quality factor, Q_{EFF}, for an electrically loaded transducer can be obtained from Equation (5.37) by setting $R=1$. Thus:

$$Q_{EFF} = |G(1)| = \left| \left[\frac{1}{Q_M}\left(\frac{1}{jR_2}+1\right) - \frac{k^2}{jR_2} \right]^{-1} \right| \tag{5.39}$$

Equation (5.39) is plotted in Figure 5.11 for $Q=10$ and four values of k. Here, it is interesting to note that since, $R_2=\omega_n R_L C_O$, there are an infinite number of transducer-load combinations which can result in the same value of R_2 and hence the same value of the Q_{EFF}. It is also interesting to note that for any particular value of R_2 the effective quality factor, Q_{EFF}, is very strongly influenced by the value of the coupling coefficient, k.

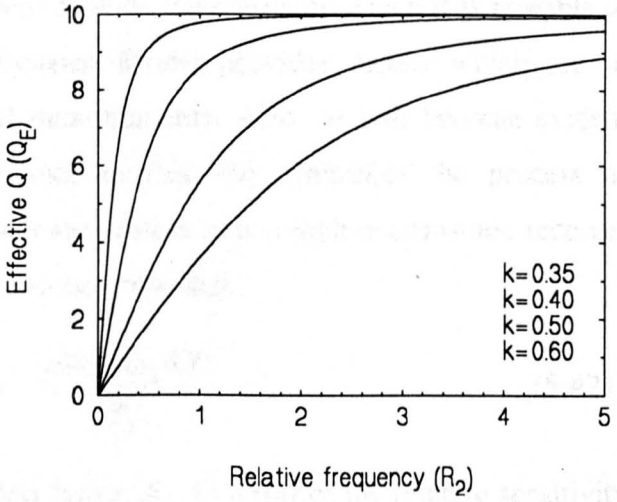

FIGURE 5.11 THE EFFECTIVE Q OF AN ELECTRICALLY LOADED TRANSDUCER FOR k EQUAL TO 0.35, 0.4, 0.5 AND 0.6 (TOP LEFT TO BOTTOM RIGHT)

5.3.4 *The Force to Voltage Transfer Function*

It will now be shown that the modified Linear Systems Model can be used to obtain a very compact and convenient mathematical expression for a plate transducer's force to voltage transfer function. From Equation (4.5) the force to voltage transfer function, in terms of relative frequency, can be written in the following form:

$$V_S(R) = \frac{-hT_F K_F U\left(\frac{1}{j\omega_n R Z_C}\right) F_{SM}}{1 - \frac{Z_F T_F K_F k^2}{j\pi R}} \tag{5.40}$$

Here, $V_S(R)$ is the signal voltage corresponding to the signal force, F_{SM}, in the coupling medium. All of the other terms have been identified previously. The only condition that applies to Equation (5.40) is that the front and back face media are identical. Substituting Equation (5.28) into Equation (5.40) gives the new transfer function:

$$V_S(R) = \left(\frac{-hT}{Z_C}\right) G(R) F_{SM} \tag{5.41}$$

5.3.5 *Electrical Impedance*

It will be found instructive to express the electrical impedance in terms of the transducer's relative sensitivity. This will provide the means by which it is possible to illustrate that the modified Linear Systems Model provides results which are in excellent agreement with experimental measurements. Also, as will become evident later, expressing the electrical impedance in this way simplifies the process of combining all of the noise sources which are present in a complete ultrasonic receiver system. From the previous analysis it can be show that:

$$K_F = \frac{jG(R)\omega_n RT}{T_F} \tag{5.42}$$

This equation expresses the reverberation factor, K_F, in terms of the relative sensitivity function, $G(R)$. From Equation (4.27) it is easy to show that, for a piezoelectric transducer with identical front and back media, the transducer's electrical impedance as a function of relative frequency, R, is given by:

$$Z_E(R) = \frac{1}{j\omega_n RC_0}\left(1 - \frac{k^2}{j\omega_n RT}K_F T_F\right) \tag{5.43}$$

Using Equation (5.85) to substitute for K_F in Equation (5.86) gives:

$$Z_E(R) = \frac{1}{j\omega_n RC_0}(1 - k^2 G(R)) \tag{5.44}$$

This is very similar to an expression for electrical impedance described by Kino in his book on acoustic waves [83]. The only difference is that *G(R)* is represented by a different mathematical function. Equation (5.44) indicates that the electrical impedance of a piezoelectric plate transducer can be found by applying a modifying factor to the component of electrical impedance which is associated with the transducer's static capacitance and which is given by the following well known equation:

$$Z_{ES}(R) = \frac{1}{j\omega_n RC_0} = \frac{1}{j\omega C_0} \tag{5.45}$$

Thus:

$$Z_E(R) = Z_{ES}(R)\, M(R) \tag{5.46}$$

where the modifying factor is given by:

$$M(R) = (1 - k^2 G(R)) \tag{5.47}$$

From this it can be seen that as R tends to zero, *G(R)* tends to unity and:

$$M(0) = (1 - k^2) \tag{5.48}$$

Equation (5.48) is of no great significance since, as R tends to zero, the electrical impedance associated with the static capacitance tends to infinity. However, if the transducer is operated at its fundamental thickness mode resonance frequency then

$R=1$, $G(R)=Q_M$ and:

$$M(1) = (1 - k^2 Q_M) \tag{5.49}$$

Equation (5.49) further illustrates the importance of a transducer's mechanical quality factor, Q_M, in the noise analysis.

Example

Consider a typical 30 mm diameter PZT-5A transducer intended for air coupled operation at a frequency (f_n) of 1.116 MHz. As will be discussed at the end of this Section, this particular frequency has been chosen because experimental data has been obtained for a PZT-5A device operating at this frequency. The device parameters are:

Wave velocity: $c=4350$ ms^{-1} [83]
Wavelength in the transducer: $\lambda=3.9 \times 10^{-3}$
Corresponding transducer thickness: $\tau=\lambda/2=1.95$ mm
Piezoelectric charge constant: $h_{33}=21.5 \times 10^8$ Vm^{-1}
Relative dielectric constant (constant strain): 830
Permittivity of free space: $\varepsilon_0=8.85 \times 10^{-12}$ Fm^{-1}
Corresponding permittivity of transducer material: $\varepsilon_{33}=7.4 \times 10^{-9}$ Fm^{-1}
Corresponding static capacitance: $C_0=2.66 \times 10^{-9}$ F
Material density: $\rho=7.75 \times 10^3$ kgm^3
Characteristic acoustic impedance: $Z_{CHA}=\rho c=34$ MRayl
Acoustic impedance of transducer: $Z_C=AZ_{CHA}=2.4 \times 10^4$
Mechanical quality factor: $Q_M=75$.

These values have been used in Equation (5.44) to plot the open circuit electrical impedance of this typical PZT-5A transducer. This involved using Equation (5.27) to obtain $G(R)$. The results are illustrated in Figures 5.12 and 5.13. Figure 5.12 represents the magnitude of the impedance and Figure 5.13 represents the current-voltage phase relationship. This is the first time that the Linear Systems Model (LSM) has been used to make this type of theoretical prediction without having to introduce

an attenuation factor (discussed previously) which forces the theory to fit with experimental observations. The extensively modified version of the LSM which has been described in this Chapter is capable of producing highly accurate predictions based only on materials parameters supplied by the manufacturer. In particular, it is the incorporation of the mechanical quality factor, Q_M, into the model which has made this possible.

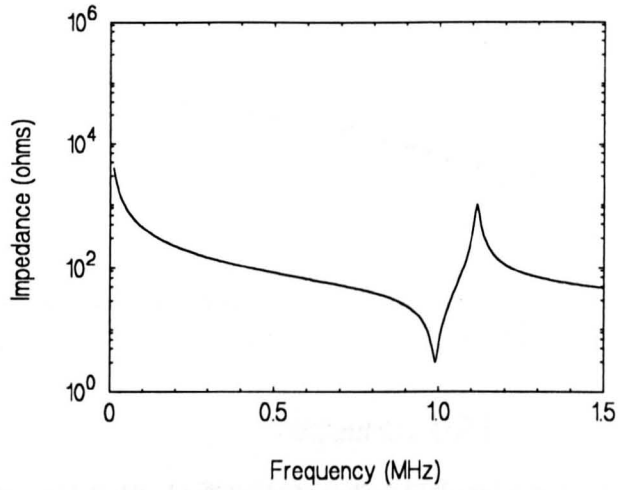

FIGURE 5.12 THEORETICAL CURVE REPRESENTING THE MAGNITUDE OF THE IMPEDANCE AS A FUNCTION OF FREQUENCY FOR A TYPICAL PZT-5A TRANSDUCER

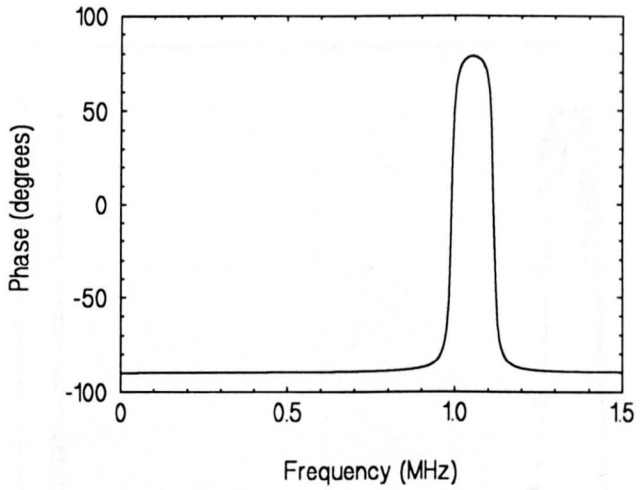

FIGURE 5.13 THEORETICAL CURVE REPRESENTING CURRENT-VOLTAGE PHASE AS A FUNCTION OF FREQUENCY FOR A TYPICAL PZT-5A TRANSDUCER

Experimental Validation

The accuracy of the theoretical predictions presented here can be judged by comparing Figures 5.12 and 5.13 with corresponding experimental results which are presented in Figures 4.5 and 4.6 respectively. These experimental results have been discussed

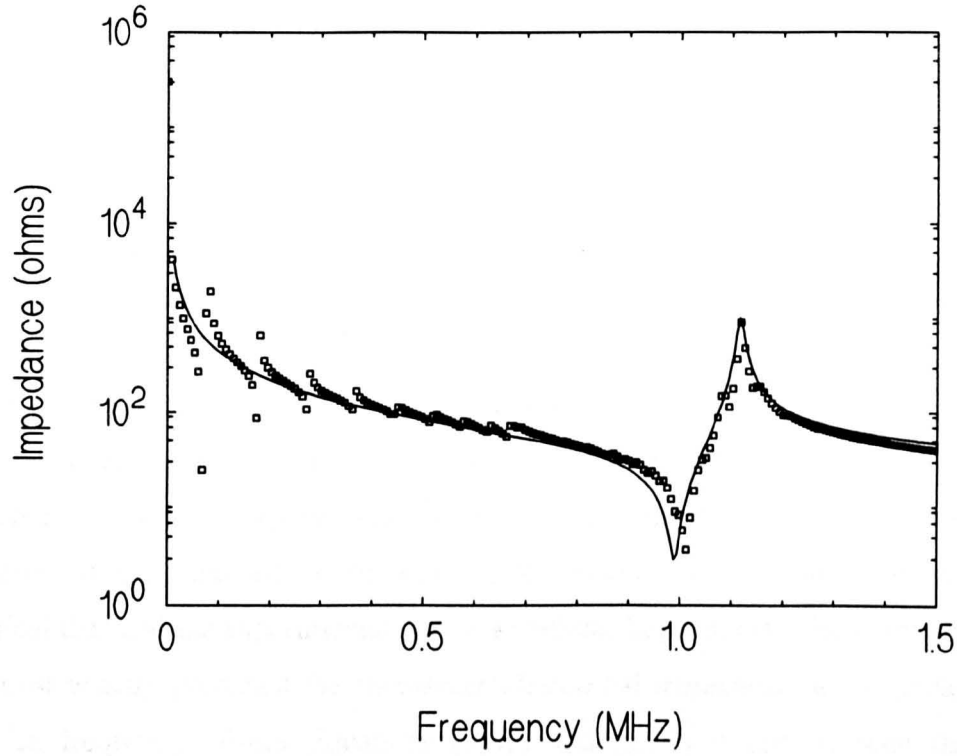

FIGURE 5.14 THEORETICAL AND EXPERIMENTAL CURVES REPRESENTING THE MAGNITUDE OF THE ELECTRICAL IMPEDANCE AS A FUNCTION OF FREQUENCY FOR A TYPICAL PZT-5A TRANSDUCER

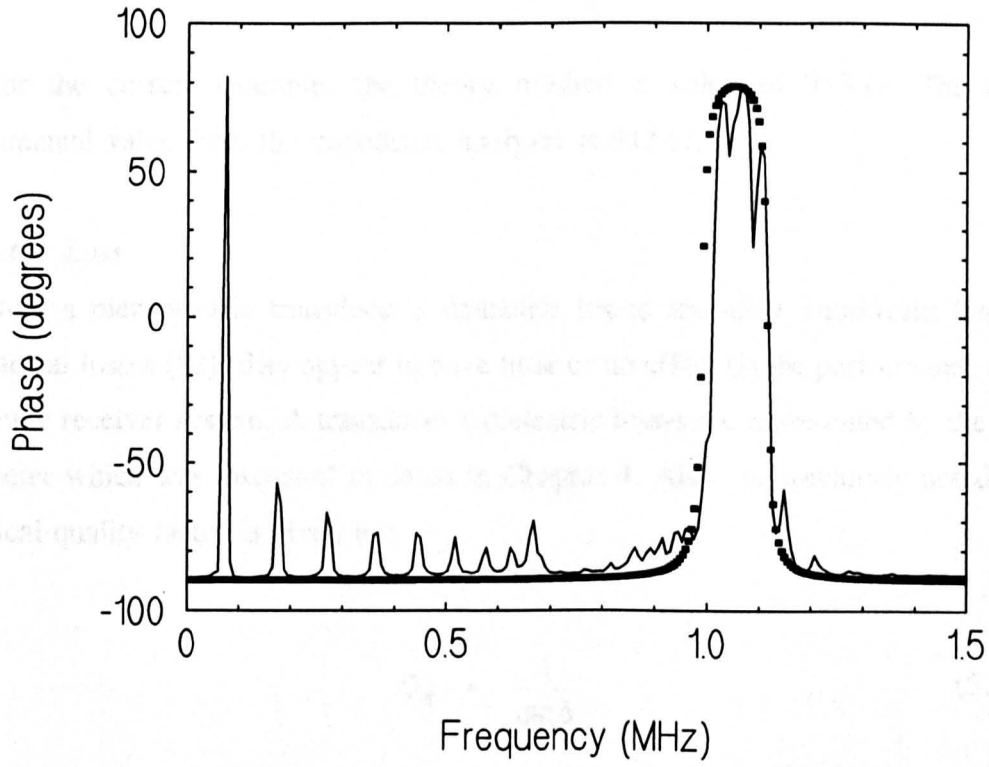

FIGURE 5.15 THEORETICAL AND EXPERIMENTAL CURVES REPRESENTING CURRENT-VOLTAGE PHASE AS A FUNCTION OF FREQUENCY FOR A TYPICAL PZT-5A TRANSDUCER

previously in Section 4.2.3. The quality of the theoretical results can only be fully appreciated by displaying the experimental results on the same graph. This has been done for the magnitude of the impedance in Figure 5.14 and for the current-voltage phase in Figure 5.15. In Figure 5.14 the hollow squares represent the experimental data and in Figure 5.15 solid squares represent the theory.

As discussed in Section 4.2.2 the experimental data which is displayed in Figures 5.14 and 6.15 was obtained using a Hewlett Packard 4194A impedance analyzer. At this stage it is important to mention that the Linear Systems Model is not capable of predicting a transducer's lateral modes of vibration. These modes are more obvious at lower frequencies in the experimental data for both magnitude and phase. However, in the region of the fundamental thickness mode resonance, the match between the theoretical data and the experimental data is excellent. In particular, the modified LSM has almost exactly predicted the transducer's electrical impedance at its fundamental resonance frequency. From Equations (5.45) and (5.49) it can be seen that this impedance is given by:

$$Z_E(R) = \frac{(1 - k^2 Q_M)}{j\omega C_0} \tag{5.50}$$

So, for the current example, the theory predicts a value of 953 Ω. The exact experimental value from the impedance analyzer is 912 Ω.

Dielectric Loss

Although a piezoelectric transducer's dielectric losses are more significant than its mechanical losses [82], they appear to have little or no effect on the performance of an ultrasonic receiver system. A transducer's dielectric losses are represented by the $tan\delta$ parameter which was discussed in detail in Chapter 4. Also, as previously noted, the electrical quality factor is given by:

$$Q_E = \frac{1}{\tan\delta} \tag{5.51}$$

From Chapter 4 it will be evident that the significance of $tan\delta$ is that the static electrical impedance of a piezoelectric transducer is not, as assumed in the LSM, the purely imaginary impedance associated with the static capacitance C_0. In reality the static electrical impedance has a real component. This means that Equation (5.44) should be modified to become:

$$Z_E(R) = \frac{(1 - k^2 G(R))}{j\omega_n R C_0 (1 - j\tan\delta)} \tag{5.52}$$

It has been confirmed that introducing the $tan\delta$ term has no measurable effect on the magnitude of $Z_E(R)$, however, its presence has a very interesting effect on the current-voltage phase characteristic. In order to appreciate this it is necessary to examine the previously discussed theoretical phase data in more detail. Equation (5.44) is plotted again in Figure 5.16, but this time over the phase angle range -90° to -80°. Equation (5.52) is plotted in Figure 5.17 over the same range for $tan\delta$=0.02 which is typical for PZT-5A [82]. It will be clear from these results, and from the detailed discussion in Sections 4.2.2 and 4.2.3, that Equation (5.52) provides a more accurate representation of a piezoelectric transducer's current-voltage phase characteristic. Figure 5.17 illustrates that, as for a real dielectric material, it is not possible for the phase angle to be exactly -90°. As mentioned at the start of this Section, the $tan\delta$ parameter has no measurable effect on the performance of an ultrasonic receiving transducer, however, it is very important in a transmitting device where it limits the magnitude of the signal that can be generated [82]. In the case of a transmitter, $tan\delta$ determines the proportion of the supplied electrical power which is converted directly into heat.

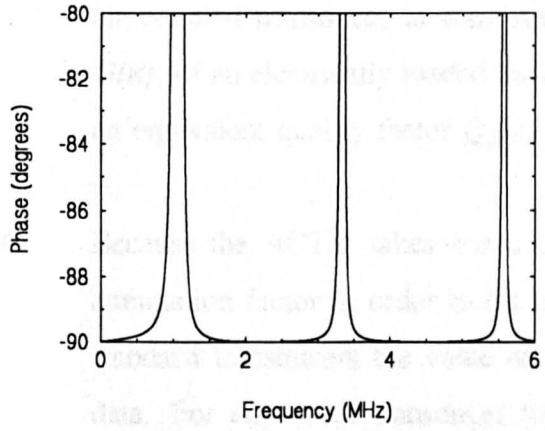

FIGURE 5.16 THEORETICAL CURRENT-VOLTAGE PHASE CURVE PRODUCED USING EQUATION (5.44)

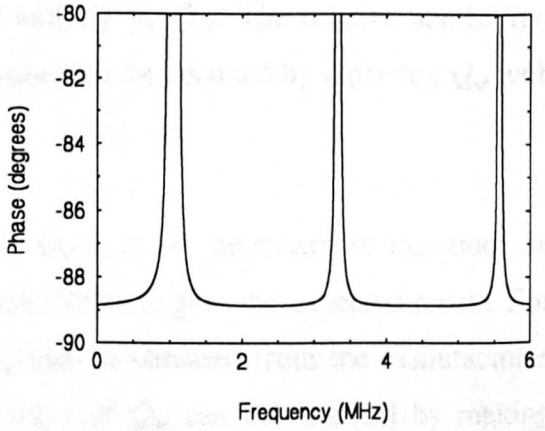

FIGURE 5.17 THEORETICAL CURRENT-VOLTAGE PHASE CURVE PRODUCED USING EQUATION (5.52)

5.4 *Conclusions*

5.4.1 *The Goal*

The single goal of the work which is described in this Chapter was the development of a modified version of the Linear Systems Model which takes account of a transducer's mechanical quality factor, Q_M. The only restriction that applies to the new model is that both the transducer's front face coupling medium and its backing medium should be a gas or any other material which produces an insignificant degree of mechanical damping compared to the transducer's intrinsic damping which is quantified by Q_M. It was essential that this new version of the model should produce results which could be experimentally verified and which were consistent with results produced by previous versions. In addition to achieving this goal, a number of other useful and interesting findings have been made.

5.4.2 *Summary of Features and Achievements*

This Section provides a summary of the main features of the Air Coupled Transducer Model (ACTM). The Section also serves to highlight the principal achievements. Both are listed below:

- A key feature of the ACTM is the open circuit mechanical gain equation which represents the relative sensitivity of a piezoelectric plate transducer:

$$G_0(R) = \frac{1}{jR}\left[\frac{1}{Q_M} + \frac{\pi}{2}\frac{1 + e^{-j\pi R}}{1 - e^{-j\pi R}}\right]^{-1}$$

  From this equation it can be seen that the resonant behaviour of an open circuit, air coupled transducer is controlled entirely by Q_M. The relative sensitivity, $G(R)$, of an electrically loaded transducer can be obtained by replacing Q_M with an equivalent quality factor Q_{EFF}.

- Because the ACTM takes account of Q_M it is not necessary to introduce an attenuation factor in order to force the model to give the expected result. For standard transducers the value of Q_M can be obtained from the manufactures data. For any other transducer the value of Q_M can be obtained by making bandwidth measurements using an impedance analyzer.

- It has been established that the quality factor for a transducer which is subjected to external mechanical loading only is given by:

$$Q_T = \frac{2Z_C}{\pi Z_1}$$

For a 34 MRayl transducer operating in air, Q_T has a value 54,000. By contrast, Q_M is 75 for a typical PZT-5A transducer. The significant difference between these values provides the justification for disregarding external damping.

- The only restriction that applies to the ACTM is that the transducer's coupling medium and its backing medium must be gas or any other material which results in a level of external damping, as quantified by Q_T, which is insignificant compared with the transducer's intrinsic damping, as quantified by Q_M.

- By using the ACTM it has been possible to obtain the following very simple expression for a transducer's force to voltage transfer function:

$$V_S(R) = \left(\frac{-hT}{Z_C}\right) G(R) F_{SM}$$

Here, F_{SM} is the signal force in the coupling medium and $V_S(R)$ is the signal voltage that would be measured across the terminals of the transducer. The other terms have been identified previously.

- Use of the ACTM also leads to the following simple expression for a transducer's electrical impedance.

$$Z_E(R) = \frac{(1 - k^2 G(R))}{j\omega_n R C_0 (1 - j\tan\delta)}$$

Because this expression also takes account of Q_M, it was possible to produce a very accurate simulation of the experimental impedance plots which were discussed in Chapter 4.

- The expressions for $V_S(R)$ and $Z_E(R)$ are essential to the development of the new receiver noise model.

- The expressions for both $V_S(R)$ and $Z_E(R)$ use the function $G(R)$ instead of the function $G_0(R)$. The function $G(R)$ is related to the function $G_0(R)$:

$$G(R) = \left[\frac{1}{G_0(R)}\left(\frac{1}{jRR_2} + 1\right) - \frac{k^2}{jRR_2}\right]^{-1}$$

where:

$$R_2 = 2\pi f_n R_L C_0$$

These equations take account of the effect of electrical loading on the transducer. As will be discussed in more detail in the next Chapter, the R_2 parameter can be thought of as a figure of merit for a complete receiver front-end (transducer and pre-amplifier). This follows because, when a transducer is connected to a pre-amplifier, R_L represents the input impedance of the amplifier. The properties of the transducer are represented by its static capacitance, C_0, and its fundamental thickness mode resonant frequency, f_n. Clearly, the performance of the front-end is controlled by R_2 and the transducer's electromechanical coupling coefficient, k.

- The modelling approach which has been described in this Chapter allows an effective quality factor to be defined for an electrically loaded transducer. This effective quality factor is given by the following equation:

$$Q_{EFF} = |G(1)| = \left|\left[\frac{1}{Q_M}\left(\frac{1}{jR_2} + 1\right) - \frac{k^2}{jR_2}\right]^{-1}\right|$$

Chapter 6

A Receiver Noise Model

6.1 Introduction

As mentioned at the start of Chapter 5, the development of the Air Coupled Transducer Model (ACTM) was an essential prelude to the development of the Receiver Noise Model (RNM) which is described in this Chapter. The ACTM will also be used to show that accounting for Johnson noise in a piezoelectric receiving transducer is exactly equivalent to accounting for force fluctuations using an approach based on the Callen and Welton theorem. Without the ACTM it would have been impossible to obtain some key results which lead to a very comprehensive understanding of the factors which control the absolute sensitivity of an ultrasonic receiver.

The present Chapter describes a receiver noise model which is suitable for predicting the MDP and MDF of both open circuit piezoelectric transducers and complete receiver systems. The model has been validated by showing that it is capable of generating a theoretical voltage noise spectrum which is in excellent agreement with experimental measurements made by Banks [85]. Also, as previously mentioned, the model is consistent with the Callen and Welton theorem. Here, it will be shown that the RNM is capable of predicting how MDP and MDF vary as a function of frequency. In addition, it will be shown that, in order to obtain accurate results over a wide range of conditions, it is necessary to account for an external noise source which was not included in the Linear Systems Noise Model (LSNM).

A significant achievement has been to shown that the closed form solutions for open circuit SNR, MDP and MDF that were described in Chapter 4 are both accurate and meaningful. The process of solving this problem has led to two very simple mathematical relationships which fully describe the absolute sensitivity of a transducer in terms of MDP and MDF. These relationships indicate that, for a given coupling medium, it is only necessary to know a transducer's acoustic impedance, Z_C, and its mechanical quality factor, Q_M, in order to calculate its resonant MDP and MDF.

6.1.1 Background

Chapter 4 described two different ways in which it is possible to model the absolute sensitivity of a receiving transducer in terms of minimum detectable force (MDF), minimum detectable power (MDP) and minimum detectable displacement (MDD). One

approach involves using the Linear Systems Noise Model (LSNM) and the other involves using an approach based on the Callen and Welton theorem. Both modelling techniques were investigated in great detail and it had appeared that they could be inconsistent. In order to establish a standard against which a receiver's absolute sensitivity could be measured it was necessary to use the models to obtain MDF and MDP values for an open circuit transducer. The open circuit condition implies that there is no electrical damping of the transducer's mechanical vibrations and that the only noise source that has to be considered is thermal noise which is produced by the transducer itself. When the LSNM was used to model the absolute sensitivity of a standard PZT-5A plate transducer, the results indicated that it would be possible for the transducer to detect a signal force with an amplitude which is smaller than the r.m.s. amplitude of the thermally generated force fluctuations in both the transducer and the coupling medium. Further, the LSNM indicated that the open circuit MDF was constant with respect to frequency. A closed form solution indicated that the MDF per unit bandwidth in the coupling medium is given by Equation (4.41) which is reproduced here:

$$MDF = \sqrt{2k_B T_A Z_1} \tag{6.1}$$

In this equation k_B is Boltzmann's constant, T_A is the absolute temperature in degrees Kelvin and Z_1 is the acoustic impedance of the coupling medium. This result indicates that the absolute sensitivity of the transducer is independent of all of its mechanical and electrical properties and that the absolute sensitivity is independent of frequency. By contrast with the LSNM result, the Callen and Welton based approach indicates that the MDF per unit bandwidth in the coupling medium is given by Equation (4.74) which is reproduced here:

$$MDF = \sqrt{\frac{4k_B T_A Z_C}{\pi Q_M}} \tag{6.2}$$

Here, Z_C is the acoustic impedance of the transducer and Q_M is its mechanical quality factor. Because this result can also be obtained directly using the laws of modern solid state physics, it was concluded that there could be a flaw in the LSNM approach. In this Chapter it will be shown that by using the ACTM it is possible to explain the apparent inconsistency between the two approaches.

6.2 *Receiver Noise Sources*

In order to construct a complete receiver noise model it is necessary to obtain a mathematical expression which can be used to represent a transducer's equivalent noise voltage. Here it will be shown that, as in the original LSNM, it is possible to calculate the transducer noise voltage by using the real part of a transducer's electrical impedance in the Johnson noise equation. This approach will be justified using both theoretical and experimental evidence. In order to provide a theoretical justification for using the Johnson noise equation it will be necessary to show that the LSNM and the ACTM both provide results which are consistent with the Callen and Welton theorem. Section 6.2.1 covers the theoretical aspects in detail and Section 6.3.2 briefly covers the experimental aspects.

6.2.1 A New Closed Form Solution

The aim of this Section is to use the ACTM to gain additional insight into the theoretical results which were obtained in Section 4.4.2 of Chapter 4. In that Section, closed form solutions were obtained for a transducer's SNR, MDF and MDP. These solutions were obtained using the equations which form the building blocks of the LSNM. In this Section, the equations which form the building blocks of the ACTM will be used to obtain a closed form solution for a transducer's MDF. Unlike the previous closed form solution for MDF, the one which is now to be derived can be applied to a transducer which has associated with it an intrinsic loss. In addition to the main goal, this exercise will provide confirmation that the ACTM behaves in a way which is completely consistent with the operation of the LSM.

The Solution for Minimum Detectable Force

From Equation (5.44) the real part of the transducer's electrical impedance is:

$$Z_{ER} = Re\left(\frac{1 - k^2 G(R)}{jR\omega_n C_0}\right) \tag{6.3}$$

Here, $G(R)$ is the relative sensitivity, k is the electromechanical coupling coefficient, R is the relative frequency, ω_n is the angular equivalent of the fundamental resonance frequency and C_0 is the transducer's static capacitance. It is immediately obvious that, since $1/(jR\omega_n C_0)$ is always imaginary, Equation (6.3) can be simplified to:

$$Z_{ER} = Re\left(\frac{k^2 G(R)}{jR\omega_n C_0}\right) \tag{6.4}$$

Using this in the Johnson noise equation gives:

$$v_{JN} = \sqrt{4k_B T_A \, Re\left(\frac{k^2 G(R)}{jR\omega_n C_0}\right)} \tag{6.5}$$

Here, k_B is Boltzmann's constant and T_A is the absolute temperature in degrees Kelvin. From equation (5.41) the magnitude of the signal voltage, $V_S(R)$, is:

$$|V_S(R)| = \left|\left(\frac{hT}{Z_C}\right) G(R) F_{SM}\right| \tag{6.6}$$

Here, F_{SM} is the signal force in the coupling medium, h is the piezoelectric charge constant, Z_C is the transducer's acoustic impedance and T is the time taken for sound waves to travel from one face of the transducer to the opposite face. From Equations (6.5) and (6.6) the voltage signal to noise ratio at the transducer terminals is:

$$SNR(R) = \frac{\left|\left(\frac{hT}{Z_C}\right) G(R) F_{SM}\right|}{\sqrt{4k_B T_A \, Re\left(\frac{k^2 G(R)}{jR\omega_n C_0}\right)}} \tag{6.7}$$

Setting the SNR to unity, the minimum detectable force is found to be:

$$MDF(R) = \frac{\sqrt{4k_B T_A \, Re\left(\frac{k^2 G(R)}{jR\omega_n C_0}\right)}}{\left|\left(\frac{hT}{Z_C}\right) G(R)\right|} \tag{6.8}$$

Using Equation (4.39) to substitute for k gives:

$$MDF(R) = \frac{(4k_B T_A Z_C)^{1/2}}{|G(R)|}\left[Re\left(\frac{G(R)}{jR\pi}\right)\right]^{1/2} \tag{6.9}$$

The $G_0(R)$ function is given by Equation (5.27) which is reproduced here:

$$G_0(R) = \frac{1}{jR}\left[\frac{1}{Q_M} + \frac{\pi}{2}\frac{1 + e^{-j\pi R}}{1 - e^{-j\pi R}}\right]^{-1} \tag{6.10}$$

This can be expanded to give:

$$G_0(R) = \frac{2Q_M[\pi Q_M \sin(\pi R) + 2j + 2j\cos(\pi R)]}{R[-4 - \pi^2 Q_M^2 - 4\cos(\pi R) + \pi^2 Q_M^2 \cos(\pi R)]} \tag{6.11}$$

Using equation (6.11) to substitute for *G(R)* in equation (6.9) leads, after considerable manipulation, to the following expression for open circuit minimum detectable force:

$$MDF(R) = \frac{\sqrt{4k_B T_A Z_C}}{\sqrt{\pi Q_M}} \tag{6.12}$$

Equation (6.12) is identical to Equation (6.2) or (4.74) which was obtained using an approach based on the Callen and Welton theorem. This proves that it is possible to analyse thermal noise in a transducer using either an electrical approach based on the Johnson noise equation or a mechanical approach based on the mechanical equivalent of the Johnson noise equation. However, a cursory inspection would appear to indicate that the closed form solution for MDF obtained using the ACTM is radically different from the one which was obtained using the LSNM. It will now be shown that this is not the case. As discussed previously, if the intrinsic losses associated with a transducer are insignificant compared to transmission losses back into the coupling medium, it is acceptable to replace Q_M with Q_T. This was, in effect, the assumption that was made in the derivation of Equation (4.41). Doing this in Equation (6.12) gives:

$$MDF(R) = \frac{\sqrt{4k_B T_A Z_C}}{\sqrt{\pi Q_T}} \tag{6.13}$$

The quality factor Q_T is given by Equation (5.24) which is reproduced here:

$$Q_T = \frac{2Z_C}{\pi Z_1} \tag{6.14}$$

Using this equation to substitute for Q_T in Equation (6.13) gives:

$$MDF(R) = \sqrt{2k_B T_A Z_1} \tag{6.15}$$

The main features of this additional analysis are as follows:

- Equation (6.15) is identical to Equation (6.1) or (4.41). The fact that it is possible to convert Equation (6.13) into Equation (6.1) or (4.41) using Equation (6.14) or (5.24) indicates that the Air Coupled Transducer Model provides results which are entirely consistent with the Linear Systems Model.

- It can now be seen why the MDF of an intrinsically lossless transducer is independent of Z_C. Equation (6.13) indicates that, as Z_C varies, the amplitude of the force fluctuations varies in a way which is consistent with the Callen and Welton theorem, however, variations in Q_T counteract this effect.

- Equation (6.15) indicates that, for a lossless open circuit transducer, the minimum detectable force (MDF) depends only on the acoustic impedance of the coupling medium. Previously this result had been thought to be completely meaningless but now Equation (6.13) makes sense of it and the other results in Section 4.4.2.

- By approaching the problem in a different way, this analysis has provided final evidence that there is not an error in the closed form solutions which were presented in Chapter 4.

6.2.2 *Thermal Noise in the Coupling Medium*

In Chapter 4 it was noted that the LSNM can predict levels of absolute sensitivity which are physically impossible. This happens because the LSNM does not account for intrinsic damping as quantified by Q_M. This in effect means that the LSNM is represented by Equation (6.13) which uses Q_T instead of Q_M. Because values of Q_T are very high (e.g. 54,000), the transducer's mechanical gain may be sufficiently high that the absolute sensitivity is limited, not by transducer noise but by thermally generated noise in the coupling medium. Since the LSNM does not account for this it is possible for the predicted absolute sensitivity to reach impossible levels.

Modelling External Noise

As in the LSNM it was initially assumed that, because the impedance difference between a typical piezoelectric plate transducer and air is so great, it would not be necessary to include the effects of external thermal noise in the RNM. However, it later became evident that, for transducer materials or transducer structures which have both a low value of Z_C and a high value of Q_M, thermal noise in the coupling medium is significant. It was therefore decided to include an equivalent voltage generator in the RNM which accounts for external noise. This will ensure that the model is suitable for future applications.

As previously discussed in Chapter 4, all of the elements of an ultrasonic receiver system produce the same level of thermally generated noise power. So, by again using the Callen and Welton theorem it is found that the force fluctuations in the coupling medium are given by:

$$F_{NM} = (4k_B T_A Z_1)^{1/2} \tag{6.16}$$

Here, Z_1 is the acoustic impedance of the coupling medium. The other terms have been defined previously. For a 30 mm diameter transducer used in air:

$$F_{NM} = 6.8\times10^{-11}\ N\sqrt{Hz}$$

As will become evident, this level of noise is not significant for the transducers which are of interest in this research, however, its possible effects in future developments will be discussed towards the end of this Chapter. The existence of external thermal noise can be accounted for in the complete RNM by introducing an additional equivalent voltage generator, $V_{EN}(R)$, into the equivalent circuit. Since any form of external noise appears to the transducer as if it is a signal, it follows that an expression for $V_{EN}(R)$ can be found using the transfer function. To do this it is only necessary to replace the signal force in the coupling medium, F_{SM}, by F_{NM} which is given by equation (6.16). Thus:

$$V_{EN}(R) = \left(\frac{hT}{Z_C}\right) G(R)(4k_B T_A Z_1)^{1/2} \tag{6.17}$$

6.3 A Complete Receiver Front-End

Note that, from this point on in the Thesis, the term *front-end* will be used to identify that part of a complete ultrasonic receiver system which consists of the receiving transducer and the pre-amplifier. As will be discussed in Chapter 7, the complete receiver system includes an extra gain stage and a filter.

6.3.1 Total Receiver Noise and Sensitivity

In this Thesis, and in the previous work by Hayward *et al.* [84], the total front-end noise is calculated using an approach which has become the standard for many different types of detection system: laser receivers for optical rangefinders and fibre-optic communications systems, radio receivers, radar receivers, sonar receivers etc.. So, as in the original Linear Systems Noise Model, the complete front-end can be represented by the equivalent circuit illustrated in Figure 6.1. Here, $V_S(R)$ is the signal voltage, $V_{JN}(R)$ is the noise voltage associated with the transducer alone, $Z_E(R)$ is the transducer's electrical impedance, $V_{EN}(R)$ is the voltage which accounts for thermal noise in coupling medium and $g(R)$ is the gain of the pre-amplifier. It should be noted that, in order to maintain consistency with the previous discussion, all of these terms are shown as functions of the relative frequency, R. Just as a reminder, the relative frequency, R, is the signal frequency measured relative to the fundamental thickness mode frequency, f_n, of the transducer. It should be obvious that the actual frequency is simply $f=Rf_n$. In the equivalent circuit, the transducer's electrical load is, as assumed previously, a pure resistance denoted by R_L. Here, R_L is the input impedance of the pre-amplifier. The pre-amplifier noise sources are represented by the equivalent voltage

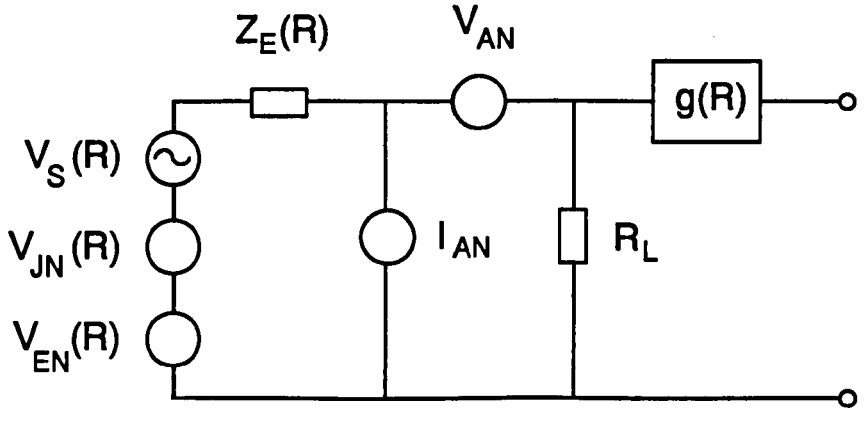

FIGURE 6.1 EQUIVALENT CIRCUIT FOR THE RECEIVER NOISE MODEL

generator V_{AN} and the equivalent current generator I_{AN}. The terminology used here is also consistent with that used in a Mathcad implementation of the Receiver Noise Model (RNM) which can be found in Appendix IV. From the equivalent circuit of Figure 6.1 it is easy to show that the total r.m.s. front-end noise is given by:

$$V_{RN}(R) = \left(\frac{R_L}{|Z_E(R)|+R_L}\right)\sqrt{V_{JN}(R)^2+V_{EN}(R)^2+V_{AN}^2+I_{AN}^2|Z_E(R)|^2} \qquad (6.18)$$

This is the voltage noise spectral density as it would appear at the input to the pre-amplifier. Here, $V_{JN}(R)$ is obtained using Equation (6.5) and V_{EN} is obtained using Equation (6.17). As discussed in Chapter 5, $G_0(R)$ is obtained using Equation (5.27) and $G(R)$ is obtained using Equation (5.37). The signal to noise ratio (SNR) is:

$$SNR(R) = \frac{V_S(R)}{[V_{JN}(R)^2+V_{EN}(R)^2+V_{AN}^2+I_{AN}^2|Z_E(R)|^2]^{1/2}} \qquad (6.19)$$

Here, the signal amplitude, $V_S(R)$, can be found using the force to voltage transfer function which is represented by Equation (5.41). Substituting for $V_S(R)$ from Equation (5.41), Equation (6.19) becomes:

$$SNR(R) = \frac{\left(\frac{-hT}{Z_C}\right)G(R)F_{SM}}{[V_{JN}(R)^2+V_{EN}(R)^2+V_{AN}^2+I_{AN}^2|Z_E(R)|^2]^{1/2}} \qquad (6.20)$$

All of the terms have been identified previously, however, note in particular that F_{SM} is the signal force in the coupling medium. By setting the SNR equal to unity the minimum detectable force is found to be:

$$MDF(R) = \frac{[V_{JN}(R)^2+V_{EN}(R)^2+V_{AN}^2+I_{AN}^2|Z_E(R)|^2]^{1/2}}{\left(\frac{-hT}{Z_C}\right)G(R)} \qquad (6.21)$$

The minimum detectable power in air can be found using:

$$MDP(R) = \frac{MDF(R)^2}{400A} \qquad (6.22)$$

where A is the area of the transducer. The equations which are listed in this Section

along with those for $Z_E(R)$, $G_0(R)$ and $G(R)$ fully describe the new Receiver Noise Model (RNM). As mentioned previously, the RNM has been implemented using Mathcad. An example of this version of the RNM can be found in Appendix IV. This example is based on a standard PZT-5A transducer and a ZN460 pre-amplifier which is the type used in all of the experimental work. The reasons for choosing this particular pre-amplifier will be discussed in Chapter 7.

6.3.2 Experimental Validation

It is clear from all of the Equations in Section 6.3.1 that the performance of the RNM is critically dependent on the accuracy with which the various noise sources have been represented. It is therefore of interest to compare a theoretical noise spectrum obtained using Equation (6.18) with an experimental spectrum. Banks [85] has conducted a wide range of experiments with a receiver front-end which has a similar specification to that which is used in Appendix IV. This receiver consists of a piezocomposite transducer connected to a ZN460 pre-amplifier. By modifying the parameters in the Appendix IV model to take account of the piezocomposite's lower characteristic acoustic impedance, Z_{CHA}, and its lower value of mechanical quality factor, Q_M, it has been possible to produce a theoretical spectrum that can be compared with the experimental data. In producing the theoretical spectrum it has been assumed that $Z_{CHA}=15$ MRayl and $Q_M=30$. The theoretical and experimental curves are illustrated in Figure 6.2. In order to produce the experimental curve it was necessary to use a conversion factor which takes account of the amplifier gain. Here a gain of 800 was used, which is lower than

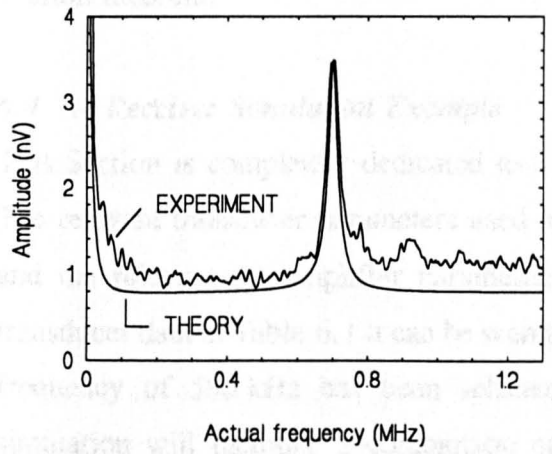

FIGURE 6.2 EXPERIMENTAL AND THEORETICAL NOISE SPECTRA FOR COMPOSITE TRANSDUCER AND ZN460 PRE-AMPLIFIER (7000 OHM INPUT)

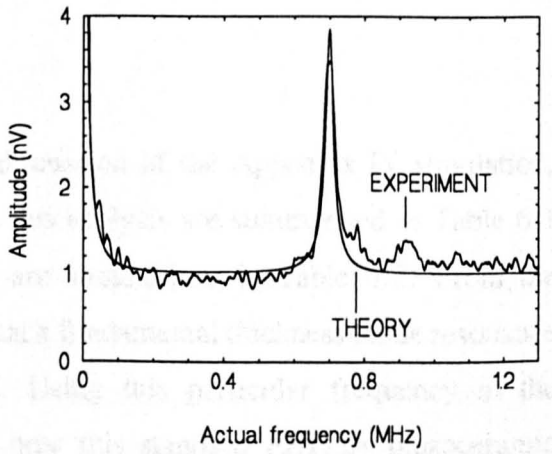

FIGURE 6.3 EXPERIMENTAL AND THEORETICAL NOISE SPECTRA FOR COMPOSITE TRANSDUCER AND ZN460 PRE-AMPLIFIER (14,000 OHM INPUT)

the value quoted on the data sheet. Using a gain of 800 can be justified since it is known form actual measurements that the gain of the ZN460 is often less than quoted by the manufacturer. In the model it was assumed that, as quoted on the data sheet, the amplifier's maximum input impedance is 7 kΩ. It is interesting to note that by changing the input impedance to 14 kΩ in the model it is possible to achieve a considerably better match between the experimental and theoretical data. The effect is illustrated in Figure 6.3. Regardless of which input impedance is used the match between the experimental and theoretical data is excellent. Unlike Banks's theoretical results [85], these results are based on the transducer's mechanical quality factor, Q_M, as used in the RNM. Figure 6.4 indicates how the transducer noise source would be influenced by changes in Q_M.

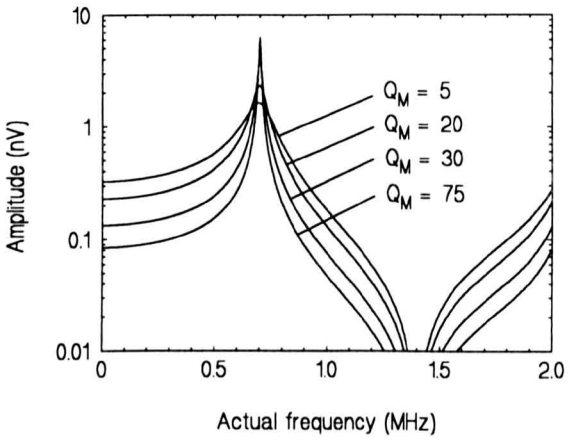

FIGURE 6.4 TRANSDUCER NOISE PLOTTED AS A FUNCTION OF FREQUENCY FOR FOUR DIFFERENT VALUES OF THE MECHANICAL QUALITY FACTOR

The experiments which have been described here provide sufficient evidence to indicate that it is correct to model the transducer noise source by using the real part of the transducer's electrical impedance in the Johnson noise equation. Also, the new closed form solution for absolute sensitivity indicates that the Johnson noise approach is entirely consistent with the alternative approach which is based on the Callen and Welton theorem.

6.4 A Receiver Simulation Example

This Section is completely dedicated to a discussion of the Appendix IV simulation. The relevant transducer parameters used in this analysis are summarised in Table 6.1 and the relevant pre-amplifier parameters are summarised in Table 6.2. From the transducer data in Table 6.1 it can be seen that a fundamental thickness mode resonance frequency of 580 kHz has been selected. Using this particular frequency in the simulation will facilitate a comparison of how this standard PZT-5A piezoceramic transducer performs in comparison to the piezocomposite transducers which were used

TABLE 6.1

TRANSDUCER PARAMETERS USED IN FIRST RECEIVER SIMULATION

NAME OF PARAMETER	ENTRY
Material type	PZT-5A
Fundamental frequency (f_n)	580 kHz
Wave velocity in material (c)	4350 ms^{-1}
Wavelength in material (λ)	7.5 x 10^{-3} m
Thickness ($\tau=\lambda/2$)	3.75 x 10^{-3} m
Transducer radius (r)	15 mm
Transducer area ($A=\pi r^2$)	7.1 x 10^{-4} m^2
Relative dielectric constant - constant strain (K_{33})	830
Permittivity of free space (ε_0)	8.85 x 10^{-12} Fm^{-1}
Static capacitance ($C_0=K_{33}\varepsilon_0\pi r^2/\tau$)	1.385 x 10^{-9} F
Material density (ρ)	7.75 x 10^3 kgm^{-1}
Characteristic acoustic impedance of material ($Z_{CHA}=\rho c$)	34 MRayl
Acoustic impedance of transducer ($Z_C=AZ_{CHA}$)	2.38 x 10^4
Modulus of elasticity (Y_{33})	10.6 x 10^{10} Nm^{-2}
Piezoelectric charge constant ($h=h_{33}$)	21.5 x 10^8 Vm^{-1}
Mechanical quality factor (Q_M)	75

TABLE 6.2

PRE-AMPLIFIER PARAMETERS USED IN FIRST RECEIVER SIMULATION

NAME OF PARAMETER	ENTRY
Pre-amplifier type	ZN460
Maximum input impedance (R_L)	7 x 10^3 Ω
Bandwidth (B_E)	6 MHz
Voltage noise spectral density (v_{AN})	800 x 10^{-12} V
Current noise spectral density (i_{AN})	1 x 10^{-12} A

with the same ZN460 pre-amplifier in all of the experimental work. The reasons for using the ZN460 pre-amplifier will be discussed in Chapter 7, along with the reasons for using a frequency of 580 kHz. The main results of the simulation are summarised in the following Sections.

6.4.1 *Effective Quality Factor and Bandwidth*

A piezoelectric transducer is subjected to additional damping when it is connected to an electrical load. This additional damping can be quantified by calculating the effective quality factor, Q_{EFF}, which can be obtained using Equation (5.39). This equation is reproduced below:

$$Q_{EFF} = |G(1)| = \left| \left[\frac{1}{Q_M} \left(\frac{1}{jR_2} + 1 \right) - \frac{k^2}{jR_2} \right]^{-1} \right| \tag{6.23}$$

Here, R_2 is given by:

$$R_2 = \frac{\omega}{\omega_L} = 2\pi f_n R_L C_0 \tag{6.24}$$

where f_n is the fundamental thickness mode resonance frequency of the transducer, C_0 is its static capacitance and R_L is the input impedance of the pre-amplifier. The R_2 parameter can be regarded as an additional figure of merit which is a characteristic of both the transducer and the pre-amplifier. In this example R_2 is found to be 35.3 and, since the thickness mode electromechanical coupling coefficient, k, is 0.49, the effective quality factor, Q_{EFF}, is 67.4. This means that the Q of the transducer has been reduced by a factor of 10% as a consequence of connecting it to the pre-amplifier. As will become evident, this does not result in a reduction in receiver sensitivity at resonance. In fact, the reduced Q may be an advantage since it corresponds to increasing the transducer bandwidth from 7.73 kHz to 8.6 kHz. These values of transducer bandwidth were obtained using Equation (5.14) which states that $B_E = f_n/Q_M$.

6.4.2 *Noise Sources*

The significant components in Equation (6.18) are plotted in Figure 6.5 as a function of the actual frequency Rf_n. In Figure 6.6, one curve represents the transducer's Johnson noise source and the other the combined effect of the amplifier sources.

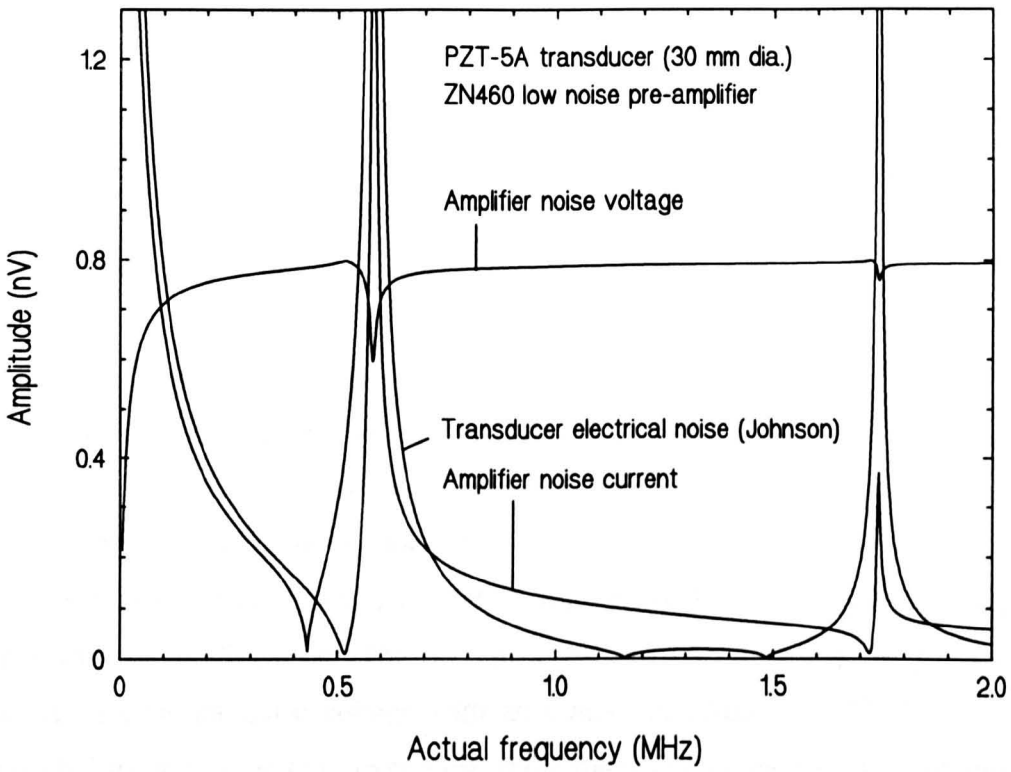

FIGURE 6.5 THE THREE MAIN RECEIVER NOISE CONTRIBUTIONS AS THEY WOULD APPEAR AT THE PRE-AMPLIFIER INPUT

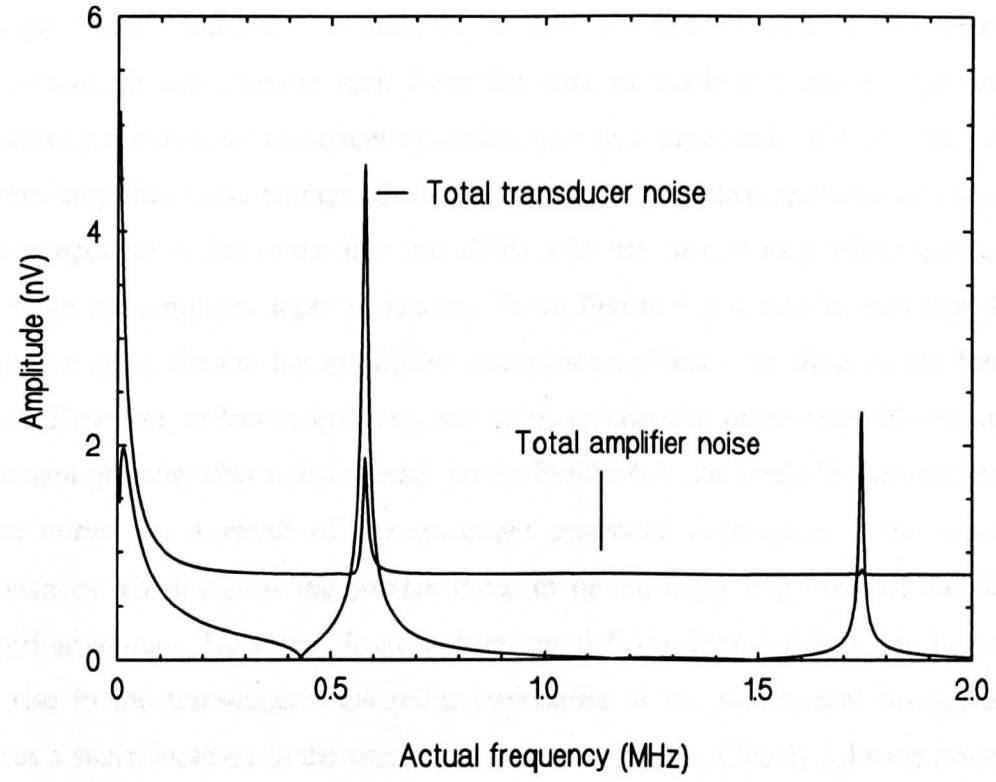

FIGURE 6.6 THE TRANSDUCER (PZT-5A PLATE) NOISE SOURCE AND THE COMBINED EFFECT OF THE AMPLIFIER (ZN460) NOISE SOURCES

Figure 6.7 represents the combined effect of all the receiver noise sources. It should be noted that all of the curves that appear in Figures 6.5, 6.6 and 6.7 represent the noise components as they would appear at the input to the pre-amplifier. Each of the individual components in Figure 6.5 was obtained by plotting Equation (6.18) with all of the other components set to zero. A similar approach was used to obtain the two curves in Figure 6.6, and Figure 6.7 was obtained simply by plotting Equation (6.18) without modification. The data in Table 6.2 indicates that the pre-amplifier produces a constant noise voltage with an r.m.s. amplitude of 800 pV/√Hz. From Figure 6.5 it can be seen that, over most of the frequency range, this has a predominant effect. The frequency dependence that has been introduced into this component is due to the fact that $Z_E(R)$ is in the current loop which also contains the finite pre-amplifier input resistance. Because of the $Z_E(R)$ influence, the amplitude of the pre-amplifier voltage noise component is reduced at low frequencies and at the mechanical resonances. It can also be seen from the data in Table 6.2 that the pre-amplifier produces a constant noise current which has an r.m.s. amplitude of 1 pV/√Hz. As with the pre-amplifier noise voltage, the frequency dependence that has been introduced into this component is due to the fact that $Z_E(R)$ is in the current loop which also contains the finite pre-amplifier input resistance. From Figure 6.5 it can be seen that the pre-amplifier noise current has an almost insignificant effect over most of the frequency range. However, at low frequencies and at the mechanical resonances this becomes the dominant pre-amplifier noise source. So, in Figure 6.6, the peaks in the total amplifier noise curve are a result of the increased electrical impedance at the mechanical resonances which causes the current noise to be the more important of the two pre-amplifier sources. However, from both Figure 6.5 and Figure 6.6, it can be seen that the rise in the transducer's electrical impedance at the mechanical resonances also causes a sharp increase in the transducer's Johnson noise. Clearly Johnson noise in the transducer dominates the total front-end noise at the mechanical resonances.

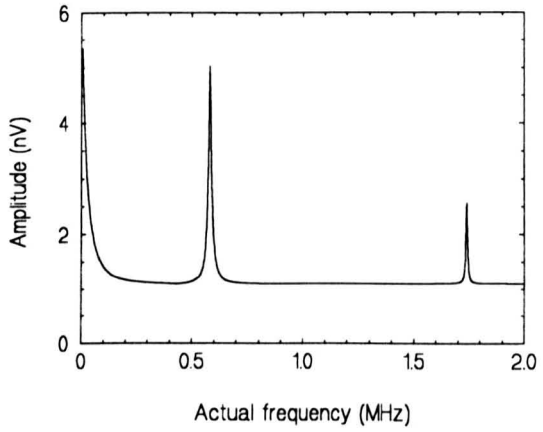

FIGURE 6.7 THE COMBINED EFFECT OF ALL THE NOISE SOURCES FOR A RECEIVER CONSISTING OF A PZT-5A TRANSDUCER AND A ZN460 PRE-AMPLIFIER

6.4.3 *Signal to Noise Ratio*

Figure 6.8 illustrates the receiver's signal to noise ratio (SNR), signal amplitude and total front-end noise as a function of frequency. These curves were generated using Equations (6.20), (5.41) and (6.18) respectively. Also plotted in Figure 6.8 is a straight line (160 dB) which represents the best possible SNR that is possible with a *non-resonant* (this is discussed in Appendix II) transducer which has the same acoustic impedance (34 MRayl) as the one under consideration here. As discussed in detail in Chapter 4, this *non-resonant* limit is purely a function of the transducer's acoustic impedance, Z_C. It is important to note that, for both the resonant and *non-resonant* transducers, the SNR has been calculated for an input force of 1 N in the coupling medium. Also, note that the signal and noise curves are not to scale. Here, multiplying factors have been used so that these curves can be displayed on the same graph. From the signal and noise curves it can be seen that, as mentioned previously, an increase in signal amplitude is accompanied by an increase in noise. As a consequence, the improvement in SNR is not as great as might be expected for a transducer with a relatively high (75) value of Q_M. In fact, as can be seen from the graph, the peak SNR

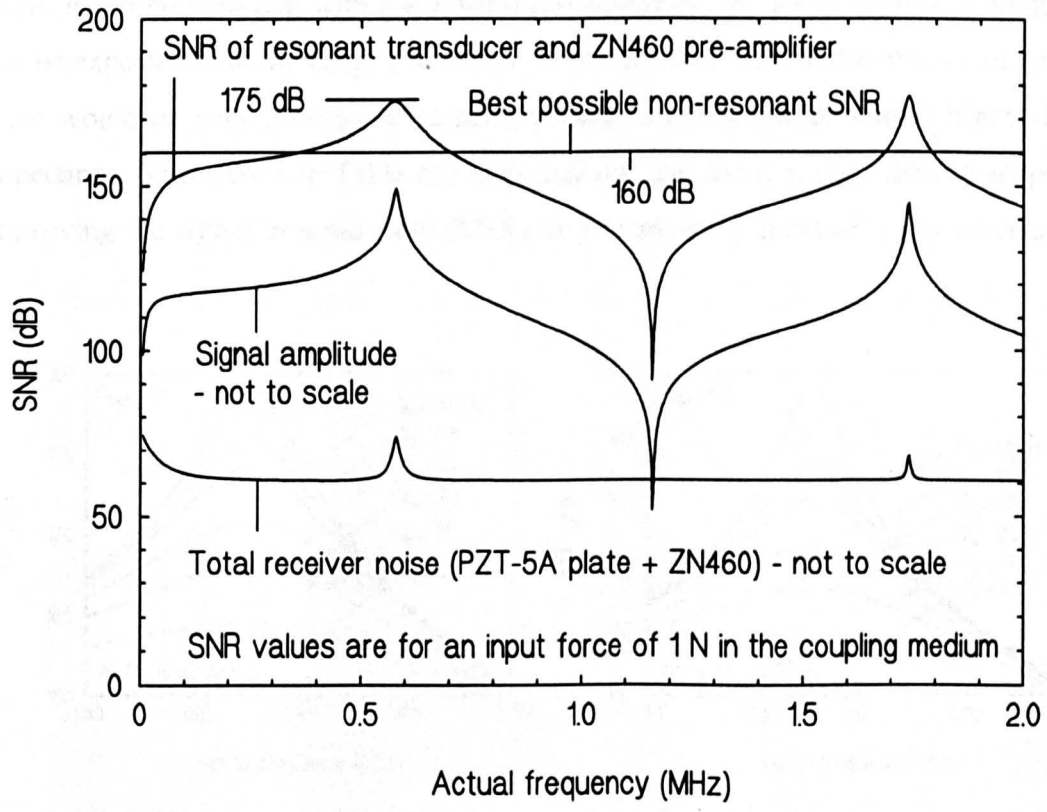

FIGURE 6.8 SIGNAL TO NOISE RATIO, SIGNAL AMPLITUDE AND TOTAL RECEIVER NOISE AMPLITUDE AS A FUNCTION OF ACTUAL FREQUENCY (PZT-5A PLATE AND ZN460 PRE-AMPLIFIER)

is 175 dB which is only 15 dB better than the 160 dB that is achievable with the equivalent *non-resonant* transducer. An improvement in SNR of 15 dB is equivalent to an improvement factor of 5.6. The effect of varying the transducer's mechanical quality factor, Q_M, is illustrated in Figure 6.9. Here, all of the other transducer and pre-amplifier parameters remain unchanged. It is interesting to note that increasing the value of Q_M above 10,000 has an almost insignificant effect on the SNR because an upper limit is set by electrical damping. This can be understood by comparing values of the effective quality factor, Q_{EFF}, with the values of Q_M. The effect of removing electrical damping is illustrated in Figure 6.10. In practice this effect could be achieved by using a pre-amplifier which has a very much higher input impedance than the ZN460 which has been used in the model. It should be noted that Figure 6.10 may not be entirely realistic since the levels of voltage and current noise remain unchanged as the input impedance of the pre-amplifier is altered. The peak values from both sets of curves are listed in Table 6.3. In this table, the values in brackets represent the improvement in SNR relative to the 160 dB that is possible with a *non-resonant* transducer with the same acoustic impedance. All of the receiving transducers which are of interest in this Thesis have a value of Q_M in the range 20 to 100. So, from the table, it can be seen that with the ZN460 pre-amplifier, the improvement in SNR that can be expected is in the range 3.6 to 5.6. It is also clear that, within this range of Q_M, there would be very little to be gained by using a pre-amplifier with a higher input impedance. The results in Table 6.3 also indicate that there is only limited scope for improving the signal to noise ratio (SNR) in a receiver by increasing the value of the

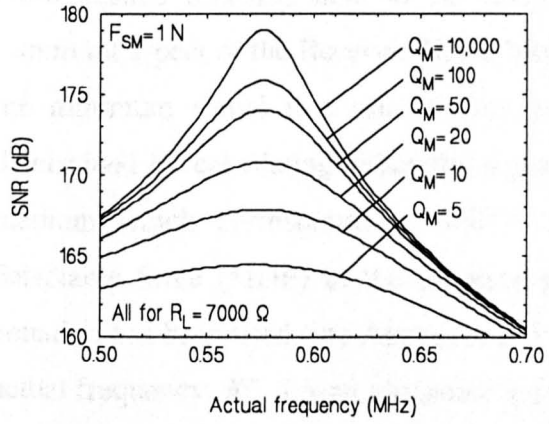

FIGURE 6.9 SIGNAL TO NOISE RATIO CLOSE TO RESONANCE FOR VARIOUS VALUES OF MECHANICAL QUALITY FACTOR (ELECTRICAL LOAD=7000 Ω)

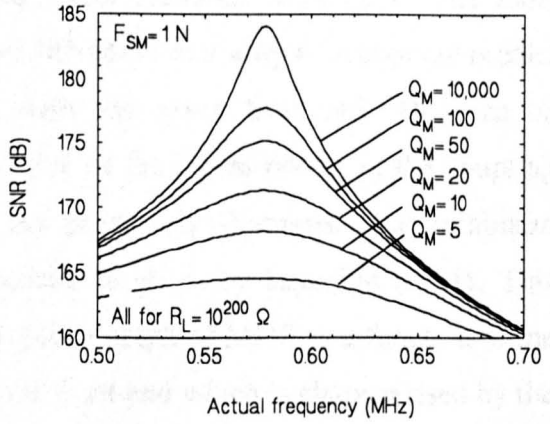

FIGURE 6.10 SIGNAL TO NOISE RATIO CLOSE TO RESONANCE FOR VARIOUS VALUES OF MECHANICAL QUALITY FACTOR (NO ELECTRICAL LOAD)

TABLE 6.3

PEAK SIGNAL TO NOISE RATIOS

Q_M	Q_{EFF} (R_L=7000 Ω)	SNR (R_L=7000 Ω)	SNR (R_L=10^{200} Ω)
10,000	145	179 dB (8.9)	184 dB (16)
100	48	175 dB (5.6)	178 dB (7.9)
50	67	174 dB (5.0)	175 dB (5.6)
20	20	171 dB (3.6)	171 dB (3.6)
10	10	168 dB (2.5)	168 dB (2.5)
5	5	165 dB (1.8)	165 dB (1.8)

Q_M is the mechanical quality factor of the transducer. Q_{EFF} is the effective quality factor of the receiver. Values in brackets represent the improvement in SNR that would be achieved relative to the 160 dB SNR that is possible with a *non-resonant* transducer which has a characteristic acoustic impedance of 34 MRayl

transducer's mechanical quality factor. So, possible improvements in absolute sensitivity are restricted partly because of the effective quality factor and partly because SNR variations are not proportional to Q_M. Table 6.3 indicates that an SNR of better than 184 dB is impractical.

6.4.4 Minimum Detectable Signal

Obviously there is nothing special about a signal force of 1 N. The previously discussed SNR results, which are based on a 1 N signal force, have been included in order to allow results obtained here to be compared with previous work [85]. The most important aspect of the Receiver Noise Model (RNM) is its ability to accurately predict the minimum signal that can be detected with any given front-end. This can be determined by calculating either the signal force or the signal power in the coupling medium which corresponds to SNR=1. As previously discussed, the minimum detectable force (MDF) in the coupling medium is given by Equation (6.21). This equation has been used (see Appendix IV) to plot a graph of MDF as a function of the actual frequency, Rf_n, for an ultrasonic receiver front-end which is characterised by the transducer parameters indicated in Table 6.1 and the pre-amplifier parameters indicated in Table 6.2. The result is illustrated in Figure 6.11. Also plotted in Figure 6.11 are

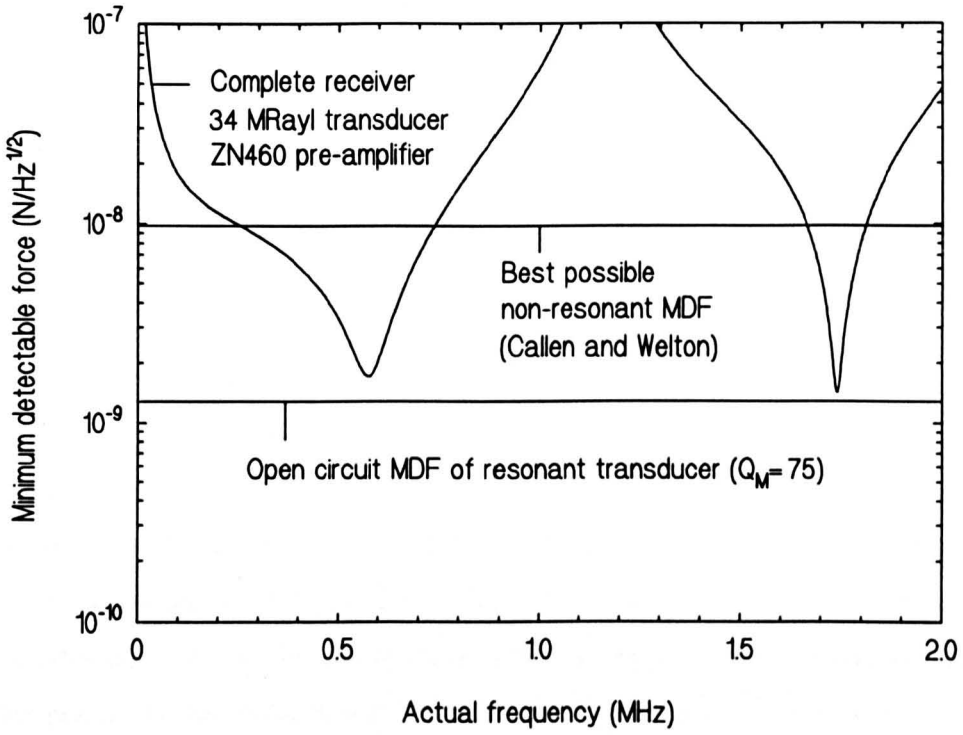

FIGURE 6.11 MINIMUM DETECTABLE FORCE AS A FUNCTION OF FREQUENCY

two horizontal straight lines. The top horizontal line corresponds to the best possible *non-resonant* MDF and was obtained using:

$$MDF_{NR} = (4k_B T_A A Z_{CHA})^{1/2}/T_F \tag{6.25}$$

Here Z_{CHA} is the transducer's characteristic acoustic impedance and A is its area. In this example $Z_{CHA}=34$ MRayl and the transducer diameter is 30 mm. For air coupling, the front face transmission coefficient T_F (force) equals 2. The other terms have been defined previously. For the example under consideration, Equation (6.25) evaluates to:

$$MDF_{NR} = 9.9\times10^{-9}\ N\sqrt{Hz}\quad (30mm\ dia.\ 34\ MRayl)$$

In Figure 6.11, the bottom horizontal line was obtained using Equation (6.12) which is reproduced below in a slightly different form:

$$MDF_{OCR} = \frac{\sqrt{4k_B T_A Z_C}}{\sqrt{\pi Q_M}} \tag{6.26}$$

As discussed in Section 6.2, this equation represents the MDF of a resonant open circuit transducer. In this Thesis this has been shown to be independent of frequency.

This version of Equation (6.12) uses the *OCR* subscript to indicate the resonant open circuit condition. It can now be seen that Equation (6.29) is of enormous value because it provides a very simple way of calculating a figure of merit against which the performance of a complete receiver system can be judged. In this example Q_M=75 which means that Equation (6.26) evaluates to:

$$MDF_{OCR} = 1.28\times10^{-9}\ N\sqrt{Hz} \quad (30mm\ dia.\ 34\ MRayl)$$

It can now be seen that the transducer's mechanical quality factor, Q_M, limits the improvement in performance (resonant compared to *non-resonant*) to a factor of $\sqrt{75}$ or 8.7. This figure can be obtained directly using Equation (6.25). From Figure 6.11, it can be seen that the receiver's MDF at the mechanical resonances closely approaches the previously discussed MDF_{OCR} limit. This was to be expected since it had already been established that, at the resonances, the transducer noise dominates the pre-amplifier noise. At the fundamental thickness mode resonance the MDF is:

$$MDF_{FR} = 1.7\times10^{-9}\ N\sqrt{Hz} \quad (30mm\ dia.\ 34\ MRayl)$$

So, at resonance, this receiver can achieve a level of absolute sensitivity which is almost as good as could be achieved with a resonant open circuit transducer. The small loss in performance is partly due to electrical damping and partly due to the addition of amplifier noise to the total system noise.

Although the performance of the receiver described here is good, MDF_{FR} is only better than MDF_{NR} by a factor of 5.8. It is interesting to compare the MDF figures quoted here with the absolute limit. In Chapter 4 it was shown (see Equation (4.72)) that if it were possible to impedance match a 30 mm diameter transducer to the surrounding coupling medium, the absolute limit of MDF would be:

$$MDF_0 = 6.8\times10^{-11}\ N\sqrt{Hz} \quad (30mm\ dia.\ impedance\ matched)$$

So, as discussed in Chapter 4, the absolute sensitivity would be improved by a factor of 146 compared to MDF_{NR}.

Clearly, operating a transducer at resonance has a similar effect to reducing the characteristic acoustic impedance, Z_{CHA}, of the material from which it is made. At

resonance, it is as if the acoustic impedance had been reduced from, in this case, 34 MRayl to 5.9 MRayl (i.e. 34/5.8). However, unlike a reduction in the characteristic acoustic impedance, operating at resonance has the unwelcome effect of reducing the transducer bandwidth.

For an air coupled transducer the minimum detectable power is given by Equation (6.22). This equation has been used (see Appendix IV) to plot the MDP of the same receiver and the result is illustrated in Figure 6.12. Also shown in Figure 6.12 are two horizontal lines which are the MDP equivalents of the two theoretical MDF limits discussed previously. It is interesting to note from both the MDF and MDP curves that the model predicts a level of absolute sensitivity at the first odd harmonic which is slightly better than at the fundamental frequency. In practice frequency dependent attenuation may prevent this. Other versions of the Linear Systems Model take account of frequency dependent attenuation.

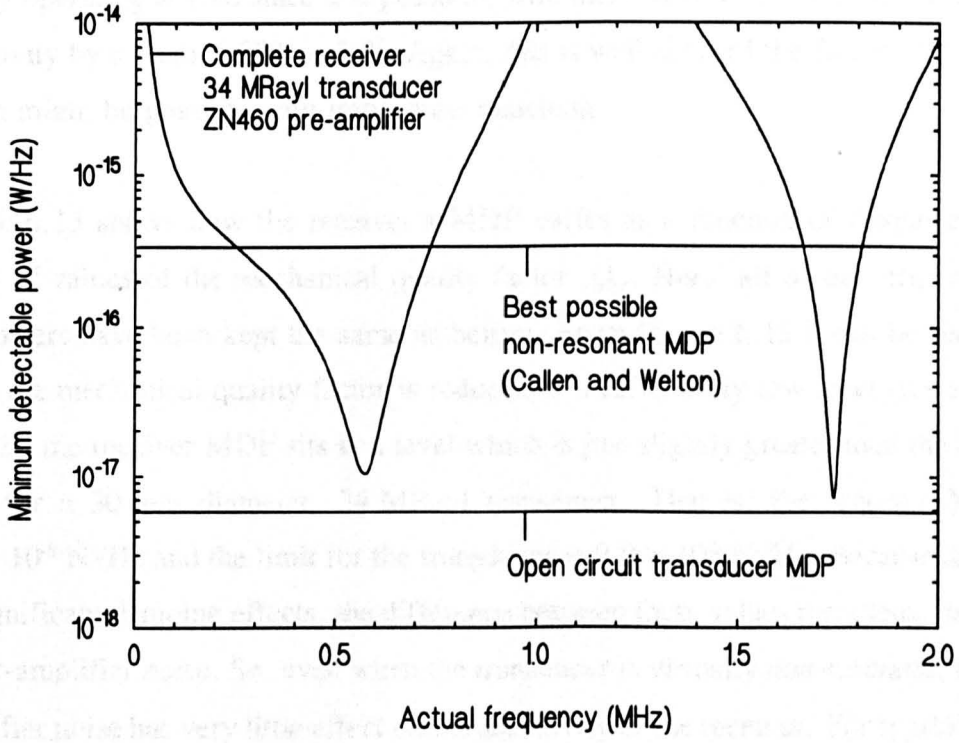

FIGURE 6.12 MINIMUM DETECTABLE POWER AS A FUNCTION OF FREQUENCY

In terms of minimum detectable power (MDP) the three important results are as

follows. From Section 4.5.8, the absolute thermal limit is:

$$MDP_0 = 1.62 \times 10^{-20}\ W/Hz$$

This is the best way to express the thermal limit since it does not involve either the transducer area or the transducer impedance. As before, this limit is only achievable by using a transducer which is impedance matched to the surrounding coupling medium. For a 34 MRayl, *non-resonant* transducer (equivalent to setting Q_M equal to $4/\pi$) used in air the best possible level of minimum detectable power is:

$$MDP = 3.4 \times 10^{-16}\ W/Hz \quad (34\,MRayl,\ Q_M = 4/\pi)$$

This value, which is a factor of 2.1 x 10^4 or 146^2 higher than MDP_0, corresponds to the top horizontal line in Figure 6.12. From Figure 6.12 it can be seen that, for this particular receiver, the best possible MDP at resonance is:

$$MDP = 1 \times 10^{-17}\ W/Hz \quad (34\,MRayl,\ Q_M = 75)$$

So, by operating at resonance it is possible, with this receiver, to improve the absolute sensitivity by a factor of 34 or 5.8^2. Again, this is well short of the factor of 2.1 x 10^4 which might be possible with impedance matching.

Figure 6.13 shows how the receiver's MDF varies as a function of frequency for a range of values of the mechanical quality factor, Q_M. Here, all of the other receiver parameters have been kept the same as before. From Figure 6.13 it can be seen that, when the mechanical quality factor is reduced to a sufficiently low level (for example Q_M=2), the receiver MDF sits at a level which is just slightly greater than the thermal limit for a 30 mm diameter, 34 MRayl transducer. That is, the receiver MDF is 1.2 x 10^{-8} N$\sqrt{\text{Hz}}$ and the limit for the transducer is 9.9 x 10^{-9} N$\sqrt{\text{Hz}}$. Because there are no significant damping effects, the difference between these values represents the effect of pre-amplifier noise. So, even when the transducer is virtually *non-resonant*, the pre-amplifier noise has very little effect on the sensitivity of the receiver. For typical values of Q_M (e.g. in the range 10 to 100) the effect of pre-amplifier noise is almost insignificant. From Figure 6.13 it can also be seen that, for high values of Q_M, the improvement in MDF is much less than might be expected. As with the SNR curves, this happens for two reasons. Firstly, a finite pre-amplifier input impedance will always

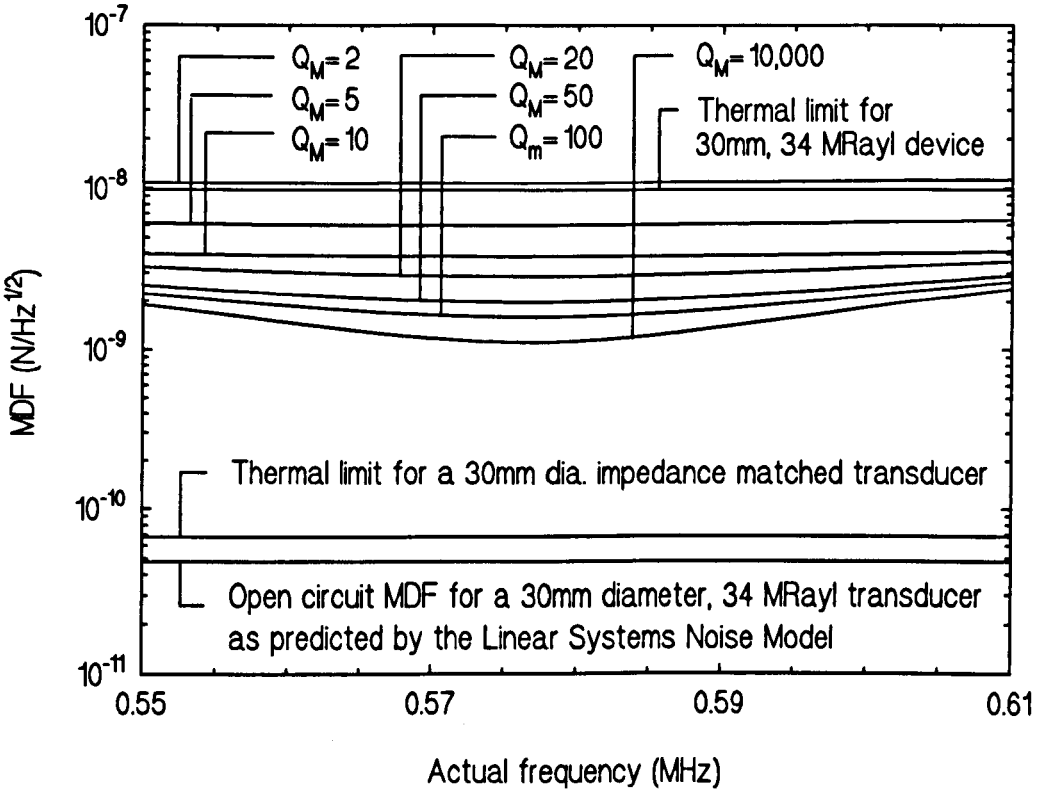

FIGURE 6.13 MINIMUM DETECTABLE FORCE AS A FUNCTION OF FREQUENCY FOR A COMPLETE RECEIVER CONSISTING OF A PZT-5A TRANSDUCER AND A ZN460 PRE-AMPLIFIER

TABLE 6.4

BEST VALUES OF MINIMUM DETECTABLE FORCE

Q_M	Q_E (R_L=7000 Ω)	MDF (N/√Hz) (R_L=7000 Ω)	MDF_{OCR} (N/√Hz) (OPEN CIRCUIT)
10,000	145	1.1×10^{-9}	1.1×10^{-10}
100	48	1.6×10^{-9}	1.1×10^{-9}
50	67	2.0×10^{-9}	1.6×10^{-9}
20	20	2.9×10^{-9}	2.5×10^{-9}
10	10	4.0×10^{-9}	3.5×10^{-9}
5	5	5.9×10^{-9}	5×10^{-9}
2	2	1.1×10^{-8}	7.8×10^{-9}

The thermal limit for a 30 mm diameter, 34 MRayl transducer used in air is 9.9×10^{-9} N/√Hz.

lead to an effective quality factor which is less than the transducer's mechanical quality factor. Secondly, variations in MDF are, as with SNR, proportional to $\sqrt{Q_M}$ and not Q_M. The minimum values from each curve in Figures 6.13 are listed in Table 6.4. Also shown in Table 6.4 are the corresponding values of MDF_{OCR}. This second set of values represents the best sensitivity that is possible with a resonant open circuit transducer which has the same acoustic impedance and mechanical quality factor as the transducer used in the complete receiver. From Table 6.4 it can be seen that, except for very high values of Q_M, connecting the ZN460 pre-amplifier to the PZT-5A plate transducer has very little effect on the achievable MDF. It is interesting to compare the various MDF values with the thermal limit for a 30 mm diameter impedance matched transducer. A line corresponding to this limit is included in Figure 6.13. Another line indicates the open circuit MDF value that was predicted by the original LSNM. As discussed previously, the LSNM line corresponds to a transducer which has no intrinsic loss. If it were possible to construct such a transducer its mechanical quality factor, Q_M, would be infinite. When Q_M is very large transducer damping is entirely due to transmission loss into the surrounding coupling medium. When this happens Q_M must be replaced by Q_T with the result that the MDF becomes independent of all of the transducer properties. As discussed previously, Q_T has a value of 54,000 for a typical air coupled transducer. When the quality factor becomes as large as this, transducer noise and amplifier noise become insignificant and thermal noise in the coupling medium becomes dominant. It is only because the LSNM does not account for this source of noise that it is possible to predict a level of MDF which is below the thermal limit. One final point about Figure 6.13 is worth noting: for all values of Q_M, it is possible to achieve a reasonably constant level of MDF over a frequency range which is in excess of the 60 kHz band covered in the illustration.

6.5 High Performance Transducers

From the Section 6.4 analysis it is now known that, by operating a piezoelectric plate transducer at its fundamental thickness mode resonance frequency, it is typically possible to improve its MDF by a factor of 5.8 compared to the *non-resonant* value which is equivalent to setting Q_M equal to $4/\pi$ in Equation (6.12). Although this may not seem all that significant, it means that a typical resonant plate transducer has an absolute sensitivity which is only a factor of 25 (1.7×10^{-9} / 6.8×10^{-11}) above the

impedance matched MDF for air. As previously discussed, a *non-resonant* plate transducer with a characteristic acoustic impedance of 34 MRayls has an MDF which is a factor of 146 higher that the impedance matched limit. It is not difficult to see how further improvements in receiver MDF and MDP could lead to a situation where thermal noise in the coupling medium (air) could become significant. The mechanical matching layers which are under development within the Ultrasonics Research Group at Strathclyde represent one possible way of significantly reducing acoustic impedance levels. With this in mind it is of interest to examine the significance of the external noise source which has been included in the RNM.

6.5.1 Ultimate Limits

From the previous analysis it is known that, by using an ultra low noise pre-amplifier, it is possible to design a receiver which has an absolute sensitivity, at resonance, which is given by Equation (6.26). If external noise is significant then it is necessary to take into account Equation (6.16) which was obtained using the Callen and Welton theorem. So, assuming that amplifier noise is not significant at or close to the transducer's fundamental resonance frequency, the receiver MDF can be found using:

$$MDF_F^2 = MDF_{OCR}^2 + F_{NM}^2 \tag{6.27}$$

Here, the F subscript has been used to indicate that this only applies at or close to the transducer's fundamental resonance frequency. Combining this with Equations (6.16) and (6.26) gives:

$$MDF_F = (4k_B T_A Z_C)^{1/2}\left[\frac{1}{\pi Q_M} + \frac{Z_1}{Z_C}\right]^{1/2} \tag{6.28}$$

In terms of signal power, the equivalent equation is:

$$MDP_F = \frac{4k_B T_A Z_C}{Z_1}\left[\frac{1}{\pi Q_M} + \frac{Z_1}{Z_C}\right] \tag{6.29}$$

In both of these equations the first term inside the brackets controls the transducer noise contribution and the second term controls the coupling medium noise contribution. From these equations it is clear that, for air coupling, the effects of external noise

become equal to the effects of transducer noise when. $Z_{CHA}/Q_M = 400\pi = 1257$. Here, Z_{CHA} is the characteristic acoustic impedance of the transducer. As noted previously, $Q_M = 75$ for a typical piezoceramic transducer. For this value of the mechanical quality factor it would be necessary to reduce the transducer's characteristic impedance to 0.09 MRayl before external noise became significant. It is interesting to note that materials with much higher values of Q_M do exist. For example, consider the common materials listed in Table 6.5. For PZT8 it would be necessary to reduce the transducer's characteristic impedance to 1.3 MRayl before external noise became significant. Equation (6.28) has been used to generate a set of curves which indicate how the MDF of a transducer varies as a function of its characteristic acoustic impedance for a range of values of its mechanical quality factor, Q_M. The results are illustrated in Figure 6.14. Also, Equation (6.29) has been used to generate a set of curves which indicate how the MDP of a transducer varies as a function of its characteristic acoustic impedance for the same range of Q_M values. The

TABLE 6.5
MATERIALS

MATERIAL	Q_M
PZT4	500
PZT4D	600
PZT8	1000
PZT7A	600
PZT7D	500

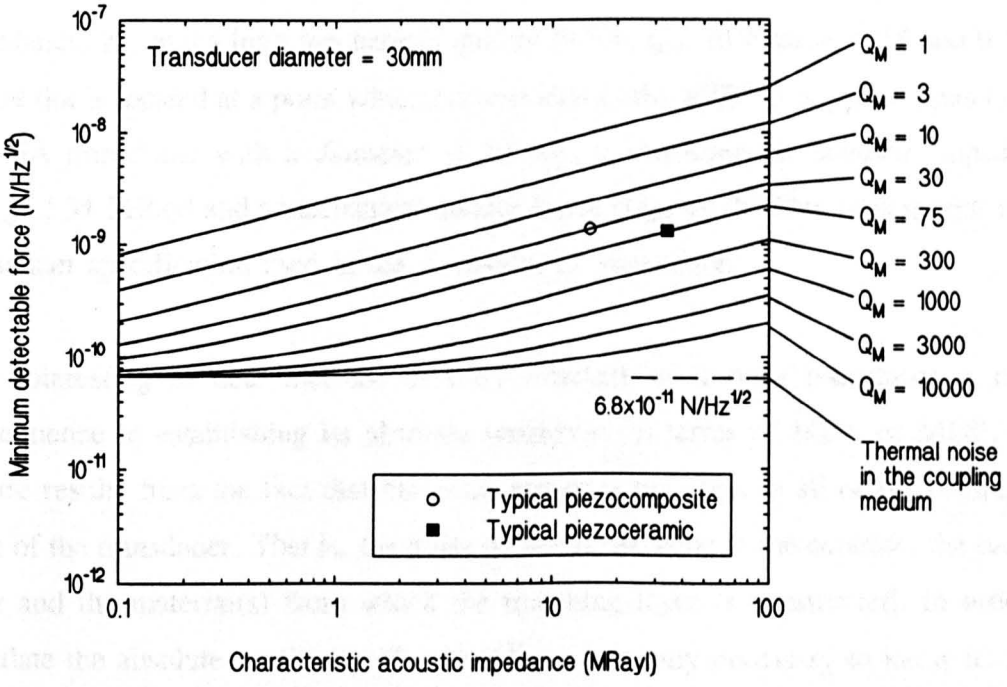

FIGURE 6.14 MDF IN AIR AS A FUNCTION OF CHARACTERISTIC ACOUSTIC IMPEDANCE (THE CURVES TAKE ACCOUNT OF THERMAL NOISE IN THE COUPLING MEDIUM)

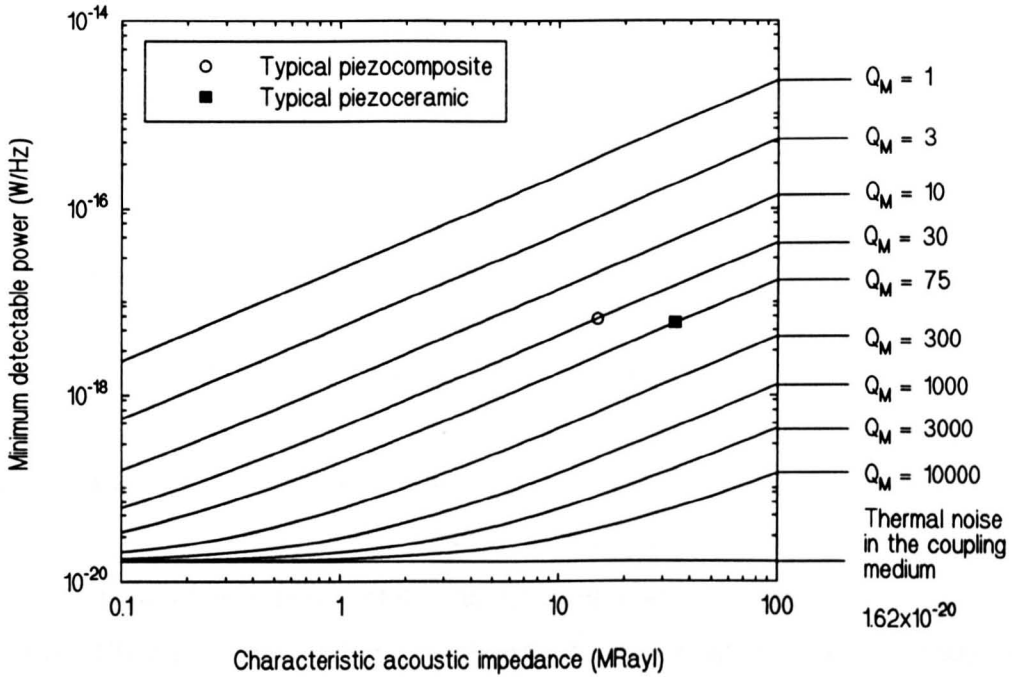

FIGURE 6.15 MDP IN AIR AS A FUNCTION OF CHARACTERISTIC ACOUSTIC IMPEDANCE (THE CURVES TAKE ACCOUNT OF THERMAL NOISE IN THE COUPLING MEDIUM)

results are illustrated in Figure 6.15. These graphs clearly indicate the importance of thermal noise in the coupling medium for transducers which have both a low acoustic impedance, Z_C, and a high mechanical quality factor, Q_M. In Figures 6.14 and 6.16, a square dot is located at a point which corresponds to the MDF of a typical open circuit PZT-5A transducer with a diameter of 30 mm, a characteristic acoustic impedance (Z_{CHA}) of 34 MRayl and a mechanical quality factor (Q_M) of 75. This corresponds to the transducer specification used in the Appendix IV simulation.

It is interesting to note that the detailed structure of a plate transducer is of no consequence in establishing its absolute sensitivity in terms of MDF or MDP. This feature results from the fact that the noise power is the same in all of the component parts of the transducer. That is, the noise power is the same in the ceramic, the passive filler and the material(s) from which the matching layer is constructed. In order to calculate the absolute sensitivity of a transducer it is only necessary to know its front face acoustic impedance and its mechanical quality factor Q_M. For a complicated design, the most difficult part of the problem would be obtaining the value of Q_M.

6.6 *Conclusions*

6.6.1 *The Goal*

The single goal of the work which is described in this Chapter was the development of an accurate and complete receiver noise model. In the previous Chapter it was found that the mechanical quality factor, Q_M, of the transducer is of major significance. The work which has been described in this Chapter reinforces the importance of that finding. As with the Air coupled Transducer Model (ACTM), the only restriction that applies to the Receiver Noise Model (RNM) is that both the transducer's front face coupling medium and its backing medium should be a gas or any other material which produces an insignificant degree of mechanical damping compared to the transducer's intrinsic damping which is quantified by Q_M. It was essential that RNM should produce results which could be experimentally verified and which were also consistent with the findings of Chapter 4. In addition to achieving the main goal, a number of other useful and interesting findings have been made.

6.6.2 *Summary of Achievements*

This Section provides a summary of the principal achievements which are as follows:

- An accurate and highly comprehensive receiver noise model has been developed. This model is suitable for predicting the MDF and MDP of both open circuit piezoelectric transducers and complete receiver systems.

- It has been confirmed that the RNM is capable of generating a theoretical voltage noise spectrum which is in excellent agreement with experimental measurements made by Banks [85].

- The RNM is capable of predicting how MDF and MDP vary as a function of frequency. MDF and MDP predictions made using the RNM are completely consistent with the findings of Chapter 4.

- It has been shown that, in order to obtain accurate results over a wide range of conditions, it is necessary to account for an additional noise source which was not included in the Linear Systems Noise Model (LSNM).

- For the receiver example which was considered in this Chapter and which is fully described in Appendix IV, thermal noise in the transducer predominates over all other noise sources when the transducer is operated at resonance. As in the LSNM, the transducer noise has been calculated by using the real part of the transducer's electrical impedance in the Johnson noise equation. Although this noise sources may appear to be electrical in origin, it has been shown that it can be represented by a mathematical relationship which depends only on the transducer's acoustic impedance, Z_C, and its quality factor, Q_M.

- It has been shown that if a transducer has a combination of a low acoustic impedance, Z_C, and a high quality factor, Q_M, it is possible for thermally generated noise in the coupling medium to become significant. The final version of the RNM takes account of external noise.

- It has been shown that for high values of Q_M it is possible for the LSNM to predict MDF and MDP values which are lower than the device limits which are set by the Callen and Welton theorem. This becomes particularly apparent if it is assumed that it is possible for the transducer to have no intrinsic losses. Under these circumstances Q_M must be replaced by Q_T, which for a typical air coupled transducer has, a value of 54,000. Because the LSM was not originally intended for air coupled applications it is effectively assumed that Q_T is much more significant than Q_M.

- For the ZN460 pre-amplifier, which will be described in Chapter 7, amplifier noise has an almost insignificant effect on the previously discussed MDF levels.

- It has been shown that, for an open circuit transducer, variations in signal amplitude as a function of frequency are accompanied by variations in the amplitude of the transducer's thermal noise voltage. Partly as a consequence of this, transducer's with a high quality factor, Q_M, do not produce the significant improvements in SNR, MDF and MDP that might at first be expected. Electrical damping is the other major factor which limits performance.

- For a complete receiver system electrical damping sets a limit on the effective quality factor, Q_{EFF}. This effect is illustrated in Figure 5.11. So, even if the transducer noise voltage did not increase with Q_M, the value of Q_{EFF} is restricted in any case. For example, consider the receiver which is defined by the values in Tables 6.1 and 6.2. For values of Q_M equal to 75, 100, 1000 and 10,000 the corresponding values of Q_{EFF} are 67, 84, 145 and 145 respectively. The value of Q_{EFF} depends only on the electromechanical coupling coefficient and the R_2 figure of merit which was defined in Section 5.3.2. This figure of merit is given by:

$$R_2 = 2\pi f_n R_L C_0$$

- By operating a 30 mm dia., 34 MRayl, PZT-5A transducer at resonance it is possible to improve the transducer's MDF from 9.9 x 10^{-9} N/$\sqrt{Hz}$ (*non-resonant* limit i.e. $Q_M=4/\pi$) by a factor of 5.8 to 1.7 x 10^{-9} N/$\sqrt{Hz}$. The restricted improvement is a consequence of the previously discussed factors. As discussed in Chapter 4, impedance matching could give an MDF of 6.8 x 10^{-11} N/$\sqrt{Hz}$.

- Figure 6.13 indicate that, for a typical receiver ($Q_M=75$), it is possible to obtain almost constant values of SNR, MDF and MDP over a bandwidth which is well in excess of the 60 kHz range displayed.

- In Section 6.2 it was shown that the closed form solution for open circuit MDF that was described in Chapter 4 is both accurate and meaningful.

- It has been shown that it is possible to obtain very simple mathematical relationships which fully describe the absolute sensitivity of a transducer in terms of MDF and MDP. These relationships indicate that, for a given coupling medium, it is only necessary to know a transducer's acoustic impedance, Z_C, and its mechanical quality factor, Q_M, in order to calculate its resonant MDF and MDP. This is so even though the transducer is described by the relatively complex list of parameters which can be found in Table 6.1. Obtaining these relationships is regarded as a major achievement.

Chapter 7

FEASIBILITY STUDY

7.1 Introduction

This Chapter brings together the work of Chapters 1 to 6 and for the first time in the Thesis shows how each aspect contributes to demonstrating the feasibility of truly practical air coupled test systems.

Examples of all of the conventional liquid coupled test systems were described briefly in Chapter 1. In Chapter 2 it was shown that, for the purpose analysis, all of these systems can be placed into one of three categories: pulse-echo, through transmission and pitch-catch. An important finding was that pulse-echo testing in air at normal pressure would probably be impossible because of the dynamic range problems, however, through transmission and pitch-catch testing would be viable provided that it was possible to find ways of compensating for the coupling losses which are many orders of magnitude worse than for the equivalent liquid coupled systems. Table 2.2 indicates that for typical pulse-echo and through transmission systems, the total insertion loss is -173 dB. For a typical pitch-catch system the total insertion loss is -168 dB. So, as indicated in Table 2.3, the total coupling losses in air are between 137 dB and 140 dB worse than in water. For a typical PZT-5A transducer, the loss at the transducer/air interfaces is -92 dB and for an aluminium test sample the associated losses are between -76 dB and -81 dB depending on the test configuration used. All of the figures in Tables 2.1, 2.2 and 2.3 are based on typical 33 MRayl PZT-5A plate transducers. The reasons for choosing to work with piezoelectric plate transducers are discussed in Chapter 3 and the absolute limits of piezoelectric receiver sensitivity are discussed in Chapter 4. In Chapters 5 and 6 it is shown that by using a resonant receiving transducer and an ultra low noise pre-amplifier it is possible to achieve an MDF of 1.7×10^{-9} N/$\sqrt{\text{Hz}}$ which, for a 30 mm diameter transducer, is equivalent to an MDP of 1×10^{-17} W/Hz. In this Chapter it will be shown that by achieving these very low levels of MDF and MDP it is possible to implement a variety of air coupled test systems. For test systems which are based on piezoceramic transducers it is possible to obtain a bandwidth of almost 10 kHz and for test systems which are based on piezocomposite transducers it is possible to obtain a bandwidth of 20 kHz. It will be shown that *real-time* (no signal averaging or digital processing) testing is possible even with very modest levels of transmitter power. This *real-time* operation is possible without the necessity to place matching layers on the front face of each transducer.

7.2 Theoretical Feasibility Study

For reasons that were discussed in Chapters 1,2 and 3, piezoelectric plates have been selected for both the receiving and transmitting devices which were used in all of the test systems described in this Thesis. The main reason for choosing piezoelectric plate transducers is that their robustness makes them suitable for use in a wide range of industrial and high pressure (e.g. 1000 p.s.i.) environments. Two basic types of plate transducer are available: piezoceramic and piezocomposite. In Chapter 6 it was shown that the resonant sensitivity of a typical piezocomposite receiver is similar to that of a typical piezoceramic receiver. The reason for this is that, although the piezocomposite transducer has a lower acoustic impedance, this is offset by its lower mechanical quality factor, Q_M.

One advantage of designing a system based on piezocomposite plates is that it can achieve the same overall sensitivity as a piezoceramic system but with an improved bandwidth. Another advantage is that radial modes are almost completely eliminated in the piezocomposite transducers. As will be discussed later, a new generation of air coupled piezocomposite transducers was used in all of the experimental work which is described in this Chapter and in Chapter 8. In order to design a complete air coupled ultrasonic test system based on piezoelectric technology it is necessary to know the absolute sensitivity of the receiver and the level of available transmitter power. The limits of receiver sensitivity have been investigated in Chapters 4, 5 and 6. Transmitter limitations are discussed briefly in the following Section.

7.2.1 Transmitter Power

The efficiency of a resonant piezoelectric transmitter is controlled by its front face coupling coefficient, T_F, its mechanical quality factor, Q_M, and its electromechanical coupling coefficient, k. For a complete transmitter system, the amount of electrical energy that is available for conversion into mechanical energy is controlled by the source voltage, the output impedance of the transmitter electronics (pulser or power amplifier) and the operational impedance of the transducer. It is possible to increase the amount of power which is delivered into the coupling medium by reducing T_F or by increasing Q_M. However, attempting to improve T_F by using piezocomposite transducers appears to lead to an unavoidable reduction in Q_M.

Regarding the transmitter electronics there are no real options other than those that reduce the amount of power which is dissipated in the electronic system itself. During the course of this research it was possible to develop a new type of electronic tone burst generator which does exactly that. A brief description of this will be provided later in the present Chapter. The output impedance of the transmitter electronics is important because, as with the electrical input impedance of a receiver pre-amplifier, it leads to damping of the transducer's mechanical vibrations. In addition, the output impedance of the transmitter electronics and the transducer's operational impedance determine the power transfer efficiency which cannot exceed 50%. It is conventional to operate a transmitting transducer at its electrical resonance in order to achieve the best possible power transfer ratio. Later it will be shown that the electrical impedance of a typical air coupled piezocomposite plate transmitter at its electrical resonance is 80 Ω compared to 4 kΩ at its fundamental thickness mode mechanical resonance (see Figure 7.5). Since many commercial power amplifiers have a source impedance of 50 Ω, the power transfer efficiency is reasonable.

If, as is often the case, power dissipation in the transmitter electronics is not important, the maximum amount of power that can be produced by a piezoelectric plate transducer is determined by the amount of heat which is generated within the device itself. This depends on the electrical and mechanical losses. If high transducer temperatures are acceptable then the limit is set, in the case of a piezoceramic device, by depoling of the ceramic, or, in the case of a piezocomposite device, by melting of the polymer. The ultimate limit is the Curie temperature of the ceramic which, for PZT-5A, is 365°C. Any attempt to use a transmitting transducer above the Curie temperature for the ceramic will result in either partial or complete depoling.

According to Grandia *et al.* [42], it is possible to generate transmitter power levels of up to 10 kW using commercially available equipment, however, the work which is described in this Thesis involves much more modest power levels. The reason for this is that the systems which were developed during the course of this research programme are intended to be truly practical, safe, reliable and suitable for use by untrained operators in a variety of industrial environments. In order for these systems to be practical and safe it was necessary to avoid high temperatures and dangerously high

voltages. For the systems to be reliable it was necessary to ensure that none of the components were operated close to their physical limits. With these restrictions in mind it was decided to arrange that the transmitting transducers would not be operated at voltages exceeding 200 V peak. An additional motivation for selecting this as the maximum voltage is that it is commonly used for transducer excitation in conventional liquid coupled test equipment. In most of the experimental work which is described in this Thesis, the transducers were driven with a standard radio frequency power amplifier which has an output impedance of 50 Ω. This amplifier has a gain of 50 dB when operated into a matched 50 Ω load. This is equivalent to a voltage gain of 316 and a power gain of 100,000. The power delivered to the transducer is given by:

$$P_T(Z_E) = \frac{Z_E V_S^2 G^2}{(Z_O + Z_E)^2} \tag{7.1}$$

Here, Z_O is the output impedance of the amplifier, Z_E is the transducer's electrical impedance at its electrical resonance and G is the amplifier's voltage gain. The amplifier has a bandwidth of over 30 MHz so it is reasonable to assume that its gain, G, is constant over the frequency range of interest (typical air channel bandwidth is 1.3 MHz) and that the transducer's electrical power is a function only of its electrical impedance, Z_E. From Equation (7.1) it can be seen that maximum power is delivered to the transducer when $Z_E=Z_O$. When this condition is met:

$$P_T(MAX) = \frac{V_S^2 G^2}{4 Z_O} \tag{7.2}$$

The amplitude, V_S, of the input signal to the power amplifier was typically 300 mV in the experimental systems. For this signal amplitude the maximum electrical power available to the transducer is 45 W. However, as mentioned previously, the electrical impedance of a typical transmitting transducer at resonance is 80 Ω so that the typical transducer electrical power is 42.5 W. Transmitter power as a function of transducer impedance is illustrated in Figure 7.1. The corresponding transducer voltages are illustrated in Figure 7.2. By using these low levels of power along with low repetition rate tone bursts (defined later) it was possible to ensure that the transmitting transducers used in this work operated at temperatures which did not significantly exceed 21°C.

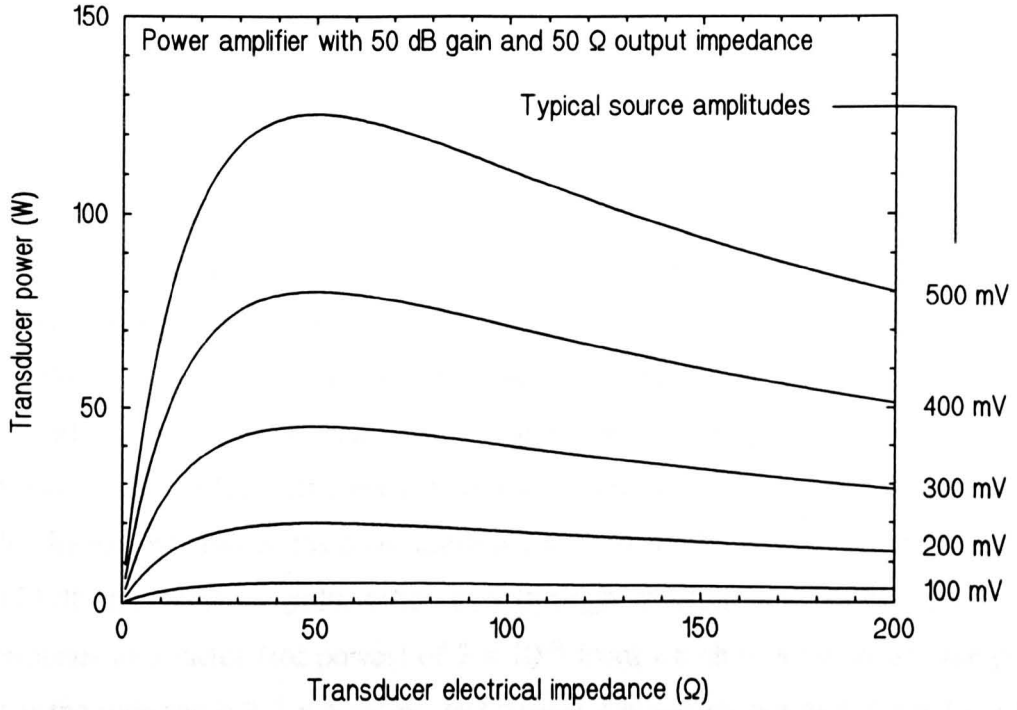

FIGURE 7.1 TRANSDUCER POWER AS A FUNCTION OF TRANSDUCER ELECTRICAL IMPEDANCE

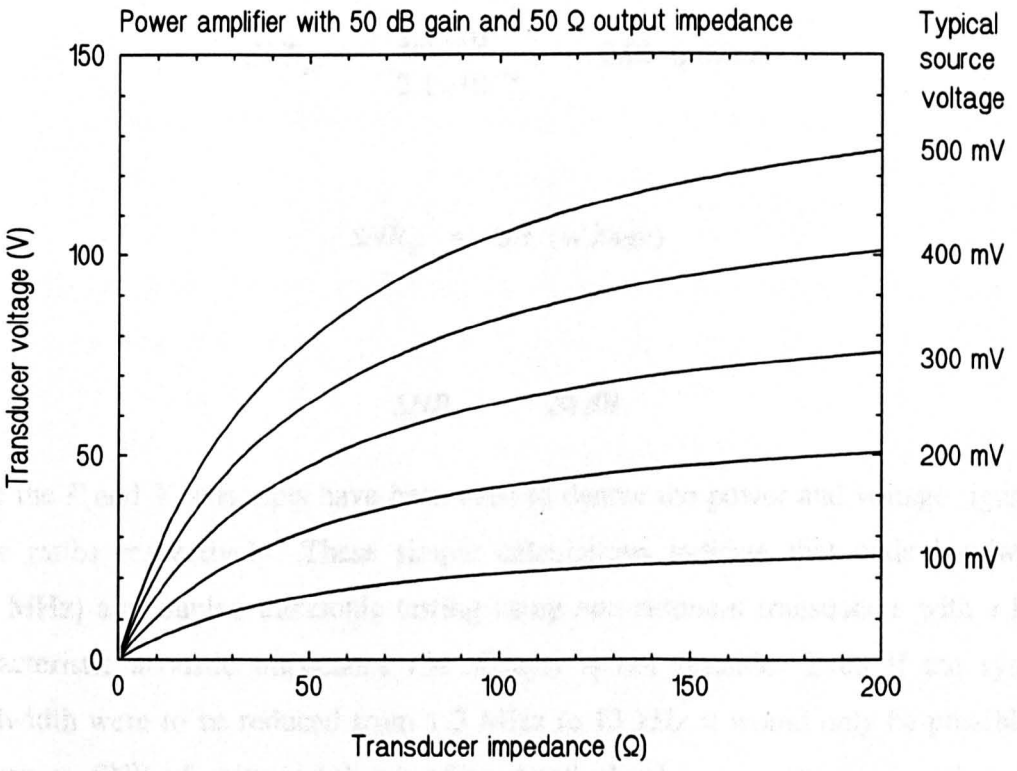

FIGURE 7.2 TRANSDUCER VOLTAGE AS A FUNCTION OF TRANSDUCER ELECTRICAL IMPEDANCE

7.2.2 *A System Based on Non-Resonant Transducers*

The feasibility of testing using air coupled transducers can now be assessed. Consider the previously discussed arrangement in which the transmitter power is 42.5 W. Initially, let it be assumed that the transmitting and receiving transducers are *non-resonant*. As discussed in Appendix II this means that, close to the frequencies of interest, they exhibit no gain in particle velocity compared to the particle velocity in an infinite medium. For now, it will also be assumed that the transmitting transducer is capable of converting electrical energy into mechanical energy with an efficiency of 100% and that the receiving transducer is capable of converting mechanical energy into electrical energy with an efficiency of 100%. From Table 2.2 it can be seen that, for an aluminium test sample, the total insertion loss (transmitter to test sample to receiver) is -173 dB for either a pulse-echo or a through transmission configuration. This corresponds to a factor (for power) of 5×10^{-18} from which it is found that the power level at the receiver is 2.1×10^{-16} W. In Chapter 2 it was shown that, for a 1 cm long air channel, the maximum available bandwidth of the channel is 1.3 MHz. From Chapters 4 and 6 it is known that the noise power at the receiver is 1.62×10^{-20} W/Hz. So, assuming that the full channel bandwidth is available, the total noise power at the receiver is 2.1×10^{-14} W. It follows that the signal to noise ratio is:

$$SNR_P = \frac{2.1\times10^{-16}}{2.1\times10^{-14}} = 0.01 \ (power)$$

or:

$$SNR_V = 0.1 \ (voltage)$$

or:

$$SNR = -20\,dB$$

Here the P and V subscripts have been used to denote the power and voltage signal to noise ratios respectively. These simple calculations indicate that wide bandwidth (1.3 MHz) air coupled ultrasonic testing using *non-resonant* transducers with a high characteristic acoustic impedance (34 MRayl) is not feasible. Even if the system bandwidth were to be reduced from 1.3 MHz to 13 kHz it would only be possible to achieve an SNR of unity and that is of no practical value.

Power Levels in the Coupling Medium

Using Equation (4.16) it can be seen that, for a 34 MRayl transducer transmitting into air, the power transmission coefficient (one face) is 1.2×10^{-5} and hence the power in the coupling medium on the transducer side of the test sample is 0.5 mW. From Table 2.2, the coupling losses associated with the aluminium test sample amount to -81 dB or a factor of 7.9×10^{-9}. This means that the signal power in the coupling medium at the receiver side of the test sample is 4 pW. These figures provide useful references against which other systems can be judged.

7.2.3 A System Based on Resonant Transducers

It is possible to use the Linear Systems Model (LSM) to model the performance of a resonant transmitting transducer in a similar way to that in which it is used to model a resonant receiving transducer [55,81]. Although many researchers employ simpler methods to determine the level of available sound power [42], the LSM method has the advantage that it accounts for, among other things, the effect of electrical damping on the transducer's mechanical resonances.

Linear Systems Transmitter Model

As with the receiver work, a version of the LSM which is appropriate to the transmitter investigation has been implemented using Mathcad and a typical example can be found in Appendix V. Because the example is based on a PZT-5A plate transducer, the material parameters are the same as those which were used in the receiver analysis and which are listed in Table 6.1. The only difference between the transmitting and receiving transducers is that the fundamental mechanical resonance of the transmitter has been chosen such that its electrical resonance frequency is coincident with the fundamental mechanical resonance of the receiving transducer. By doing this it is possible to arrange that the transmitter is operating at a frequency which is within the relatively narrow band of frequencies over which the receiver is most sensitive. The LSM has been used to calculate both the force and the power in the coupling medium (air) for the same values of transmitter voltage (95 V) and source impedance (50 Ω) as were used in Section 7.2.1. Force as a function of frequency is illustrated in Figure 7.3 and power as a function of frequency is illustrated in Figure 7.4. From Figure 7.4 it can be seen that the peak power (i.e. at 580 kHz) in the coupling medium

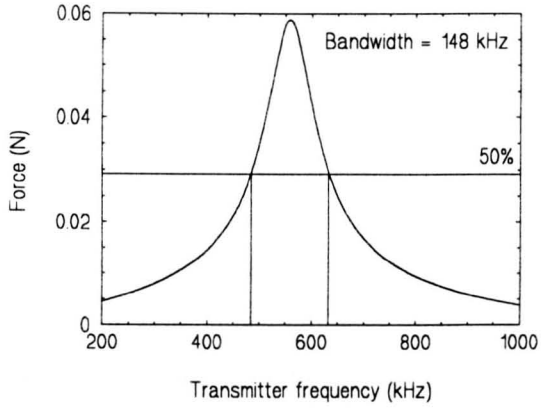

FIGURE 7.3 FORCE IN THE COUPLING MEDIUM AS A FUNCTION OF FREQUENCY (PREDICTED USING THE LINEAR SYSTEMS MODEL)

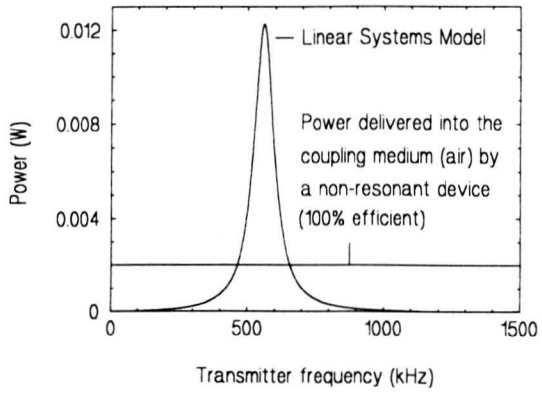

FIGURE 7.4 POWER IN THE COUPLING MEDIUM AS A FUNCTION OF FREQUENCY (PREDICTED USING THE LINEAR SYSTEMS MODEL)

on the transmitter side of the test sample is 12 mW compared to 0.5 mW for the previously considered 100% efficient, *non-resonant* system. So, the LSM indicates that, by operating at the transducer's electrical resonance frequency, it is possible to increase the power in the coupling medium by a factor of 24. From Table 2.2 it can be seen that the coupling losses associated with the aluminium test sample amount to -81 dB or a factor of 7.9×10^{-9}. This means that the signal power in the coupling medium at the receiver side of the test sample is 9.4×10^{-11} W. From Section 6.4.4 it is known that for a standard PZT-5A plate (Z_{CHA}=34 MRayl and Q_M=75) and a ZN460 pre-amplifier, it is possible to achieve a resonant (580 kHz) receiver MDP of 1×10^{-17} W/Hz. As discussed in Section 6.4.1, this receiver has an effective quality factor, Q_E, of 67.4 and hence a bandwidth of 8.6 kHz which is considerably narrower than the transmitter's 148 kHz bandwidth. If 8.6 kHz is used as the system bandwidth then the full MDP in the coupling medium is 8.6×10^{-14} W and the signal to noise ratio is:

$$SNR_P = \frac{9.4\times10^{-11}}{8.6\times10^{-14}} = 1093 \quad (power)$$

or:

$$SNR_F = 33 \ (force)$$

or:

$$SNR = 30\,dB$$

Summary

The analysis that has been performed in this Section clearly indicates that, provided that the system bandwidth can be reduced to 8.6 kHz, it is possible to use resonant PZT-5A piezoceramic transducers to perform air coupled testing. It is important to note that the resonant (Q_M=75) system which has been described in this Section is 50 dB more sensitive than the *non-resonant* (see Appendix II) system described in Section 7.2.1. Details of how this has been achieved are summarised in Table 7.1. This level of performance requires the use of an ultra low noise pre-amplifier (e.g. the ZN460).

TABLE 7.1
SUMMARY OF RESONANT AND NON-RESONANT SYSTEM CHARACTERISTICS

PROPERTY	NON-RESONANT	RESONANT (Q=75)	RELATIVE GAIN
SIGNAL GENERATOR AMPLITUDE	300 mV	300 mV	N.A.
POWER AMPLIFIER GAIN (dB)	50 dB (R_L=50 Ω)	50 dB (R_L=50 Ω)	N.A.
POWER AMPLIFIER GAIN (POWER)	10^5 (R_L=50 Ω)	10^5 (R_L=50 Ω)	N.A.
POWER AMPLIFIER GAIN (VOLTAGE)	316 (R_L=50 Ω)	316 (R_L=50 Ω)	N.A.
POWER AMPLIFIER SOURCE VOLTAGE	95 V	95 V	N.A.
POWER AMPLIFIER O/P IMPEDANCE	50 Ω	50 Ω	N.A.
TRANSMITTER POWER (ELECTRICAL)	42.5 W	N.A.	N.A.
TRANSMITTER EFFICIENCY	100%	56%	N.A.
TRANSMITTER POWER (MECHANICAL)	42.5 W	N.A.	N.A.
POWER IN AIR AT TRANSMITTER	0.5 mW	12 mW	24 UP
SIGNAL POWER IN AIR AT RECEIVER	4 pW	94 pW	24 UP
SIGNAL POWER IN RECEIVER	2.1 x 10^{-16} W	N.A.	N.A.
RECEIVER EFFICIENCY	100%	56%	N.A.
BANDWIDTH	1.3 MHz	8.6 kHz	151.2
RECEIVER SENSITIVITY (W/Hz)	3.44 x 10^{-16} W/Hz	1 x 10^{-17} W/Hz	34.4
RECEIVER SENSITIVITY (W)	4.47 x 10^{-10} W	8.6 x 10^{-14} W	5201
NOISE POWER (W/Hz)	1.62 x 10^{-20} W/Hz	1.62 x 10^{-20} W/Hz	N.A.
NOISE POWER (W)	2.1 x 10^{-14} W	1.4 x 10^{-16} W	151 DOWN
SIGNAL TO NOISE RATIO	-20 dB	30 dB	50 dB

NOTE: The resonant system has been analyzed using the Linear Systems Model and is based on standard PZT-5A piezoceramic transducers. The transducers in both systems have an acoustic impedance of 34 MRayl and the test sample is aluminium with an acoustic impedance of 17 MRayl. Receiver performance is based on the ZN460 pre-amplifier. The abbreviation N.A. indicates that the data is either not applicable or not available.

All of the transducer specifications which have been used in the main theoretical examples in this Thesis have been based on standard piezoceramic devices which have a characteristic acoustic impedance of 34 MRayl and a mechanical quality factor of 75. By deliberately working with one particular transducer specification it has been possible to ensure that all of the theoretical results are consistent. This approach has also allowed direct comparisons to be made between different test configurations and different receiver configurations. In addition, the transducer parameters which have been used can easily be checked against the manufactures data.

Piezocomposite Transducers

When this research programme was initiated it was believed that the superior properties of composite piezoelectric materials would be highly significant in the air coupled work, however, this judgement was made in the absence of the receiver noise analysis which is described in Chapter 6 of this Thesis. It is now known that the sensitivity (MDF or MDP) of a piezocomposite transducer is not significantly different from that of a receiver which uses a standard PZT-5A plate transducer. This can be explained as follows. The sensitivity (MDF) of a *non-resonant* (see Appendix II), air coupled, piezoelectric plate transducer is given by Equation (6.25) which is reproduced below:

$$MDF_{NR} = (k_B T_A B Z_C)^{1/2} \tag{7.3}$$

Here, k_B is Boltzmann's constant, T_A is the absolute temperature, B is the bandwidth and Z_C is the acoustic impedance of the transducer. The acoustic impedance of a typical piezocomposite transducer is 5 MRayl compared to 34 MRayl for a typical PZT-5A piezoceramic transducer. This means that the best possible improvement in MDF that can be achieved by using a piezocomposite device instead of a piezoceramic device is approximately $\sqrt{7}$. Unfortunately, a $\sqrt{7}$ improvement in absolute sensitivity is not necessarily achievable with a resonant transducer. The absolute receiver sensitivity depends not only on the transducer's acoustic impedance, Z_C, but on its mechanical quality factor, Q_M. This is evident from Equation (6.26) which is reproduced below:

$$MDF_{OCR} = \sqrt{\frac{4 k_B T_A Z_C}{\pi Q_M}} \tag{7.4}$$

This equation indicates that, if it were possible to keep Q_M constant, it would again be

possible to achieve an approximate $\sqrt{7}$ improvement in MDF by using a composite transducer instead of a ceramic transducer. However, in practice, the Q_M of a piezocomposite transducer is always significantly less than that of the piezoceramic material from which it is manufactured. So, the possible $\sqrt{7}$ or 8.5 dB advantage is severely eroded. In fact, some piezocomposite transducers may be less sensitive than their piezoceramic equivalents. It can now be seen that the results which are summarised in Table 7.1 would not have been significantly different if the resonant transducer analysis had been based on piezocomposite rather than piezoceramic transducers. However, this is only strictly true provided that pre-amplifier noise is insignificant compared to transducer noise. As previously discussed, this has been made possible by using the ZN460 ultra low noise pre-amplifier. The reasons for using this amplifier are discussed in Section 7.3. Piezocomposite transducers were used in all of the experimental work which is described in the remainder of this Thesis. The original reasons for using piezocomposite transducers are also discussed in Section 7.3.

7.3 An Ultra Low Noise Receiver

This Section of the Thesis is concerned with the detailed design of an ultra low noise receiver based on piezocomposite transducer technology. The piezocomposite transducers are discussed in Section 7.3.1 and the pre-amplifier is discussed in Section 7.3.2.

7.3.1 The Transducers

A brief description of 1-3 connectivity piezoceramic composite transducer technology was provided in Section 3.4.4 and an illustration of the transducer structure is provided in Figure 3.9. A physical model [96] can be used to investigate the material properties which govern the thickness-mode oscillations of this type of PZT-rod/polymer composite device. This model is valid provided that the lateral periodicity of the rods is much smaller than all of the relevant acoustic wavelengths. A computerised implementation of the model is available within the Ultrasonics Research Group (URG) at Strathclyde and this was used to design the composite transducers which were employed in the experimental investigation.

The design of a piezocomposite transducer for a particular application involves

choosing suitable component materials and selecting an appropriate ceramic volume fraction. The URG has conducted an extensive investigation [47] aimed at determining the optimum transducer volume fractions for 1-3 connectivity transmitter/receiver pairs used in air. The conclusions of this investigation are as follows. For an air backed transducer transmitting into air, maximum sensitivity (overall efficiency) occurs with volume fractions of 70% or greater. Simulations indicate that it may be possible to extend this upwards if high volume fraction devices can be manufactured with lower aspect ratios. For an air coupled receiver operating into a 10 MΩ load, peak sensitivity (this definition of sensitivity does not take account of transducer noise) with volume fractions in the 10% - 15% range. However, the design of a 10% composite is difficult because of the influence of inter-pillar resonances within the composite structure. These inter-pillar resonances can interfere with and degrade the desired thickness mode operation. The extent of the degradation is a function of pillar shape and distribution, in addition to choice of passive material. An accurate prediction of the performance of these low volume fraction devices is only possible using finite element analysis (FEM).

Figure 7.5 shows how the electrical impedance of a 20% ceramic volume fraction transducer varies as a function of frequency. This plot was obtained for a real device using a Hewlett Packard 4194A impedance analyzer. A significant difference between this impedance plot and the piezoceramic impedance plots which were discussed in Section 4.2.2 is the absence of radial modes. Indicated in Figure 7.5 are the positions of the electrical and mechanical resonances. Maximum pressure output is obtained from the device if the frequency of the applied electrical signal matches the electrical resonance frequency. However, maximum sensitivity is obtained in reception if the frequency of the incident pressure waves is matched to the mechanical resonance. Clearly it is possible to improve the signal to noise ratio in pitch-catch mode by arranging to frequency match the

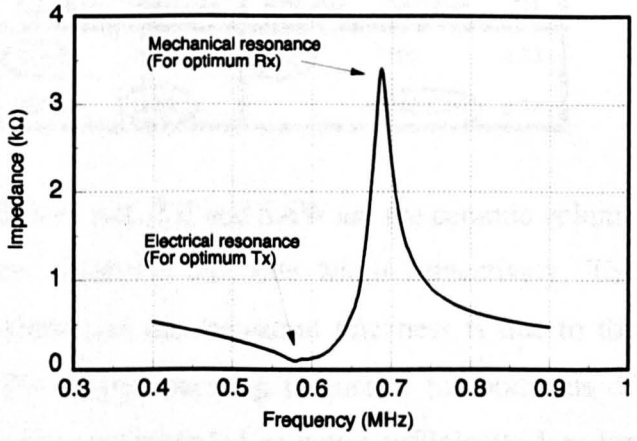

FIGURE 7.5 IMPEDANCE PLOT OF THE PIEZOCOMPOSITE TRANSMITTING TRANSDUCER (VOLUME FRACTION=20%) USED IN THE EXPERIMENTAL INVESTIGATION

transducers. As will be discussed later in the present Section, the improvement in performance that can be achieved using frequency matching can be predicted using the previously discussed Linear Systems Model. This improvement in performance was accounted for in the Section 7.2.2 analysis.

Two sets of piezocomposite transducers were manufactured for use in the first experimental system. In accordance with the findings of the previously mentioned investigation, one set was to consist of a 10% receiver, frequency matched to a 70% transmitter, and the other set was to consist of a 20% receiver frequency, matched to a 20% transmitter. It was anticipated that the second set of transducers would be less difficult to manufacture. The previously mentioned computer model was used to obtain all of the information necessary to manufacture the transducers. All of the relevant data (computed data and data from measurements made on the completed transducers) is

TABLE 7.2
DETAILS OF TRANSDUCERS USED IN THE FIRST AIR COUPLED EXPERIMENTS

PZT5A 30mm ⌀	INPUT				COMPUTED		MEASURED		
	VF	AR	TH	SAW	F(E) kHz	F(M) kHz	F(E) kHz	F(M) kHz	TH
Tx(20%)	0.2	0.1	2.45	0.3	578.5	686.1	580	688	2.55
Rx(20%)	0.2	0.1	2.90	0.3	486.9	577.4	487	566	3.03

PZT5H 30mm ⌀	INPUT				COMPUTED		MEASURED		
	VF	AR	TH	SAW	F(E) kHz	F(M) kHz	F(E) kHz	F(M) kHz	TH
Tx(70%)	0.7	0.34	2.50	0.17	598.2	785.3	670	767	2.53
Rx(10%)	0.1	0.18	2.65	1.10	537.7	610.3		540 (730)	2.77

summarised in Table 7.2. In Table 7.2, VF, AR, TH and SAW are the ceramic volume fraction, pillar aspect ratio, transducer thickness and saw width respectively. The difference between the specified thickness and the measured thickness is due to the thickness of the painted electrodes. The target operating frequency for both sets of transducers was 600 kHz. This frequency was regarded as being sufficiently low for attenuation in air to be insignificant over the operating ranges under consideration. It was also sufficiently high to be of practical value in some of the anticipated NDT

applications. From Table 7.2 it can be seen that frequency matching of the 20% pair of transducers was reasonably successful, with the transmitter operating at 580 kHz and the receiver operating at 566 kHz. Frequency matching of the second pair of transducers (70%,10%) was not successful. At 670 kHz the measured electrical resonance of the 70% transmitter was much higher than had been expected. Also, the impedance plot of the 10% receiver had two peaks: a small peak at 540 kHz and a large peak at 730 kHz. The peak at 730 kHz was due to inter-pillar resonances. Because of the problems with the second pair of transducers (70%,10%) all of the initial experiments were conducted using the 20% pair of transducers. Figure 7.6 illustrates superimposed impedance analyzer plots for the 20% transmitter and the 20% receiver. From this it can be seen that the transducers have been manufactured in such a way that the mechanical resonance of the receiver is very close to the electrical resonance of the transmitter. The improvement in sensitivity that can be obtained by frequency matching of the transducers was quantified by using the Linear Systems Model to simulate pitch-catch operation of the transducers when the transmitter is driven with a typical 20 cycle tone burst. Figure 7.7 illustrates the simulated output from the receiver for two identical 20% transducers and Figure 7.8 illustrates the simulated output from the receiver for frequency matched

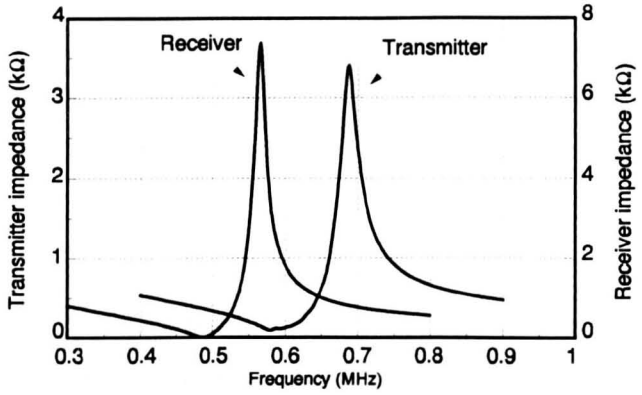

FIGURE 7.6 IMPEDANCE PLOTS OF THE FREQUENCY MATCHED PIEZOCOMPOSITE TRANSDUCERS (VF=20%) USED IN THE EXPERIMENTAL INVESTIGATION

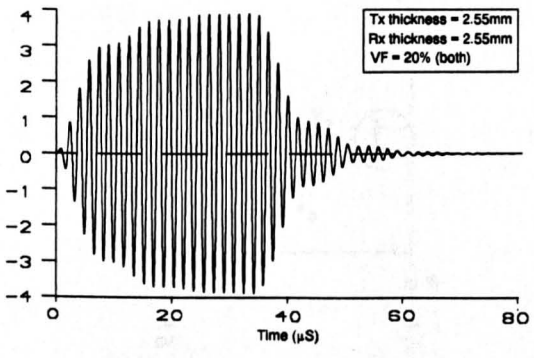

FIGURE 7.7 SIMULATED RECEIVER OUTPUT WITH TWO IDENTICAL 20% VOLUME FRACTION TRANSDUCERS USED IN PITCH-CATCH MODE

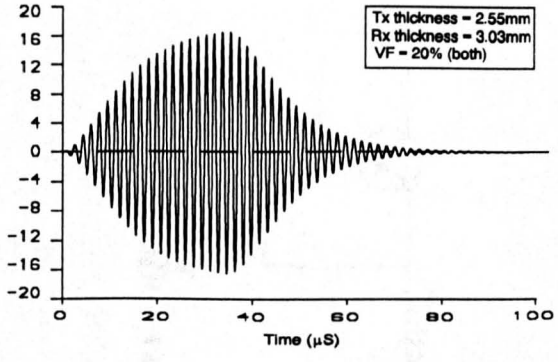

FIGURE 7.8 SIMULATED RECEIVER OUTPUT WITH TWO FREQUENCY MATCHED 20% VOLUME FRACTION TRANSDUCERS USED IN PITCH-CATCH MODE

transducers. The only parameter that was changed between the first simulation and the second simulation was the thickness of the receiving transducer. In the experimental investigation a ZN460 pre-amplifier was used. As discussed in Chapter 6, this has an input impedance of 7 kΩ. This value of pre-amplifier input impedance was used in the simulations. By comparing Figures 7.7 and 7.8 it can be seen that frequency matching improves the sensitivity of the 20% transducer pair by a factor of 4 (12 dB). As mentioned previously, this improvement in performance was accounted for in the Section 7.2.2 analysis. From Figure 7.6 it can be seen that the bandwidth of the piezocomposite receiving transducer is 20 kHz and hence it has a Q_M of 29. So, although the characteristic acoustic impedance of the transducer has been reduced by 50% compared to a standard PZT-5A piezoceramic transducer, Equation (7.4) indicates that there is no significant difference in sensitivity (MDF or MDP).

7.3.2 The Pre-Amplifier

A low noise amplifier can be designed using either bipolar transistors or field effect transistors. Regardless of which technology is used, thermal noise at the input to the pre-amplifier is accounted for by the two noise generators (v_a and i_a) which were included in the previously discussed Receiver Noise Model. This model can be used to predict the performance a complete receiver front-end (combined transducer and pre-amplifier). So, in the following investigation it is only necessary to obtain values for v_a and i_a. The noise models for a field effect transistor (FET) and a bipolar transistor are illustrated in Figure 7.9 and 7.10 respectively. Although two noise generators are indicated in Figure 7.9, it is only necessary to include the voltage source for most practical applications. The current source takes account of the gate leakage current and

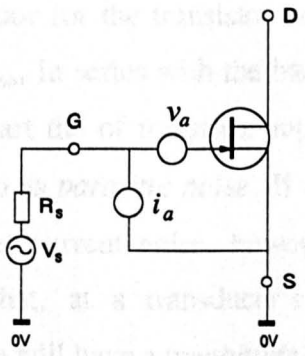

FIGURE 7.9 NOISE MODEL OF A FIELD EFFECT TRANSISTOR

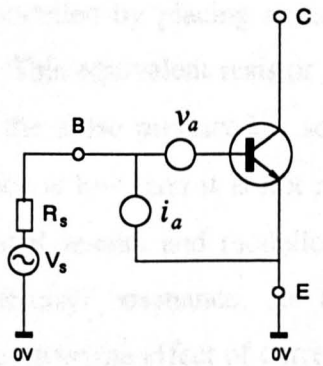

FIGURE 7.10 NOISE MODEL OF A BIPOLAR TRANSISTOR

its value can be calculated using the shot noise equation, however, because the input impedance of a field effect transistor is very high it is not normally necessary to do this. The value of the voltage noise source can be calculated using the following equation:

$$v_a = \frac{4k_B T_A \Gamma_T}{g_m} \tag{7.5}$$

Here, k_B is Boltzmann's constant, T_A is the absolute temperature and g_m is the transconductance of the device. Γ_T is a numerical factor which takes account of the material from which the device is fabricated. With silicon (Si) devices $\Gamma_T = 0.7$ and with gallium arsenide (GaAs) devices $\Gamma_T = 1.1$. For a typical small signal device with $g_m = 2$ mA/V the value of v_a is 2.4 x 10^{-9} V/$\sqrt{}$Hz [97].

It will now be shown that for some applications bipolar transistors offer more flexibility and better performance. It is not always appreciated that, under certain circumstances, it is possible to reduce the total system noise (detector and pre-amplifier) by increasing the collector current of the transistor. The reason for this can be seen by looking at the simple equation which provides the value of v_a:

$$v_n = k_B T_A \sqrt{\frac{2}{qI_C}} \tag{7.6}$$

Here, k_B is Boltzmann's constant, q is the electronic charge constant, T_A is the absolute temperature and I_C is the collector current. Although it is possible to reduce the voltage noise by increasing the collector current there is a limit and this is set by the so-called *base-spreading resistance*. The effect of the base spreading resistance is to introduce a noise floor for the transistor and this is usually modelled by placing an equivalent resistor, r_{bb}, in series with the base of the transistor. This equivalent resistor is in fact the real part the of transistor input impedance and the noise produced is sometimes referred to as *parasitic noise*. If the source impedance is low then it is not necessary to consider current noise, however, both experimental results and modelled results indicate that, at a transducer's fundamental mechanical resonance, its electrical impedance will have a magnitude of a few kΩ and therefore the effect of current noise, i_a, is very significant. Fortunately, since r_{bb} is small and appears in series with R_s it can

be neglected in this analysis. For a bipolar transistor, current noise arises as a consequence of shot noise generated by the collector current, I_C. The shot noise equation is:

$$i_s = \sqrt{2qI_C} \tag{7.7}$$

hence the current noise at the input is:

$$i_a = \sqrt{\frac{2qI_C}{h_{FE}}} \tag{7.8}$$

where h_{FE} is the DC current gain of the transistor and is well defined. Equations (7.6) and (7.8) have been used to plot graphs of transistor voltage noise and current noise respectively. The results are shown in Figures 7.11 and 7.12 respectively. For a transistor with a current gain of 100 these graphs indicate that when, for example, the transistor collector current is set at 0.35 mA, the voltage noise is 800 nV/√Hz and the current noise is 1 pA/√Hz. The significance of this example will become obvious later. An important observation is that, for an amplifier which uses a bipolar transistor as its first stage, it is possible to control the relative values of the two current generators. This feature of a bipolar transistor is of great value because it allows the system designer to easily optimise the design for a particular source impedance. In many applications this means that optimum results can be obtained without resorting to the use of troublesome transformer coupling. Both experimental results and modelled results indicate that a piezoelectric receiving transducer has, at its fundamental

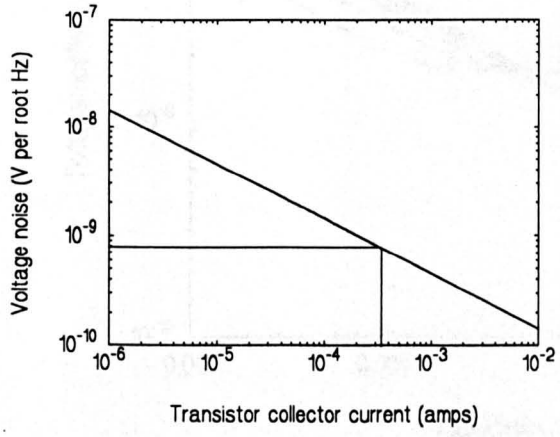

FIGURE 7.11 BIPOLAR TRANSISTOR VOLTAGE NOISE SOURCE AS A FUNCTION OF COLLECTOR CURRENT

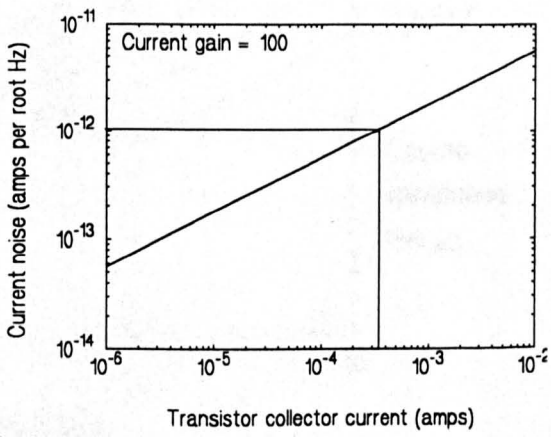

FIGURE 7.12 BIPOLAR TRANSISTOR NOISE CURRENT SOURCE AS A FUNCTION OF COLLECTOR CURRENT

thickness mode resonance frequency, an electrical impedance which is typically a few kΩ. The exact value depends on the device specification. Consider, for example, a receiving transducer which has an electrical impedance of 4 kΩ at its fundamental thickness mode resonance frequency. For this typical device, the r.m.s. amplitudes of the two bipolar noise sources have been plotted as a function of collector current and the results are illustrated in Figure 7.13. In Figure 7.13 the transducer impedance has been used to convert the current noise into an equivalent voltage noise. It can now be seen that, for any particular transducer impedance, it is possible to minimise receiver noise by selecting the correct bias current for the first stage transistor in the pre-amplifier. This option is not available with field effect transistors and is of particular value when a pre-amplifier is required to provide low noise operation with a high source impedance.

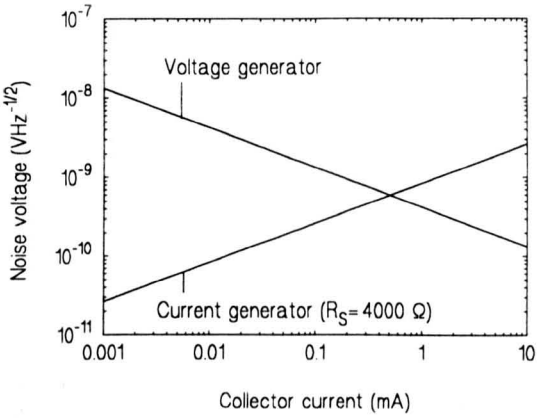

FIGURE 7.13 BOTH OF THE BIPOLAR TRANSISTOR NOISE SOURCES AS A FUNCTION OF COLLECTOR CURRENT

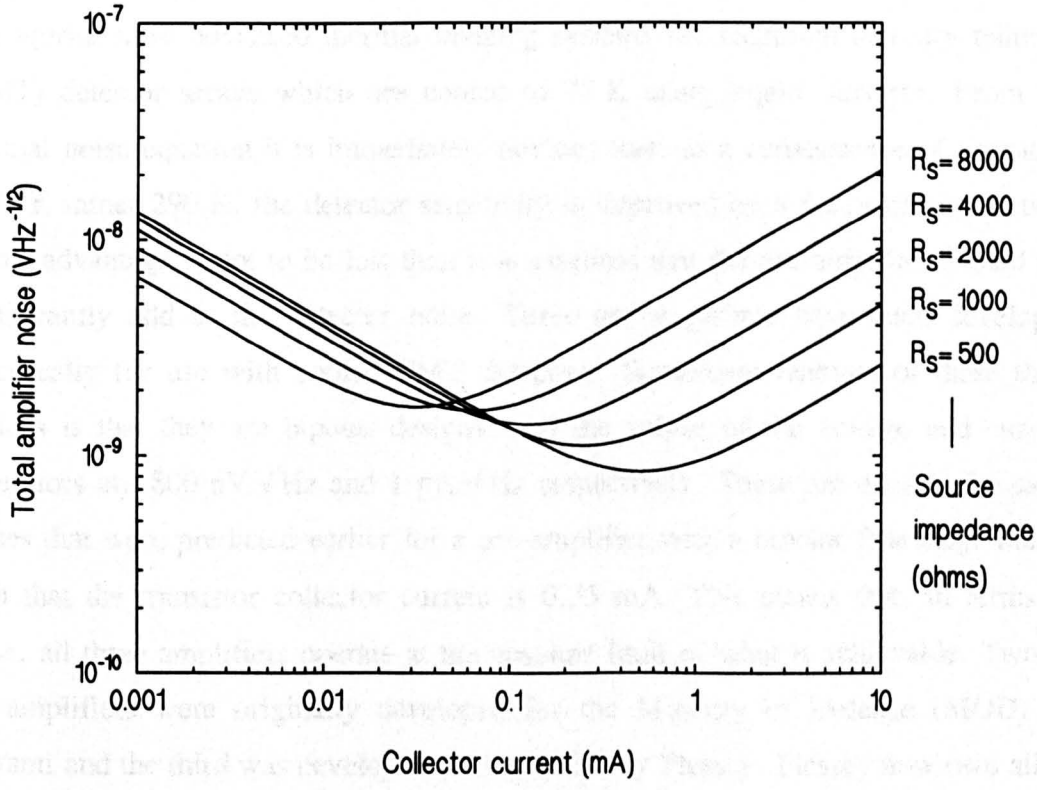

FIGURE 7.14 BIPOLAR TRANSISTOR NOISE AS A FUNCTION OF COLLECTOR CURRENT FOR A RANGE OF SOURCE IMPEDANCES

Total transistor noise as a function of collector current is plotted in Figure 7.14 for a range of different source impedances. The equivalent circuit of the Receiver Noise Model (see Figure 6.1) was used when generating these curves. As with the RNM the curves represent the total noise as it would be observed at the input to the pre-amplifier. The minimum noise voltages from the curves are listed in Table 7.3 along with the corresponding collector current and source impedance. From this table it can be seen that, even for a very high source impedance of 8 kΩ, the total amplifier noise is only 1.7 nV/√Hz compared to the 2.4 nV/√Hz which can be achieved with a typical FET. The table also indicates that, if it is possible to reduce the source impedance to 500 Ω, the total noise can be reduced to 0.8 nV/√Hz.

TABLE 7.3
BIPOLAR NOISE VOLTAGES

Source impedance	Collector current	Total noise
500 Ω	0.50 mA	0.8 nV/√Hz
1000 Ω	0.25 mA	1.1 nV/√Hz
2000 Ω	0.13 mA	1.4 nV/√Hz
4000 Ω	0.06 mA	1.6 nV/√Hz
8000 Ω	0.03 mA	1.7 nV/√Hz

Pre-Amplifier Selection

The worlds most advanced thermal imaging systems use cadmium mercury telluride (CMT) detector arrays which are cooled to 77 K using liquid nitrogen. From the thermal noise equation it is immediately obvious that, as a consequence of operating at 77 K rather 290 K, the detector sensitivity is improved by a factor of almost two. If this advantage is not to be lost then it is essential that the pre-amplifier should not significantly add to the detector noise. Three pre-amplifiers have been developed specifically for use with cooled CMT detectors. Significant features of these three devices is that they are bipolar designs, and the values of the voltage and current generators are 800 nV/√Hz and 1 pA/√Hz respectively. These are exactly the same values that were predicted earlier for a pre-amplifier with a bipolar first stage biased such that the transistor collector current is 0.35 mA. This means that, in terms of noise, all three amplifiers operate at the absolute limit of what is achievable. Two of the amplifiers were originally developed for the Ministry of Defence (MOD) by Ferranti and the third was developed for the MOD by Plessey. Plessey now own all of the technology and the amplifiers are designated ZN460, ZN459 and SL561. For this

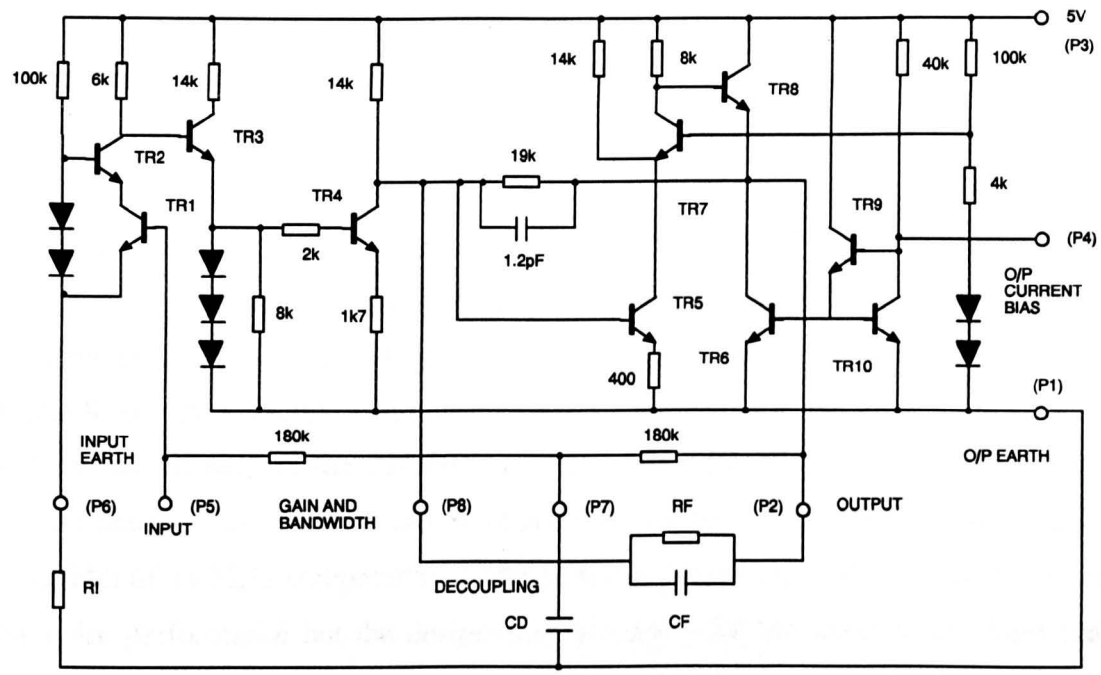

FIGURE 7.15 CIRCUIT DIAGRAM OF THE PLESSEY (FERRANTI) ULTRA LOW NOISE PRE-AMPLIFIER

research application, the ZN460 pre-amplifier is a particularly interesting device because the package includes pins which allow the amplifier to be configured in a variety of different ways. A circuit diagram of the amplifier is illustrated in Figure 7.15. Here, all of the components are internal to the integrated circuit package except for R1, RF, CD and CF. The key component in the first stage of the amplifier is TR1 which normally provides a gain of 100. Transistor TR2 behaves as a variable resistor which can be externally controlled by R1 to provide first stage feedback which alters the input impedance and gain of the amplifier. If R1=0 (i.e. pin 6 is taken to ground) then the pre-amplifier provides its best possible noise performance, has an input impedance of 7 kΩ and a gain of 60 dB. However, if for example, R1=470 Ω then the noise performance is degraded, the input impedance is increased and the gain is reduced to 40 dB. The gain of the amplifier can be reduced without degrading the noise performance by including RF, and by including CF it is possible to reduce the bandwidth. It is not difficult to show that the voltage drop across the 6 kΩ resistor in the collector circuit of TR2 is 2.6 volts. This makes good sense since, for a supply voltage of 5 V, it allows an almost equal voltage swing in each direction. It follows that the collector currents in both TR1 and TR2 are 0.4 mA. This is very close to the value of 0.35 mA which was previously calculated as being the value of collector current that

results in an 800 nV/√Hz voltage source and a 1 pA/√Hz current source. It follows that, if the ZN460 is used as a pre-amplifier with a piezoceramic transducer which has an operational impedance of a few kΩ, it should be possible to obtain noise performance which is close to the absolute theoretical limits. Comparing the values of the voltage and current noise generators quoted in the ZN460 specification with those which were previously calculated for a bipolar transistor, it is clear that the transistors used in the first stages of the device are not limited by base spreading resistance. This is a feature of the integrated circuit technology and it would be difficult, if not impossible, to build an amplifier using discrete components which could provide the same level of noise performance. However, the ZN460 has some of the advantages of a discrete design because many of its functions can be controlled externally. The ZN459, which has a bandwidth of 15 MHz compared to 6 MHz for the ZN460, provides a similar level of low noise performance but the design does not allow for the same level of external control. During the course of this research the ZN460 was used exclusively but a number of other low noise pre-amplifiers were identified. For example, the Analog Devices AD797, which is regarded as the current industry standard for low noise operational amplifiers, has an input voltage noise generator with a typical value of 1.7 nV/√Hz. It has a very high input impedance and hence no value is quoted for input current noise. With this device it is not possible to simultaneously obtain adequate gain and bandwidth without including a second operational amplifier in the complete design. Also, external components which must be included at the input degrade the noise performance. An excellent device which is intended for SONAR applications is the AH0013 manufactured by OEI but this is very expensive and suffers from the same problems as the AD797.

7.3.3 The Complete Receiver

During the design phase it was arranged that the ZN460 pre-amplifier would be placed in the same metal housing that contains the ultrasonic receiving transducer. The maximum gain (60 dB) of the pre-amplifier was utilised and no attempt was made to restrict its bandwidth. In this way it was possible to keep the external component count down to the absolute minimum and mount the ZN460 on a 30 mm diameter printed circuit board (PCB) which sits directly behind the 30 mm diameter piezocomposite transducer. By adopting this strategy it was found that it is possible to almost

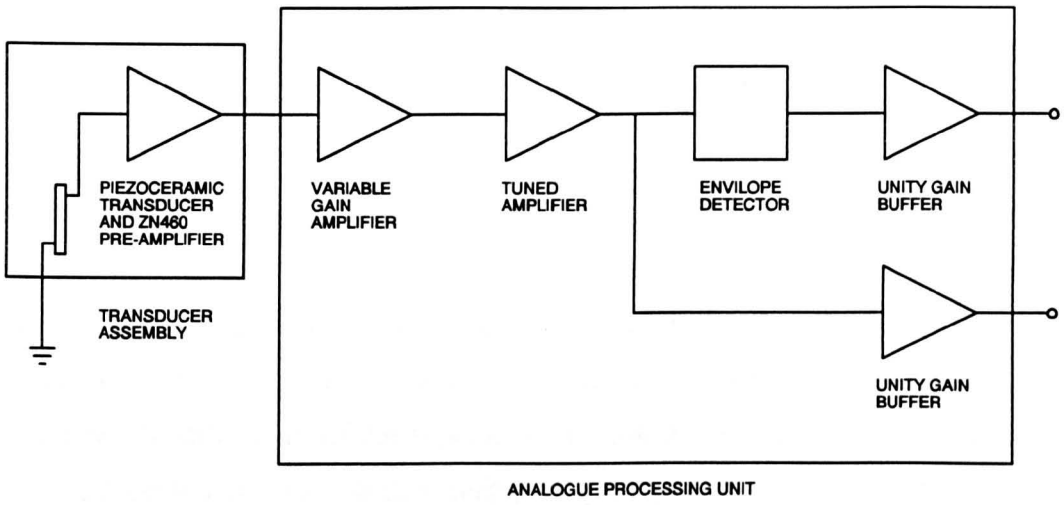

FIGURE 7.16 THE COMPLETE ULTRASONIC RECEIVER

completely eliminate electrical interference problems. A block diagram of the complete receiver is illustrated in Figure 7.16.

The Analogue Processing Unit

The main function of the Analogue Processing Unit (APU) is to control the system bandwidth and provide extra gain. The unit is housed in a small metal case which can be placed several metres away from the transducer assembly. The APU contains a mains power supply unit which provides +5 volts DC for the pre-amplifier and ±15 volts for the processing board. The analogue processing board provides additional amplification, filtering and envelope detection. Here, the additional amplification is obtained using an integrated circuit (IC) video amplifier which is configured as a variable gain stage and the filtering is obtained using an identical IC which is configured as a gain stage with a variable centre frequency. Envelope detection is performed using discrete components. Unity gain buffer stages are employed to simultaneously provide radio frequency (RF) and envelope detected outputs. Front panel controls allow adjustment of gain, filter centre frequency and filter bandwidth. The gain can be varied from 0 to 500 and the centre frequency can be varied from 0.25 MHz to 1.5 MHz. At a centre frequency of 580 kHz the bandwidth can be reduced to a minimum value of 10 kHz.

System Bandwidth

As discussed previously, the piezocomposite transducer used in the initial experiments is a 20% ceramic volume fraction device with a fundamental thickness mode resonance frequency of 580 kHz, a mechanical quality factor, Q_M, of 30 and a corresponding bandwidth of 20 kHz. In order to obtain the best possible signal to noise ratio it is essential that the bandwidth of the receiver electronics is matched to the bandwidth of the receiving transducer. This was achieved using the previously described APU. In order for the system to be efficient it is also necessary that the bandwidth of the transmitted signal should not contain frequency components which fall outside the receiver bandwidth. In all of the experimental work this was arranged by transmitting a 10 to 20 cycle tone burst with a centre frequency of 580 kHz. Using this type of signal has the additional advantage that, after envelope detection, the recovered signal is in a form which is convenient for digitisation.

7.4 Experimental Feasibility Study

The aim of the experimental feasibility study was to confirm that the new receiver could be used to implement air coupled test systems which are equivalent to the liquid coupled test systems described in Chapter 1. Success in doing this would automatically validate the theory which is described in Chapters 4,5,6 and 7 of this Thesis and represent a very significant step forward in the field of ultrasonic testing.

7.4.1 The Experiments

As discussed in Chapters 1 and 2, pulse-echo testing was not considered to be viable because of the additional dynamic range problems. The test configurations that were of interest are as follows:

1 Through transmission inspection
2 Shear wave inspection
3 Lamb wave and Rayleigh wave inspection

Other than the previously described piezocomposite transducers and the new receiver, no special equipment was required for the through transmission testing. However, in the case of the shear wave testing and the Lamb wave testing, it was necessary to

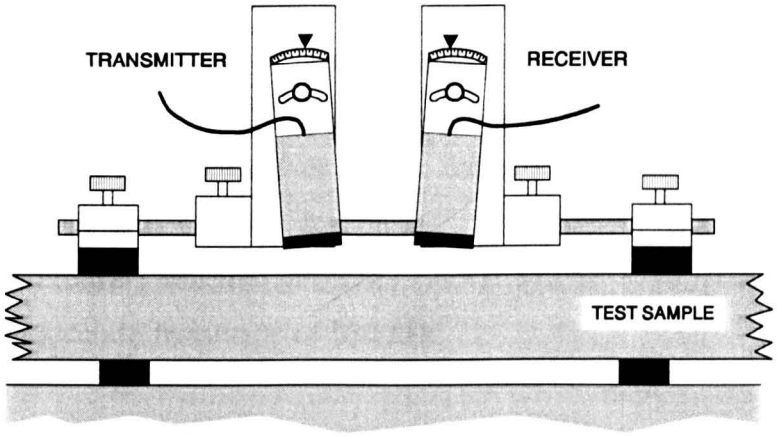

FIGURE 7.17 PRECISION MANIPULATOR USED IN THE SHEAR WAVE AND LAMB WAVE EXPERIMENTS

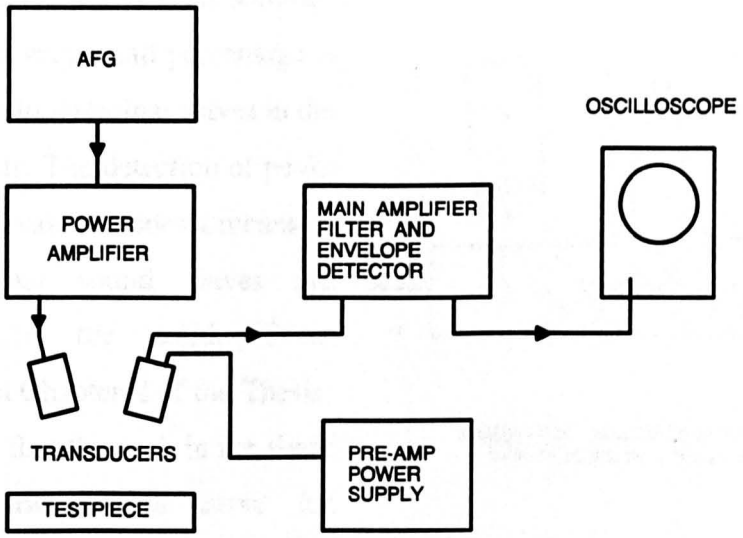

FIGURE 7.18 BLOCK DIAGRAM OF THE SYSTEM ELECTRONICS

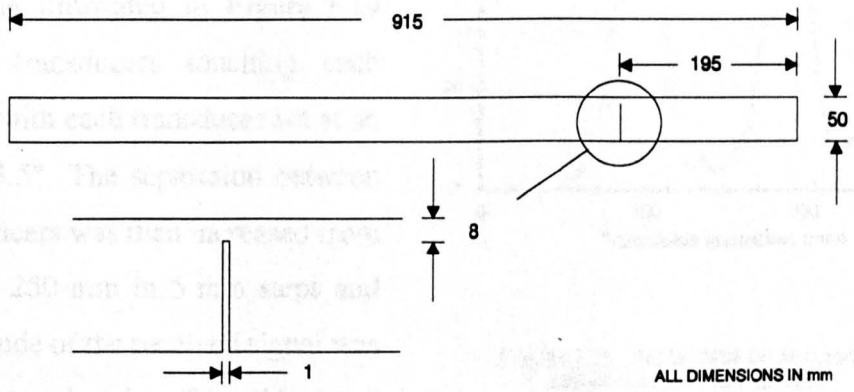

FIGURE 7.19 ALUMINIUM TEST SAMPLE USED IN MANY OF THE EXPERIMENTS

design and build a precision manipulator which could be used to set the transducers at predetermined angles. This manipulator is illustrated in Figure 7.17. A block diagram of the basic electronic configuration used in all of the experiments is illustrated in Figure 7.18. Although Figure 7.18 shows the transducers in a configuration which is appropriate to either shear wave or Lamb wave inspection, the same electronic configuration could also be used for through transmission testing. As mentioned previously, the arbitrary function generator (AFG) was set to provide 10 to 20 cycle tone burst with a centre frequency of 580 kHz.

Shear Wave and Through Transmission Experiments

As illustrated in Figure 7.20, when shear waves are generated in a long solid bar there are multiple internal reflections within the bar. Almost 100% of the shear wave energy is internally reflected at each solid/air interface but a very small percentage is converted into longitudinal waves in the surrounding air. The detection of peaks at regular intervals provides a means of confirming that sound waves are propagating in the solid. From Figure 2.19 in Chapter 2 of the Thesis, it can be seen that the peak in the shear wave echo transmission curve for air/aluminium occurs at an angle of 3.5°. The manipulator holding the transducers was placed on top of the test sample illustrated in Figure 7.19 with the transducers touching each other and with each transducer set at an angle of 3.5°. The separation between the transducers was then increased from 50 mm to 250 mm in 5 mm steps and the amplitude of the received signal was recorded at each point. Over this range

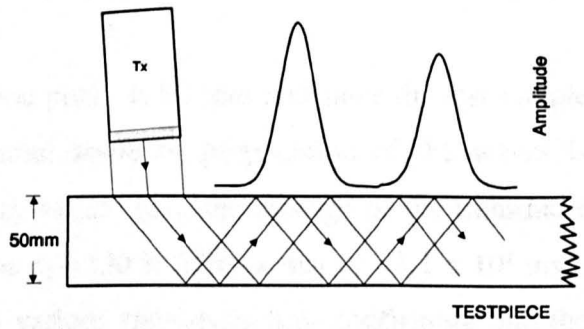

FIGURE 7.20 MULTIPLE SHEAR WAVE REFLECTIONS IN A SOLID BAR

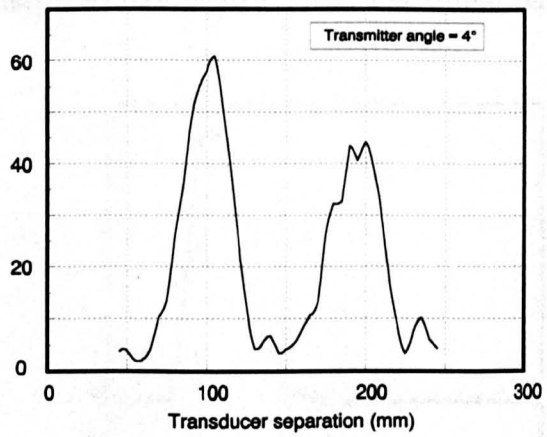

FIGURE 7.21 DETECTION OF MULTIPLE SHEAR WAVE IN ALUMINIUM

two large peaks in the amplitude of the received signal were observed. It was found that the amplitudes of the two peaks could be maximised by increasing the transmitter angle to 4° and the receiver angle to 4.5°. It is now known that the angles had to be increased because the transmitter has a beam divergence of 1.8° and the receiver has a similar field of view. The apparent difference between the transmitter angle and the receiver angle is due, among other things, to measurement errors and inaccurate mounting of the transducers in their holders. Another scan was conducted with the transducers set at the increased angles and a plot of the data recovered during this scan is illustrated in Figure 7.21. The result plotted in Figure 7.21 provides a clear indication that sound waves are being reflected from face to face inside the test sample. To confirm that these waves are shear waves it is necessary to measure their velocity and this can be done using Snell's law:

$$\frac{\sin\theta_1}{\sin\theta_2} = \frac{c_1}{c_2} \tag{7.9}$$

The separation between the first and second peaks is 95 mm and since the test sample is 50 mm thick it follows that the internal angle of propagation of the waves is θ_2=43.5°. Taking the external angle as θ_1=4.25° (i.e. the average of the transducer angles) and the velocity of sound in air as c_1=330 it follows that c_2=3.1 x 10^3 ms^{-1}. This figure agrees with values quoted in various references thus confirming that the peaks in Figure 7.21 are due to shear wave reflections. Proof that the detected waves pass through the bulk of the aluminium was provided by moving the transducer manipulator along the test sample until a deep slot (see Figure 7.19) was sitting half

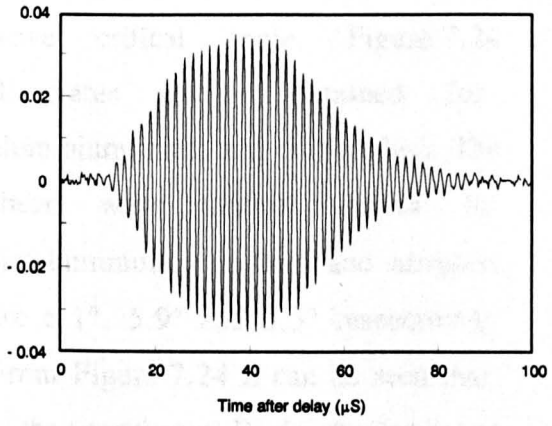

FIGURE 7.22 RADIO FREQUENCY SIGNAL RECORDED (AFTER DELAY) DURING THE SHEAR WAVE EXPERIMENT

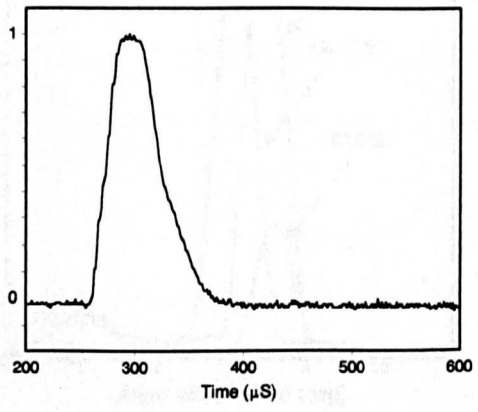

FIGURE 7.23 ENVELOPE DETECTED SIGNAL RECORDED (NO DELAY) DURING THE SHEAR WAVE EXPERIMENT

way between the two transducers. With the slot in place the path for shear waves reflected from the bottom surface of the test sample is blocked and no signals are detected. As will be noted again later, placing the slot in this position does not prevent the propagation of other modes along the surface of this test sample. A typical signal obtained with the receiver sitting on the first shear wave peak is illustrated in Figure 7.22. Figure 7.23 illustrates a typical signal recorded at the output from the envelope detector under the similar conditions. These signals were recorded without signal averaging, or any other form of processing, at the outputs from the Analogue Processing Unit. At the end of the shear wave experiment it was shown that it is possible to obtain similar signals in through transmission mode. In order to do this it was necessary to remove the transducers from the manipulator and place them facing each other with the same test sample placed between them. This Thesis is not concerned with through transmission testing, however, Kelly [2,4] has continued the through transmission work and an eight channel version of the new receiver was built for this purpose.

Rayleigh Wave Experiments

During the experimental investigation it was also shown that the new receiver makes it possible to detect Rayleigh waves in sufficiently thick test samples. This was demonstrated using exactly the same equipment as used in the shear wave experiments. For a given material, Rayleigh waves can be generated by adjusting the transducers so that they are each sitting at an angle which is close to the shear wave critical angle. Figure 7.24 illustrates results obtained for aluminium, steel and crown glass. The shear wave critical angles for air/aluminium, air/steel and air/glass are 6.1°, 5.9° and 5.5° respectively. From Figure 7.24 it can be seen that, in the experiment, Rayleigh waves start to propagate in aluminium, steel and

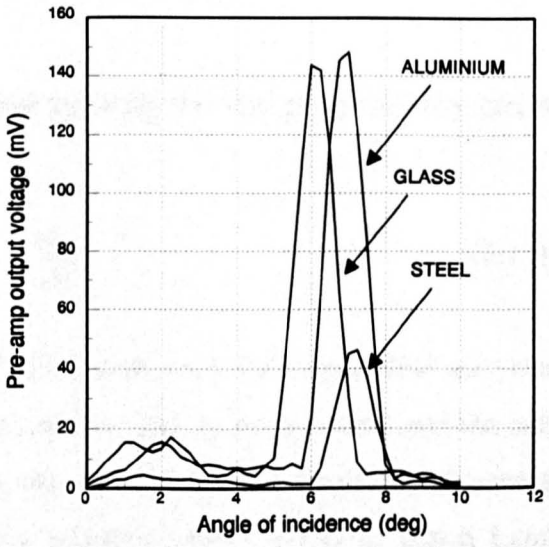

FIGURE 7.24 SIGNAL AMPLITUDES RECORDED DURING THE RAYLEIGH WAVE EXPERIMENTS

glass at angles of 5.8°, 6° and 5° respectively. As mentioned in Chapter 1, Rayleigh waves propagate in a layer of material close to the surface of the test sample. It was possible to prove this by again using the aluminium test sample illustrated in Figure 7.19. As in the shear wave experiments a slot, cut from the back of the test sample to within 8 mm of the surface, was placed half way between the two transducers. In this case there was no alteration in the amplitude of the detected signal thus confirming that the waves were propagating along the surface.

Lamb Wave Experiments

As discussed in Chapter 1, Lamb waves are two-dimensional propagating vibrations in free plates that may be symmetric or antisymmetric with respect to the middle of the plate. The velocities of Lamb waves are dispersive and in any plate of thickness *2d* and at a particular frequency *f* there will be a finite number of propagating modes which may be determined from the number of real roots of the Rayleigh-Lamb equation. The phase velocities or wave numbers of Lamb waves as a function of the frequency-thickness product, *fd*, my be obtained by solving the following transcendental equations [23]:

$$\frac{\tanh\ \pi fd\sqrt{\dfrac{v_S^2-v^2}{v_S^2v^2}}}{\tanh\ \pi fd\sqrt{\dfrac{v_L^2-v^2}{v_L^2v^2}}} = \frac{4\sqrt{\left(1-\dfrac{v^2}{v_L^2}\right)\left(1-\dfrac{v^2}{v_S^2}\right)}}{\left(2-\dfrac{v^2}{v_S^2}\right)} \qquad (7.10)$$

In these equations v is the phase velocity and knowing this the group velocity can be found from [37,98]:

$$v_g = \frac{\partial\omega}{\partial k} \qquad (7.11)$$

where k is the wave number. In Equation (7.10) v_L and v_S are the longitudinal and shear wave velocities respectively. For a given material v_L and v_S are constants and the only variables in Equation (7.10) are the phase velocity (v) and the frequency thickness-product (fd). A number of researchers have described experiments in which Lamb waves have been generated in a solid which is immersed in a liquid. In these

investigations the usual method of initiating and detecting Lamb waves has been to use the coincidence principle which was discussed in Chapter 1. The same technique has been used in the air coupled experiments which will now be described. Exactly the same equipment as was used in the shear wave and Rayleigh wave experiments was used to set the transducers at the appropriate angles. It was possible to initiate various Lamb wave modes in thin sheets of material made from a wide variety of materials which included aluminium, steel, copper, perspex, glass fibre, and carbon fibre.

One experiment involved using steel plates to identify one particular mode which was found to be relatively easy to generate. A wide variety of different plate thicknesses were available and this made it possible to plot a dispersion curve for what is now known to be the a_o mode. The experimental results are illustrated in Figure 7.25 along with theoretical curves for the phase and group velocities obtained from Equations (7.10) and (7.11). There is clearly excellent agreement between the experimental data and the theoretical group velocity curve. In making these measurements the frequency of the transmitting transducer was kept constant at 580 kHz and only the thickness of the steel was varied to obtain different values of the frequency-thickness product. The group velocity was measured by timing multiple reflections between the ends of the steel plates. An example of these multiple reflection is illustrated in Figure 7.26. By turning the plate in its own plane it was possible to

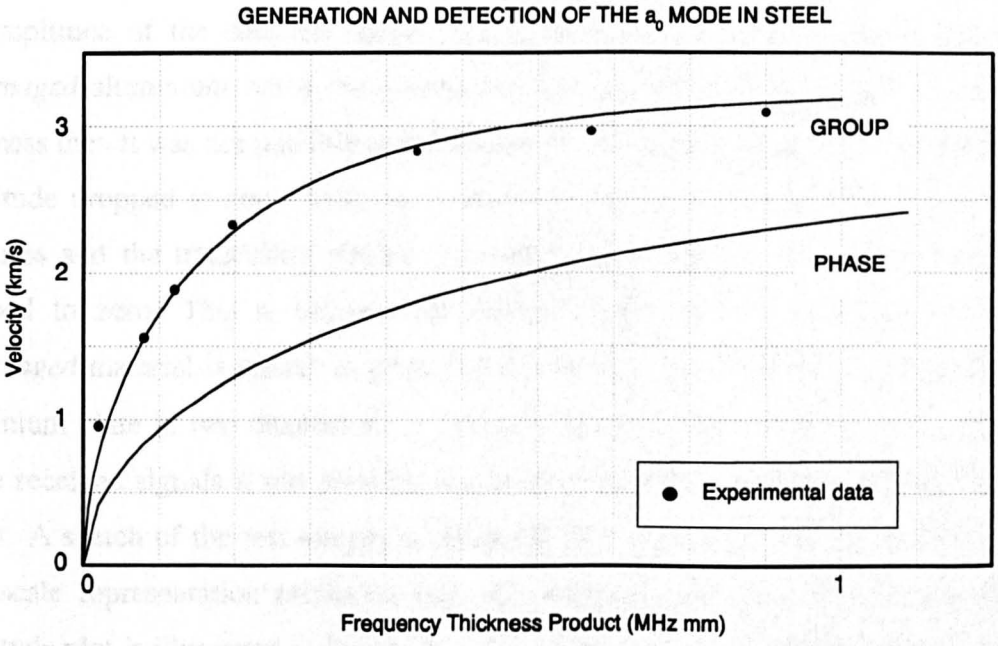

FIGURE 7.25 EXPERIMENTAL AND THEORETICAL DISPERSION CURVES FOR LAMB WAVES IN STEEL

make the multiple reflections vanish leaving only one detected signal which corresponded to the direct path between the transmitting transducer and the receiving transducer. This was done to confirm that none of the additional signals were due to the generation and detection of other Lamb wave modes. It was also possible to suppress the multiple reflections by applying light finger pressure to the plate at any point on the transmission path. The generation and detection of Lamb waves using air coupled transducers will be discussed further in Chapter 8.

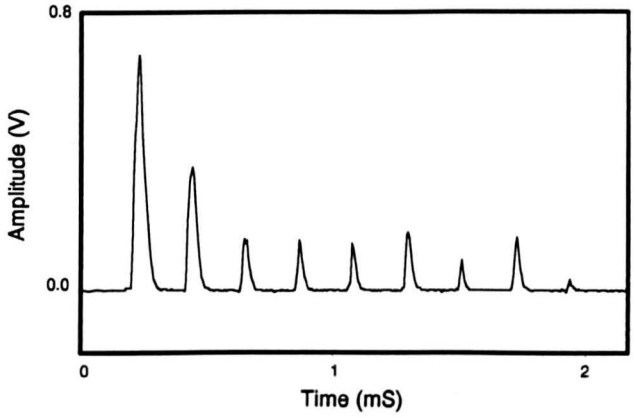

FIGURE 7.26 MULTIPLE LAMB WAVE REFLECTIONS IN A STEEL PLATE

Another experiment with Lamb waves involved *imaging* an *artificial defect* in a 1.1 mm thick aluminium plate. The *defect* was created by milling away 50% of the material thickness in a 30 mm diameter disc located close to the centre of the aluminium plate. In order to create an *image* of the *defect*, the transducer angles were adjusted to initiate a strong Lamb wave mode (a_0) in an area of *undamaged* aluminium. The test sample was then scanned by hand with both transducers locked together so that there was a small fixed separation between them. During scanning there was very little change in the amplitude of the detected signal as long as both transducers were placed over *undamaged* aluminium but if the transmitter was positioned over an area of reduced thickness then it was not possible to initiate the chosen Lamb wave mode and the signal amplitude dropped to zero. With the receiver placed over the same area of reduced thickness and the transmitter placed over undamaged material, the signal level also dropped to zero. This is because the chosen mode which is propagating in the *undamaged* material is unable to propagate in the *damaged* material. By scanning the aluminium plate in two dimensions at 100 mm intervals and recording the amplitude of the received signals it was possible to generate an *image* of the area containing the defect. A sketch of the test sample is illustrated in Figure 7.27. Figure 7.28 shows a grey scale representation produced with the recorded data and a three dimensional amplitude plot is illustrated in Figure 7.29. In this imaging experiment the diameter of

each of the transducers was 30 mm and the separation between their centres was 40 mm. Because the signal amplitude drops to zero when either the transmitter or the receiver is over damaged material the effective dimensions of the scanning aperture in the experimental system is 30 mm by 70 mm.

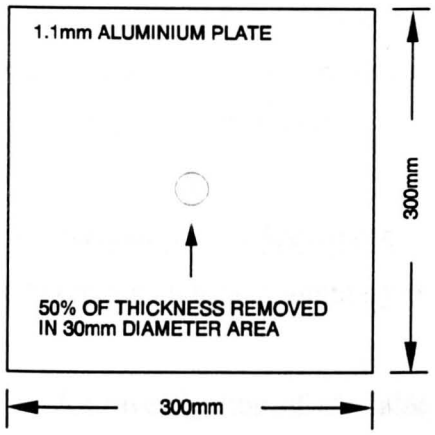

FIGURE 7.27 ALUMINIUM TEST SAMPLE USED IN AN EXPERIMENT TO DETECT AN ARTIFICIAL DEFECT

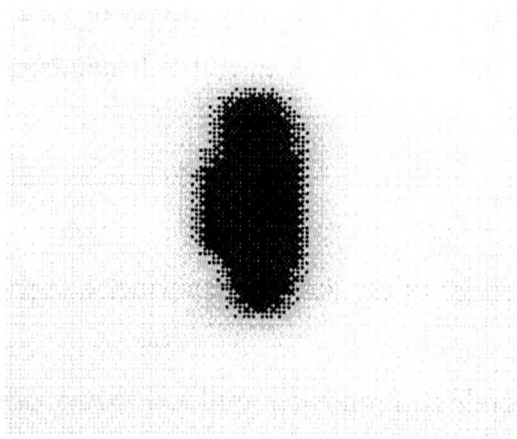

FIGURE 7.28 LAMB WAVE IMAGE OF AN AREA CLOSE TO THE CENTRE OF THE PLATE

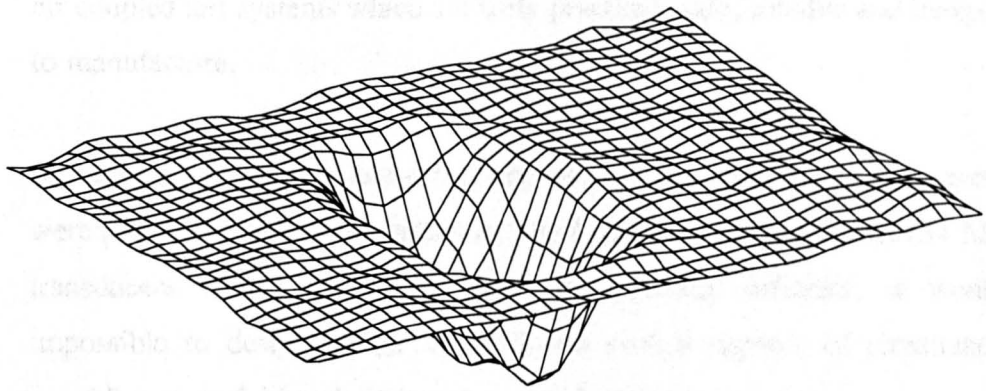

FIGURE 7.29 RELATIVE SIGNAL AMPLITUDE IN A REGION CLOSE TO THE CENTRE OF THE PLATE

7.5 Conclusions

7.5.1 The Goal

The goal of the work which is described in this Chapter was to assess the feasibility of using air coupled piezoelectric transducers for ultrasonic testing. A theoretical approach was used to establish the signal to noise ratios that might be expected from systems which do not employ signal averaging or any other form of digital processing. Such systems are sometimes referred to as *real-time* systems. The work also involved designing a system which would provide experimental evidence of the feasibility of *real-time* air coupled testing.

7.5.2 Summary of Achievements

This Section provides a summary of the principal achievements which are as follows:

- An investigation of available transmitter power has been conducted. Although it may be possible to obtain up to 10 kW [42] of power from a piezoelectric transducer it was decided that, for the experimental systems described in this Thesis, the transmitter power levels would not exceed 42.5 W. A transmitter power of 42.5 W was used in all of the theoretical signal to noise calculations and a transmitter power of 42.5 W or less was used in all of the experimental work. By using relatively low levels of transmitter power it is possible to design air coupled test systems which are truly practical, safe, reliable and inexpensive to manufacture.

- By using a very simple and direct approach it has been shown that, even if it were possible to obtain *non-resonant* (see Appendix II) piezoelectric (34 MRayl) transducers which are 100% electromechanically efficient, it would be impossible to design an air coupled test system capable of simultaneously providing a useful bandwidth and a useful signal to noise ratio.

- For an ultrasonic test system which uses the full bandwidth of the air channel (e.g. 1.3 MHz for a 1 cm path) and which is based on 100% efficient *non-resonant* (see Appendix II) transducers which have an acoustic impedance of 34 MRayl, the best possible signal to noise ratio is -20 dB.

- For 100% efficient, *non-resonant* (see Appendix II) transducers which have an acoustic impedance of 34 MRayl it would be necessary to reduce the system bandwidth to 13 kHz in order to achieve an SNR of unity. This calculation provides a useful bench mark against which practical systems can be judged.

- By using a theoretical approach based on the Linear Systems Model it has been shown that a resonant system based on two typical PZT-5A transducers (34 MRayl) is capable of providing a signal to noise ratio of 30 dB in an 8.6 kHz bandwidth. A system which is based on two typical piezocomposite transducers provides a similar signal to noise ratio but in a 20 kHz bandwidth. Compared to a *non-resonant* (Appendix II) system which uses the full channel bandwidth, these systems provide a 50 dB improvement in system sensitivity.

- The theory indicates that it is only possible to achieve a 50 dB improvement in system sensitivity provided that an ultra low noise pre-amplifier is used in the receiver. By using an ultra low noise pre-amplifier it is possible to arrange that amplifier noise is almost insignificant compared to transducer noise.

- The theoretical noise limitations of both field effect (FET) and bipolar transistors has been investigated. It has been found that, for high impedance sources, a pre-amplifier which uses bipolar technology can provide slightly better performance than one which uses FET technology.

- It has been shown that it would be possible to design a bipolar transistor amplifier which, in terms of noise, could be perfectly matched to any particular receiving transducer. This would be achieved by controlling the collector current in the first transistor stage of the amplifier.

- The ZN460 pre-amplifier has been identified as being suitable for the construction of ultra sensitive air coupled test systems. This amplifier was originally developed for military thermal imaging applications and is normally used with cadmium mercury telluride (CMT) detectors which are cooled to liquid nitrogen temperature (77 K).

- Noise in the ZN460 pre-amplifier is characterised by an 800 pV/√Hz voltage generator and a 1 pA/√Hz current generator. For a particular transistor collector current these figures represent fundamental limits which cannot be improved upon other than by reducing the temperature.

- By using the Linear Systems Model it has been shown that by using frequency matched transducers it is possible to achieve a typical 12 dB improvement in system sensitivity. This improvement is included in the previously discussed figures.

- An ultra sensitive receiver system has been designed and constructed. The new receiver consists of a 20% ceramic volume fraction piezocomposite transducer, a ZN460 pre-amplifier, a main amplifier, a tuneable filter section and an envelope detector.

- It has been shown that, by using the new receiver, it is possible to implement a number of different air coupled test configurations. By using a 20% ceramic volume fraction transducer which delivers 42.5 W of transmitter power it has been shown that the new receiver is capable of providing a useful signal to noise ratio and a useful bandwidth in all of these configurations.

- The new receiver has been used to demonstrate the viability of air coupled shear wave and through transmission testing (one and eight element versions).

- The new receiver has been used to demonstrate the viability of air coupled Rayleigh wave testing. Experiments have been conducted in aluminium, glass and steel.

- The new receiver has been used to demonstrate the viability of air coupled Lamb wave testing. The potential for defect *imaging* has been demonstrated.

- An experimental dispersion curve for the a_0 Lamb wave mode has been obtained for steel. The result is in excellent agreement with theory.

Chapter 8

LAMB WAVE STUDY

8.1 Introduction

The purpose of this Chapter is to investigate in detail one possible way of exploiting the new air coupled technology. As previously stated, pulse-echo is the most versatile and convenient configuration for most ultrasonic testing applications, however, the theoretical results discussed in Chapter 2 indicate that an air coupled version of the standard pulse-echo configuration is not viable because of the dynamic range required. Having said this, recent results obtained by the Ultrasonics Research Group (URG) indicate that it is possible to implement a pseudo pulse-echo system [99]. This system uses two transducers, in a configuration which is similar to that of Figure 1.9, and is based on a version the resonance technique which is described in Section 1.5.5 of this Thesis. Also, as will be discussed in Chapter 9, air (gas) coupled pulse-echo inspection is viable at high pressure.

Although genuine air coupled pulse-echo inspection at normal pressure is not feasible with currently available piezoelectric transducers, the experimental investigation described in Chapter 7 indicates that any other type of air coupled configuration is possible. For example it would be possible to design an air coupled test system which is based on the generation and detection of shear waves, however, this is not the most attractive option. The main objection to using shear waves is that, because of the relatively low frequencies involved, it would not be possible to measure the depth at which a defect is located with a sufficiently high degree of accuracy. Air coupled systems are more suited to applications where it is only necessary to detect the presence of a defect and record its position in the plane of the test scan. If there is no requirement to measure the depth of a defect then through transmission and Lamb wave inspection are the most appropriate options. The main advantage of designing a test system which is based on the generation and detection of Lamb waves is that the two transducers can either be on the same side of the test sample or on opposite sides. The only real disadvantage with the Lamb wave technique is that it is not possible to use focused transducers since this would not be consistent with the coincidence principle. Detailed investigations of both the Lamb wave and through transmission techniques were undertaken at Strathclyde during the course of this work. The Lamb wave investigation was conducted by the author of this Thesis and is described in this Chapter. Through transmission applications are being assessed by Kelly [2,4].

8.2 Lamb Wave Theory

During the course of this investigation it became evident that a detailed derivation of the necessary Lamb wave equations was not readily available. Most text books present the main results and in some cases a few intermediate steps. The derivation which is presented here uses the Appendix in *Physical Acoustics and the Properties of Solids* [100] by Mason as a starting point. Performing this derivation has provided an invaluable insight into the problems associated with designing Lamb wave test systems.

8.2.1 General Theory

Consider a thin plate made from a lossless isotropic medium. As illustrated in Figure 8.1, it has been arranged that the plate is symmetrical about the x-y plane. Let

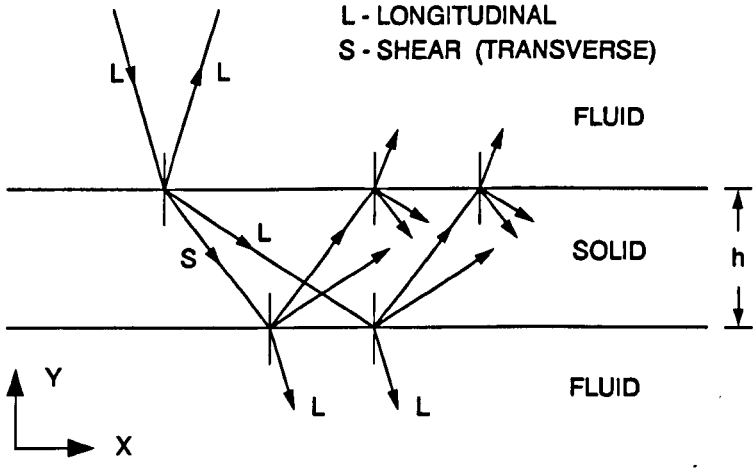

FIGURE 8.1 SECTION OF A THIN PLATE MADE FROM A LOSSLESS ISOTROPIC MEDIUM

S_1, S_2 and S_3 be the tensional strains along the x, y and z axes respectively. If u, v and w are the displacements of an elemental cube of material ($dx\ dy\ dz$) parallel to the x, y and z axes respectively then it follows that:

$$S_1 = \frac{\partial u}{\partial x} \qquad S_2 = \frac{\partial v}{\partial y} \qquad S_3 = \frac{\partial w}{\partial z} \tag{8.1}$$

For convenience let:

$$\Delta = S_1 + S_2 + S_3 \tag{8.2}$$

The equations of motion for a lossless isotropic medium can be written as [100]:

$$\rho\frac{\partial^2 u}{\partial t^2} = (\lambda + \mu)\frac{\partial \Delta}{\partial x} + \mu\nabla^2 u \tag{8.3}$$

$$\rho\frac{\partial^2 v}{\partial t^2} = (\lambda + \mu)\frac{\partial \Delta}{\partial y} + \mu\nabla^2 v \tag{8.4}$$

$$\rho\frac{\partial^2 w}{\partial t^2} = (\lambda + \mu)\frac{\partial \Delta}{\partial z} + \mu\nabla^2 w \tag{8.5}$$

where:

$$\nabla^2 = \frac{\partial^2}{\partial x^2} + \frac{\partial^2}{\partial y^2} + \frac{\partial^2}{\partial z^2} \tag{8.6}$$

In these equations ρ is the density of the medium, μ is the shear modulus and λ is Lamé's constant. The equations of motion are a consequence of Hooke's law and Newton's second law of motion. If it is assumed that all cross sections of the plate parallel to the x-y plane are identical and there is no particle motion in the z direction then the problem becomes two dimensional and it is only necessary to satisfy Equations (8.3) and (8.4). The solution to this pair of partial differential equations is:

$$u = \frac{\partial \phi}{\partial x} + \frac{\partial \psi}{\partial y}, \qquad v = \frac{\partial \phi}{\partial y} - \frac{\partial \psi}{\partial x} \tag{8.7}$$

where ϕ and Ψ are auxiliary functions satisfying the Equations:

$$\rho\frac{\partial^2 \phi}{\partial t^2} = (\lambda + 2\mu)\nabla^2\phi, \qquad \rho\frac{\partial^2 \psi}{\partial t^2} = \mu\nabla^2\psi \tag{8.8}$$

It is known that internal disturbances in an extended isotropic medium, as opposed to the thin plate being considered here, travel at either the longitudinal wave velocity (V_L) or the shear wave velocity (V_S). These velocities are related to the material constants by:

$$V_L = \sqrt{\frac{\lambda + 2\mu}{\rho}} \tag{8.9}$$

and:

$$V_S = \sqrt{\frac{\mu}{\rho}} \tag{8.10}$$

Combining Equations (8.8), (8.9) and (8.10) gives:

$$\frac{\partial^2\phi}{\partial t^2} = V_L^2\nabla^2\phi \tag{8.11}$$

$$\frac{\partial^2\psi}{\partial t^2} = V_S^2\nabla^2\psi \tag{8.12}$$

Since ϕ must be periodic with respect to both x and t it is possible to write:

$$\phi = F(y)e^{i(\omega t - kx)} \tag{8.13}$$

Here, $F(y)$ is a function of y only and represents the amplitude of ϕ. Differentiating:

$$\frac{\partial^2\phi}{\partial t^2} = -\omega^2 F(y)e^{i(\omega t - kx)} \tag{8.14}$$

Substituting for $F(y)$ from Equation (8.13) then gives:

$$\frac{\partial^2\phi}{\partial t^2} = -\omega^2\phi \tag{8.15}$$

In a similar way differentiating twice with respect to x gives:

$$\frac{\partial^2\phi}{\partial x^2} = -k^2\phi \tag{8.16}$$

Expanding Equation (8.11) for the two dimensional case gives:

$$\frac{\partial^2\phi}{\partial t^2} = V_L^2\left(\frac{\partial^2\phi}{\partial x^2} + \frac{\partial^2\phi}{\partial y^2}\right) \tag{8.17}$$

Substituting Equations (8.15) and (8.16) into Equation (8.17) leads to:

$$\frac{\partial^2\phi}{\partial y^2} = \left(k^2 - \frac{\omega^2}{V_L^2}\right)\phi \tag{8.18}$$

Lamb waves are due to the superposition of the longitudinal and shear wave modes

which exist independently in an extended medium. As a consequence of this superposition, Lamb waves have associated with them both a phase velocity, V, and a group velocity, V_g. The phase velocity of a wave is related to the wave number, k, and the angular frequency, ω, by:

$$V = \frac{\omega}{k} \tag{8.19}$$

Substituting Equation (8.19) into Equation (8.18) gives:

$$\frac{\partial^2 \phi}{\partial y^2} = k^2 \left(1 - \frac{V^2}{V_L^2}\right) \phi \tag{8.20}$$

For convenience define:

$$\alpha = k \sqrt{1 - \frac{V^2}{V_L^2}} \tag{8.21}$$

Thus:

$$\frac{\partial^2 \phi}{\partial y^2} = \alpha^2 \phi \tag{8.22}$$

Since Ψ must also be periodic with respect to both x and t it is possible to write:

$$\psi = G(y) e^{i(\omega t - kx)} \tag{8.23}$$

Where $G(y)$ is a function of y only and represents the amplitude of the function Ψ. Following the same procedure as with ϕ it then follows that:

$$\frac{\partial^2 \psi}{\partial y^2} = \beta^2 \psi \tag{8.24}$$

where:

$$\beta = k \sqrt{1 - \frac{V^2}{V_S^2}} \tag{8.25}$$

In some of the literature ϕ and Ψ are referred to as potential functions which are associated with longitudinal and shear waves respectively. In order to see how these

functions vary with respect to y it is necessary to solve (8.22) and (8.24). These are ordinary differential equations with standard solutions:

$$\phi = pe^{\alpha y} + qe^{-\alpha y} \tag{8.26}$$

$$\psi = re^{\beta y} + se^{-\beta y} \tag{8.27}$$

From Equations (8.13) and (8.23) it is known that the terms p, q, r and s each include a function of x and t. Therefore the solutions must be rewritten in the form:

$$\phi = F(y)e^{i(\omega t - kx)} = (ae^{\alpha y} + be^{-\alpha y})e^{i(\omega t - kx)} \tag{8.28}$$

$$\psi = G(y)e^{i(\omega t - kx)} = (ce^{\beta y} + de^{-\beta y})e^{i(\omega t - kx)} \tag{8.29}$$

Using hyperbolic functions the solutions become:

$$\phi = (A\sinh \alpha y + B\cosh \alpha y)e^{i(\omega t - kx)} \tag{8.30}$$

$$\psi = (C\sinh \beta y + D\cosh \beta y)e^{i(\omega t - kx)} \tag{8.31}$$

Let T_2 represent the tensional stress parallel to the y axis and T_6 represent the shear stress about the z axis and parallel to the y axis. This terminology is consistent with reference [100]. In order to obtain the Lamb wave frequency equation it is necessary to satisfy the conditions that T_2 and T_6 vanish at the two values $y=\pm h/2$ where h is the thickness of the plate. Appropriate expressions for T_2 and T_6 can be obtained as follows. First consider T_2. From reference [100]:

$$T_2 = \lambda\nabla^2\phi + 2\mu S_2 \tag{8.32}$$

For the two dimensional case:

$$\nabla^2\phi = \frac{\partial^2\phi}{\partial x^2} + \frac{\partial^2\phi}{\partial y^2} \tag{8.33}$$

Substituting from Equations (8.16) and (8.22):

$$\begin{aligned} \nabla^2\phi &= (\alpha^2 - k^2)\phi \\ &= (\alpha^2 - k^2)\times(A \sinh \alpha y + B \cosh \alpha y)e^{i(\omega t - kx)} \end{aligned} \tag{8.34}$$

From Equations (8.1) and (8.7):

$$S_2 = \frac{\partial v}{\partial y} = \frac{\partial}{\partial y}\left(\frac{\partial \phi}{\partial y} - \frac{\partial \psi}{\partial x}\right) \tag{8.35}$$

Substituting from Equation (8.22) this becomes:

$$S_2 = \alpha^2\phi - \frac{\partial^2 \psi}{\partial x \partial y} \tag{8.36}$$

Differentiating Equation (8.31) with respect to x gives:

$$\frac{\partial \psi}{\partial x} = -ik\,(C \sinh \beta y + D \cosh \beta y)e^{i(\omega t - kx)} \tag{8.37}$$

Differentiating this equation with respect to y then gives:

$$\frac{\partial^2 \psi}{\partial x \partial y} = -ik\, e^{i(\omega t - kx)}\,(\beta C \cosh \beta y + \beta D \sinh \beta y) \tag{8.38}$$

Substituting Equations (8.30) and (8.38) into Equation (8.36) gives:

$$\begin{aligned} S_2 = {} & (\alpha^2 A \sinh \alpha y + \alpha^2 B \cosh \alpha y \\ & + ik\beta C \cosh \beta y + ik\beta D \sinh \beta y)e^{i(\omega t + kx)} \end{aligned} \tag{8.39}$$

Substituting Equations (8.34) and (8.39) into Equation (8.32) gives:

$$\begin{aligned} T_2 = {} & [\lambda(\alpha^2 - k^2)A \sinh \alpha y + \lambda(\alpha^2 - k^2)B \cosh \alpha y \\ & + 2\mu\alpha^2 A \sinh \alpha y + 2\mu\alpha^2 B \cosh \alpha y + 2ik\beta\mu C \cosh \beta y \\ & + 2ik\beta\mu D \sinh \beta y]e^{i(\omega t - kx)} \end{aligned} \tag{8.40}$$

This can be rewritten as:

$$\begin{aligned} T_2 = {} & [(\lambda\alpha^2 - \lambda k^2 + 2\mu\alpha^2)A \sinh \alpha y \\ & + (\lambda\alpha^2 - \lambda k^2 + 2\mu\alpha^2)B \cosh \alpha y \\ & + 2ik\beta\mu C \cosh \beta y + 2ik\beta\mu D \sinh \beta y]e^{i(\omega t - kx)} \end{aligned} \tag{8.41}$$

As shown in Appendix VI:

$$\lambda\alpha^2 - \lambda k^2 + 2\mu\alpha^2 \equiv \mu(k^2 + \beta^2) \tag{8.42}$$

Hence Equation (8.41) becomes:

$$T_2 = [(k^2 + \beta^2)\mu A \sinh \alpha y + (K^2 + \beta^2)\mu B \cosh \alpha y + 2ik\beta\mu C \cosh \beta y + 2ik\beta\mu D \sinh \beta y]e^{i(\omega t - kx)} \quad (8.43)$$

It is now necessary to obtain a suitable expression for T_6. From reference [100]:

$$T_6 = \mu S_6 \quad (8.44)$$

where S_6 is the shearing strain about the z axis and is given by:

$$S_6 = \frac{\partial v}{\partial x} + \frac{\partial u}{\partial y} \quad (8.45)$$

Using Equation (8.7):

$$S_6 = \frac{\partial^2 \phi}{\partial x \partial y} - \frac{\partial^2 \psi}{\partial x^2} + \frac{\partial^2 \phi}{\partial x \partial y} + \frac{\partial^2 \psi}{\partial y^2} \quad (8.46)$$

Combining Equations (8.44), (8.46) and (8.24) gives:

$$T_6 = \mu \left(2\frac{\partial^2 \phi}{\partial x \partial y} - \frac{\partial^2 \psi}{\partial x^2} + \beta^2 \psi \right) \quad (8.47)$$

Differentiating Equation (8.28) with respect to x gives:

$$\frac{\partial \phi}{\partial x} = -ik(A \sinh \alpha y + B \cosh \alpha y)e^{i(\omega t - kx)} \quad (8.48)$$

Differentiating this equation with respect to y gives:

$$\frac{\partial^2 \psi}{\partial x \partial y} = -ik(\alpha A \cosh \alpha y + \alpha B \sinh \alpha y)e^{i(\omega t - kx)} \quad (8.49)$$

Differentiating Equation (8.29) twice with respect to x gives:

$$\frac{\partial^2 \psi}{\partial x^2} = -k^2(C \sinh \beta y + D \cosh \beta y)e^{i(\omega t - kx)} \quad (8.50)$$

Substituting Equations (8.49) and (8.50) into Equation (8.47) gives:

$$T_6 = [A(-2ik\alpha\mu) \cosh \alpha y + B(-2ik\alpha\mu) \sinh \alpha y + C\mu(k^2 + \beta^2)\sinh \beta y + D\mu(k^2 + \beta^2)\cosh \beta y]e^{i(\omega t - kx)} \quad (8.51)$$

If h is the thickness of the plate then the boundary conditions are:

$$T_2 = T_6 = 0 \quad at \quad y = \pm h/2 \tag{8.52}$$

For convenience let:

$$\begin{aligned} n &= 2ik\beta\mu \\ p &= -2ik\alpha\mu \\ q &= \mu(k^2 + \beta^2) \\ s_\alpha &= \sinh(\alpha h/2) \\ s_\beta &= \sinh(\beta h/2) \\ c_\alpha &= \cosh(\alpha h/2) \\ c_\beta &= \cosh(\beta h/2) \end{aligned} \tag{8.53}$$

At $y=+h/2$ Equations (8.43) and (8.51) become:

$$\begin{aligned} T_2 = 0 &= qs_\alpha A + qc_\alpha B + nc_\beta C + ns_\beta D \\ T_6 = 0 &= pc_\alpha A + ps_\alpha B + qs_\beta C + qc_\beta D \end{aligned} \tag{8.54}$$

At $y=-h/2$ Equations (8.43) and (8.51) become:

$$\begin{aligned} T_2 = 0 &= -qs_\alpha A + qc_\alpha B + nc_\beta C - ns_\beta D \\ T_6 = 0 &= pc_\alpha A - ps_\alpha B - qs_\beta C + qc_\beta D \end{aligned} \tag{8.55}$$

In matrix notation these four simultaneous equations become:

$$\begin{bmatrix} qs_\alpha & qc_\alpha & nc_\beta & ns_\beta \\ pc_\alpha & ps_\alpha & qs_\beta & qc_\beta \\ -qs_\alpha & qc_\alpha & nc_\beta & -ns_\beta \\ pc_\alpha & -ps_\alpha & -qs_\beta & qc_\beta \end{bmatrix} \begin{bmatrix} A \\ B \\ C \\ D \end{bmatrix} = \begin{bmatrix} 0 \\ 0 \\ 0 \\ 0 \end{bmatrix} \tag{8.56}$$

The elements of the matrices in Equation (8.56) may be rearranged as follows:

$$\begin{bmatrix} qs_\alpha & ns_\beta & nc_\beta & qc_\alpha \\ pc_\alpha & qc_\beta & qs_\beta & ps_\alpha \\ -qs_\alpha & -ns_\beta & nc_\beta & qc_\alpha \\ -pc_\alpha & -qc_\beta & qs_\beta & ps_\alpha \end{bmatrix} \begin{bmatrix} A \\ D \\ C \\ B \end{bmatrix} = \begin{bmatrix} 0 \\ 0 \\ 0 \\ 0 \end{bmatrix} \tag{8.57}$$

The square matrix was obtained by interchanging the second and fourth columns and multiplying the bottom row by -1. Elements B and D in the left hand column matrix have been interchanged to correspond to the changes in the square matrix. It is possible to partition the above matrix as shown below:

$$\begin{bmatrix} X_1 & X_2 \\ -X_1 & X_2 \end{bmatrix} \begin{bmatrix} Y_1 \\ Y_2 \end{bmatrix} = \begin{bmatrix} 0 \\ 0 \end{bmatrix} \tag{8.58}$$

where:

$$[X_1] = \begin{bmatrix} qs_\alpha & ns_\beta \\ pc_\alpha & qc_\beta \end{bmatrix} \qquad [X_2] = \begin{bmatrix} nc_\beta & qc_\alpha \\ qs_\beta & ps_\alpha \end{bmatrix} \tag{8.59}$$

and:

$$[Y_1] = \begin{bmatrix} A \\ D \end{bmatrix} \qquad [Y_2] = \begin{bmatrix} C \\ B \end{bmatrix} \tag{8.60}$$

Expanding (8.58) results in the following two equations:

$$[X_1]\{Y_1\} + [X_2]\{Y_2\} = 0 \tag{8.61}$$

$$-[X_1]\{Y_1\} + [X_2]\{Y_2\} = 0 \tag{8.62}$$

The only non-trivial solutions of these equations are:

$$[X_1]\{Y_1\} = 0 \qquad [X_2]\{Y_2\} = 0 \tag{8.63}$$

Substituting from Equations (8.59) and (8.60) these become:

$$\begin{bmatrix} qs_\alpha & ns_\beta \\ pc_\alpha & qc_\beta \end{bmatrix} \begin{bmatrix} A \\ D \end{bmatrix} = 0 \tag{8.64}$$

and:

$$\begin{bmatrix} nc_\beta & qc_\alpha \\ qs_\beta & ps_\alpha \end{bmatrix} \begin{bmatrix} C \\ B \end{bmatrix} = 0 \tag{8.65}$$

Any solution of these second order systems or any combination of their solutions is a solution of the original fourth order system. From Equations (8.30) and (8.31) it follows that when $A=D=0$:

$$\phi = B(\cosh \alpha y)e^{i(\omega t - kx)} \tag{8.66}$$

$$\psi = C(\sinh \beta y)e^{i(\omega t - kx)} \tag{8.67}$$

It also follows that, when $B=C=0$:

$$\phi = A(\sinh \alpha y)e^{i(\omega t - kx)} \tag{8.68}$$

$$\psi = D(\cosh \beta y)e^{i(\omega t - kx)} \tag{8.69}$$

8.2.2 *Expressions for Particle Displacement*

Recall from (8.7) that the displacement in a direction parallel to the x axis is given by:

$$u = \frac{\partial \phi}{\partial x} + \frac{\partial \psi}{\partial y} \tag{8.70}$$

and the displacement in a direction parallel to the y axis is given by:

$$v = \frac{\partial \phi}{\partial y} - \frac{\partial \psi}{\partial x} \tag{8.71}$$

Using Equations (8.66) and (8.67) the displacements become:

$$u_s = -ikB \cosh(\alpha y)e^{i(\omega t - kx)} + \beta C \cosh(\beta y)e^{i(\omega t - kx)} \tag{8.72}$$

$$v_s = \alpha B \sinh(\alpha y)e^{i(\omega t - kx)} + ikC \sinh(\beta y)e^{i(\omega t - kx)} \tag{8.73}$$

Using Equations (8.68) and (8.69) the displacements become:

$$u_a = -ikA \sinh(\alpha y)e^{i(\omega t - kx)} + \beta D \sinh(\beta y)e^{i(\omega t - kx)} \tag{8.74}$$

$$v_a = \alpha A \cosh(\alpha y)e^{i(\omega t - kx)} + ikD \cosh(\beta y)e^{i(\omega t - kx)} \tag{8.75}$$

On analysing Equations (8.72) and (8.73) it becomes obvious that the displacement u_s has the same signs in the upper and lower halves of the plate while the displacement v_s has opposite signs. This means that Equations (8.72) and (8.73) represent motion which is symmetrical about the medial plane of the plate hence the s subscript. Looking at Equations (8.74) and (8.75) it is clear that the displacement u_a has opposite signs in

the upper and lower halves of the plate while the displacement v_a has the same signs. This means that Equations (8.74) and (8.75) represent motion which is antisymmetrical about the medial plane of the plate hence the *a* subscript. From this analysis it is clear that both symmetrical and antisymmetrical Lamb wave modes can propagate in a plate independently of one another.

8.2.3 Phase Velocity as a Function of Frequency

The frequency equations for the symmetrical modes are obtained as follows. The determinant of the square matrix in Equation (8.65) must equal zero ie:

$$\begin{vmatrix} nc_\beta & qc_\alpha \\ qc_\beta & ps_\alpha \end{vmatrix} = 0 \tag{8.76}$$

hence:

$$npc_\beta s_\alpha = q^2 c_\alpha s_\beta \tag{8.77}$$

or:

$$\frac{c_\alpha s_\beta}{c_\beta s_\alpha} = \frac{np}{q^2} \tag{8.78}$$

Substituting from Equation (8.53):

$$\frac{\cosh(\alpha h/2)\sinh(\beta h/2)}{\cosh(\beta h/2)\sinh(\alpha h/2)} = \frac{(2ik\beta\mu)(-2ik\alpha\mu)}{\mu^2(k^2 + \beta^2)} \tag{8.79}$$

hence:

$$\frac{\tanh(\beta h/2)}{\tanh(\alpha h/2)} = \frac{4k^2\alpha\beta}{(k^2 + \beta^2)^2} \qquad (SYMMETRICAL) \tag{8.80}$$

By employing numerical methods it is possible to use this equation to plot phase velocity dispersion curves for the symmetrical Lamb wave modes. In exactly the same way as for the symmetrical modes it is possible to obtain an equation which can be

used to plot phase velocity as a function of frequency thickness product for the antisymmetrical modes. This equation is obtained by noting that the determinant of the square matrix in Equation (8.64) must equal zero i.e.:

$$\begin{vmatrix} qs_\alpha & ns_\beta \\ pc_\alpha & qc_\beta \end{vmatrix} = 0 \tag{8.81}$$

hence:

$$npc_\alpha s_\beta = q^2 s_\alpha c_\beta \tag{8.82}$$

or:

$$\frac{c_\alpha s_\beta}{s_\alpha c_\beta} = \frac{q^2}{np} \tag{8.83}$$

Substituting from Equation (8.53):

$$\frac{\cosh(\alpha h/2)\sinh(\beta h/2)}{\sinh(\alpha h/2)\cosh(\beta h/2)} = \frac{\mu^2(k^2 + \beta^2)^2}{(2ik\beta\mu)(-2ik\alpha\mu)} \tag{8.84}$$

or:

$$\frac{\tanh(\beta h/2)}{\tanh(\alpha h/2)} = \frac{(k^2 + \beta^2)^2}{4k^2\alpha\beta} \qquad (ANTISYMMETRICAL) \tag{8.85}$$

By employing numerical methods it is possible to use this equation to plot phase velocity dispersion curves for the antisymmetrical Lamb wave modes.

8.2.4 Group Velocity as a Function of Frequency

In general group velocity is given by:

$$V_g = \frac{d\omega}{dk} \tag{8.86}$$

As previously mentioned, it is only possible to plot the Lamb wave phase velocity, V, as a function of frequency, f, by obtaining data from the above equations using

numerical methods. Once a set of numerical data has been obtained it is then possible to perform numerical differentiation to obtain $dV/d(fh)$ where h is the thickness of the plate. To plot the group velocity as a function of frequency it is therefore necessary to obtain an equation which links group velocity to $dV/d(fh)$. This can be done as follows. From Equation (8.19):

$$V_g = \frac{d}{dk}(kV) = V + k\frac{dV}{dk} \tag{8.87}$$

hence:

$$V_g = V + k\frac{dV}{d\omega}\frac{d\omega}{dk} \tag{8.88}$$

hence:

$$V_g = V + k\frac{dV}{d\omega}V_g \tag{8.89}$$

hence:

$$V_g\left(1 - \frac{\omega}{V}\frac{dV}{d\omega}\right) = V \tag{8.90}$$

hence:

$$V_g = \frac{V}{\left(1 - \frac{\omega}{V}\frac{dV}{d\omega}\right)} \tag{8.91}$$

Since $\omega=2\pi f$ it follows that:

$$\frac{\omega}{V}\frac{dV}{d\omega} = \frac{f}{V}\frac{dV}{df} = \frac{(fh)}{V}\frac{dV}{d(fh)} \tag{8.92}$$

hence:

$$V_g = \frac{V}{\left(1 - \frac{(fh)}{V}\frac{dV}{d(fh)}\right)} \tag{8.93}$$

It was not possible to find this equation in any of the literature. Equation (8.93) can be used to plot the Lamb wave group velocity, V_g, as a function of frequency.

8.2.5 *Interpretation of the Theory*

Equations (8.72) to (8.75) indicate that two types of particle displacement are possible in a thin plate: symmetrical and antisymmetrical. Here the term *thin* applies to the situation where the thickness is comparable to the wavelength of the wave which is propagating in the plate. These two basic types of particle motion are illustrated in Figures 1.4 and 1.5 which can be found in Chapter 1 of this Thesis. To understand how Lamb waves are produced in practice, consider again the situation illustrated in Figure 8.1. As the plate thickness is reduced and the fluid/solid boundaries move closer together a point is reached where it is impossible for longitudinal and shear waves to propagate independently along the plate. When this happens it is evident that energy will propagate best down the plate at those frequencies for which the various reflected components combine in or out of phase at regular intervals along the length of the plate. At other frequencies of excitation, energy is propagated along the length of the plate in a random manner and it is not therefore possible to transmit a coherent signal from one part of the plate to another. The possible Lamb wave modes can be found by using Equations (8.80) and (8.85) to plot phase velocity dispersion curves. As discussed

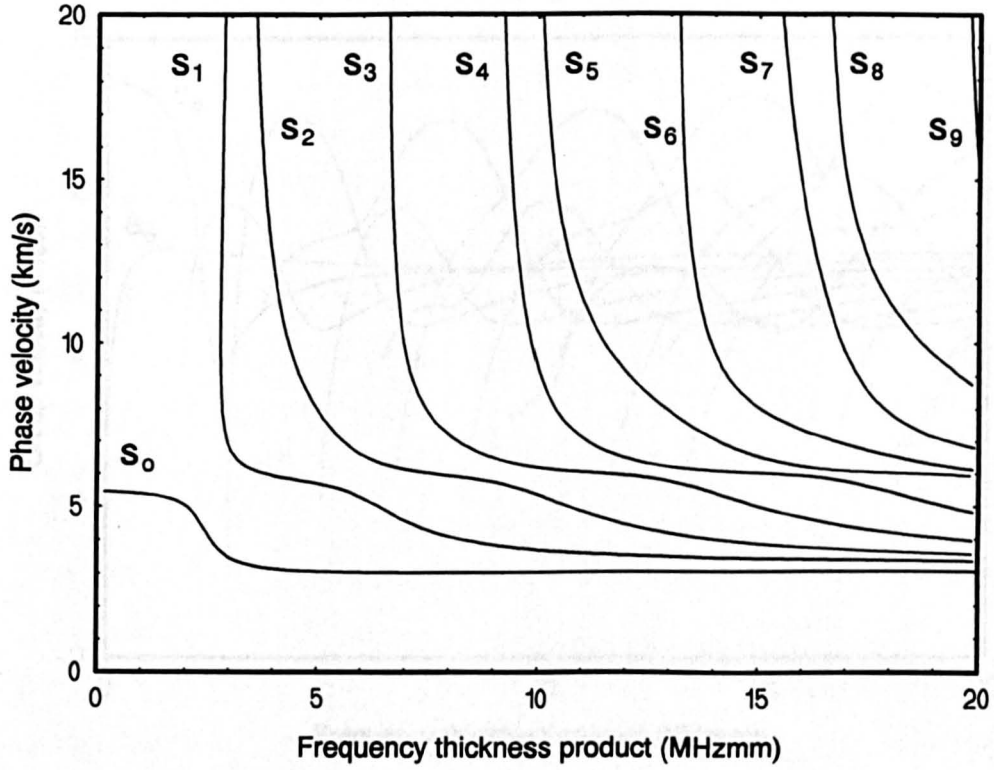

FIGURE 8.2 PHASE VELOCITY DISPERSION CURVES IN STEEL (SYMMETRICAL MODES)

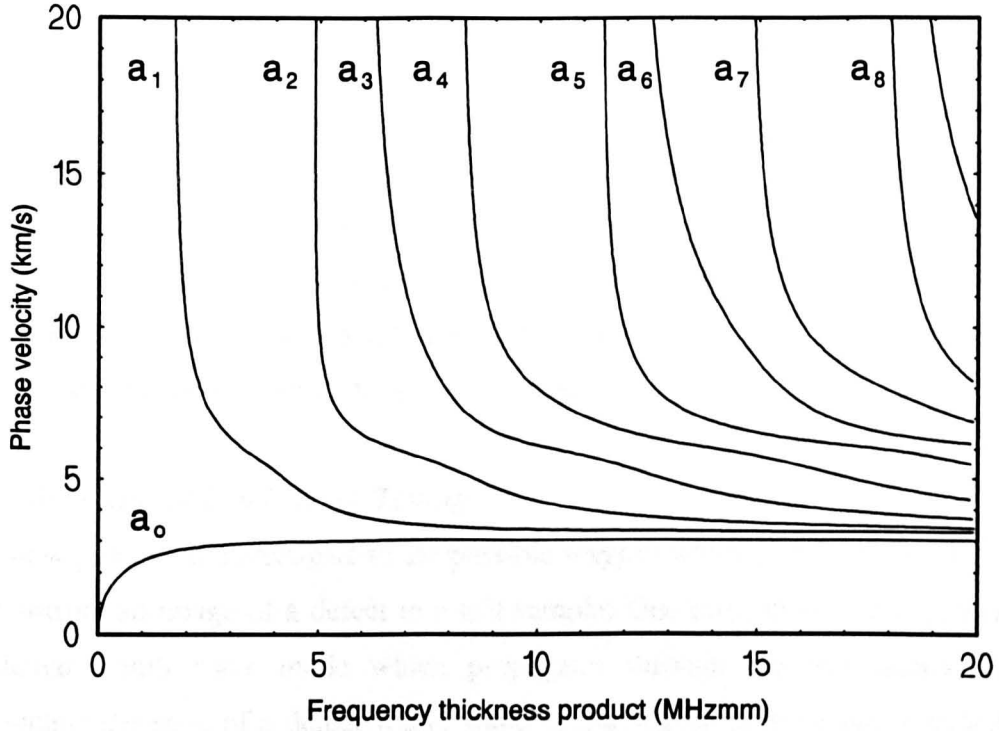

FIGURE 8.3 PHASE VELOCITY DISPERSION CURVES IN STEEL (ANTISYMMETRICAL MODES)

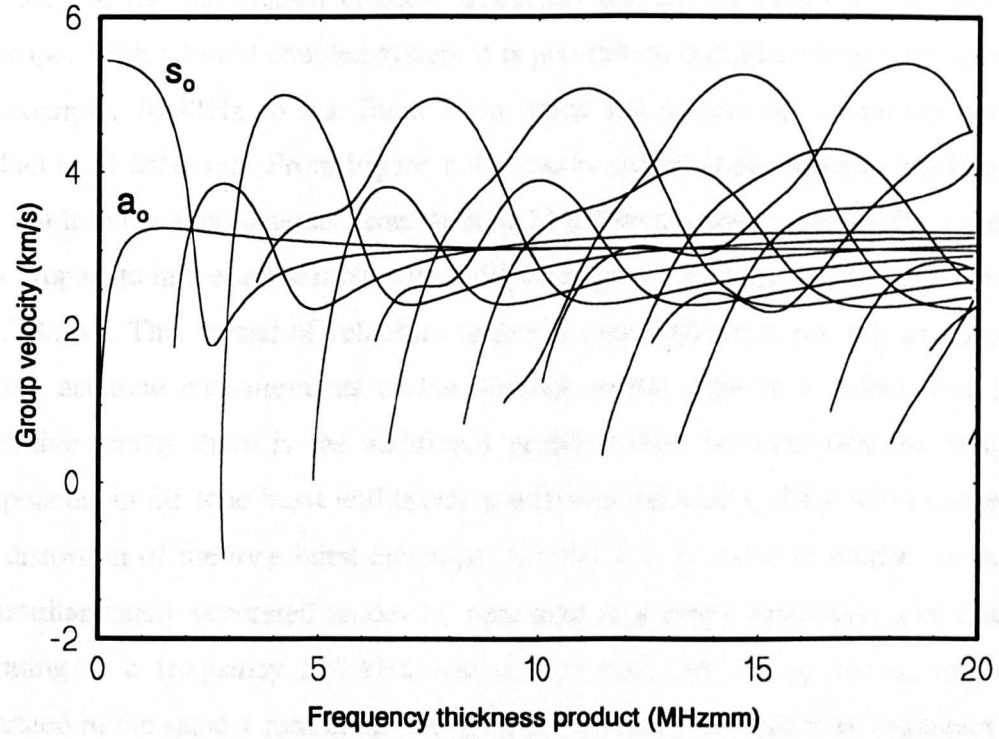

FIGURE 8.4 GROUP VELOCITY DISPERSION CURVES IN STEEL (ALL MODES)

previously, it is only possible to plot phase velocity as a function of frequency-thickness product by solving these equations numerically. This has been done for steel using specially developed computer software and the results are illustrated in Figure 8.2 (symmetrical modes) and Figure 8.3 (antisymmetrical modes). Also, Equation (8.93) has been used to plot group velocity dispersion curves for steel and the results are illustrated in Figure 8.4 (both symmetrical and antisymmetrical modes). All of the curves cover a frequency-thickness range of 1 to 20 MHzmm. Put another way, the curves represent all of the possible Lamb wave modes that can exist in a 1 mm thick steel plate over the frequency range 0 to 20 MHz.

8.3 Air Coupled Lamb Wave Testing

It is now possible to investigate to the possible ways in which Lamb waves can be used to construct an image of a defect in a test sample. One method involves generating a particular Lamb wave mode which propagates through the test sample until it encounters the edge of a defect where some of the energy in the wave is reflected. If the waves are transmitted in the form of a tone burst then it is possible to measure the total time taken for this to travel to the edge of the defect and back to a receiving device. In order to construct a precision scanning system based on this technique it is necessary to use the highest possible frequency and the shortest possible tone burst envelope. With a liquid coupled system it is possible to consider using a frequency of, for example, 10 MHz so that for a 1 mm thick test sample the frequency thickness product is 10 MHzmm. From Figure 8.4 it can be seen that operating at this frequency will result in the simultaneous generation of 10 different Lamb wave modes which will each propagate in the test sample with a different group velocity in the range 0.8 kms^{-1} to 4.7 kms^{-1}. This spread of velocities makes it very difficult to use this technique for making accurate measurements of the distance to the edge of a defect. For highly dispersive modes there is the additional problem that, because different frequency components in the tone burst will travel at different velocities, there will be stretching and distortion of the tone burst envelope. Clearly it is possible to reduce the number of simultaneously generated modes by operating at a lower frequency. For example, operating at a frequency 500 kHz will ensure that only the s_o and a_o modes are generated in the same 1 mm thick test sample. Reducing the operating frequency in an air coupled system has the additional advantage that signal frequency is then within the

channel bandwidth discussed in Chapter 2 (1.3 MHz for a 1 cm air gap). The disadvantage of operating at a lower frequency is that both the measurement accuracy and the resolution of the system are reduced. There are a number of other problems associated with detecting and imaging defects by looking for Lamb wave reflections from edges. Many of these problems are associated with the way in which Lamb waves interact with different types of defect. For example, the magnitude of the reflection will be influenced by the angle of the defect edges relative to the direction of propagation. Also, with this technique the distance between the transducer(s) and the defect is large and variable, and if the material under test is highly attenuative then this results in a significant loss of signal and large variations in amplitude. When using a single sided imaging system with difficult materials there is an enormous advantage to be gained by keeping the distance between the transducer(s) and the defect (i.e. the part of the path which is inside the test sample) constant and as short as possible.

An alternative way of using Lamb waves to construct an image of a defect in a test sample is to simply measure the ability of the material to support a particular Lamb wave mode. By using this method it is possible to overcome most of the previously discussed problems. A feature of this technique is that the accuracy and the resolution of the system are determined by the physical size of the transducers and not by the frequency of operation. As discussed briefly at the end of Chapter 7, the method involves using two transducers placed at the correct angles for generating and detecting a particular Lamb wave mode in parts of the test sample which contain no defects. By placing the two transducers as close together as possible it is possible to transmit a signal of constant amplitude from one transducer to the other via the test sample. The amplitude of the signal will remain constant for as long as both transducers are sitting over material of the correct thickness. Having fixed the separation and orientation of the transducers they can then be used to scan the test sample to find variations in thickness, composition or structure. If either the transmitter or the receiver is placed over part of the test sample which is different to that used during tuning of the system, the amplitude of the received signal is reduced. The technique is very sensitive and even a small variation in material thickness will result in a significant reduction in the magnitude of the received signal. Larger variations in thickness (e.g. 50%) will cause the received signal to vanish completely.

8.4 A Prototype System

8.4.1 System Description

A fully automated test system, which is based on the previously discussed imaging technique, was developed to demonstrate the enormous potential of the new air coupled technology. As illustrated in Figure 8.5 the main building blocks of the system are a mechanical scanner, a personal computer (PC) equipped with a digitising card, a pair of piezocomposite transducers, an ultra low noise pre-amplifier which is integrated into the receiver package and a *real-time* signal recovery module consisting of an analogue filter and an envelope detector. As discussed previously, the term *real-time* should be read to mean that no signal averaging or any other form of digital processing was required to produce the ultrasonic images which are to be discussed here. Another important element of the system is the specially written computer software which enables the PC to simultaneously control the scanner, digitise analogue data from the envelope detector and construct an internal image of the test sample in *real-time*. The automated Lamb wave scanner has been used to produce images of defects in thin plates made from various materials including carbon fibre. Images constructed by the system are normally displayed on the computer screen in real-time and consist of a colour coded map which indicates signal amplitude as a function scanner head position.

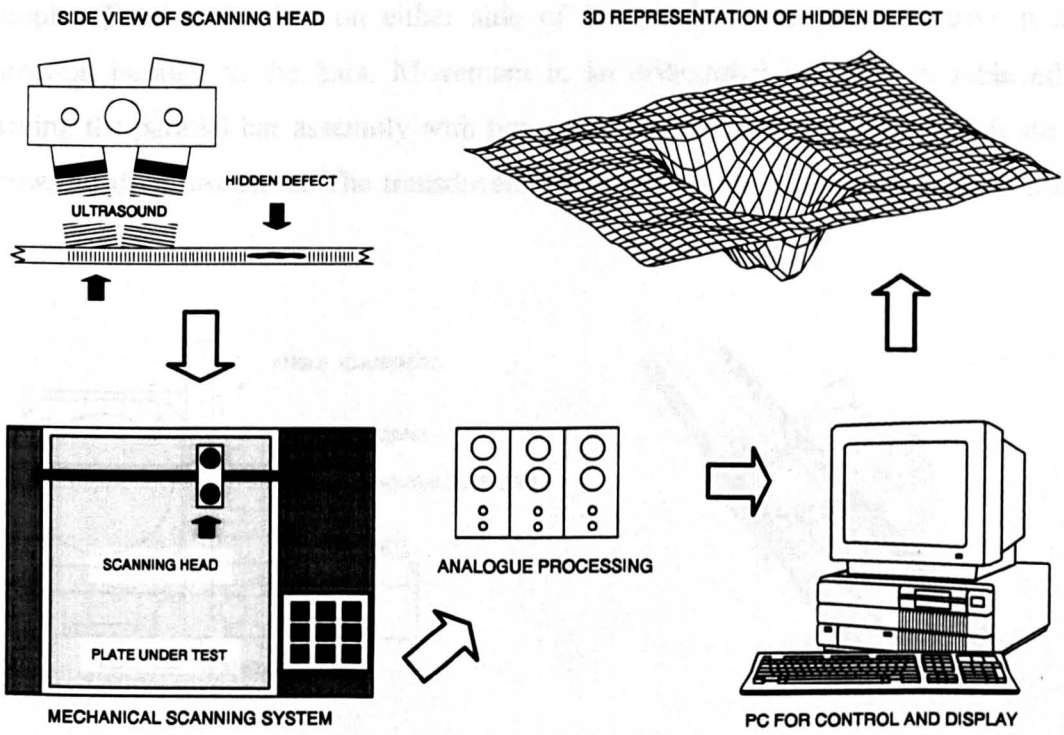

FIGURE 8.5 MAIN BUILDING BLOCKS OF THE AUTOMATED LAMB WAVE SCANNER

8.4.2 System Design

Transducers

As discussed in Chapter 7, the initial Lamb wave experiments were performed using 30 mm diameter piezoceramic composite transducers which both have a 20% ceramic volume fraction. In order to improve the resolution of the system and reduce the weight of the transducer assemblies, smaller piezoceramic composite transducers were designed and manufactured for use with the scanner. The transmitter is a 15 x 15 mm device with a 70% ceramic volume fraction and the receiver is a 15 mm diameter device with a 20% ceramic volume fraction. As with the 30 mm diameter devices the new transducers are frequency matched to operate at 580 kHz. The design of the 70% transducer is based on the latest results obtained using the linear systems and finite element models mentioned previously. As in the initial experiments there is no requirement for mechanical matching layers.

Scanner Configuration

The transducer assembly is illustrated in Figure 8.6. Within the scanner this assembly is bolted onto a moving platform which is supported on a pair of parallel bars. The platform assembly is illustrated in Figure 8.7. Under computer control the platform can be moved along two orthogonal axes in a plane parallel to the top surface of the test sample. Tensioned wires on either side of the platform are used to drive it in a direction parallel to the bars. Movement in an orthogonal direction is achieved by driving the parallel bar assembly with two more sets of tensioned wires which are not shown in the illustration. The transducers sweep across the surface of the test sample

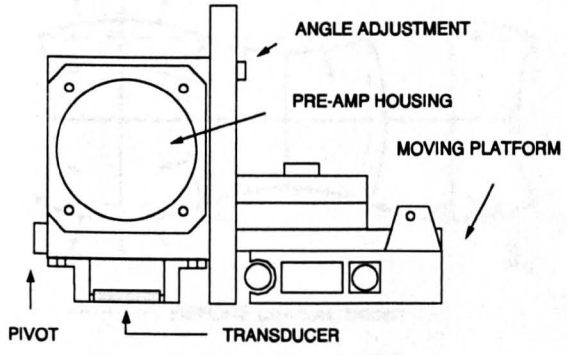

FIGURE 8.6 ULTRASONIC TRANSDUCER ASSEMBLY

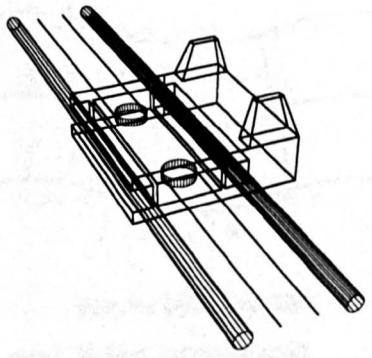

FIGURE 8.7 MOVING PLATFORM FOR TRANSDUCERS

at a fixed height which is set at between 5 and 10 mm. A block diagram of the system electronics is illustrated in Figure 8.8. As in the initial set of experiments, the transmitting transducer is driven with a 10 to 20 cycle tone burst which has a centre frequency of 580 kHz.

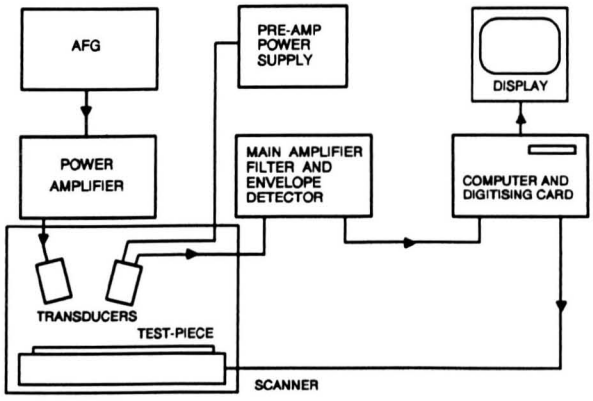

FIGURE 8.8 BLOCK DIAGRAM OF SYSTEM ELECTRONICS

Lamb Wave Modes

Many of the results which are discussed later involve the use of test samples made from 1 mm thick aluminium plates. As mentioned previously the transducers are designed to operate at a frequency of 580 kHz. For aluminium and for a frequency thickness product of 0.58 MHzmm the only possible modes that can be generated in the test sample are the first symmetrical (s_o) mode, which is illustrated in Figure 8.9, and the first anti-symmetrical (a_o) mode, which is illustrated in Figure 8.10. By using a computer model which is based on the previously described theory it is possible to predict the relative magnitudes of the in plane and out of plane displacements for both of these modes. The out of plane displacement for the s_o mode is illustrated in Figure 8.11 and the out of plane displacement for the a_o mode is illustrated in Figure 8.12. In these figures relative displacement is plotted as a function of depth. A depth of 0 corresponds to the top of the test plate and a depth of +1 corresponds to

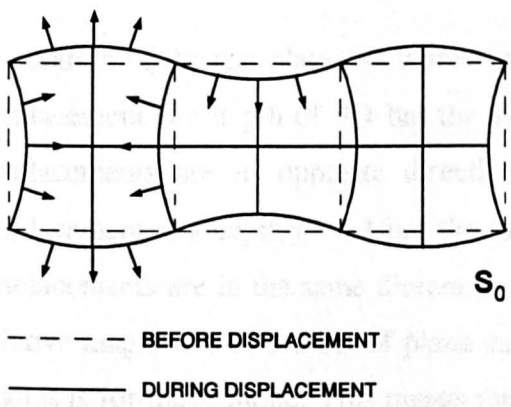

FIGURE 8.9 FIRST SYMMETRICAL LAMB WAVE MODE

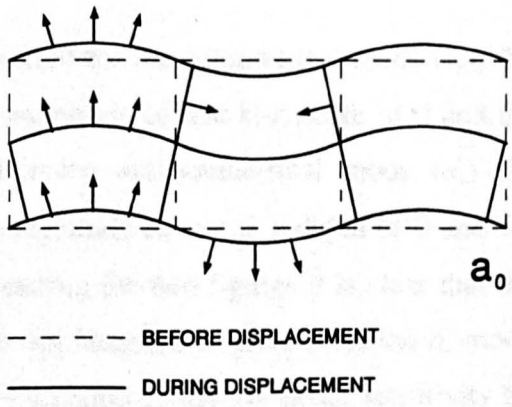

FIGURE 8.10 FIRST ANTISYMMETRICAL LAMB WAVE MODE

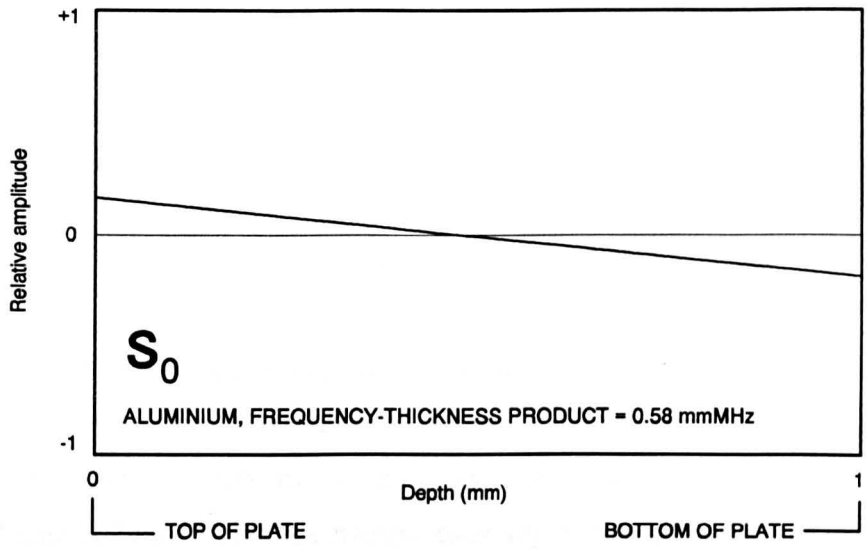

FIGURE 8.11 OUT OF PLANE DISPLACEMENT FOR THE FIRST SYMMETRICAL MODE
(1 mm THICK ALUMINIUM PLATE, 580 kHz)

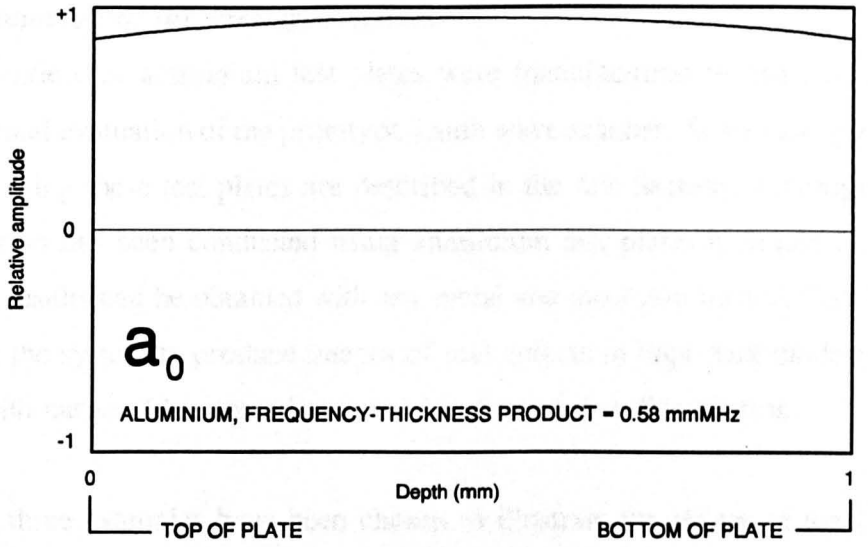

FIGURE 8.12 OUT OF PLANE DISPLACEMENT FOR THE FIRST ANTISYMMETRICAL MODE
(1 mm THICK ALUMINIUM PLATE, 580 kHz)

the bottom of the test plate. As would be expected for the symmetrical mode (s_o), the displacement at a depth of +1 has the same magnitude as that at a depth of 0 and the displacements are in opposite directions. For the antisymmetrical mode (a_o) the displacement at a depth of +1 has the same magnitude as that at a depth of 0 and the displacements are in the same direction. Comparing the two figures it is clear that the relative magnitude of the out of plane surface displacement is greater for the a_o mode than it is for the s_o mode. This means that it is possible to achieve better sensitivity by using the a_o mode rather than the s_o mode. For 1 mm thick aluminium plates and

various other test samples this has been confirmed by experiment. The phase velocity of the required mode can be found using the previously mentioned computer model. Knowing this, the angle of the transducers can be found using the coincidence principle which was discussed in Chapter 1. The necessary equation is reproduced below:

$$\sin(\theta) = \frac{V_i}{V} \tag{8.94}$$

Here, V_i is the velocity of the incident ultrasonic wave in air (340 ms^{-1}), θ is the angle of incidence and V is the phase velocity of the Lamb wave mode generated in the test sample. The phase velocity of the a_o mode for a frequency thickness product of 0.58 MHzmm is 2 kms^{-1} and the corresponding angle for the transducers is 9.8 degrees. All of the single sided scans obtained with 1 mm thick aluminium plates were produced with both transducers sitting at this angle.

8.5 Evaluation of the Prototype System

A wide variety of aluminium test plates were manufactured in order to conduct an experimental evaluation of the prototype Lamb wave scanner. Some examples of results obtained using these test plates are described in the this Section. Although a detailed investigation has been conducted using aluminium test plates it should be noted that excellent results can be obtained with any metal and most non-metals. To illustrate the ability of the system to produce images of real defects in important modern materials, results with carbon fibre test plates are also presented in this Section.

The first three examples have been chosen to illustrate the ability of the Lamb wave scanner to construct images of a number of basic shapes. Each of the three test plates was manufactured from a 1 mm thick aluminium plate into which a *defect* was introduced by removing 50% of the material thickness. The test plates along with their corresponding Lamb wave images are illustrated in Figures 8.13 to 8.21. In each case the test plate was scanned across its smooth undamaged face. Figure 8.13 illustrates a simple rectangular *defect* and Figure 8.14 is the corresponding Lamb wave image. From Figure 8.14 alone it is clear that there is excellent contrast between areas of different thickness on the plate. This is only possible because of the high levels of signal to noise ratio that can be achieved using the new receiver. As with all of the

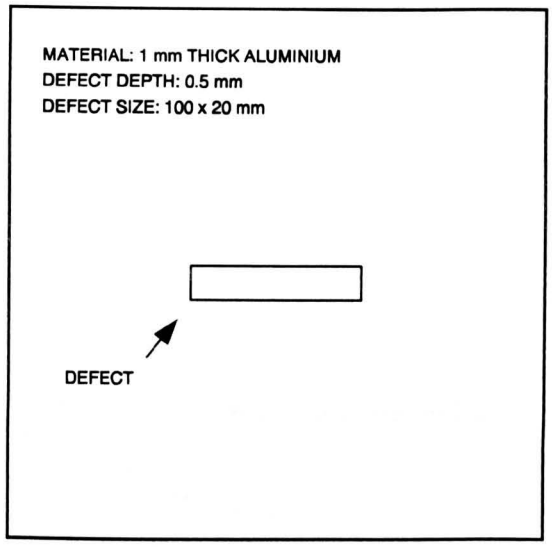

FIGURE 8.13 A RECTANGULAR *DEFECT* CREATED IN A THIN ALUMINIUM PLATE

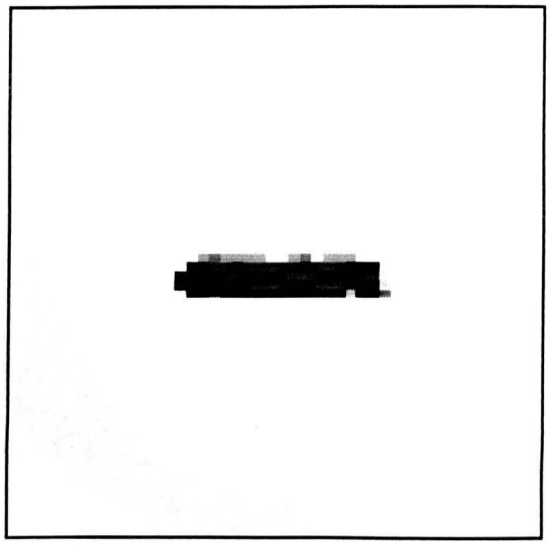

FIGURE 8.14 LAMB WAVE IMAGE OF THE RECTANGULAR *DEFECT*

results presented in this Section, these images were produced in real-time. As before, the term *real-time* should be read to mean that no signal averaging, data processing or image processing was involved in producing any of the images. Also, all of the results in this Thesis were obtained without applying front face matching layers to either of the transducers. Figure 8.15 is a plot of relative signal amplitude as a function of scanner head position over the same test plate. This 3D plot helps to emphasise the steep transition from a strong signal to a weak signal as the scanner head moves from thick material to thin material. Also evident from the 3D amplitude plot is the consistent

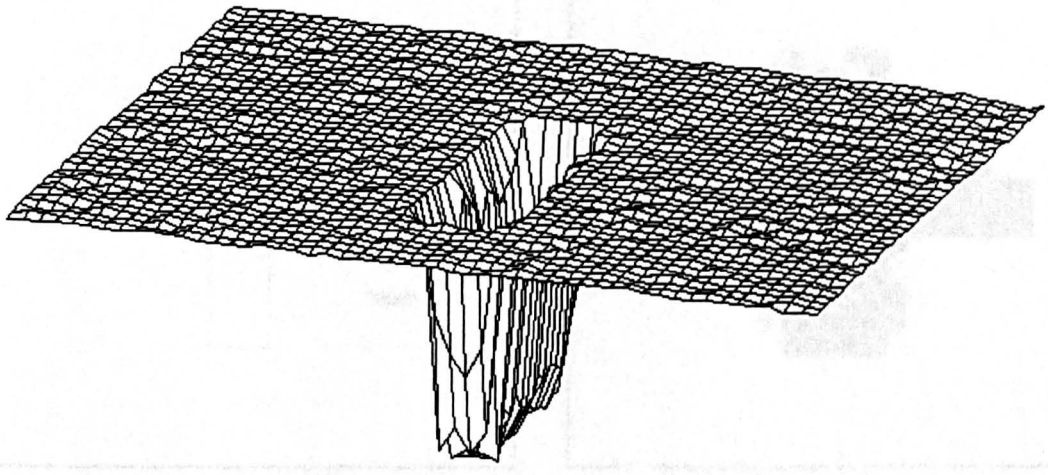

FIGURE 8.15 RELATIVE SIGNAL AMPLITUDE AS A FUNCTION OF TRANSDUCER HEAD POSITION ON THE PLATE

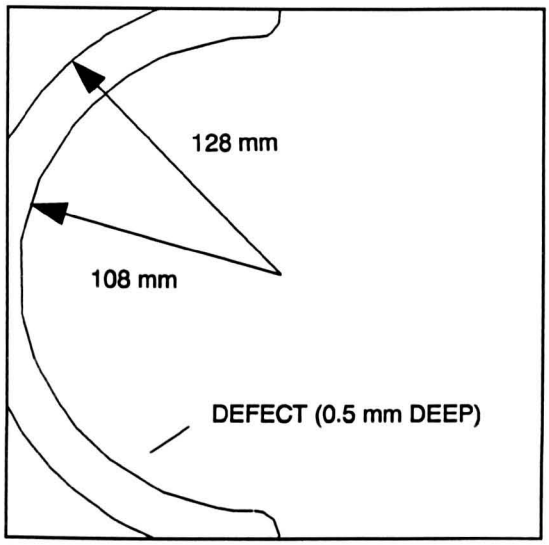

FIGURE 8.16 A SEMICIRCULAR *DEFECT* CREATED IN A 1 mm THICK ALUMINIUM PLATE

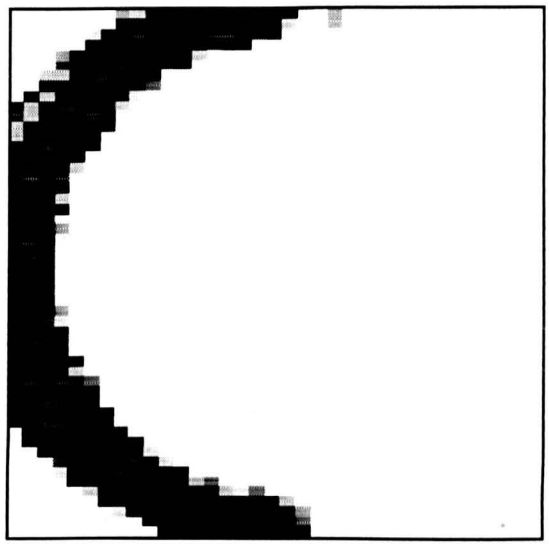

FIGURE 8.17 LAMB WAVE IMAGE OF THE SEMICIRCULAR *DEFECT*

nature of the signal as the scanner head moves over areas of constant thickness. Figures 8.16 and 8.18 illustrate a semicircular *defect* and a cross shaped *defect* respectively. The Lamb wave image of the semicircular *defect* is illustrated in Figure 8.17 and the Lamb wave image of the cross shaped *defect* is illustrated in Figure 8.19. The first thing to note about both of the images is the clarity with which the shapes of the *defects* have been revealed. In Figure 8.17 the image appears to be clipped at the edges because it was not possible to take the scanner head sufficiently close to the edges of the test plate. From Figure 8.19 it can be seen that there is a double image of the cross

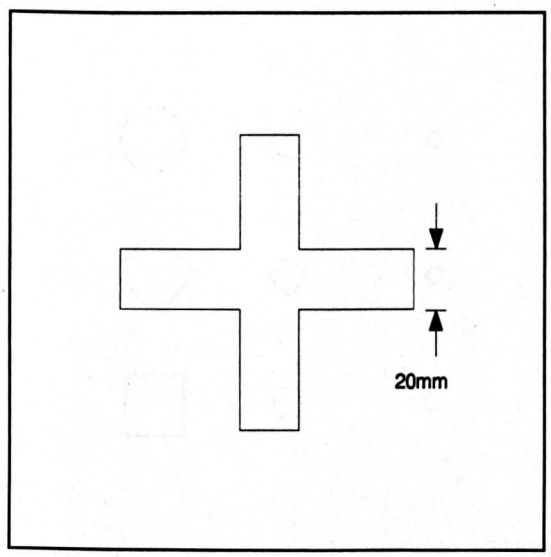

FIGURE 8.18 A *DEFECT* CREATED IN A 1 mm THICK ALUMINIUM PLATE BY REMOVING 50% OF THE MATERIAL THICKNESS IN A CROSS SHAPED AREA

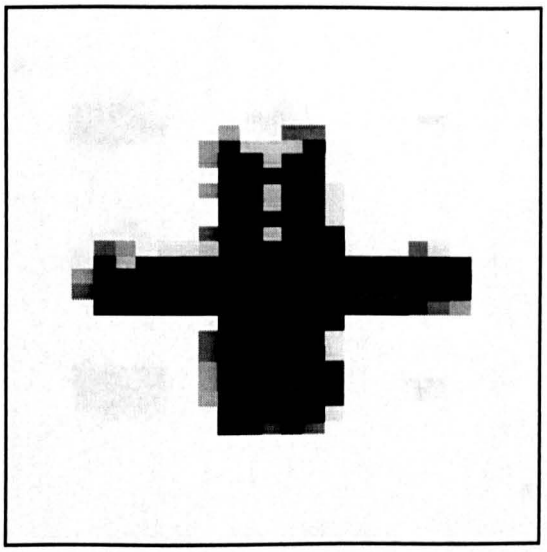

FIGURE 8.19 LAMB WAVE IMAGE OF THE CROSS SHAPED *DEFECT*

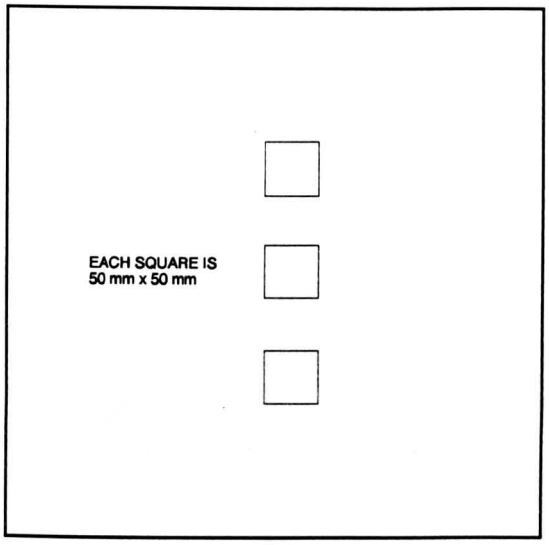

FIGURE 8.20 *DEFECTS* CREATED IN A 1 mm THICK ALUMINIUM PLATE BY REMOVING 50% OF THE MATERIAL THICKNESS IN 3 SQUARE SHAPED AREAS

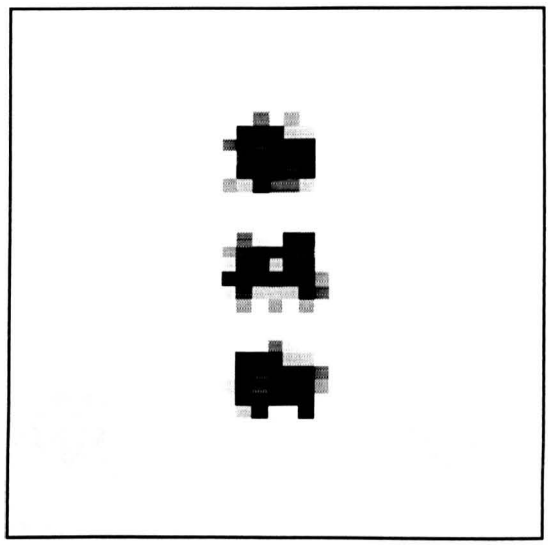

FIGURE 8.21 LAMB WAVE IMAGE OF THE 3 SQUARE SHAPED *DEFECTS*

shaped *defect*. This is due to the fact that the signal amplitude goes from high to low when either the transmitting transducer or the receiving transducer is placed over the *defect*. Figure 8.20 illustrates a test sample consisting of an aluminium plate with three square *defects* introduced into it. The corresponding Lamb wave image of Figure 8.21 illustrates the ability of the system to resolve these individual *defects*. The last two examples in this Section illustrate the ability of the Lamb wave scanner to produce images of defects in *difficult* materials. Figure 8.22 is a drawing of a 3 mm thick carbon fibre test sample supplied by British Aerospace (Warton). This test sample

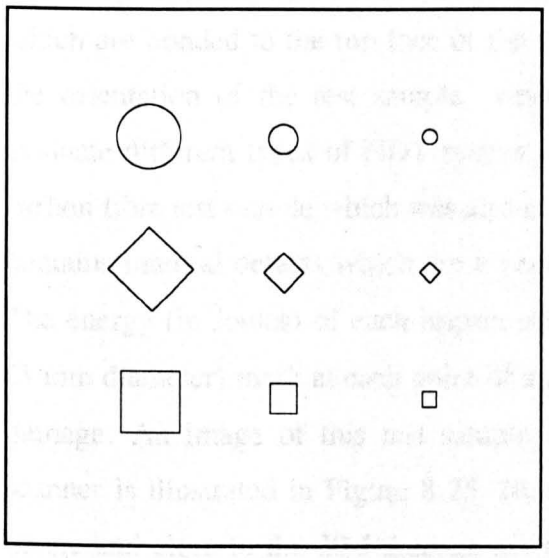

FIGURE 8.22 A 3 mm THICK CARBON FIBRE PLATE WITH DELAMINATIONS OF VARIOUS SHAPES AND SIZES. THE LARGEST SQUARE IS 24 mm WIDE

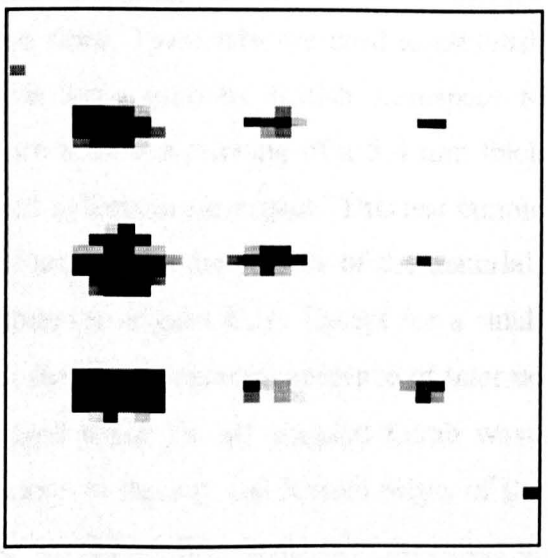

FIGURE 8.23 LAMB WAVE IMAGE OF A CARBON FIBRE PLATE CONTAINING A RANGE OF DELAMINATIONS OF DIFFERENT SHAPES AND SIZES

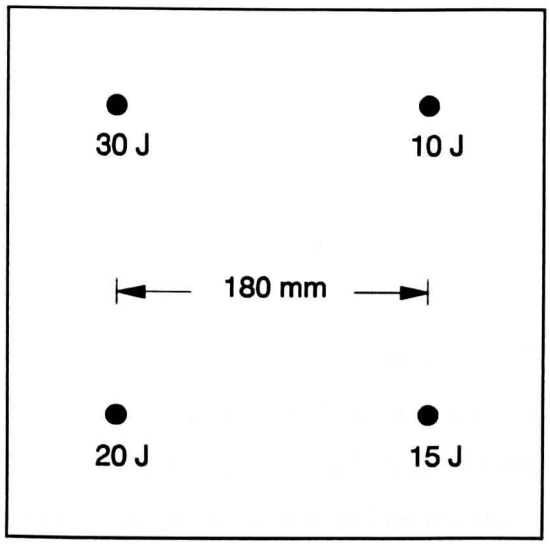

FIGURE 8.24 A 5.4 mm THICK CARBON FIBRE PLATE WITH IMPACT DAMAGE (30, 20, 15 AND 10 JOULES)

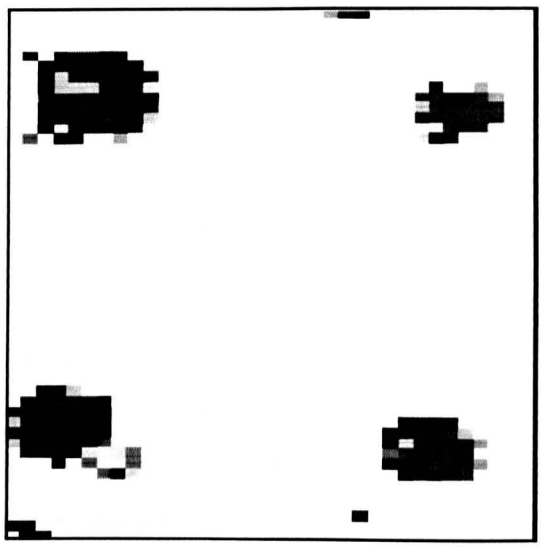

FIGURE 8.25 LAMB WAVE IMAGE OF AN IMPACT DAMAGED CARBON FIBRE PLATE

contains internal delaminations of various shapes and sizes and can be regarded as an ultrasonic *test-card* which can be used in a similar way to the type which is used for assessing optical imaging systems. There is no external evidence of the delaminations and they can only be located using an NDT (non-destructive testing) system. The largest circle is approximately 24 mm in diameter and the smallest one is approximately 6 mm in diameter. An image of this test sample obtained using the air coupled Lamb wave scanner is illustrated in Figure 8.23. From this it can be seen that all of the delaminations have been detected and imaged with striking contrast and clarity. The marks close to the top left and bottom right of the image are due to thin metal tabs which are bonded to the top face of the carbon fibre. These tabs are used to establish the orientation of the test sample when it is being used by British Aerospace to evaluate different types of NDT system. Figure 8.24 is a drawing of a 5.4 mm thick carbon fibre test sample which was also supplied by British Aerospace. This test sample contains internal defects which are a result of impacts on the surface of the material. The energy (in Joules) of each impact is indicated in Figure 8.24. Except for a small (3 mm diameter) mark at each point of impact there is no external evidence of internal damage. An image of this test sample obtained using the air coupled Lamb wave scanner is illustrated in Figure 8.25. Marks close to the top and bottom edges of the image and close to the 20 J damage are again caused by thin metal tabs cemented to the surface of the test sample.

8.6 System Limitations

8.6.1 Available Modes

In Chapter 2 of this Thesis it was shown that the air channel has a finite bandwidth which is determined by attenuation. For example, if the total length of the air channel is 10 mm then the channel bandwidth is 1.3 MHz. In order to ensure that attenuation would not be a significant loss factor in this work it was arranged that all of the air coupled systems would operate at a frequency of 580 kHz. As discussed in Section 7.4.1, the experimental work indicated that the a_0 mode is the only one that can be generated and detected over a wide range of frequency-thickness values. Other modes can be generated and detected in particular plates but it is not possible to track them across a range of thicknesses. So, with the air coupled systems which are described in this Thesis, the a_0 mode has been found to be the most useful. For the plate thicknesses of interest, the s_0 mode is also available but the theory indicates that this is of less value because, as illustrated by Figures 8.11 and 8,12, its relative out of plane displacement is considerably lower than for the a_0 mode.

8.6.2 Plate Thickness

From Figure 8.3 it can be seen that, for steel, use of the a_0 mode restricts the frequency-thickness product to approximately 3 MHzmm. For higher frequency-thickness values the Lamb wave degenerates into a Rayleigh wave which propagates along the surface of the test sample. With transducers which operate at 580 kHz, a frequency-thickness product of 3 MHzmm is equivalent to a plate thickness of 5.2 mm. For most materials of interest, use of the air coupled Lamb wave test system is restricted to applications where the plate thickness does not exceed approximately 5 mm. It is only possible to state approximate values because there is no definite point at which Lamb waves degenerate into Rayleigh waves. On inspection of Figure 8.3 it might be thought that, for the a_0 mode, there is no lower limit to the plate thickness that can

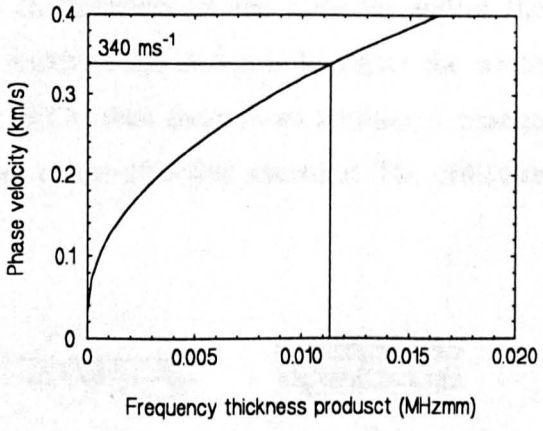

FIGURE 8.26 PHASE VELOCITY AS A FUNCTION OF FREQUENCY-THICKNESS PRODUCT IN ALUMINIUM

be measured with a particular frequency. However, the coincidence principle does set a lower limit. From Equation (8.94) it can be seen that it is not possible for the Lamb wave phase velocity to be lower than the velocity of sound in air. Figure 8.26 shows an example of how the lower limit of plate thickness can be found for an aluminium test sample. This phase velocity dispersion curve indicates that the lower limit of frequency thickness-product is 11.3 x 10^{-3} MHzmm. So, for a frequency of 580 kHz the minimum thickness of aluminium is 0.2 mm.

8.6.3 Defect Width and Length

Figure 8.27 illustrates how one line of a Lamb wave image is created. This diagram defines the length and the width of the *defect* with respect to the scan axis. Figure 8.28

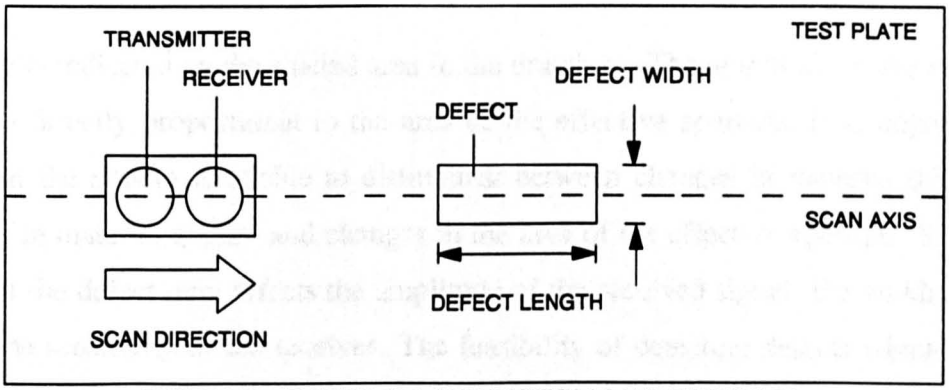

FIGURE 8.27 CREATION OF A SINGLE LINE IN A LAMB WAVE IMAGE

illustrates what happens when both the transmitting transducer and the receiving transducer are over the defect. If, as illustrated in Figure 8.28(A), the defect is at least as wide as the diameter of the transducers, then the signal amplitude changes by an amount which depends only on the change in thickness of the material and/or the change in material quality. However, if the width of the defect is less than the width of transducers, as in Figures 8.28(B) and 8.28(C), then there is an additional change in signal amplitude which depends on the area of the effective aperture. The effective

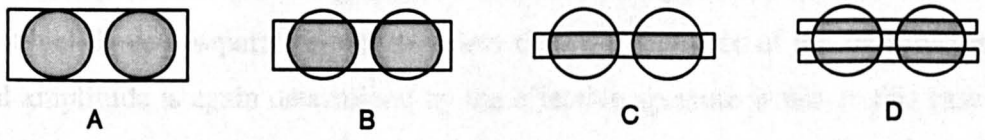

FIGURE 8.28 EFFECTIVE APERTURE OF THE SYSTEM

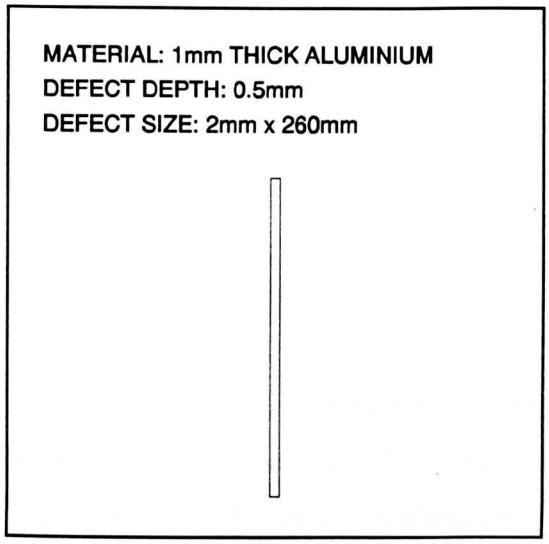

FIGURE 8.29 THE ALUMINIUM TEST PLATE USED TO TEST THE LIMITS OF DEFECT WIDTH

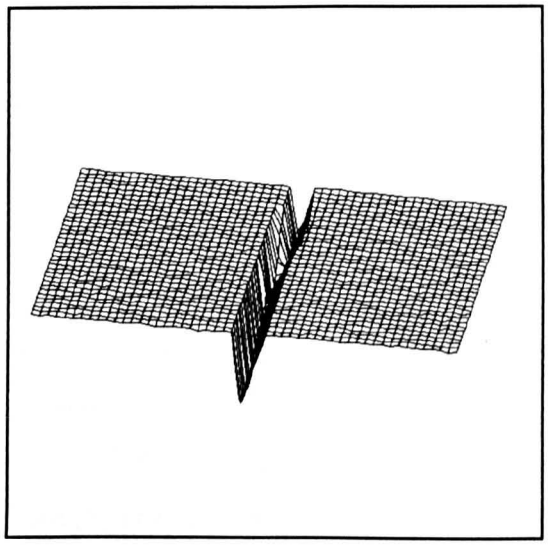

FIGURE 8.30 LAMB WAVE IMAGE OF A 1 mm THICK ALUMINIUM PLATE WITH A LONG THIN *DEFECT*

aperture is indicated by the shaded area in the drawings. The amplitude of the received signal is directly proportional to the area of the effective aperture. It is important to note that the system is unable to distinguish between changes in material thickness, changes in material quality and changes in the area of the effective aperture. Since the width of the defect only affects the amplitude of the received signal, the width limit is set by the sensitivity of the receiver. The feasibility of detecting defects which have a width which is significantly less than the diameter of the transducers was investigated experimentally using the test plate illustrated in Figure 8.29. This test sample consists of a 1 mm thick aluminium plate with a 2 mm wide, 260 mm long slot. As with the previous test plates, material was removed from the slot to a depth of 0.5 mm and it was scanned across its undamaged face. The result of the scan is illustrated in Figure 8.30 which is a 3D plot of relative signal amplitude. From Figure 8.30 it is clear that it would have been possible to further reduce the width of the slot. As previously discussed, the ultimate width limit depends only on system sensitivity. Although the width of slot that can be detected depends only on the system sensitivity, the resolution depends on the diameter of the transducers. This is illustrated by Figure 8.28(D). From this diagram it is clear that the system is unable to resolve two slots which have a separation which is less than the diameter of the transducers. The signal amplitude is again determined by the effective aperture which in this case is the sum of the four shaded areas. The preceding discussion of defect width also applies to

defect length, however, the situation becomes confused because of the creation of a double image. An explanation of how the double image is formed has been provided previously. Later it will be shown that this double image can be removed using relatively simple image processing techniques.

8.6.4 Transducer Dimensions

From the previous discussion it is clear that the limit of resolution can be improved by reducing the diameter of the transducers. One limit to how small the transducers can be made is set by the available signal to noise ratio (SNR). The prototype Lamb wave scanner uses 15 mm diameter transducers and can provide an SNR of 30 dB with most types of test sample. Based on SNR considerations only, it would be possible to reduce the transducer diameter to 7.5 mm which would allow the system to provide a 24 dB SNR. Without finding a way of further improving the SNR, it is not possible to consider making the transducers significantly smaller than this. Another limit is set by the coincidence principle which was discussed in Section 1.5.7 of this Thesis. From Figure 1.13 it can be seen that, in order to generate and detect a Lamb wave in a plate, it is necessary to arrange that the pressure distribution in the air outside the plate is coincident with the out of plane pressure distribution of the required mode inside the plate. An alternative representation of this situation is provided in Figure 8.31. From this diagram it can be seen that the coincidence principle will only produce the desired effect provided that the pressure distribution in air extends over a sufficiently long path. However, this method of generating Lamb waves will be effective even when the pressure distribution in air is less than one wavelength long (i.e. the wavelength of the

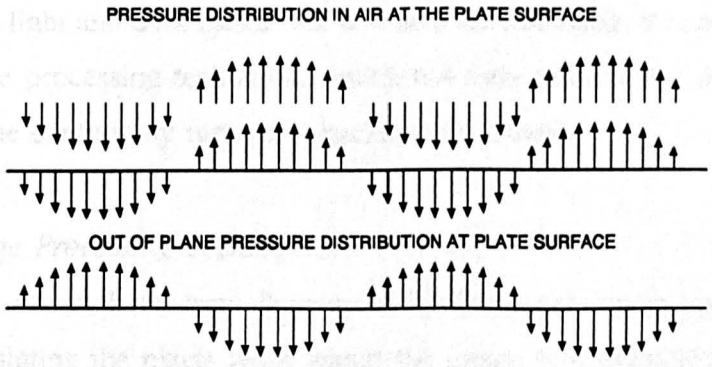

FIGURE 8.31 GENERATING AND DETECTING LAMB WAVES USING THE COINCIDENCE PRINCIPLE

Lamb wave). The method will only fail completely when the pressure distribution in air is effectively flat. For example, if the transducer diameter was so small that the pressure distribution in air was only one tenth of a wavelength (Lamb wave) long, then the surface of the plate would see a single pressure point which has a time varying amplitude. Obviously there is no definite lower limit of transducer diameter at which the coincidence principle becomes invalid. However, a good design target would be to say that the transducers should be at least one wave length (Lamb wave) in diameter. So, to generate and detect the a_0 mode in a 1 mm thick steel plate at a frequency of 580 kHz, the transducers should have a diameter of at least 3.5 mm. This figure is based on a Lamb wave phase velocity of 2 kms^{-1}.

8.6.5 Image Processing

Background

From the preceding analysis it is clear that, with improved air coupled transducers, it should be possible to design a non-contact Lamb wave scanner which is capable of 3.5 mm resolution in a direction perpendicular to the direction of scanning. However, in the scanning direction, the limit of resolution will be closer to 7 mm because of the double image problem. Sophisticated algorithms are available for correcting many types of image defects but most of these operate in the frequency domain and tend to be slow to implement [101]. During the course of this investigation a final year engineering student was tasked with investigating the possibility of using standard 2D deconvolution algorithms to improve the quality of the Lamb wave images [102]. It was found that, although deconvolution can sometimes provide an improvement in resolution, the image contrast is greatly reduced. Also, the method often introduced artifacts into the processed image which did not exist in the original. For example the processed image often contained light and dark bands. As will now be discussed, it is possible to devise dedicated image processing techniques which not only remove the double image but also improve the contrast by removing background clutter.

Dedicated Image Processing Techniques

The techniques which have been developed for the Lamb wave system operate by directly manipulating the pixels from which the image is constructed. They are very fast and could be implemented during scanning so that there is no requirement for later

processing of the data. The method of removing the double image is based on the observation that every point on the test sample is effectively scanned twice: once by the transmitting transducer and once by the receiving transducer. So, the final image consists of two identical images which are superimposed but shifted by an amount which is equivalent to the separation between the centres of the two transducers. Although this has obvious disadvantages, it also introduces a simple way of checking the image for pixel errors. For example, consider a test plate with one small circular defect which has a diameter which is smaller than the diameter of the transducers. This defect must produce two identical pixel distributions in the final image. If an isolated pixel appears in a Lamb wave image it can be immediately rejected as an error. One way of checking for errors is to multiply together the amplitudes of pixels which are separated by the equivalent of the transducer separation. This has the effect of emphasising genuine artifacts and de-emphasising artificial artifacts. One of the artificial artifacts that is removed is the secondary image. So, by scanning through the image one line at a time it is possible to use amplitude data from each pixel pair (separated by the equivalent of the transducer separation) to produce on new pixel. During the course of this investigation it was also found that interpolation dramatically improves the image resolution. Edge detection was also found to be useful. It is beyond the scope of this Thesis to investigate the absolute limits of the processing techniques which have been mentioned but their value can be judged from the following examples.

Figure 8.20 illustrates a 1 mm thick aluminium plate containing three 0.5 mm deep *defects* (the area of each is 50 x 50 mm). As illustrated in Figure 8.32, this plate was scanned to produce an image which consists of 35 rows and 52 columns. Only pixels close to the *defects* are shown. The data has been interpolated to produce an image which contains 373 x 409 pixels and the result is illustrated in Figure 8.33. Whereas the double image may not have been obvious in Figure 8.32, it is strikingly obvious in Figure 8.33. The quality of this image can then be further improved by using the previously described process to remove the double image. The result is illustrated in Figure 8.34. Figure 8.35 shows the result of performing edge detection. The effectiveness of applying these three simple image processing techniques can be judged by comparing Figure 8.35 with the test plate drawing (Figure 8.20). Results for other test plates are displayed in Figures 8.36 to 8.43.

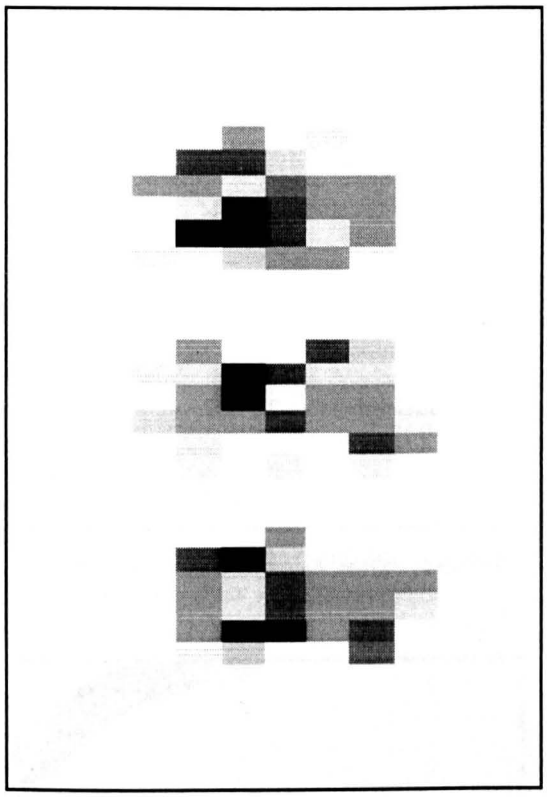

FIGURE 8.32 PART OF ORIGINAL LAMB WAVE IMAGE OF 3 SQUARE *DEFECTS* IN AN ALUMINIUM PLATE (35 x 52 PIXELS IN FULL IMAGE)

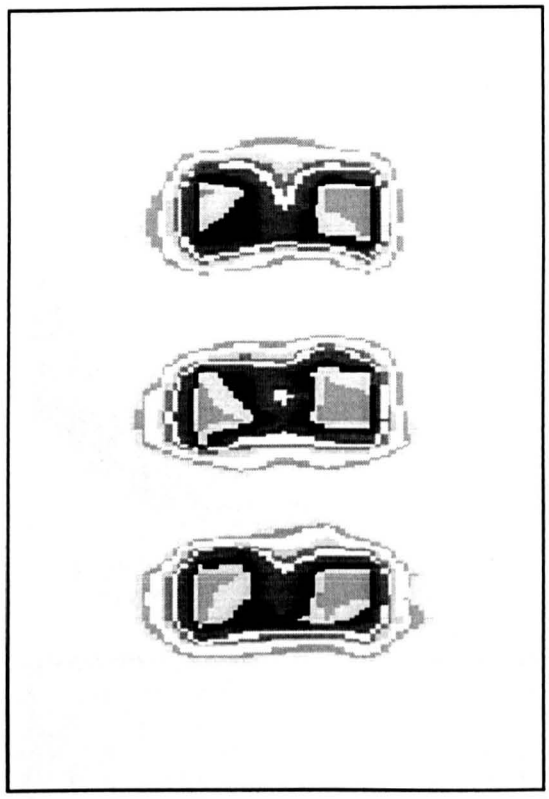

FIGURE 8.33 PART OF INTERPOLATED LAMB WAVE IMAGE OF 3 SQUARE DEFECTS IN AN ALUMINIUM PLATE (273 x 409 PIXELS IN FULL IMAGE)

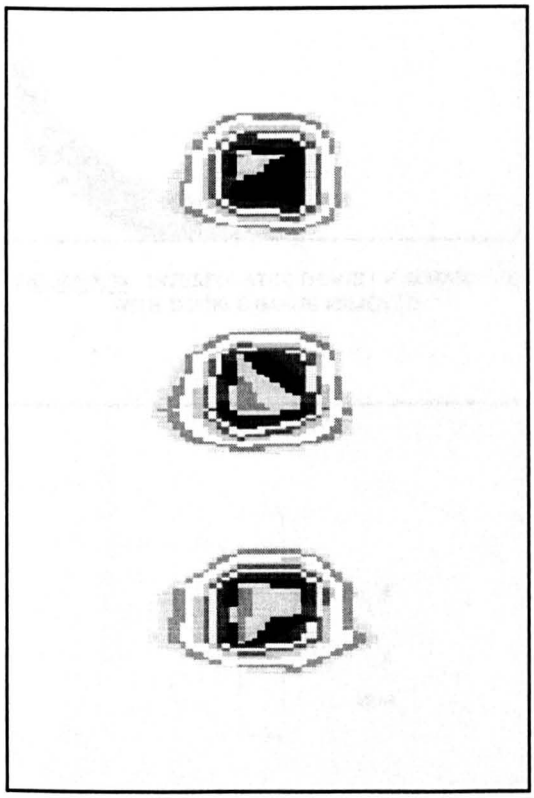

FIGURE 8.34 VERSION WITH DOUBLE IMAGE REMOVE

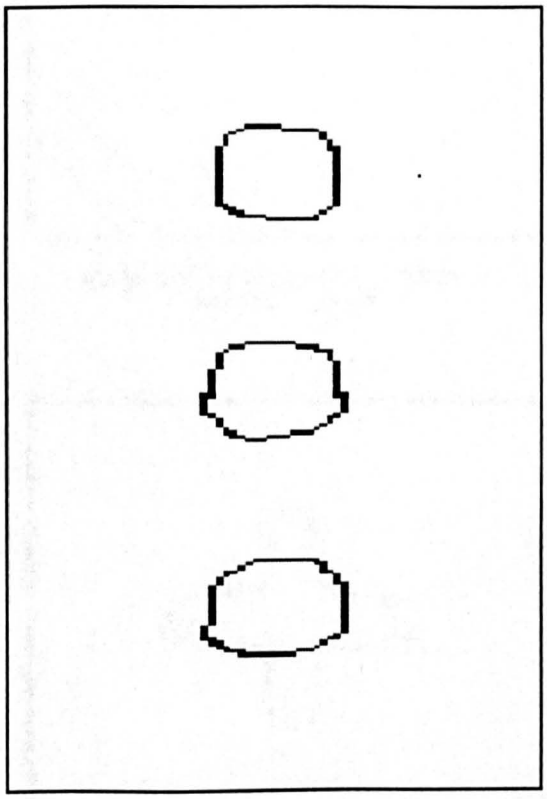

FIGURE 8.35 EDGE DETECTED VERSION OF IMAGE

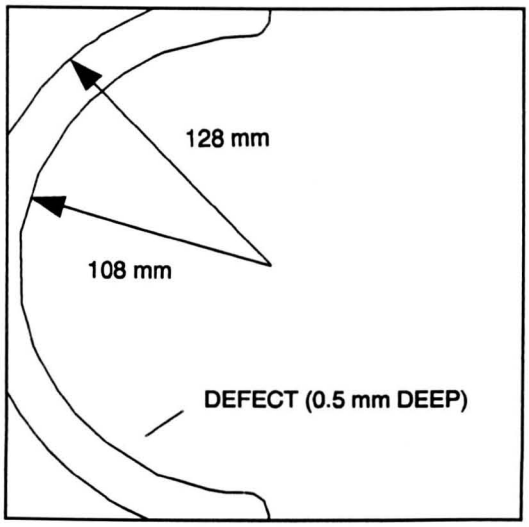

FIGURE 8.36 A SEMICIRCULAR *DEFECT* CREATED IN A 1 mm THICK ALUMINIUM PLATE

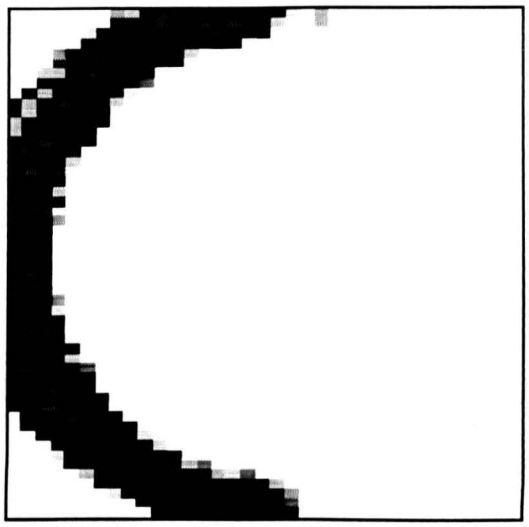

FIGURE 8.37 ORIGINAL LAMB WAVE IMAGE OF SEMICIRCLE (35 x 52 PIXELS IN FULL IMAGE)

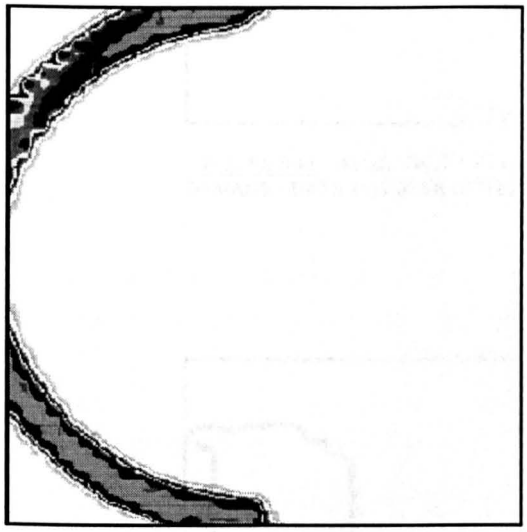

FIGURE 8.38 INTERPOLATED IMAGE OF SEMICIRCLE WITH DOUBLE IMAGE REMOVED

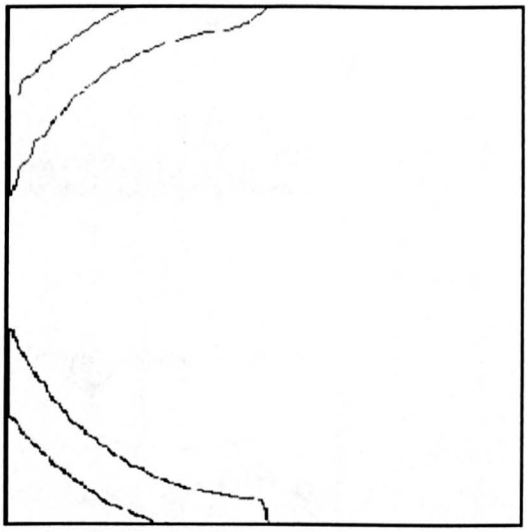

FIGURE 8.39 EDGE DETECTED VERSION OF SEMICIRCLE IMAGE

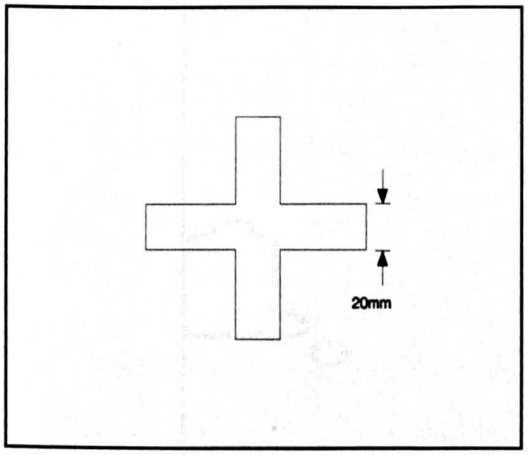

FIGURE 8.40 A CROSS SHAPED *DEFECT* IN A 1 mm THICK ALUMINIUM PLATE

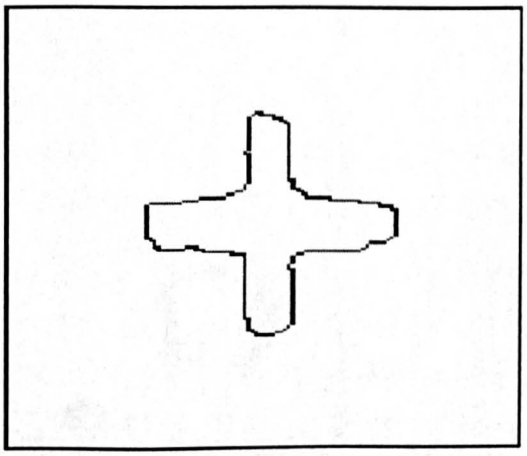

FIGURE 8.41 FULLY PROCESSED IMAGE OF THE CROSS SHAPED *DEFECT*

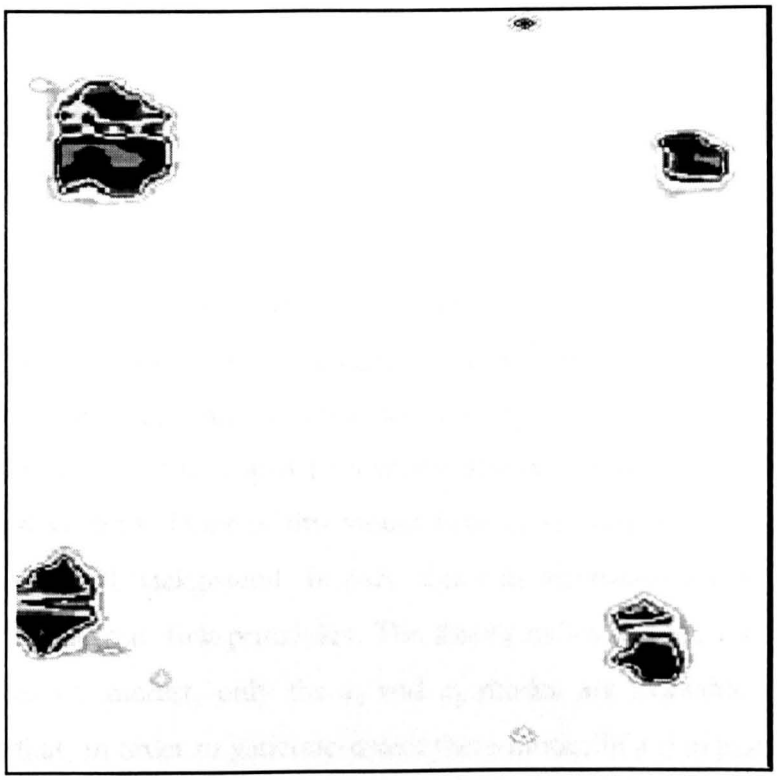

FIGURE 8.42 IMAGE OF A 5.4 mm THICK CARBON FIBRE PLATE WITH IMPACT DAMAGE - DATA HAS BEEN INTERPOLATED AND THE DOUBLE IMAGE REMOVED

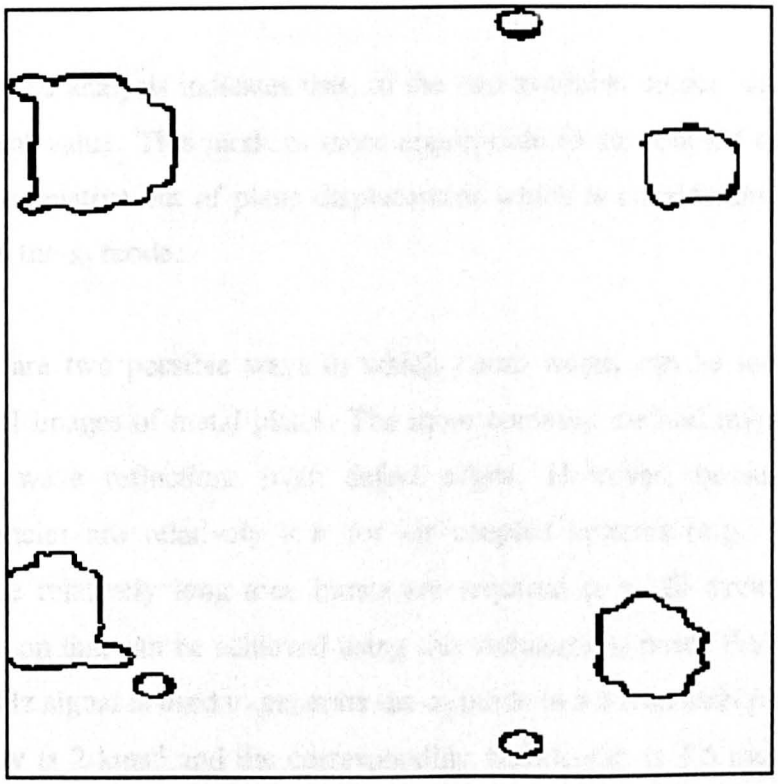

FIGURE 8.43 IMPACT DAMAGE IN CARBON FIBRE - DATA HAS BEEN INTERPOLATED, THE DOUBLE IMAGE REMOVED AND EDGE DETECTION APPLIED

8.7 Conclusions

8.7.1 The Goal

During the feasibility study it became evident that both Lamb wave inspection and through transmission inspection can be implemented with a high degree of effectiveness using the new air coupled technology. The goal of the work which is described in this Chapter was the design, construction and evaluation of a prototype Lamb wave test system. This system was to use air coupled piezoelectric transducers and was to be based on the new receiver which is described in Chapter 7. Importantly, development of the prototype system has helped to identify design criteria for future air coupled Lamb wave test systems. None of this would have been possible without establishing a thorough theoretical background. In part, this was achieved by deriving all of the necessary equations from first principles. The theory indicates that, for the frequency-thickness values of interest, only the s_0 and a_0 modes are available. An important observation is that, in order to generate/detect these modes in a thin plate using angled air coupled transducers it is necessary to achieve an angular tolerance of about 0.5°.

8.7.2 Summary of Achievements

The principal achievements are as follows:

- A detailed analysis indicates that, of the two available modes, only the a_0 is of practical value. This mode is more appropriate to air coupled testing because it has a relative out of plane displacement which is considerably greater than that of the s_0 mode.

- There are two possible ways in which Lamb waves can be used to produce internal images of metal plates. The more common method involves detecting Lamb wave reflections from defect edges. However, because the signal frequencies are relatively low for air coupled systems (e.g. 580 kHz) and because relatively long tone bursts are required (e.g. 20 cycles), the image resolution that can be achieved using this technique is poor. For example, if a 580 kHz signal is used to generate the a_0 mode in a 1 mm steel plate, the phase velocity is 2 kms^{-1} and the corresponding wavelength is 3.5 mm. This means that a 20 cycle tone burst will extend over a distance of 70 mm.

- The 70 mm image resolution which is possible with the edge reflection technique is of very limited value for producing images of defects in thin plates (e.g less than 5 mm thick). In this Chapter it has been shown that a better approach is to employ a technique which involves measuring the ability of a plate to support a particular mode. Image resolution then depends on the diameter of the transducers.

- The images which have been described in this Chapter were produced using 15 mm transducers. No transducer matching layers were required.

- It has been shown that it will be possible to reduce the diameter of the transducers to 7.5 mm while continuing to maintain a useful signal to noise ratio.

- By, for example, applying matching layers it will be possible to make a further reduction in transducer diameter, however, another limit is set by the coincidence principle. If it is assumed that the transducer diameter should not be less than one wavelength, then the limit for a 580 kHz signal is 3.5 mm. In this analysis it has been assumed that, for such small diameters, beam divergence will not be excessive in the near field. This assumption is supported by beam profile measurements which have been made by other members of the Ultrasonics Research Group at Strathclyde. Beam divergence would be excessive in the far field.

- It has been shown that, by using 15 mm diameter air coupled transducers, it is possible to produce *real-time* (no signal averaging or processing) images of many different types of defect. Images of artificial defects in aluminium show excellent contrast and a level of image resolution which is better than might be expected. Both delaminations and impact damage in carbon fibre have been detected and imaged. Although not discussed in this Thesis, the Lamb wave system has been used with many other metals other then aluminium and steel. It has also been used with glass, plastics and laminates.

- It has been shown that the width of defect that can be detected is limited only by the available signal to noise ratio. A long thin slot (2 mm wide) in a 1 mm thick plate can be detected without difficulty. As previously discussed, the ability of the system to resolve separate defects is limited by the diameter of the transducers.

- Image resolution along the direction of scanning is limited by the formation of a double image. It has been shown that this double image can be removed by using a relatively simple image processing technique. The quality of the Lamb wave images can be improved very significantly by interpolating the data. Edge detection has also been implemented.

Chapter 9

High Pressure Study

9.1 Introduction

9.1.1 Background

This Chapter illustrates that, even before the original EPSRC funded project had ended, the potential of the air coupled work had been recognised by industry. As has now been mentioned several times, the original aim of this PhD research was to investigate how ultra low noise techniques could be used to allow the liquid coupling used in conventional ultrasonic testing systems to be replaced with air at normal pressure. An additional aim was to investigate the improvements in air coupled sensitivity that could be achieved using special piezocomposite transducers developed at Strathclyde University. Some of the research findings were published [1,2,3,4] at an early stage in the work and as a consequence a number of commercial organisations expressed interest. Among these organisations was the British Gas On Line Inspection Centre (Cramlington) who funded most of the research which is described in this Chapter. British Gas currently use a *magnetic flux leakage (MFL)* technique for the inspection of gas pipe lines which are used to transport large volumes of gas over long distances. It is not clear why British Gas would wish to switch to using gas coupled ultrasonic techniques but it is known that the MFL technique is only suitable for use with metal pipes. However, their interest has made it possible to assess the performance of the low noise receiver and the piezocomposite transducers in a high pressure environment.

9.1.2 Available Techniques

As with the research which was conducted at atmospheric pressure, the basic techniques which are available at higher pressures are pulse-echo, through transmission and pitch-catch. However, a basic British Gas requirement was that the University should only investigate techniques which would be suitable for the automated inspection of pressurised pipes from a platform (PIG) which is propelled along the inside of a pipe. Because through transmission techniques would be of no value under these conditions they were not investigated during this study. A particularly exciting feature of this part of the PhD research programme is the pulse-echo work. Here, it has been possible to show that, by using a single piezocomposite transducer, it is possible to perform limited pulse-echo testing in a high pressure environment. As will become evident, the work which is described in this Chapter would not have been possible without the preliminary work which is described in the preceding Chapters.

9.1.3 Project Organisation

It should be noted that this investigation was conducted on a part time basis over a period of less than three months. During this time it was necessary to attend planning meetings with representatives from British Gas, install the necessary equipment at Strathclyde and rapidly perform a series of agreed experiments. In order to conduct a more thorough investigation it would have been desirable to have had access to the necessary equipment for a much longer period of time. It would then have been possible to **(a)** devise better experiments than the ones which are described here, **(b)** spend more time on each experiment, **(c)** refine the experiments and **(d)** repeat the experiments where necessary. Unfortunately, there was insufficient time and funding to allow for any of this. However, just before writing this Chapter the author of this Thesis reviewed the principal findings of the study at a formal British Gas presentation. All of the indications suggest that the work will go further.

9.1.4 Project Goals

The principal aims of the high pressure study were as follows:

- To investigate fundamentally ultrasonic wave propagation in the gaseous environment over a range of pressures and hence determine operational and design limitations for practical inspection.
- To investigate the performance of different ultrasonic transducers in a pressurised air coupled environment, using available laboratory apparatus.
- To evaluate the feasibility of normal incidence, shear and Lamb wave inspection methods for a range of pressures, test materials and surface finish.
- To provide recommendations for a more detailed research programme.

9.2 Special Equipment

All of the high pressure experiments described in this PhD Thesis were conducted in a nitrogen environment using a pressure vessel which was provided by British Gas PLC (Pipeline Integrity International, Cramlington). A schematic representation of the basic experimental configuration is illustrated in Figure 9.1. Installation and operation of the pressure vessel are discussed in the original report [103].

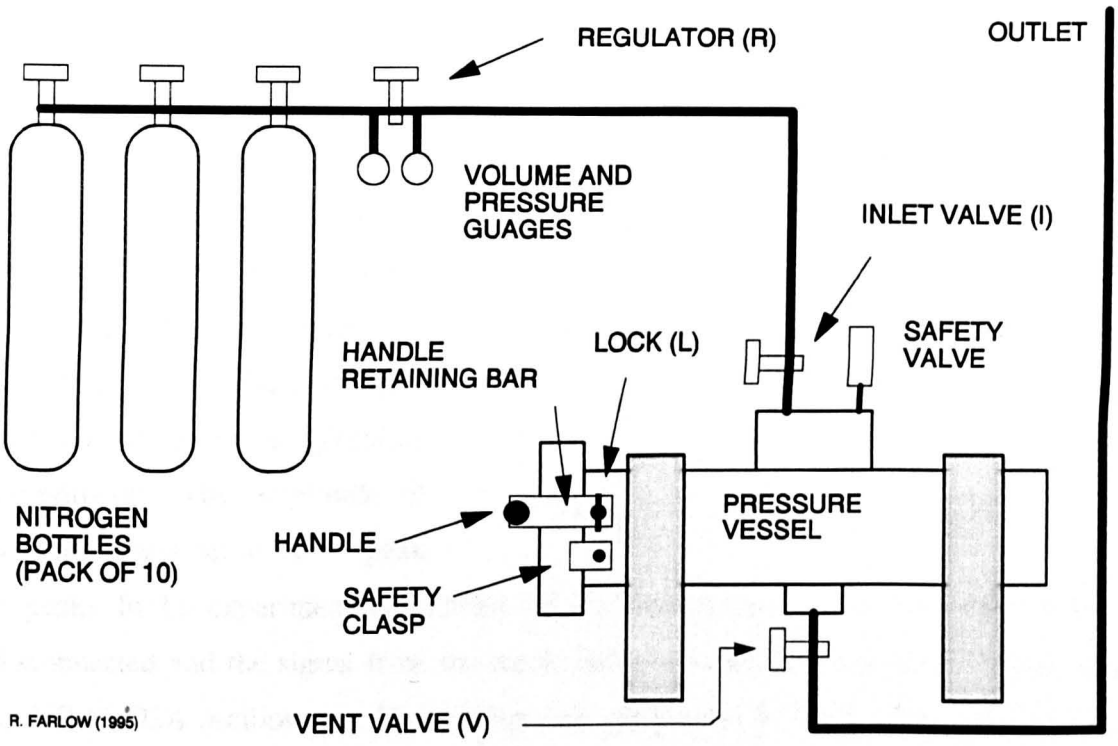

FIGURE 9.1 BASIC EXPERIMENTAL CONFIGURATION FOR THE HIGH PRESSURE WORK

9.3 Initial Experiments

The main aim of the first experiments was to allow familiarisation with the equipment, however, they are significant and were found to be useful during the later stages of the project. These experiments with the pressure vessel were conducted using the same pair of 30 mm diameter piezocomposite transducers as were used in the original air coupled experiments [1]. Both ultrasonic transducers have a ceramic volume fraction of 20% and operate at a matched frequency of 560 kHz.

9.3.1 Efficiency as a Function of Pressure with Low Transmitter Power

An experiment was devised to investigate the efficiency of through air transmission as a function of pressure. As illustrated in Figure 9.2, the previously mentioned transducers were clamped face to face on a wooden base with the separation between them fixed at 100 mm. By removing screws which normally hold the lid to the body of each housing it was arranged that there was a small air gap which would allow fast equalisation of the pressure inside each housing as the external pressure was altered. In this first experiment the transmitting transducer was driven directly from an

HP 33120A function generator (no power amplifier) which was adjusted to provide 10 cycle tone bursts (560 kHz) at a repetition frequency of 100 Hz. Except for the fact that no power amplifier was used, the arrangement was the same as that which was used in many of the *normal pressure* experiments. The amplitude of the signal was set at 10 V (peak to peak). In this experiment the internal pre-amplifier in the receiver package was also disconnected and the signal from the receiving transducer was monitored directly on an HP 65402A oscilloscope. The oscilloscope input impedance was set at 50 Ω.

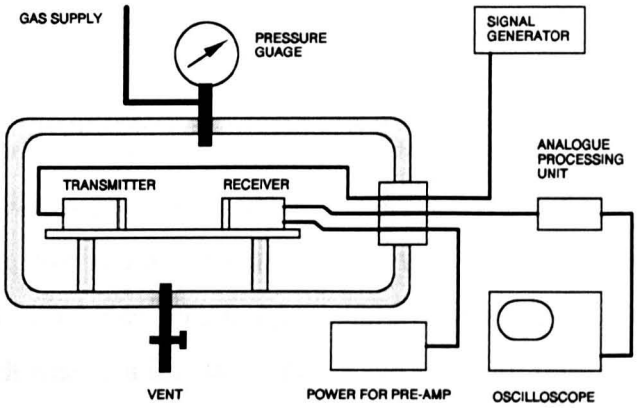

FIGURE 9.2 SCHEMATIC REPRESENTATION OF FIRST AND SECOND EXPERIMENTS

Results

The results of the first experiment were as follows. It was found that, at normal atmospheric pressure (1 bar) and with no signal averaging used on the oscilloscope, it was not possible to detect a signal at the receiver. The pressure in the vessel was then gradually increased. At a point well before the pressure reached the 10 bar mark on the gauge it became possible to detect signals at the receiver. It is not possible to be more precise than this because the pressure gauge supplied with the vessel was not suitable for making accurate measurements at pressures below 10 bar. At pressures of 10 bar and above the amplitude of the received signal was measured as a function of the pressure in the vessel. The results of this experiment are illustrated in Figure 9.3. The following observations were made during the course of this experiment.

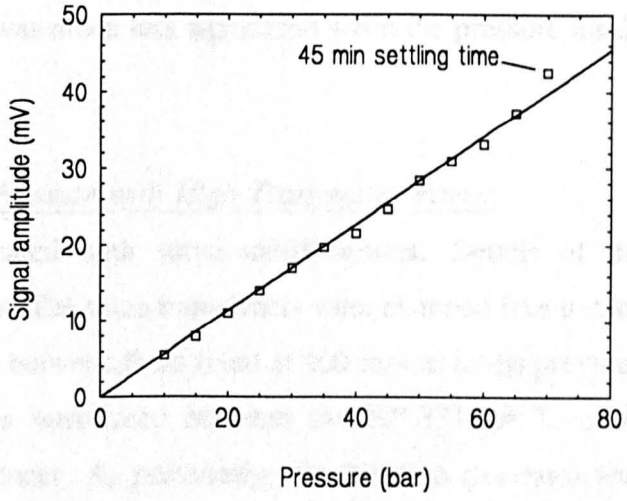

FIGURE 9.3 THROUGH AIR TRANSMIT-RECEIVE EFFICIENCY AS A FUNCTION OF PRESSURE

During periods when gas was being introduced or removed from the vessel the velocity of the sound waves travelling between the transmitter and the receiver changed significantly. This large change in velocity was due to a rapid change in the temperature of the gas. For a period of up to 10 minutes the velocity of the sound waves was observed to drift back towards its original value. During pressurisation the velocity stabilised at a value which was slightly higher than it was perviously and during depressurisation it stabilised at a value which was slightly lower than it was previously. The final velocity in each case is a function only of the pressure inside the vessel. The importance of leaving a sufficient settling time between measurements was not fully appreciated until towards the end of this experiment. Most of the readings were taken after leaving the vessel to settle for only a few minutes. The reading at 65 bar was taken after leaving the vessel to settle for a longer but unmeasured period and the reading at 70 bar was taken after leaving the vessel to settle for 45 minutes.

At low internal pressures it was not possible to observe the received signal while gas was entering or leaving the vessel. This was due to acoustic noise and disturbance of the gas inside the vessel. This effect was much less significant when the pressure inside the vessel was high.

9.3.2 *Efficiency as a Function of Pressure with High Transmitter Power*

The previous experiment was repeated with some modifications. Details of the experimental procedure are as follows. The same transducers were clamped face to face on a wooden base with the separation between them fixed at 100 mm as in the previous experiment. A power amplifier was introduced between the HP 33120A function generator and the transmitting transducer. As previously, the function generator was adjusted to provide 10 cycle tone bursts (560 kHz) at a repetition frequency of 100 Hz. The amplitude of the signal was set at 400 mV (peak to peak). Again, the internal pre-amplifier in the receiver package was disconnected and the signal from the receiving transducer was monitored directly on an HP 65402A oscilloscope. This time the oscilloscope input impedance was set at 1 MΩ.

With the new arrangement it was possible to detect a signal at normal atmospheric pressure (1 bar). As the pressure in the vessel was gradually increased measurements

of both signal amplitude and velocity were made but this time the gas in the vessel was allowed to settle for exactly 10 minutes before taking each reading. However, it should be noted that a longer settling time would be required for truly accurate measurements. The circumstances discussed in the introduction forced a compromise. Signal amplitude as a function of pressure is illustrated in Figures 9.4 and a graph of sound velocity as a function of pressure is illustrated in Figure 9.5. In this second experiment the signal to noise ratio was greatly improved as a consequence of using the power amplifier. This made it easier to take accurate readings and it was noted that the signal was more stable during pressurisation and depressurisation. As mentioned previously, the pressure gauge supplied with the vessel was not suitable for making measurements below a pressure of 10 bar hence the readings of signal amplitude and time delay at a pressure of 5 bar can be disregarded. The reading at 70 bar was repeated after leaving the vessel standing for 1 hour. During this period there was no variation in signal amplitude or time delay. This would appear to indicate that the 10 minute settling time used in this experiment was sufficient to ensure adequate accuracy. Further confirmation of this would be required especially at lower pressures.

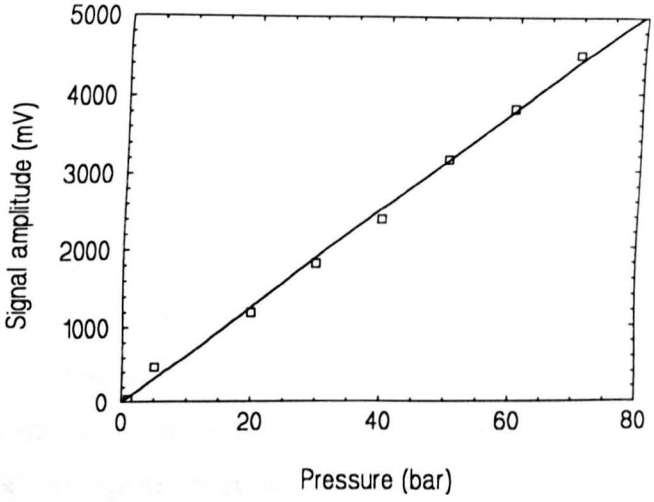

FIGURE 9.4 THROUGH AIR TRANSMIT-RECEIVE EFFICIENCY AS A FUNCTION OF PRESSURE

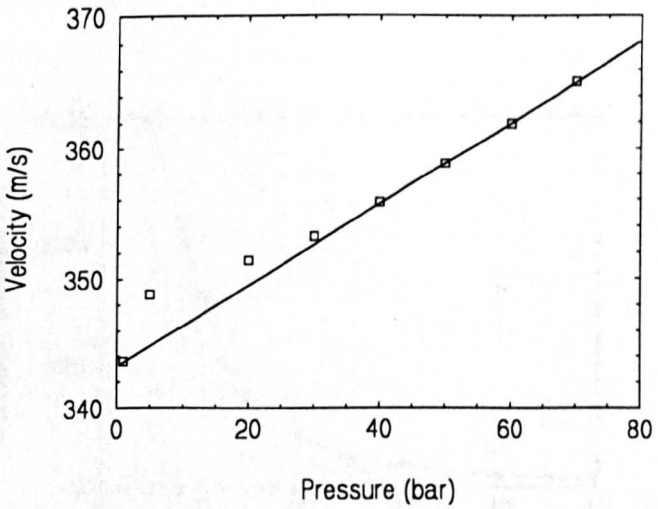

FIGURE 9.5 VELOCITY OF SOUND IN THE VESSEL AS A FUNCTION OF PRESSURE

9.3.3. *Initial Lamb Wave Experiment*

Details of an experiment involving the generation and detection of Lamb waves in a high pressure environment follow. In this experiment the equipment used was identical to that which was used in the original air coupled experiments [1]. The same transducers as were used in the previous two experiments were placed on a manipulator which allowed them to be set at the correct angle (9.9°) for generating and detecting the a_o Lamb wave mode in a 1 mm thick aluminum plate. As in the previous experiment a 55 dB power amplifier was used between the HP 33120A function generator and the transmitting transducer. Again, the function generator was adjusted to provide 10 cycle tone bursts (560 kHz) at a repetition frequency of 100 Hz. The amplitude of the signal was set at 400 mV (peak to peak). In this experiment the internal pre-amplifier in the receiver package was used to provide 60 dB of voltage gain and its output was monitored directly on an HP 65402A oscilloscope. With this arrangement it was possible to generate and detect Lamb waves (a_o mode) at normal atmospheric pressure (1 bar). As the pressure in the vessel was gradually increased the amplitude of the transmitter excitation was decreased in such a way that the output from the receiver pre-amplifier remained constant at 80 mV. This method was adopted because it was found that even a relatively small increase in pressure resulted in pre-amplifier saturation due to the improved coupling efficiency. A graph of transmitter signal amplitude as a function of pressure is provided in Figure 9.6.

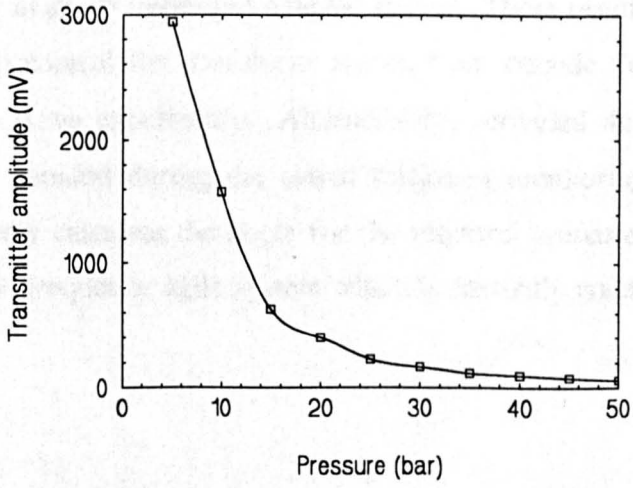

FIGURE 9.6 TRANSMITTER DRIVE VOLTAGE AS A FUNCTION OF PRESSURE (PRE-AMP OUTPUT MAINTAINED AT 80 mV)

The following observations were made during the course of this first Lamb wave experiment. For values of pressure between 1 bar and 15 bar there was a much more rapid increase in signal amplitude as a function of pressure compared to the previous two experiments. It is believed that this is because four solid/fluid interfaces are

involved compared to two solid/fluid interfaces in the previous experiments. For values of pressure above 15 bar the rate of increase in signal amplitude as a function of pressure slowed down rapidly. It is believed that this happens because there is a significant change in sound velocity. This can be confirmed by looking at Figure 9.5 from which it can be seen that between 1 bar and 70 bar the velocity of sound waves in the vessel changes by 21.5 m/s. As discussed previously, the angle of the transducers for a given Lamb wave mode is found using the coincidence principle:

$$\sin(\theta) = \frac{V_i}{V_p}$$

Here, V_i is the velocity of the incident sound wave in the external fluid and V_p is the phase velocity of the required Lamb wave mode. The phase velocity of the a_o mode in 1 mm thick aluminium is 2 km/s. From Figure 9.5 the velocity of sound in nitrogen at 1 bar is 344 m/s and from the above equation the angle of the transducers is 9.9°. At a pressure of 70 bar Figure 9.5 indicates that the velocity of sound is 365 m/s and from the above equation the correct angle for the transducers is 10.5°. This means that at 70 bar the transducer angles are set at an angle which is 0.6° less than the correct angle. This is a very significant error in an air (nitrogen) coupled system. These results indicate that it may be necessary to control the transducer angles from outside the pressure vessel in any future Lamb wave experiments. Alternatively, provided that extreme pressure variations can be avoided during the actual thickness monitoring phase, it may be possible to accurately calculate the angle for the required pressure. Another approach would be to use the frequency agile system which is currently under development at Strathclyde [7].

9.4 Detailed Experiments

At this stage in the project the pressure vessel had been successfully installed, commissioned and tested. A pair of 20% ceramic volume fraction piezoceramic composite transducers had been tested at pressures of up to 70 bar with no evidence of reduced performance, physical deterioration or damage to the devices. The low noise pre-amplifier and its associated electronic components had also been successfully tested to a pressure of 70 bar. Pressurisation times were found not to be restrictive and two or three pressurisations to 70 bar were possible from one bank of bottles. It was found

that accurate measurements require long settling times after each change in pressure. Each change in pressure also involves a change in temperature. In order to make more accurate measurements it would be necessary to monitor the internal temperature of the pressure vessel.

Before performing any further experiments the pressure gauge used in the early experiments was replaced with a more accurate one. This gauge was calibrated in pounds per square inch (psi) rather than bar. It had also been hoped to introduce a sensor into the vessel which would allow its internal temperature to be monitored, however, this was not possible within the time available.

The aim of the detailed experiments was to investigate methods of using ceramic-polymer composite transducers for thickness testing in a high pressure environment.

9.4.1. An Investigation of Pulse-Echo Techniques

At atmospheric pressure it would be difficult, if not impossible, to adopt pulse-echo ultrasonic testing without using liquid coupling between the transducer and the test-piece. As discussed in Chapter 2, the main problem with trying to use this technique is that the amplitude of the signal reflected from the front face of the test-piece is many orders of magnitude greater than the amplitude of signals resulting from any internal reflections. With air coupling at atmospheric pressure it is currently not possible to design a pre-amplifier and associated electronics which have sufficient dynamic range to allow detection of internal reflections which appear a short time after a large front face reflection. It was believed that this problem would become less significant as the gas pressure is increased and the aim of the next set of experiments was to investigate this possibility. In these experiments, unlike the previous ones, a conventional pulser receiver unit was used to generate and detect the signals. Details of this pulser receiver unit can be found in Appendix VII. Using this type of equipment involves driving the transmitting transducer with high voltage (~200 volts) impulses rather than the tone bursts used in all of the previous work. Also, the receiver noise voltage density is more than 4 times higher than with the amplifier used before and the electronic bandwidth is 35 MHz compared to 6 MHz for the pre-amplifier.

Experiments with a 400 kHz Transducer

The transducer used in the first pulse-echo experiment was a 400 kHz piezoceramic composite which has a mechanical matching layer (polymer) applied to its front face. A special test-piece was manufactured and this is illustrated in Figure 9.7. The internal

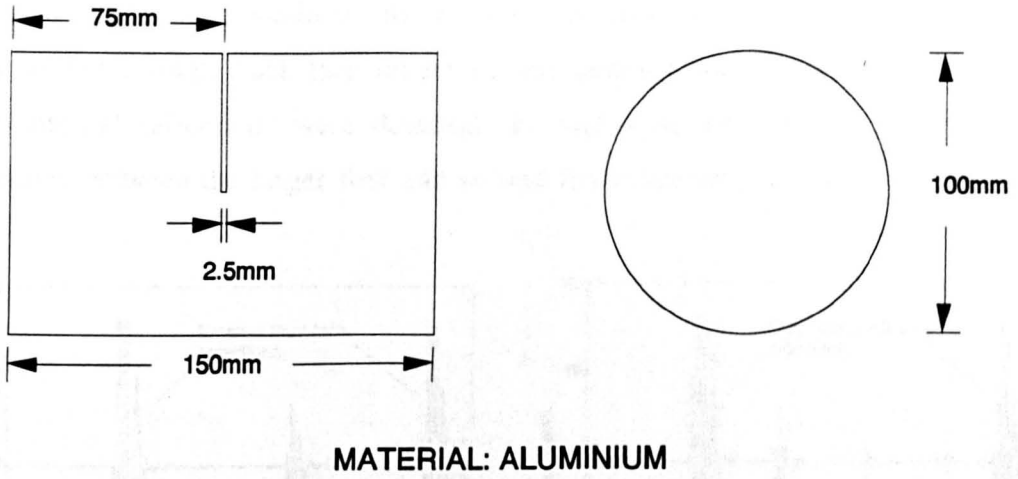

FIGURE 9.7 SPECIAL TEST-PIECE USED IN THE PULSE-ECHO EXPERIMENTS

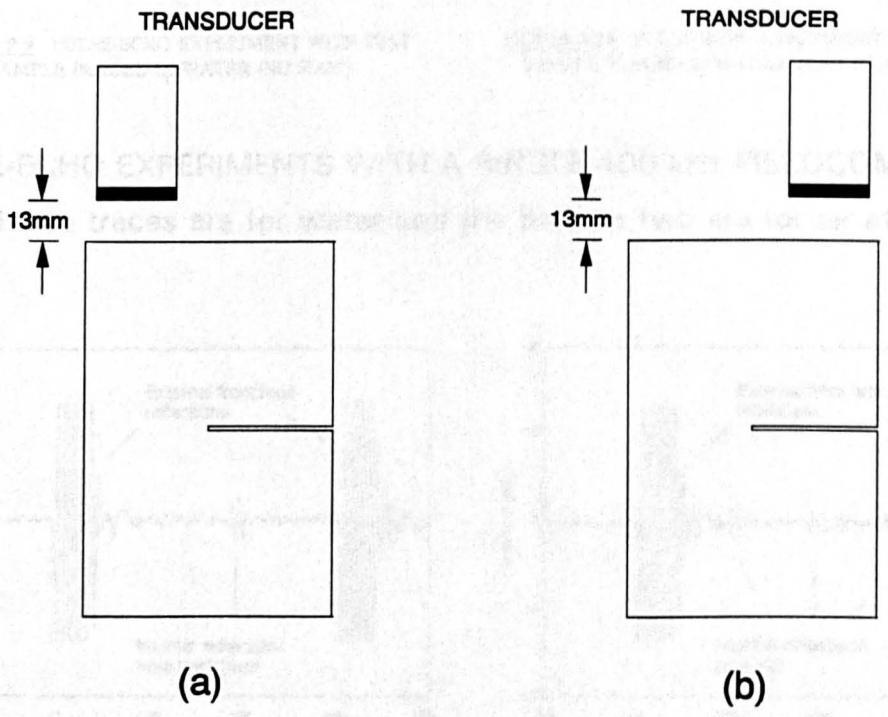

FIGURE 9.8 ARRANGEMENT FOR THE HIGH PRESSURE PULSE ECHO EXPERIMENTS

ultrasonic reflections from this test-piece were initially investigated by placing it in a water bath along with the 400 kHz piezocomposite transducer. As illustrated in Figure 9.8, it was possible to place the transducer above the test-piece so that it would detect either (a) ultrasonic reflections from the back face of the test-piece or (b) ultrasonic reflections from the slot. Results obtained with no slot are illustrated in Figure 9.9 and results obtained with the slot in position are illustrated in Figure 9.10. With no slot a single back face reflection was detected and with the slot in position three internal reflections were detected. In each case the internal reflections are positioned between the larger first and second front face reflections.

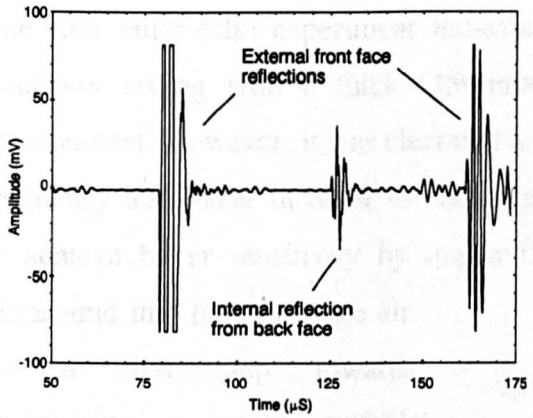

FIGURE 9.9 PULSE-ECHO EXPERIMENT WITH TEST SAMPLE PLACED IN WATER (NO SLOT)

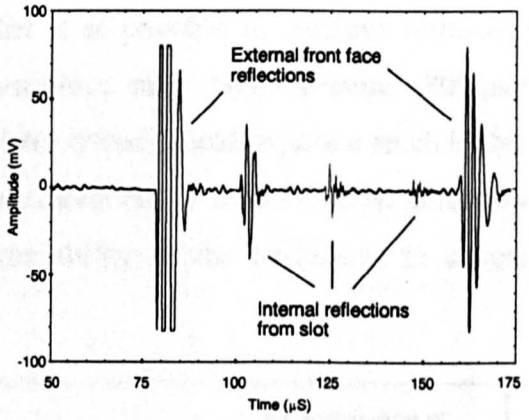

FIGURE 9.10 PULSE-ECHO EXPERIMENT WITH TEST SAMPLE PLACED IN WATER (SLOT IN POSITION)

PULSE-ECHO EXPERIMENTS WITH A SINGLE 400 kHz PIEZOCOMPOSITE

The top two traces are for water and the bottom two are for air at 800 psi.

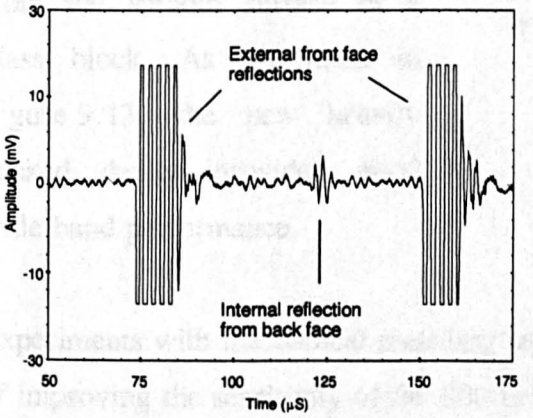

FIGURE 9.11 PULSE-ECHO EXPERIMENT WITH TEST SAMPLE PLACED IN PRESSURE VESSEL (NO SLOT)

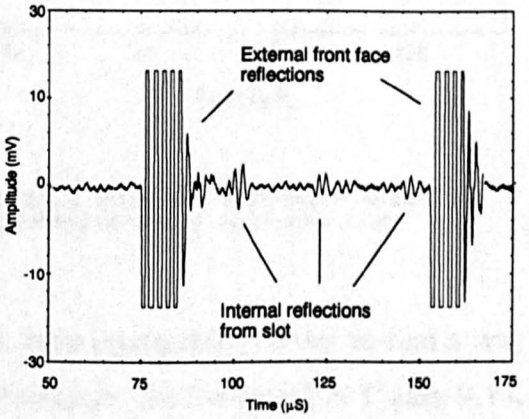

FIGURE 9.12 PULSE-ECHO EXPERIMENT WITH TEST SAMPLE PLACED IN VESSEL (SLOT IN POSITION)

The previous experiment was repeated without water coupling by placing the transducer and the special test-piece inside the pressure vessel. Results obtained at a pressure of 800 psi are illustrated in Figures 9.11 and 9.12. Figure 9.11 shows a single back face reflection obtained with no slot and Figure 9.12 shows three internal reflections obtained with the slot in position. In both cases the internal reflections appear in exactly the same positions as they do in the water coupled experiment. The significant difference between the water coupled results and the 800 psi air coupled results is the relative amplitudes of the internal and the external reflections.

Experiments with a 600 kHz Transducer

The first pulse-echo experiment indicated that it is possible to perform ultrasonic thickness testing with a thick (150 mm) test-piece in a high pressure (800 psi) environment. However, it was clear that a realistic system would require a much higher frequency transducer in order to obtain useful resolution. It would also be necessary to achieve better sensitivity by improving the ability of the transducer to couple ultrasound into high pressure air.

As a first step towards engineering a more suitable transducer, a 600 kHz device was designed and manufactured. The new device was evaluated in a simple experiment which involved monitoring ultrasonic reflections from the smooth surface of a glass block. As illustrated in Figure 9.13, the new heavily backed device provided good wide band performance.

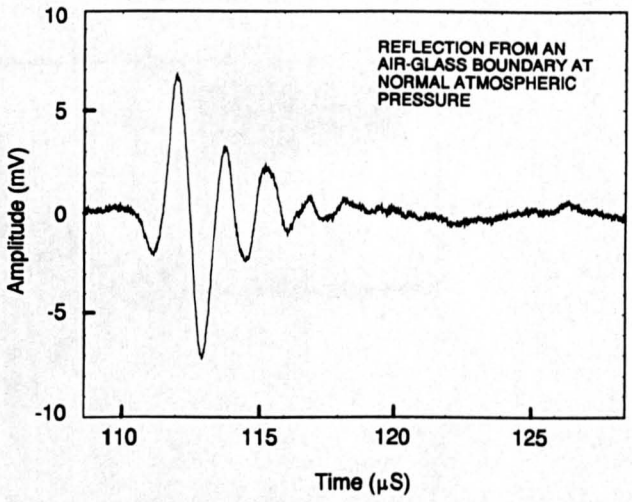

FIGURE 9.13 PULSE-ECHO RESPONSE OF 600 kHz TRANSDUCER WITH NO MATCHING LAYER

Experiments with mechanical matching layers were conducted in order to find a way of improving the sensitivity of the 600 kHz transducer. As illustrated in Figure 9.14, it was possible to obtain a very significant improvement in sensitivity by temporarily applying a membrane-filter matching layer to the front face of the 600 kHz transducer.

Encouraged by this result it was decided to permanently bond the matching layer to the front face of the transducer using a very thin layer of soft setting epoxy resin. As illustrated in Figure 9.15, this resulted in a further improvement in sensitivity, however, the device now features an unwanted resonance which limits its resolution.

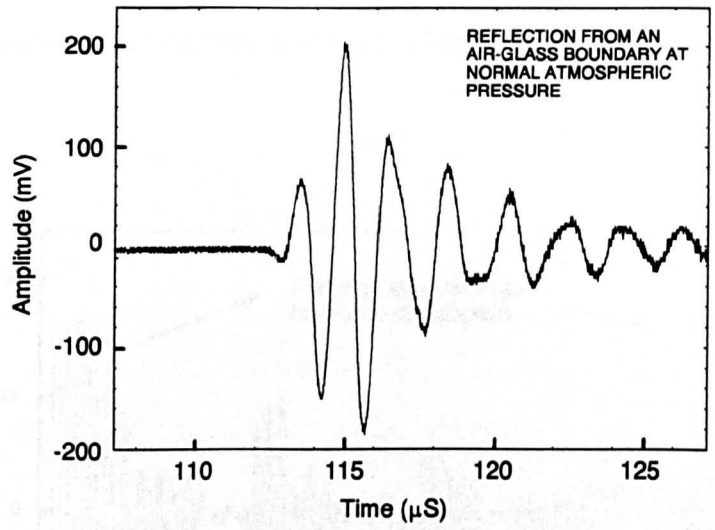

FIGURE 9.14 PULSE-ECHO RESPONSE OF 600 kHz TRANSDUCER WITH TEMPORARY MATCHING LAYER

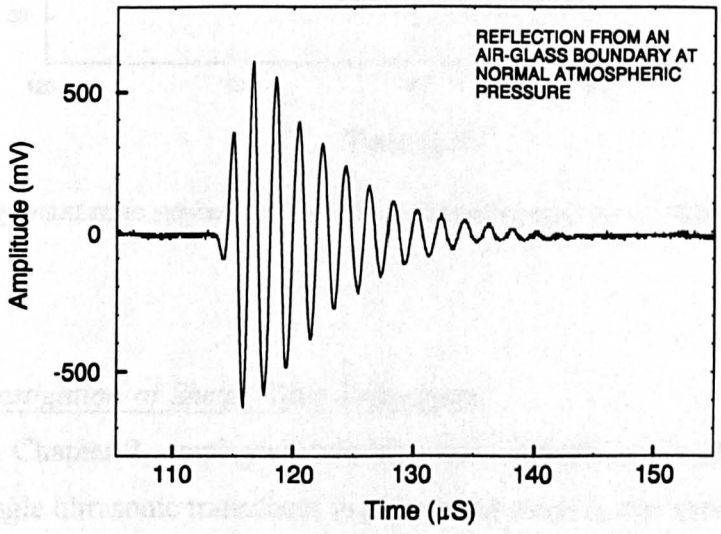

FIGURE 9.15 PULSE-ECHO RESPONSE OF 600 kHz TRANSDUCER WITH PERMANENT MATCHING LAYER

A significant result obtained with the 600 kHz transducer at 1000 psi is illustrated in Figures 9.16. This experiment was conducted in the pressure vessel using the test-piece illustrated in Figure 9.7 and using the configuration illustrated in Figure 9.8(b). Three

internal reflections form the slot are clearly visible but it should be noted that these are the second, third and fourth internal reflections with the first internal reflection being almost lost in the ringing produced by the first external reflection from the front face of the test-piece. Comparing this result with that of Figure 9.12 it can be seen that the new transducer provides considerably more sensitivity but, as a consequence of the effect described above, the resolution is poor. Clearly further transducer development is required.

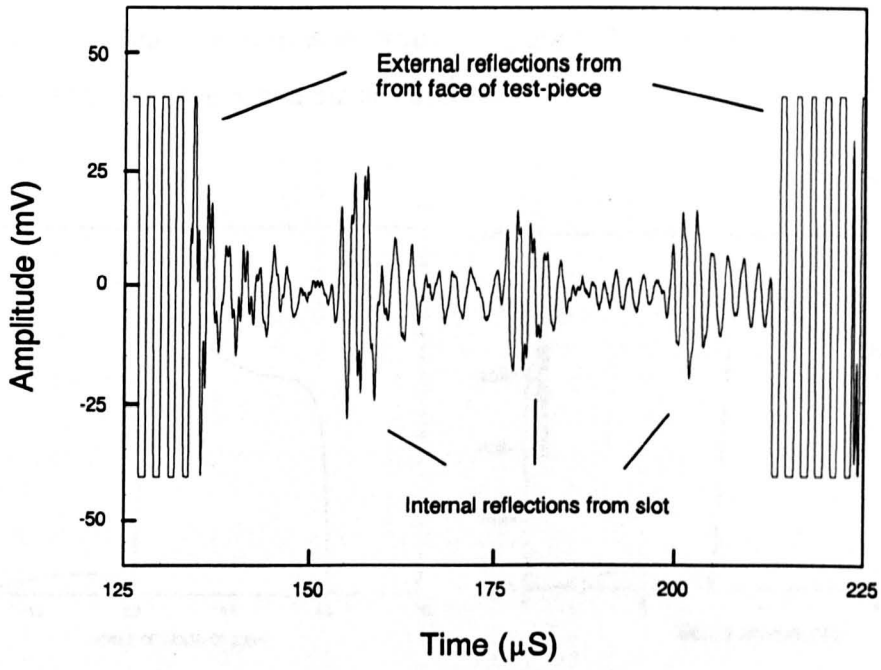

FIGURE 9.16 PULSE-ECHO EXPERIMENT WITH 600 kHz TRANSDUCER PLACED IN PRESSURE VESSEL

9.4.2. *An investigation of Shear Wave Techniques*

As discussed in Chapter 2, employing two ultrasonic transducers in pitch-catch mode rather than a single ultrasonic transducer in pulse-echo mode is one method of avoiding the dynamic range problems previously discussed. When a pressure wave is incident on a solid from a fluid at any angle other than at 90 degrees relative to the surface, mode conversion takes place and both longitudinal and shear waves are generated in the solid provided that it is sufficiently thick. By operating beyond the critical angle for longitudinal waves it is possible to generate shear waves alone and these can be used for thickness testing. The most suitable range of angles for a particular external

medium and a particular solid can be determined by plotting the echo transmission coefficient [1]. Figures 9.17 and 9.18 illustrate the echo transmission coefficient for air at atmospheric pressure and air at a pressure of 1000 psi. By plotting both curves together on the same graph, as in Figure 9.19, it can be seen that it should be possible to set the transducer angles at atmospheric pressure before conducting an experiment at 1000 psi. This was the approach adopted during the course of the shear wave investigation. Figure 9.19 also helps to show how the system sensitivity will be improved by operating at a higher than normal pressure, however, in a full analysis it would be necessary to take into account improvements in coupling efficiency at both the transmitter/air and air/receiver interfaces. Figure 9.20 shows the echo transmission coefficient curves for water and air at 1000 psi.

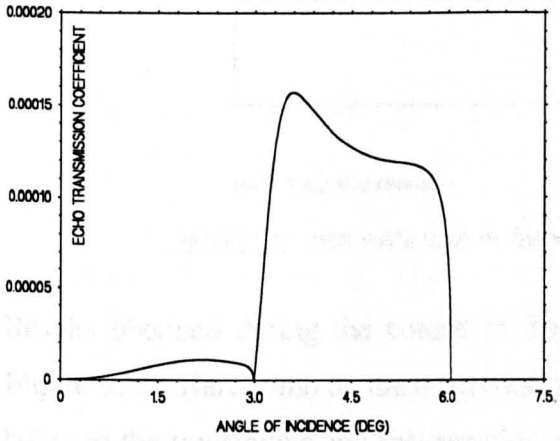

FIGURE 9.17 ECHO TRANSMISSION COEFFICIENT FOR AIR AT NORMAL PRESSURE

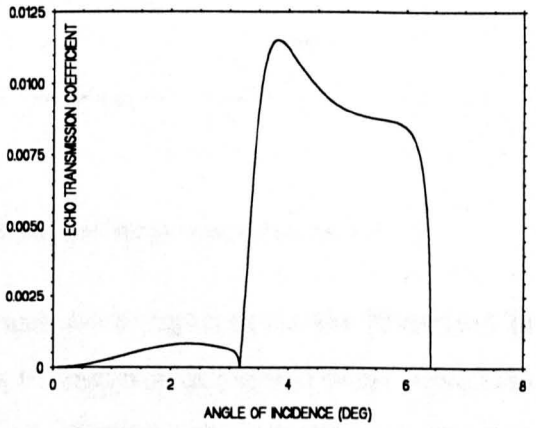

FIGURE 9.18 ECHO TRANSMISSION COEFFICIENT FOR AIR AT A PRESSURE 1000 PSI

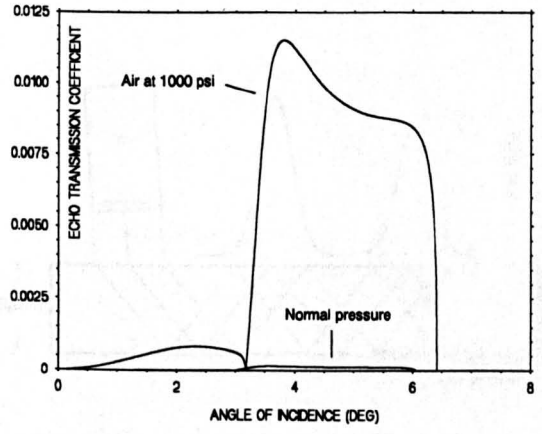

FIGURE 9.19 ECHO TRANSMISSION COEFFICIENT FOR AIR AT NORMAL PRESSURE AND 1000 PSI

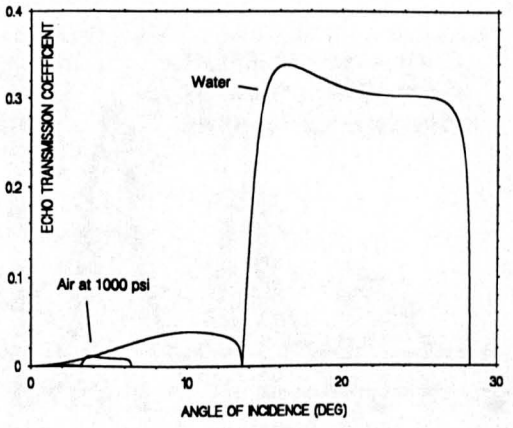

FIGURE 9.20 ECHO TRANSMISSION COEFFICIENT FOR WATER AND AIR AT A PRESSURE OF 1000 PSI

The shear wave experiments were conducted using the same pair of 30 mm diameter piezocomposite transducers as were used in the original air coupled experiments [1]. Both ultrasonic transducers have a ceramic volume fraction of 20% and operate at a matched frequency of 560 kHz. The transducers were set at the correct angles using data from Figure 9.19. The test-piece used in these experiments is illustrated in Figure 9.21. As illustrated in Figure 9.22 the transmitter was fixed in position at one end of the test-piece and the receiver was scanned across the surface in order to detect multiple internal shear wave reflections.

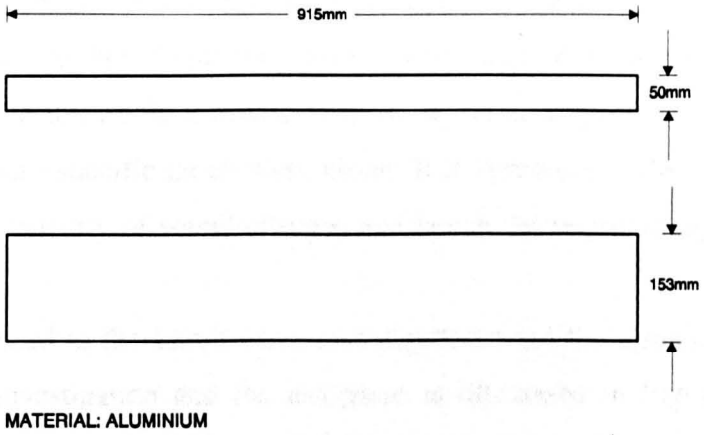

FIGURE 9.21 TEST-PIECE USED IN THE HIGH PRESSURE SHEAR WAVE EXPERIMENTS

Results obtained during the course of the shear wave experiments are illustrated in Figure 9.23. Here, time on the horizontal axis is directly proportional to the separation between the transmitter and the receiver. At each pressure three peaks corresponding to internal shear wave reflections are clearly visible. The distance between the peaks is directly proportional to the thickness of the test-piece.

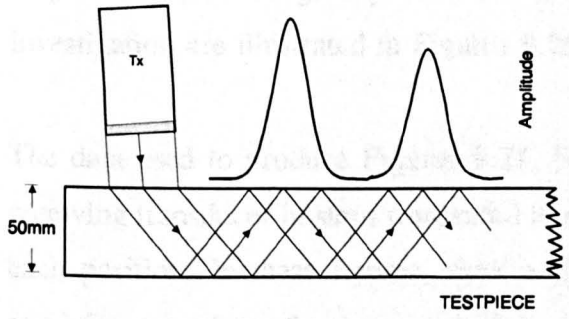

FIGURE 9.22 HIGH PRESSURE SHEAR WAVE EXPERIMENT

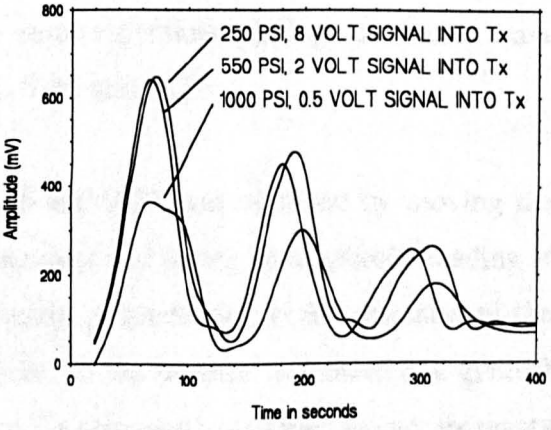

FIGURE 9.23 MULTIPLE SHEAR WAVE REFLECTIONS IN A 50 mm THICK ALUMINIUM PLATE

9.4.3. *An Investigation of Lamb Wave Techniques*

As demonstrated by the previous experiment, it is not difficult to construct a system suitable for generating and detecting shear waves over a wide range of environmental pressures. The reason for this is that shear waves can be generated and detected efficiently over a range of angles. By comparing Figures 9.17, 9.18 and 9.19 with Figure 9.20 it can be seen that the range of angles in air is small compared to that in water. Although the range of angles in air is not as wide as in water it is more than adequate to facilitate easy alignment of the system. As illustrated by the initial Lamb wave experiment (Section 9.3.3), it is more difficult to construct a system based on this technique which is capable of operating over a wide range of environmental pressures. This is because the ultrasonic transducers must be set at a specific angle in order to generate and detect a specific Lamb wave mode. If the pressure of the external medium changes then the velocity of sound changes and hence the required angle changes.

The transducers used in the Lamb wave investigation were the same as those used in the shear wave investigation and the test-piece is illustrated in Figure 9.24. It was calculated that, for the a_0 Lamb wave mode, it would be necessary to increase the angle at which the transducers are set by 0.6 degrees in order to compensate for increasing the pressure from atmospheric to 1000 psi. Ideally this experiment would have been arranged so that it was possible to move the transducers as a pair across the plate but it was not possible to arrange this with the equipment available. As an alternative the transmitter was fixed in position and the receiver was moved in a line passing through the defect and perpendicular to its longer side. It was expected that while the receiver was in position above metal of the correct thickness a strong signal would be detected but when the receiver was placed over material of reduced thickness the signal amplitude would be greatly reduced. The results obtained during the Lamb wave investigation are illustrated in Figures 9.25, 9.26 and 9.27.

The data used to produce Figures 9.25, 9.26 and 9.27 was obtained by moving the receiving transducer in steps (measured in seconds) and taking an amplitude reading at each position. In these figures, time is directly proportional to the distance of the receiving transducer from one end of the plate. It can be seen that there is a gradual increase in attenuation as the distance between the transmitter and the receiver increases

but when the receiver is directly over the defect there is a sharp decrease in the amplitude of the received signal.

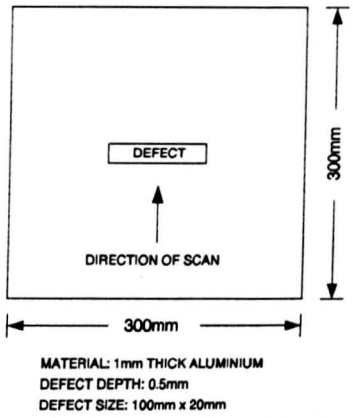

FIGURE 9.24 TEST-PIECE USED IN THE HIGH PRESSURE LAMB WAVE EXPERIMENTS

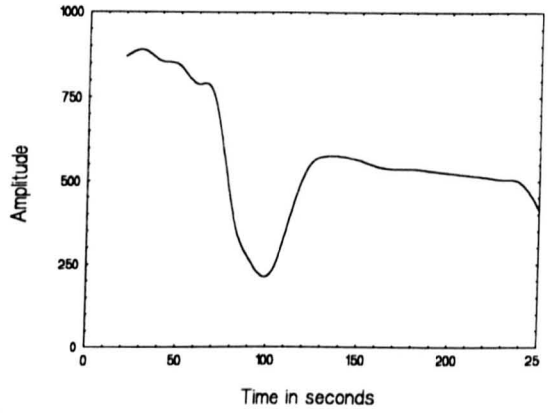

FIGURE 9.25 LAMB WAVE SCAN OF 1 mm ALUMINIUM PLATE AT 250 PSI

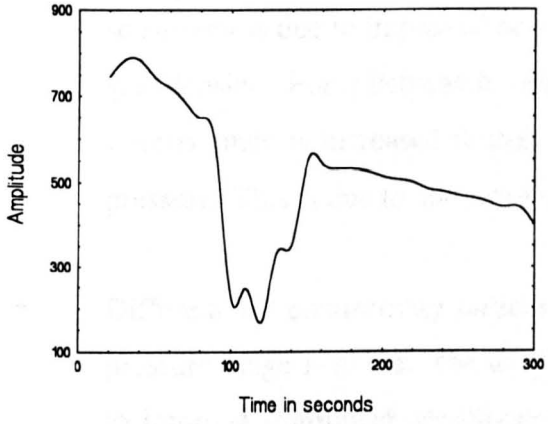

FIGURE 9.26 LAMB WAVE SCAN OF 1 mm ALUMINIUM PLATE AT 500 PSI

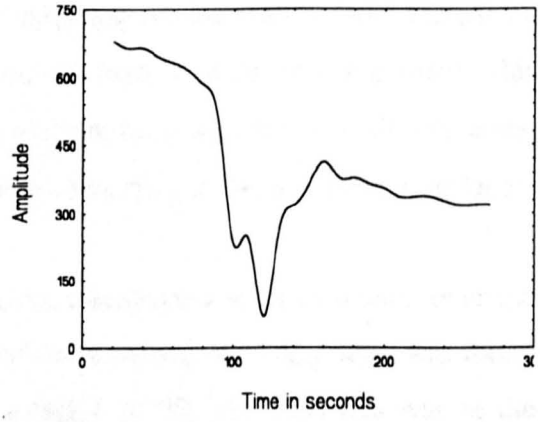

FIGURE 9.27 LAMB WAVE SCAN OF 1 mm ALUMINIUM PLATE AT 1000 PSI

9.5 Electrostatic Transducers

Although the main aim of the high pressure study was to investigate piezoceramic composite transducers, the opportunity was taken to investigate electrostatic transducers. An electrostatic transducer which had previously been constructed by Kelly [104] was tested over the 70 bar pressure range. In this case the sensitivity decreased significantly with pressure, with considerable degradation in pulse shape and bandwidth, even at relatively low levels (10 bar). Although the exact cause is unclear, the degradation is believed to be caused by compression of the miniature air pockets that are necessary to enable electrostatic vibration.

9.6 Conclusions

Although time and funding were very limited significant progress was made during the course of the high pressure study. The principal findings are as follows:

- The ultrasonic velocity in nitrogen was found to vary from 344 ms^{-1} to 366 ms^{-1} over the pressure range 1 to 70 bar. This variation, although apparently small, is sufficient to necessitate changing the transducer angles in both shear and Lamb wave testing configurations. Failure to adjust the transducer angles has a significant effect on sensitivity, especially for a Lamb wave system.

- For a pair of gas coupled transducers operating in direct transmit/receive mode (i.e. with no intermediate test specimen), the received signal amplitude was found to increases linearly with pressure. This improvement in system sensitivity is due to improved acoustic matching arising mainly from increasing gas density. For pitch-catch operation through a solid test specimen, this improvement is increased further, approximating a square law with increasing pressure. This is due to additional acoustic matching at the test-piece interfaces.

- Different 1-3 connectivity piezocomposite transducers were evaluated over the pressure range 1-70 bar. The addition of a customised matching layer was found to improve transducer sensitivity by a factor of 20, although this was at the expense of pulse bandwidth and resolution.

- An electrostatic transducer [104] was tested over the 70 bar pressure range. The device failed to operate even at relatively a low pressure (10 bar). This form of transducer is not recommended for through air operation at elevated pressures.

- In a very significant experiment, gas-coupled pulse-echo thickness testing was demonstrated using a single transducer.

- Pitch-catch shear wave testing was demonstrated using two transducers.

- Pitch-catch Lamb wave testing was demonstrated using two transducers.

Chapter 10

Conclusions and Suggestions for Future Work

10.1 Concluding Summary

The success of this research programme demonstrates that, although it is over a hundred years since Koenig [16] first produced ultrasonic waves, it is still possible to make significant theoretical and experimental contributions to the science of ultrasound, and push the technology beyond what had been its accepted limits. Following a brief overview, the various contributions made by this Thesis are discussed in detail.

10.1.1 A Brief Overview of the Thesis

The gas coupled ultrasonic research described here could be said to be a continuation of the work which was started in 1907 when Altberg [17] performed his pioneering experiments involving the generation and detection of sound waves in air at a frequency of 300 kHz. Unfortunately for Altberg, it is very unlikely that he could have foreseen what is probably the most exciting application of his work, that is, using these waves to probe the internal structure of solid objects. It is also unlikely that he could have foreseen the new air coupled transducer technologies which were to replace his spark discharge technique. The most significant of these are the electrostatic technology which was discussed briefly in Chapter 1 and the piezocomposite technology which features in all of this work. By itself, the first ever use of piezocomposite transducers for real-time[1] air coupled testing makes this work unique. However, the significance of this contribution is greatly enhanced by an unprecedented set of experiments which show that, unlike electrostatic transducers, piezocomposites can be used in a variety of test configurations at pressures of up to 1000 psi. Taking the technology to the limits of what is possible has involved producing a theory which allows the absolute sensitivity of piezoelectric plate transducers to be predicted. This major contribution to the field of air coupled ultrasound occupies Chapters 4,5 and 6 of this Thesis. By applying the new theory and by designing an ultra low noise ultrasonic receiver system based on air coupled piezocomposite transducer technology, it has been shown that it is possible to produce clear Lamb wave images of defects in almost any type of material. These real-time[1] images can now be produced on a routine basis using an automated Lamb wave scanner which was specially developed for this project. The ability of this scanner to detect delaminations and impact damage in carbon fibre plates has proved to be of

1 No signal averaging or any other form of processing required

particular interest to industry. The high quality and industrial relevance of this research has guaranteed the continued support of EPSRC and various commercial organisations including British Aerospace, British gas, Rolls Royce, and the Ford Motor Company.

10.1.2 Basic Ground Work

It is interesting to note that, even with modern transducer technology, air coupled testing at normal atmospheric pressure is typically conducted at frequencies similar to those which were used by Altberg. For example, all of the transducers used in this work were designed to operate at frequencies close to 600 kHz. The reason for this is that, as discussed in Section 2.4 of this Thesis, the air channel behaves as a low pass filter which, for a 1 cm path length, restricts the 3 dB upper cut off frequency to 1.3 MHz. Attenuation in air ensures that any increase in the path length will result in a reduction in the upper cut off frequency. So, without placing unrealistic restrictions on the path length, the frequencies available for ultrasonic testing in air at normal atmospheric pressure are restricted to a few hundred kHz.

At an early stage in this investigation it was discovered that all of the available text books on elastic waves completely disregard the possibility of transmitting sound waves through a gas into a solid. As with an ordinary mirror which reflects almost all of the light which is incident upon it, a gas/solid interface is normally thought of as a 100% reflector. However, in reality, it is possible for a very small percentage of a sound waves energy to cross a solid/air boundary and vice versa. This is what makes gas coupled ultrasonic testing of materials and structures possible. Chapter 2 of this Thesis paves the way to a proper understanding of the problems associated with gas coupled testing. In particular, it contributes to the field of ultrasonic testing by providing a thorough theoretical investigation of the various ways in which gas coupled ultrasound can be used to penetrate solid objects. Pearson's [53] unpublished work was found to be invaluable during this part of the theoretical investigation.

10.1.3 Experimental Work

Although the feasibility of air coupled ultrasonic testing was first demonstrated experimentally by Luukkala *et al.* [12,13] during the early 1970's, serious attempts at commercial exploitation did not start until the early 1990's. In the UK, the most

ambitious air coupled test systems are currently being developed by the University of Strathclyde in collaboration with British Aerospace [2,4]. These through transmission systems replace conventional water jet systems and use the same basic components (piezocomposite transducers, ultra low noise pre-amplifiers and electronic filter units etc.) which were developed in 1994 at the start of the *Ultrasonic Testing Without Coupling Fluids* project, which is discussed in Chapter 1 of this Thesis. A novel feature of all the Strathclyde systems is the use of new piezocomposite transducers which were specially developed for air coupled applications [47,48]. These transducers, which consist of piezoceramic rods supported in a passive polymer, provide superior air coupled performance to the homogeneous piezoelectric plates used by Rogovsky [14] in 1991. A major goal, which was achieved close to the start of this project, was to demonstrate for the first time that piezocomposite transducers can be used for real-time air coupled testing. As discussed in Chapter 7, it was shown that air coupled piezocomposites can be used to generate and detect longitudinal waves, shear waves, Lamb waves and Rayleigh waves in appropriate test samples. In Chapter 8 it was shown that the air coupled generation and detection of Lamb waves using piezocomposite transducers provides a particularly valuable way of inspecting thin plates which can be made from almost any material. Compared to the previously mentioned through transmission systems which have since been constructed using the same component parts as the original Lamb wave system, the current Lamb wave systems continue to have the advantage that internal images can be produced using a pair of transducers which are both located on the same side of the test plate. Although the transducer angles must be set with a high degree of accuracy (typically 0.5°), these *single sided* systems provide the only realistic way of using air coupled ultrasonic transducers for *in service* testing. One of the few problems with the original Lamb wave system was the formation of a double image. The development of a unique technique which allows the removal of this double image constitutes one of the less obvious contributions to be made to the field of non-destructive testing (NDT) during this research programme.

An as yet unpublished contribution to the NDT field, which is discussed in Chapter 9, was to show that all of the gas coupled techniques which were developed for use at normal atmospheric pressure can also be used at pressures of up to 1000 psi. During

this investigation it was shown that piezocomposites were capable of operating over the entire range of available pressures whereas electrostatic devices failed at a pressure which was just a few psi. above atmospheric. In general, piezocomposite transducers have been shown to provide a robust alternative to the electrostatic transducers favoured by many other researchers working in the field of air coupled ultrasonic testing.

10.1.4 The Absolute Sensitivity Theory

Some of the most significant contributions which this Thesis makes to the field of ultrasonics are concerned with a fundamental aspect of sound detection theory which has not until now been fully understood. While investigating the performance limitations of various ultrasonic test systems which employ gas coupled transducers, it became evident that the accepted definition of receiver sensitivity can be very misleading. This is particularly true when discussing ultrasonic transducers which are used for non-destructive testing. The problem is less apparent in SONAR applications where alternative figures of merit are used to properly describe the performance of ultrasonic receivers. However, even in the SONAR field, it appears that existing theories of receiver sensitivity fail to reveal some important fundamental relationships which are derived in this Thesis.

It is the advent of air coupled test systems, such as those discussed in this Thesis, that has served to expose the flawed definition of sensitivity. In order to detect the much lower amplitude signals which are characteristic of air coupled systems, it is necessary to use a pre-amplifier which produces a much lower level of noise than is normally found in conventional[1] ultrasonic test systems. In Chapter 7 of this Thesis it was shown that a pre-amplifier which is designed to operate close to its own theoretical noise limit produces a level of noise which is comparable to the level of noise produced by a typical receiving transducer. It is the possibility of using ultra low noise pre-amplifiers that has led, in this work, to an interest in the absolute sensitivity of receiving transducers. Although a transducer's absolute sensitivity may only be of academic interest in connection with conventional[1] ultrasonic test systems it is of critical importance when attempting to design the best possible air coupled systems.

1 Dry or liquid coupled

As discussed in Chapter 4, absolute sensitivity can be defined in terms of minimum detectable power (MDP), minimum detectable force (MDF) or minimum detectable displacement (MDD). The theoretical aspects of absolute sensitivity are best understood using MDP, and MDD is relevant when assessing a transducer experimentally using, for example a laser vibrometer, however, MDF appears to be the most acceptable parameter when discussing NDT applications. One of the main contributions which this Thesis makes to the field of gas coupled ultrasonic testing is to show that the absolute sensitivity of an open circuit piezoelectric plate transducer can be expressed using the following expression:

$$MDF = \sqrt{\frac{4k_B T_A Z_C B}{\pi Q_M}} \tag{10.1}$$

Here, k_B is Boltzmann's constant, T_A is the absolute temperature in degrees Kelvin, B is the bandwidth, Z_C is the acoustic impedance of the transducer and Q_M is its intrinsic mechanical quality factor. Equation (10.1) provides a meaningful figure of merit for transducers which are surrounded by a gaseous coupling medium, however, it should only be regarded as an extreme example which emerges from a more general theory. In this Thesis, another extreme example was considered by investigating what happens to a transducer's absolute sensitivity when its intrinsic damping, as quantified by Q_M, is insignificant compared to external damping. For this condition it was shown that:

$$MDF = \sqrt{2k_B T_A Z_1 B} \tag{10.2}$$

where Z_1 is the acoustic impedance of the coupling medium. This intriguing result indicates that, for a transducer which has no intrinsic losses, the minimum detectable force in the coupling medium is completely independent of all of the transducer's properties. Further, the sensitivity of the transducer is determined purely by the acoustic impedance, Z_1, of the coupling medium. However, for a 34 MRayl transducer used in air it would be necessary for the transducer to have a Q_M which is significantly higher than 54,000 for this situation to arise. Also, for very high values of Q_M it would be necessary to take account of thermal noise in the coupling medium.

Prof. Richard Feynman, in his highly acclaimed *Lectures on Physics*, makes frequent reference to the importance of symmetry, especially with regard to the fundamental laws of physics. Interestingly, Equation (10.1) does indicate a type of symmetry since the frequency independent nature of the MDF is a consequence of the transducer's voltage noise spectrum tracking its force to voltage transfer function. So, a change in one parameter is exactly balanced by a change in another parameter, and that is the symmetry. Regarding the LSM approach, symmetry in the mathematics is a consequence of recognising that the real part of a transducer's complex electrical impedance is a function of frequency. This is easily confirmed using an impedance analyzer and it is this feature which leads to the voltage noise spectrum which can be observed using a spectrum analyzer. It would appear that many investigators who have attempted to obtain an accurate mathematical expression for a transducer's MDP (or its equivalent) have failed to use what is actually the real part of the transducer's electrical impedance in their derivations. Instead, they have used the loss tangent ($tan\delta$) in calculating the transducer noise voltage. As discussed in detail in Chapter 4, it is correct to use the loss tangent to calculate the noise voltage for unpoled piezoelectric materials but is certainly not correct to do this with poled piezoelectric materials. Using the loss tangent in the derivation may result in this parameter appearing in the answer (an expression for SNR, MDP or some similar parameter) along with many other transducer parameters which should have cancelled out due to the previously mentioned symmetry. It is interesting to note that, if an accurate expression for transducer MDP is to be obtained using an electrical approach (i.e. an approach based on the Johnson noise equation), it is necessary to have access to a transducer model which yields mutually consistent expressions for the transducer's electrical impedance and its force to voltage transfer function. Here, mutually consistent should be read to mean that the equations operate in such a way that electrical and mechanical energy are conserved within the model. The Linear Systems Model (LSM) satisfies this condition and it is the use of the LSM which makes this work unique. Of course, it would have been possible to use an alternative model such as the KLM model. Oakley has recently attempted to do this [105]. Although his goal was not to obtain an expression for MDP or MDF it is interesting to note that Oakley's approach may be flawed because he appears to have used the loss tangent to calculate the transducer noise.

Equation (10.1) appears to eliminate many conventional transducer design options. For example, there is no apparent reason to design a receiving transducer with a high value of electromechanical coupling coefficient. Equation (10.1) also eliminates the possibility of manipulating or selecting the electrical properties of the transducer materials in order to improve the SNR. It is now evident that, for gas coupled applications, the only important transducer parameters are Z_C and Q_M. This means that, as was always the case, it makes sense to design a transducer with as low a value of Z_C as possible, however, Equation (10.1) indicates that the absolute sensitivity (MDF) of the transducer varies in proportion to $\sqrt{Z_C}$. Conventional sensitivity (for example, volts per newton) varies in proportion to Z_C.

Although the absolute sensitivity theory which has been presented in this Thesis appears to eliminate many of the conventional transducer design options, the same is not necessarily true for the complete receiver front end (transducer plus pre-amplifier). As mentioned previously, if the pre-amplifier is excessively noisy (i.e. the pre-amplifier produces a level of voltage noise which is significantly greater than the level of voltage noise produced by the transducer itself) then most of the conventional rules apply. For example, it then makes sense to design a receiving transducer which has a high value of electromechanical coupling coefficient. Also, if the pre-amplifier input impedance is not sufficiently high compared to the transducer's electrical impedance at its fundamental mechanical resonance frequency, electrical damping makes it necessary to replace Q_M by an effective value, Q_{EFF}. This subject is discussed in detail in Chapter 6.

From the observations which have been made in this summary it should be clear that, in order to achieve the best possible air coupled receiver performance using a piezoelectric plate transducer, careful pre-amplifier design is at least as important as careful transducer design. In this Thesis it has been shown that by using an ultra low noise pre-amplifier it is possible to achieve a level of absolute sensitivity which is transducer limited. The low noise aspects of the air coupled work described in this Thesis distinguishes it from the work of previous investigators such as Luukkala *et al.* and Rogovsky. Without the low noise receiver design it would have been impossible, without signal processing, to produce the high quality Lamb wave images which are featured in this Thesis.

10.2 Commercial Exploitation

Many people who have seen the new air coupled systems demonstrated are impressed by the fact that it is possible to obtain so much information about the internal structure of a solid object with so little equipment. This is particularly so now that the massive ENI power amplifiers used in the early work have been replaced by a compact and highly efficient driver designed by the author of this Thesis. The new driver units are housed in a metal case which is identical to the one in which the receiver's main amplifier, filter and envelope detector are housed. Each metal case measures 8 x 5 x 4 inches. These two electronic units, along with a head unit which holds two piezocomposite transducers plus the receiver pre-amplifier, form the essential building blocks of all the current Lamb wave systems. Perhaps surprisingly, the cost of manufacturing the three sub-units is insignificant compared to the cost of the scanning equipment which is required to produce an ultrasonic image. For example, one of a number of possible Lamb wave test configurations involves using the three sub-units in conjunction with an Andscan position measurement system which is supplied by Krautkramer and which can cost over £20,000 in its most complete form. A goal of the Strathclyde team is to replace the Andscan with a device which operates like a computer mouse and which would, for example, be connected to the serial port of a personal computer (PC) in the normal way. This *mouse* would also contain air coupled transducers capable of generating Lamb waves in appropriate test samples. Dedicated computer software would combine signal amplitude data with positional data to create image defects on the screen of a PC in the same way as is done with the Andscan.

Development of a simple self-contained *lamb wave mouse* is not the only available avenue to commercial exploitation of the air coupled technology. As mentioned in Section 10.1.3, an ambitious eight element through transmission system which is intended to replace water jet systems is currently being developed by the University of Strathclyde in collaboration with British Aerospace. This system uses eight channel versions of the ultra low noise pre-amplifiers and electronic filter units used in this research programme. As with the single element units, these components were designed by the author of this Thesis. The author is also contributing to the development of an eight element Lamb wave system for the CANDIA consortium which again includes British Aerospace as a partner.

10.3 Future Research

This Section is concerned with the exciting scientific challenges that await anyone who is in the fortunate position of being able to continue this research.

10.3.1 The Ultimate Air Coupled Transducer

As discussed in Chapter 4, the ultimate value of room temperature (295 K) minimum detectable power (MDP) is 1.62 x 10^{-20} W/$\sqrt{Hz}$. Except by reducing the temperature of the entire test system (the transducers and the coupling medium etc.) and/or by using signal averaging, it is physically impossible to detect a signal power in air, or in any other material, which falls below this level. During this research programme it has been shown that, by using an ultra low noise pre-amplifier, it is possible, at resonance, to achieve this level of absolute sensitivity within the transducer material. For a typical 34 MRayl piezoceramic plate transducer with a Q_M of 75 this is equivalent (see Section 6.4.4) to obtaining an MDP of 1 x 10^{-17} W/$\sqrt{Hz}$ in air. The proposed project would involve the development of a new air coupled transducer technology capable of achieving an MDP of 1.62 x 10^{-20} W/$\sqrt{Hz}$ in air itself. Put another way, this clearly defined project would involve developing a receiving transducer which either has a very high value of Q_M or which is perfectly impedance matched to air. These possibilities were discussed in Section 6.6. An obvious disadvantage of designing a transducer with a very high value of Q_M would be its greatly restricted bandwidth, and technical problems would include the very real possibility that electrical damping would greatly restrict the actual value of absolute sensitivity that could be achieved. In fact, it would not be possible to investigate high Q transducers using the ZN460 pre-amplifier used in all of this research. As discussed in Section 6.4.1, even for a transducer which has a relatively low Q_M of 75, the 7 kΩ input impedance of the ZN460 results in electrical damping of the transducer leading to an effective quality factor, Q_{EFF}, of 67.4. A much more rewarding line of research will, as has always been the case, involve looking at methods of achieving improved impedance matching to air. The ultimate goal should be the development of a low Q, and hence wide bandwidth, ultrasonic receiver which is perfectly impedance matched to air. This might seem impossible, but then air coupled testing also looked to be impossible before the early 1970's. It is very unlikely that a suitable device could be constructed using piezoelectric materials and, despite the fact that they are air backed, electrostatic transducers are not capable of operating at

the thermal limit in air. Mechanical matching can provide spectacular improvements in sensitivity but again it is unlikely that this avenue of research will lead to the ultimate air coupled transducer. What is required is a new approach which builds on the fundamental laws of physics and which disregards all of the old prejudices concerning which one of the existing technologies is best.

10.3.2 Advanced Piezoelectric Transducers

Although it is unlikely that ultrasonic transducers based on piezoelectric technology could ever achieve the ultimate air coupled sensitivity discussed in the previous Section, there are some new and untried approaches which could lead to a significant improvement in receiver sensitivity. One of these was discussed in Section 3.4.1. and involves the use of bimorphs. A bimorph offers an attractive way of constructing a piezoceramic transducer with reduced stiffness, however, the analysis which was presented in Section 3.4.1 indicates that it would be difficult to produce a device capable of operating at a sufficiently high frequency. Also, because a bimorph does not produce a uniform displacement across its surface, it would not be possible to fabricate a source of ultrasound with a good directivity pattern using a single device. As discussed in Chapter 3, using the bimorph concept to construct an efficient high frequency source with a good directivity pattern would involve constructing quite complex piezoceramic structures on a very small scale and then arranging them in the form of a relatively large two dimensional array. For best performance each bimorph element would be operated at its resonance frequency. A possible configuration was suggested in Chapter 3 and is illustrated in Figure 3.5. Building an ultrasonic transducer of this type would involve using micromachining technology similar to that used for constructing small silicon components. As discussed in Section 3.4.1, Hoffmann *et al.* have reported (1994) the fabrication of micromechanical cantilever resonators with integrated optical interrogation [62]. Although this work does not involve the use of piezoceramic materials it is of considerable interest because of the operating frequencies involved. By transmitting light across a 2 μm gap from the free end of the cantilever to the end of a fixed wave guide, it was possible to produce a vibration detector capable of operating in the 80 kHz to 120 kHz frequency range. The corresponding cantilever lengths are in the range 170 μm to 140 μm. In order to construct an air coupled transducer it would be necessary to fabricate an array of

similar devices using piezoelectric materials.

10.3.3 Related Research Themes

As a further credit to the quality and industrial relevance of the research which is described in this Thesis, many of the most obvious avenues of continued research are already being investigated by the teams at Strathclyde University and Imperial College. Most, but not all of the current work is being supported by a new contract which was enthusiastically awarded to Strathclyde and Imperial by EPSRC following the success of the *Ultrasonic Testing Without Coupling Fluids* project. This contract supports a large number of activities, some of which are concerned with the generation and detection of Lamb waves using dry coupled interdigital transducers, and others which are a more direct extension of the air coupled work described in this Thesis. One of the most important air coupled projects involves an investigation of a frequency agile Lamb wave scanner which does not require the angles of the air coupled transducers to be adjusted in order for the system to test plates of different thickness. In addition to locating defects, this system will be capable of monitoring the thickness of a plate over its entire surface area. Related activities involve the development of new wide bandwidth piezocomposite transducers, an investigation of alternative electrostatic designs, and an investigation of methods which will facilitate control of the air channel. This latter activity is particularly relevant to the inspection of very hot shell like structures such as those which might, for example, be found in an oil refinery. British gas, who funded the high pressure experiments described in this Thesis, continue to show an interest in the use of gas coupled techniques for the inspection of pipe lines and recently Rolls Royce has suggested the use of air coupled techniques for the inspection of jet engine fan blades. As previously mentioned, British Aerospace is supporting the development of an ambitious eight element through transmission system and the CANDIA consortium is supporting the development of an eight element Lamb wave scanner.

References

Frequently used Acronyms and Abbreviations

IEEE Trans UFFC - IEEE Transactions on Ultrasonics, Ferroelectrics, Frequency and Control

IEEE Trans SU - IEEE Transactions on Sonics and Ultrasonics

Proc IEEE US Symp - Proceedings of the IEEE Ultrasonics Symposium

Review of progress in QNDE - Review of Progress in Quantitative Nondestructive Evaluation

JASA - The Journal of the Acoustical Society of America

JAP - The Journal of Applied Physics

---

1 R. Farlow and G. Hayward, "Real-time ultrasonic techniques suitable for implementing non-contact NDT systems employing piezoceramic composite transducers", *Insight*, vol. 36, no. 12, pp. 926-935, Dec. 1994.

2 R. Farlow, S. P. Kelly, and G. Hayward, "Advances in air coupled NDE for rapid scanning applications", *Proc IEEE US Symp*, vol. 2, p. 1099, 1994.

3 R. Farlow and G. Hayward, "An automated ultrasonic NDT scanner employing advanced air-coupled 1-3 connectivity composite transducers", *Insight* vol. 38, no.1, pp. 41-50, Jan. 1996.

4 S. P. Kelly, R. Farlow and G. Hayward, "Applications of through-air ultrasound for rapid NDE scanning in the aerospace industry", *IEEE Trans UFFC* vol. 43, no. 4, p. 581, July 1996.

5 S. G. Pierce, B. Culshaw, W. R. Philp, F. Lecuyer, R. Farlow, "Broadband Lamb wave measurements in aluminium and carbon/glass fibre composite materials using non-contact laser generation and detection", *Ultrasonics* vol. 35, pp. 105-114, 1997.

6 R. Farlow and G. Hayward, "The absolute sensitivity of a piezocomposite transducer", *Proc IEEE US Symp (Toronto)*, 1997.

7 R. Banks, R. Farlow, and G. Hayward, "A frequency-agile ultrasonic Lamb wave scanner for NDE systems", *Insight*, vol. 39, no. 11, pp. 780-784, 1997.

8 M. Castaings, P. Cawley, R. Farlow and G. Hayward", Air-coupled ultrasonic transducers for the detection of defects in plates", *Review of progress in QNDE*, vol. 15, pp. 1083-1090, Plenum Press, 1996.

9 M. Castaings and P. Cawley, "The generation, propagation and detection of Lamb waves in plates using air-coupled ultrasonic transducers", *JASA*, vol. 100,

no. 5, pp. 3070-3077, 1996.

10 R. Farlow and G. Hayward, "The thermally limited sensitivity of a piezoelectric plate transducer", *Proceedings of the Royal Society, London* - to be submitted in mid to late 1998.

11 R. Farlow, R. Banks and G. Hayward, "Noise modelling of thickness drive piezoceramic transducers", *JASA*, - to be submitted in mid to late 1998.

12 M. Luukkala, P. Heikkila and J. Surakka, "Plate wave resonance: a contactless test method", *Ultrasonics*, vol. 9, no. 4, pp. 201-208, Oct. 1971.

13 M. Luukkala and P. Merilainen, "Metal plate testing using airborne ultrasound", *Ultrasonics*, vol. 11, no. 5, pp. 218-221, Sep. 1973.

14 A. J. Rogovsky, "Development and application of ultrasonic dry-contact and air-contact c-scan systems for nondestructive evaluation of aerospace composites", *Materials Evaluation*, vol. 49, pp. 1491-1497, Dec. 1991.

15 D. Reilly and G. Hayward, "Through air transmission for ultrasonic non-destructive testing", *Proc IEEE US Symp*, 1991, pp 763-766.

16 J. R. Frederick, *Ultrasonic Engineering*. New York: Wiley, p. 5. 1965.

17 W. Altberg, *Annalen der Physik*, vol. 23, no. 4, pp. 267-276, 1907.

18 S. Sokolov, *Elek. Nachr.-Tech*, vol. 6, pp. 454-461, 1929.

19 F. A. Firestone, "The supersonic reflectoscope for interior inspection", *Metal Progress.*, vol. 48, pp. 505-512, 1945.

20 F. A. Firestone, *JASA*, vol. 17, p. 364, 1946.

21 F. A. Firestone & J. R. Frederick, *JASA*, vol. 18, p. 200, 1946.

22 C. H. Desh, D. O. Sproule and W. J. Dawson, "The Detection of Cracks in Steel by Means of Supersonic Waves", *Journal of the Iron and Steel Institute*, vol. 1, p. 319, 1946.

23 I. A. Viktorov, *Rayleigh and Lamb Waves, Physical Theory and Applications*. New York: Plenum, 1967.

24 W. C. Worlton, "Ultrasonic testing with Lamb waves", *Non-Destructive Testing*, vol. 15, pp. 218-222, 1957.

25 W. C. Worlton, "Experimental confirmation of Lamb waves at megacycle frequencies", *JAP*, vol. 32, pp. 967-971, 1961.

26 T. L. Mansfield, "Lamb wave inspection of aluminium sheet", *Materials Evaluation*, vol. 33, pp. 96-100, 1975.

27 D. F. Ball and D. Shewring, "Some problems in the use of Lamb waves for the inspection of cold-rolled steel sheet coil", *Non-Destructive Testing*, vol. 6, pp. 138-145, 1973.

28 M. G. Silk and K. F. Bainton, "The propagation in metal tubing of ultrasonic wave modes equivalence to Lamb waves", *Ultrasonics*, vol. 17, no. 1, pp. 11-19, 1973.

29 S. I. Rokhlin, "Lamb wave interaction with lap-shear adhesive joints: theory and experiment", *JASA*, vol. 89, pp. 2758-2765, 1991.

30 S. I. Rokhlin and F. Bendec, "Coupling of Lamb waves with the aperture between two elastic sheets", *JASA*, vol. 73, pp. 55-60, 1983.

31 J. L. Rose, M. C. Fuller, J. B. Nestleroth and Y. H. Jeong, "An ultrasonic global inspection technique for an offshore K-Joint", *Soc. Petrol. Eng. J*, vol. 23, pp. 358-364, 1983.

32 P. M. Bartle, "Acoustic pulsing for in-service monitoring", *Non-Destructive Testing (Proc, 12th World Conf.)*, J. Boogard and G. M. van Dijk, Eds. Amsterdam: Elsevier, 1989, pp. 254-257.

33 D. Alleyne and P. Cawley, "The interaction of Lamb waves with defects", *IEEE Trans UFFC*, vol. 39, no. 3, pp. 381-397, 1992.

34 D. Alleyne and P. Cawley, "A two-dimensional Fourier transform method for the measurement of propagating multimode signals", *JASA*, vol. 89, no. 3, pp. 1159-1169, 1991.

35 D. Alleyne and P. Cawley, "Optimization of Lamb wave inspection techniques", *NDT&E International*, May 1992.

36 N. Guo and P. Cawley, "The interaction of Lamb waves with delaminations in composite laminates", *JASA*, vol. 94, no. 4, pp. 2240-2246, 1993.

37 T. K. Lockett, "Lamb and torsional waves and there use in flaw detection in tubes", *Ultrasonics*, pp. 31-37, Jan. 1973.

38 B. Drinkwater and P. Cawley, "An ultrasonic wheel probe alternative to liquid Coupling", *Insight*, vol. 30, no. 6, pp. 430-433, June 1994.

39 J. Krautkramer and H. Krautkramer, *Ultrasonic Testing of Materials, 4th Fully Revised Edition*. Berlin: Springer-Verlag, 1989.

40 "Huge savings in large-area and complex surface inspection using laser-ultrasonics", *Insight*, vol. 38, no. 1, pp. 13-15, Jan. 1996.

41 D. A. Hutchins, W. M .D. Wright, G. Hayward and A. Gachagan, "Air-coupled piezoelectric detection of laser-generated ultrasound", *IEEE Trans UFFC*, vol. 41, no. 1, pp. 796-805, 1994.

42 W. A. Grandia and C. M. Fortunko, "NDE applications of air-coupled ultrasonic transducers", *Proc IEEE US Symp (Seattle)*, 1995.

43 *Condenser microphones and microphone preamplifiers for acoustic measurements; data handbook*, Bruel & Kjaer, 1982

44 W. Kuhl *et al.*, "Condenser transmitters and microphones with solid dielectric for airborne transducers", Acustica 4(5), April 1954, pp. 519-532.

45 D. W. Schindel *et al.*, "The design and characterisation of micromachined air-coupled capacitance transducers", *IEEE Trans UFFC*, vol. 42(1), Jan. 1995, pp. 42-50.

46 M. I. Haller and B. T. Khuri-Yakub, "A surface micromachined electrostatic ultrasonic air transducer", *IEEE Trans UFFC*, vol. 43, no. 1, pp. 1-6, 1996.

47 A. Gachagan, "An evaluation of 1-3 connectivity composite transducers for air-coupled ultrasonic applications", PhD Thesis, University of Strathclyde, 1996.

48 G. Hayward and A. Gachagan, "An evaluation of 1-3 connectivity transducers for air coupled applications, " *JASA*, vol. 99(4), pp. 2148-2157, 1996.

49 J. T. Bennett, "Development of finite element modelling system for 1-3 piezocomposites", PhD Thesis, University of Strathclyde, 1995.

50 BRITE-EURAM-II, "NDT & NDE for maintenance of structural parts - final technical report", Contract No. BRE2-CT92-0313, Project No. BE5879, Period 1st May 1993 to 30th October 1996

51 W. Galbraith and G. Hayward, "Development of a membrane hydrophone for use in air-coupled ultrasonic transducer calibration", *IEEE Trans UFFC*-submitted in early 1998.

52 J. Blitz and G. Simpson, *Ultrasonic Methods of Non-destructive Testing*, Chapman & Hall.

53 J. Pearson, "Personal notes on the transmission and reflection of sound waves at media boundaries", University of Strathclyde, Glasgow.

54 L. M. Brekhovskikh, *Waves in Layered Media*, Academic Press, 1960.

55 G. Hayward, "Time and Frequency Domain Modelling of the Piezoelectric Transducer", PhD Thesis, University of Strathclyde, 1981.

56 P. N. T. Wells, *Biomedical Ultrasonics*. Academic Press, 1977

57 A. Gachagan *et al.*, "Characterization of air coupled transducers", *IEEE Trans UFFC*, vol. 43, no. 4, pp. 678-689, 1996.

58 T. E. Gomez, S. P. Kelly and G. Hayward, "An integrated impedance matching layer for air coupled ultrasonic applications", - to be published in 1998.

59 A. J. Moulson and J. M. Herbert, *Electroceramics: Materials, Properties, Applications*. Chapman and Hall.

60 T. Ono, "Optical beam deflector using a piezoelectric bimorph actuator", Sensors and Actuators, A21-A23, pp. 726-728, 1990.

61 A. B. Frazier, C. H. Ahn and M. G. Allen, "Development of micromachined devices using polyimide-based processes", Sensors and Actuators, A45, pp. 47-55, 1994.

62 Hoffmann *et al.*, "Micromechanical cantilever resonators with integrated optical interrogation", Sensors and Actuators, A44, pp. 71-75, 1994.

63 Mullard Technical Information 24, "Designing ultrasonic systems using PXE air transducers", 1975

64 Mullard, "Piezoelectric air transducers application note", 1972

65 M. Babic, "A 200kHz ultrasonic transducer coupled to the air with a radiating membrane", *IEEE Trans UFFC*, vol. 38, no. 3, pp. 252-255, 1991.

66 Q. C. Xu, S. Yoshikawa, J. R. Belsick and R. E. Newnham, "Piezoelectric composites with high sensitivity and high capacitance for use at high pressures", *IEEE Trans UFFC*, vol. 38, no. 6, pp. 634-638, 1991.

67 H. P. Savakus, K. A. Klicker and R. E. Newman, "PZT epoxy piezoelectric transducers: a simplified fabrication process", *Materials Research Bulletin*, vol 16, pp. 667-680, 1980.

68 T. A. Gururaja *et al.*, "Piezoelectric composite materials for ultrasonic transducer applications, Part I: Resonant modes of vibration of PZT rod-polymer composites", *IEEE Trans SU*, vol. SU32-4, pp. 481-498, July 1985.

69 T. A. Gururaja *et al.*, "Piezoelectric composite materials for ultrasonic transducer applications, Part II: Evaluation of ultrasonic medical applications", *IEEE Trans SU*, vol. SU32-4, pp. 499-513, July 1985.

70 M. N. Jackson, "Simulation and control of thickness-mode piezoelectric transducers", PhD Thesis, University of Strathclyde, 1984.

71 M. Gronauer, D. Buttner and J. Fricke, "Sound velocities in SiO_2 aerogel tiles - internal report", University of Wurtzburg.

72 R. Gerlach *et al.*, "Modified SiO_2 aerogels as acoustic impedance matching layers in ultrasonic devices", *Journal of Non-Crystalline Solids*, 1992

73 N. H. Fletcher and S. Thwaites, "Multi-horn matching plate for ultrasonic transducers", *Ultrasonics*, vol. 30, no. 2, pp. 67-72, 1992.

74 M. Schwartz, *Information Transmission, Modulation and Noise, Third Edition*. Mc Graw-Hill, 1983.

75 R. P. Feynman, R. B. Leighton and M. Sands, *The Feynman Lectures on Physics*. Addison-Wesley, 1970.

76 J. B. Johnson, "Thermal agitation of electricity in conductors", *Physical Review*, vol. 32, pp. 97-109, 1928.

77 H. Nyquist, "Thermal agitation of electric charge in conductors", *Physical Review*, vol. 32, pp. 110-113, 1928.

78 J. J. Brophy, *Basic Electronics for Scientists*. Mc Graw-Hill, 1966.

79 G. Hayward, "Using a block diagram approach for the evaluation of electrical loading effects on piezoelectric reception", *Ultrasonics*, vol. 24, p. 156, 1986.

80 G. Hayward, "A systems feedback representation of piezoelectric operational impedance", *Ultrasonics*, vol. 22, pp. 153-162, 1984.

81 G. Hayward, "The influence of pulser parameters on the transmission response of piezoelectric transducers", *Ultrasonics*, vol. 23, pp. 103-112, 1985.

82 *Piezoelectric Ceramics - Data Book for Designers*. Morgan Matroc.

83 G. S. Kino, *Acoustic Waves: Devices Imaging and Analog Signal Processing*. Prentice-Hall, 1987.

84 G. Hayward *et al.*, "A Model for Low Noise Design of Ultrasonic Transducers", *Proc IEEE US Symp (Cannes)*, pp. 971-974, 1995.

85 R. A. Banks, "An Investigation of Intrinsic Noise in Piezoelectric Receiver Systems", M Phil. Thesis, University of Strathclyde, 1996

86 H. B. Callen and T. A. Welton, "Irreversibility and generalized Noise", *Physical Review*, vol 83, No. 1, pp. 34-40, July 1951.

87 *Chambers Science and Technology Dictionary*. Chambers, 1984.

88 E. S. Boltz and C. M. Fortunko, "Absolute sensitivity limits of various ultrasonic transducers", *Proc IEEE US Symp*, pp. 951-954, 1995.

89 P. Debye, Ann. Physik, 43, 49, 1914.

90 I. Waller, Dissertation, Uppsala, 1925.

91 H. Ott, Ann. Physik, [5], 23, 169, 1935.

92 A. A. Maradudin, E. W. Montroll and G. H. Weiss, "Theory of lattice dynamics in the harmonic approximation", *Solid State Physics Supplement 3*, Seitz and Turnbull eds., 1963.

93 V. Tarnow, "The lower limit of detectable sound pressure", *JASA*, vol. 82(1), July 1987.

94 J. P. Den Hartog, *Mechanical Vibrations*. Dover, 1984.

95 R. Buckley, *Oscillations and Waves*. Adam Hilger, 1985.

96 W. A. Smith *et al.*, "Tailoring the Properties of Composite Piezoelectric Materials for Medical Ultrasonic Transducers", *Proc IEEE US Symp*, pp. 642-647, 1985.

97 H. Kressel (editor), *Semiconductor Devices for Optical Communication - Topics in Applied Physics*, vol. 39, Springer-Verlag, 1980.

98 R. S. Longhurst, *Geometrical and Physical Optics*, Longman, 1967.

99 S. Whiteley, G. Hayward and D. Reilly, "Thickness measurement using air-coupled ultrasound", *Insight* vol. 39, no.11, pp. 770-775, Nov. 1997.

100 W. P. Mason, *Physical Acoustics and the Properties of Solids*, Van Nostrand, 1958.

101 L. P. Yaroslavsky and H. J. Caulfield, "Deconvolution of multiple images of the same object", Applied Optics, vol. 33, no. 11, pp. 2157-2162, 1994.

102 Jorgen Lovlie, "Project report", University of Strathclyde, April 1997.

103 G. Hayward, R. Farlow, W. Galbraith, *On Line Air Coupled Inspection in a High Pressure Gaseous Environment*. Department of Electronic and Electrical Engineering, University of Strathclyde, 1995.

104 S. P. Kelly, "Notes on the manufacture of electrostatic transducers", Ultrasonics Research Group, University of Strathclyde.

105 C. Oakley, "Calculation of ultrasonic transducer signal-to-noise ratios using the KLM model", *IEEE Trans UFFC*, vol. 44, no. 5, pp. 1018-1026, 1997.

R. Farlow and G. Hayward, "Real-time ultrasonic techniques suitable for implementing non-contact NDT systems employing piezoceramic composite transducers", *Insight*, vol. 36, no. 12, pp. 926-935, Dec. 1994.

R. Farlow, S. P. Kelly, and G. Hayward, "Advances in air coupled NDE for rapid scanning applications", *Proc IEEE US Symp,* vol. 2, p. 1099, 1994.

R. Farlow and G. Hayward, "An automated ultrasonic NDT scanner employing advanced air-coupled 1-3 connectivity composite transducers", *Insight* vol. 38, no.1, pp. 41-50, Jan. 1996.

S. P. Kelly, R. Farlow and G. Hayward, "Applications of through-air ultrasound for rapid NDE scanning in the aerospace industry", *IEEE Trans UFFC* vol. 43, no. 4, p. 581, July 1996.

M. Castaings, P. Cawley, R. Farlow and G. Hayward, "Air-coupled ultrasonic transducers for the detection of defects in plates", *Review of progress in QNDE*, vol. 15, pp. 1083-1090, Plenum Press, 1996.

S. G. Pierce, B. Culshaw, W. R. Philp, F. Lecuyer, R. Farlow, "Broadband Lamb wave measurements in aluminium and carbon/glass fibre composite materials using non-contact laser generation and detection", *Ultrasonics* vol. 35, pp. 105-114, 1997.

R. Farlow and G. Hayward, "The absolute sensitivity of a piezocomposite transducer", *Proc IEEE US Symp (Toronto),* 1997.

R. Banks, R. Farlow, and G. Hayward, "A frequency-agile ultrasonic Lamb wave scanner for NDE systems", *Insight*, vol. 39, no. 11, pp. 780-784, 1997.

M. Castaings, P. Cawley, R. Farlow and G. Hayward, "Single sided inspection of composite materials using air coupled ultrasound", *Journal of Nondestructive*

Evaluation, vol. 17, no.1, pp. 37-45, 1998.

R. Farlow and G. Hayward, "The thermally limited sensitivity of a piezoelectric plate transducer", *Proceedings of the Royal Society, London* - to be submitted in mid to late 1998.

R. Farlow, R. Banks and G. Hayward, "Noise modelling of thickness drive piezoceramic transducers", *JASA*, - to be submitted in mid to late 1998.

Appendix I

TRANSDUCER MATERIALS

PROPERTIES OF BARIUM TITANATE AND LEAD ZIRCONATE TITANATE

Material	$BaTiO_3$	PZT-4	PZT-5A	PZT-5H	PZT-7A	PZT-8
Compliance, s^E, and stiffness, c^E, under constant field, E						
s_{11}^E ($10^{-12}m^2/N$)	8.6	12.3	16.4	16.5	10.7	11.5
s_{12}^E ($10^{-12}m^2/N$)	-2.6	-4.05	-5.74	-4.78	-3.2	-3.38
s_{13}^E ($10^{-12}m^2/N$)	-2.7	-5.31	-7.22	-8.45	-4.6	-4.69
s_{33}^E ($10^{-12}m^2/N$)	9.1	15.5	18.8	20.7	13.9	13.5
s_{44}^E ($10^{-12}m^2/N$)	22.2	39.0	47.5	43.5	39.5	31.9
s_{66}^E ($10^{-12}m^2/N$)	22.4	32.7	44.3	42.6	29.7	27.8
c_{11}^E ($10^{10}N/m^2$)	16.3	13.9	12.1	12.6	14.8	13.7
c_{12}^E ($10^{10}N/m^2$)	5.0	7.78	7.54	7.96	7.62	6.97
c_{13}^E ($10^{10}N/m^2$)	4.7	7.43	7.52	8.41	7.42	7.16
c_{33}^E ($10^{10}N/m^2$)	15.0	11.5	11.1	11.7	13.1	12.4
c_{44}^E ($10^{10}N/m^2$)	4.5	2.56	2.11	2.30	2.53	3.14
c_{66}^E ($10^{10}N/m^2$)	4.46	3.05	2.26	2.35	3.37	3.6
Piezoelectric coefficients						
d_{31} ($10^{-12}C/N$)	-58	-123	-171	-274	-60	-97.4
d_{33} ($10^{-12}C/N$)	149	289	374	593	150	225
d_{15} ($10^{-12}C/N$)	242	496	584	741	362	333
h_{31} ($10^8V/m$)	-6.8	-9.2	-7.3	-5.0	-10.2	-7.8
h_{33} ($10^8V/m$)	14.1	26.8	21.5	18.0	45.8	26.9
h_{15} ($10^8V/m$)	9.3	19.7	15.2	11.3	23.0	13.1
Dielectric constants under constant stress, T, and constant strain, S						
$\varepsilon_{11}^T/\varepsilon_0$	1300	1475	1730	3130	840	1291
$\varepsilon_{33}^T/\varepsilon_0$	1200	1300	1700	3400	425	1020
$\varepsilon_{11}^S/\varepsilon_0$	620	730	916	1700	460	898
$\varepsilon_{33}^S/\varepsilon_0$	590	635	830	1470	235	582
Electrical loss coefficient, tanδ, mechanical loss coefficient, Q_m						
tanδ	0.006	0.004	0.020	0.020	0.017	0.004
Q_m	400	500	75	65	600	1000
Material density						
ρ (kg/m^3)	5500	7500	7750	7500	7600	7600

Appendix II

THE QUALITY FACTOR

A2.1 Quality Factor Definition

The resonant efficiency of an oscillator is usually described in terms of the *quality factor, Q,* which is fundamentally defined by the following equation [95]:

$$Q = \frac{f_n}{f_2 - f_1} \tag{A2.1}$$

Here, f_n is the undamped natural frequency of the oscillator, and f_2 and f_1 are the frequencies either side of f_n for which the oscillator power drops to 50% of its peak value. All properties of free or forced oscillators can be described in terms of Q. For example, the resonant/zero frequency amplitude ratio is given by [95]:

$$\frac{\textit{resonant amplitude}}{\textit{zero frequency amplitude}} = Q\left(1 - \frac{1}{4Q^2}\right)^{-1/2} \tag{A2.2}$$

Provided the value of Q is not too close to unity, Equation (A2.2) approximates to:

$$\frac{\textit{resonant amplitude}}{\textit{zero frequency amplitude}} = Q \tag{A2.3}$$

Equation (A2.3) can be applied very accurately to the mechanical vibrations associated with all of the air coupled receiving transducers considered in this Thesis since, for example, a PZT-5A plate has a *mechanical quality factor,* Q_M, of 75. So, for an air coupled plate transducer:

$$\frac{d_R}{d_0} = Q_M \tag{A2.4}$$

where d_R is the amplitude of the particle displacement at the undamped natural resonance frequency and d_0 is the amplitude of the particle displacement at zero frequency. From Equation (A2.4) it follows that:

$$\frac{v_R}{v_0} = Q_M \tag{A2.5}$$

where v_R is the amplitude of the particle velocity at the undamped natural resonance frequency and v_0 is the amplitude of the particle velocity at zero frequency. In this Thesis a slightly different figure of merit for an oscillator has been introduced and this is defined by the following equation:

$$Q_\infty = \frac{v_R}{v_\infty} \tag{A2.6}$$

where v_∞ is the amplitude of the particle velocity in an infinite medium (no boundaries). Although Q_∞ has been found to be very useful in the work on noise, it is of little practical value. For example, Q_M and not Q_∞ is used when making experimental measurements. From Equations (A2.5) and (A2.6) it can be seen that:

$$Q_M = \left(\frac{v_\infty}{v_0}\right) Q_\infty \tag{A2.7}$$

For a plate transducer, the ratio v_∞/v_0 depends on the degree of external mechanical damping which has been applied. In the case of an air coupled transducer the ratio v_∞/v_0 is very small but finite. As will now be illustrated, the value of v_∞/v_0 for an air coupled plate transducer can be found using the original version of the Linear Systems Model.

A2.2 Linear Systems Model Analysis

As previously mentioned, a transducer's static or zero frequency displacement is a function of the degree of mechanical loading [79]. This feature can be demonstrated

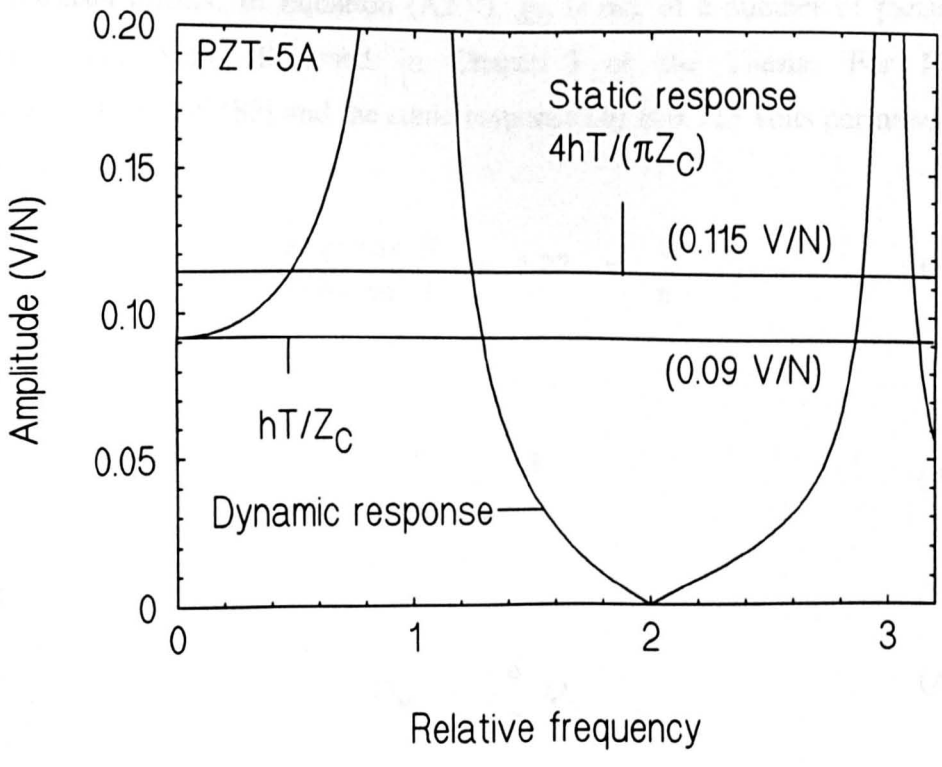

FIGURE A2.1 COMPARISON OF STATIC AND DYNAMIC RESPONSES FOR A 30 mm DIAMETER PZT-5A TRANSDUCER

with the aid of Figure A2.1 which was produced using the original Linear Systems Model, and which is based on a 30 mm diameter PZT-5A transducer with a fundamental thickness mode resonant frequency of 580 kHz. From this basic specification it can be shown that the transducer has a thickness (τ) of 3.24 mm and an area (A) of 7.1 x 10^{-4} m^2. From Appendix I, the piezoelectric charge constant (h_{33}) for PZT-5A is 21.5 x 10^8 V/m. The curve in Figure A2.1 represents a lightly damped response which is typical of an air coupled transducer. As indicated by the bottom horizontal line, this curve tends to a value (A) of 0.09 volts per newton as the frequency tends to zero. This value was obtained using Equation (5.15) which is reproduced here:

$$\frac{V_0(0)}{F_1(0)} = \frac{-k^2}{hC_0} = \frac{-hT}{Z_C} \cdot \qquad \text{(A2.8)}$$

The top horizontal line was obtained using:

$$\frac{V_0}{F_1} = \frac{g_{33}\tau}{A} \qquad \text{(A2.9)}$$

The difference between the last two equations is that Equation (A2.8) is based on a model which takes account of plate resonances and Equation (A2.9) assumes that there are no resonant effects. In Equation (A2.9), g_{33} is one of a number of piezoelectric constants which were discussed in Chapter 3 of the Thesis. For PZT-5A, g_{33}=24.9 x 10^{-3} Vm/N [83] and the static response (B) is 0.115 volts per newton. The ratio of the values is:

$$\frac{Response\ B}{Response\ A} = 1.27 = \frac{4}{\pi} \qquad \text{(A2.10)}$$

Hence:

$$\frac{v_\infty}{v_0} = \frac{4}{\pi} \qquad \text{(A2.11)}$$

Hence:

$$Q_M = \left(\frac{4}{\pi}\right) Q_\infty \qquad \text{(A2.12)}$$

Equation (A2.12) explains the existence of the $4/\pi$ terms which are conspicuous in the

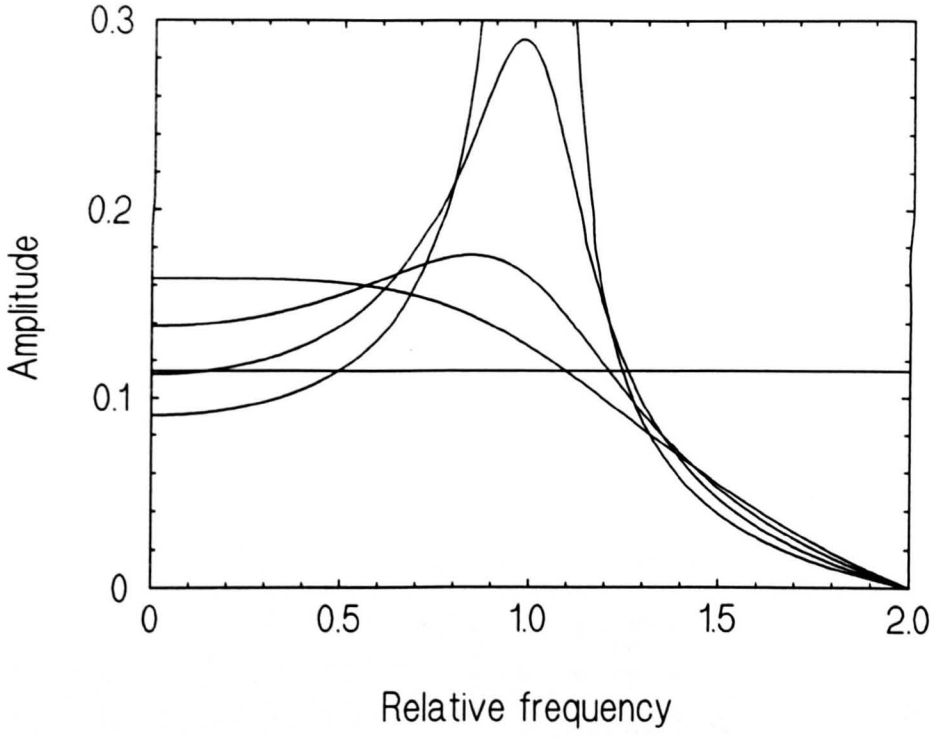

FIGURE A2.2 THE EFFECT OF INCREASED DAMPING ON THE ZERO FREQUENCY RESPONSE OF A PLATE TRANSDUCER

equations which have been derived for air coupled SNR, MDP and MDF. However, it should be noted that since Equation (A2.8) only applies to a lightly damped transducer, the same is true of Equation (A2.12). The effect of increased damping on the zero frequency response of a plate transducer is illustrated in Figure A2.2 which was obtained using the Mathcad model described in Appendix III. Here, it can be seen that as the level of damping is increased, the amplitude at the fundamental thickness mode resonance frequency decreases and the zero frequency amplitude increases. So, Equation (A2.12) can only be used for air coupled plate transducers.

A2.3 A Non-resonant Transducer

Reference has occasionally been made to a *non-resonant* transducer. This can be defined as a hypothetical transducer for which the force to voltage transfer function is described by Equation (2.9). So, over its entire frequency range this transducer exhibits no gain in particle velocity compared to the particle velocity in an infinite medium or a semi-infinite half-space. Since all real structures possess resonant properties the *non-resonant* definition should be considered as a mathematical convenience which provides a reference against which real devices can be compared. The particle velocity in a real transducer equals the particle velocity in a *non-resonant* transducer when $Q_M=4/\pi$.

Appendix III

Mathcad Version of the Original
Linear Systems Model

ORIGINAL LINEAR SYSTEMS NOISE MODEL

This is a Mathcad version of the original Linear Systems Noise Model (LSM). The input parameters are for a PZT-5A piezoceramic plate transducer and a ZN460 ultra low noise pre-amplifier:

$f := 1000, 10000 .. 2 \cdot 10^6$			Frequency range of interest
$fo := .58 \cdot 10^6$			Resonant frequency of transducer
$K_{33} := 916$			Relative dielectric constant
$\varepsilon_0 := 8.85 \cdot 10^{-12}$			Permettivity of free space
$d := 30 \cdot 10^{-3}$	$r := \frac{d}{2}$	$A := \pi \cdot r^2$	Diameter, radius, area
$v := 4350$	$\lambda := \frac{v}{fo}$	$\lambda = 0.007$	Wave velocity [Kino] and wave length
$W := \frac{\lambda}{2}$	$W = 0.00375$		Transducer thickness
$Co := \frac{K_{33} \cdot \varepsilon_0 \cdot \pi \cdot r^2}{W}$	$Co = 1.528 \cdot 10^{-9}$		Transducer static capacitance
$h_{33} := 21.5 \cdot 10^8$	$h := h_{33}$		Piezoelectric charge constant
$\rho := 7750$	$\rho \cdot v = 3.371 \cdot 10^7$		Density, characteristic impedance
$Zc := \rho \cdot v \cdot A$	$Zc = 2.383 \cdot 10^4$		Impedance (mech.) of transducer
$Z1 := 400 \cdot A$	(air)		Impedance (mech.) of front face medium
$Z2 := 400 \cdot A$	(air)		Impedance (mech.) of rear face medium
$T := \frac{1}{2 \cdot fo}$	$T = 8.621 \cdot 10^{-7}$		Transit time from front face to back face
$k := \sqrt{\frac{h^2 \cdot Co \cdot T}{Zc}}$	$k = 0.505$		Electromechanical coupling coefficient
$wo := 2 \cdot \pi \cdot fo$	$wo = 3.644 \cdot 10^6$		Mechanical resonance - angular
$w(f) := 2 \cdot \pi \cdot f$			Frequency range of interest - angular
$Rf := \frac{Zc - Z1}{Zc + Z1}$	$Rf = 1$		Front face reflection coefficient (force)
$Rb := \frac{Zc - Z2}{Zc + Z2}$	$Rb = 1$		Rear face reflection coefficient (force)
$Tf := \frac{2 \cdot Zc}{Zc + Z1}$	$Tf = 2$		Transmission coefficient (front face)
$Tb := \frac{2 \cdot Zc}{Zc + Z2}$	$Tb = 2$		Transmission coefficient (back face)
$La := .02$ (intrinsic damping factor)			Loss due to attenuation of sound
$Ra := 3 \cdot 10^3$			Preamplifier input impedance (typical)
$va := 1 \cdot 10^{-9}$			Pre-amplifier voltage noise generator
$ia := 1 \cdot 10^{-12}$			Pre-amplifier current noise generator

FORCE TO VOLTAGE TRANSFER FUNCTION AND ELECTRICAL IMPEDANCE

$$Kf(f) := \frac{\left(1 - e^{-j \cdot w(f) \cdot T - La}\right) \cdot \left(1 - Rb \cdot e^{-j \cdot w(f) \cdot T - La}\right)}{1 - Rf \cdot Rb \cdot e^{-j \cdot 2 \cdot w(f) \cdot T - 2 \cdot La}}$$

Reverberation factor (front face)

$$Kb(f) := \frac{\left(1 - e^{-j \cdot w(f) \cdot T - La}\right) \cdot \left(1 - Rf \cdot e^{-j \cdot w(f) \cdot T - La}\right)}{1 - Rf \cdot Rb \cdot e^{-j \cdot 2 \cdot w(f) \cdot T - 2 \cdot La}}$$

Reverberation factor (back face)

$$U(f) := \frac{j \cdot w(f) \cdot Co \cdot Ra}{1 + j \cdot w(f) \cdot Co \cdot Ra}$$

Forward path attenuation factor (FPA)

$$Zf(f) := \frac{1}{1 + j \cdot w(f) \cdot Co \cdot Ra}$$

Feedback factor (controls secondary piezoelectric action)

$$Vf(f) := \frac{-h \cdot Tf \cdot Kf(f) \cdot U(f) \cdot \frac{1}{j \cdot w(f) \cdot Zc}}{1 - Zf(f) \cdot \left(\frac{Tf \cdot Kf(f)}{2} + \frac{Tb \cdot Kb(f)}{2}\right) \cdot \frac{k^2}{j \cdot w(f) \cdot T}}$$

Force to voltage transfer function

$$Zt(f) := \frac{1}{j \cdot w(f) \cdot Co} \cdot \left[1 - \frac{k^2}{j \cdot w(f) \cdot T} \cdot \left(Kf(f) \cdot \frac{Tf}{2} + Kb(f) \cdot \frac{Tb}{2}\right)\right]$$

Electrical impedance

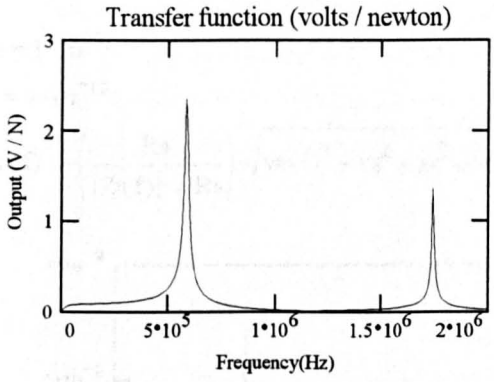

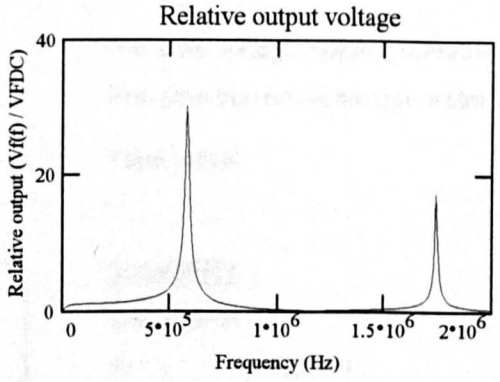

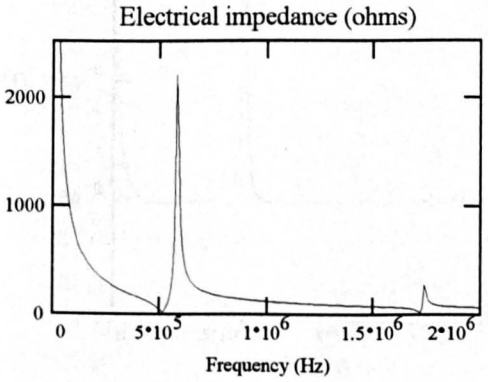

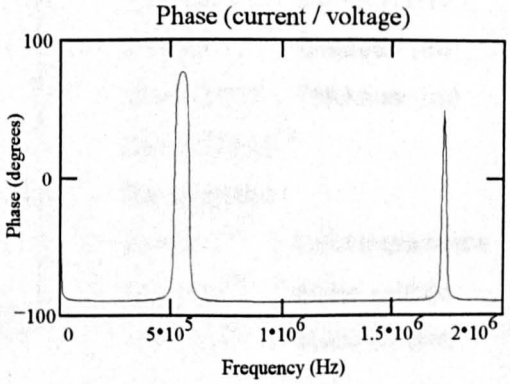

TRANSDUCER NOISE

The thermal noise produced by the transducer can be calculated from the real part of the electrical impedance:-

$Kb := 1.38 \cdot 10^{-23}$ — Boltzmann's constant

$Tr := 293.15$ — Temperature (293.15 K is 20 deg C)

$Pn := 4 \cdot Kb \cdot Tr \qquad Pn = 1.618 \cdot 10^{-20}$ — Noise power

$vn(f) := \sqrt{4 \cdot Kb \cdot Tr \cdot Re(Zt(f))}$ — Transducer thermal noise (volts - r.m.s.)

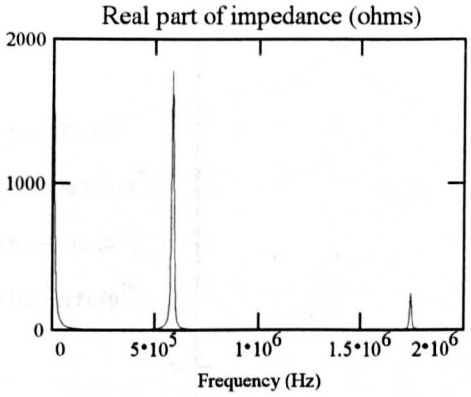

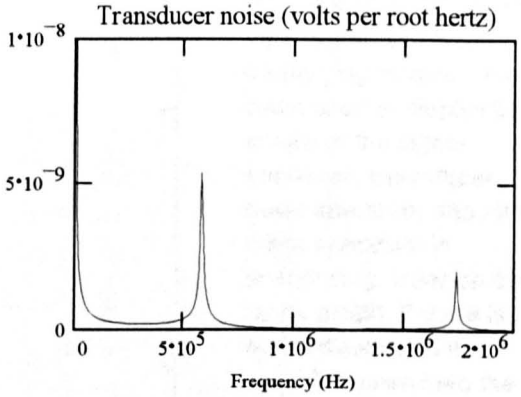

Additional noise from pre-amplifier:-

$va = 1 \cdot 10^{-9}$ — Pre-amp voltage noise generator

$ia = 1 \cdot 10^{-12}$ — Pre-amp current noise generator

$vnt(f) := \left(\frac{Ra}{|Zt(f)| + Ra}\right) \cdot \sqrt{vn(f)^2 + va^2 + ia^2 \cdot (|Zt(f)|)^2}$ — Total noise

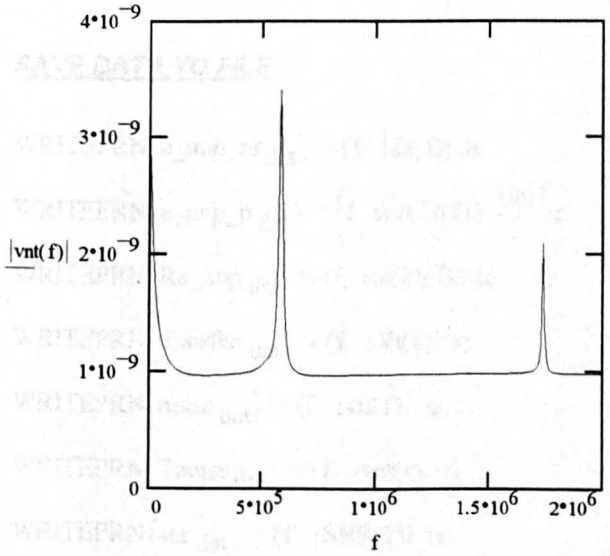

SUMMARY

Transducer:-

$Rf = 1$ $\qquad Rb = 1$

$k = 0.505$ $\qquad \rho \cdot v = 3.371 \cdot 10^{7}$

$d = 0.03$ — Diameter (m)

$W = 0.00375$ — Thickness (m)

$Co = 1.528 \cdot 10^{-9}$

Pre-amplifier:-

$Ra = 3 \cdot 10^{3}$ — Input impedance

$va = 1 \cdot 10^{-9}$ — Noise voltage

$ia = 1 \cdot 10^{-12}$ — Noise current

SIGNAL TO NOISE RATIO

For an input force of 1 newton per root hertz (r.m.s.) the signal to noise ratio can be found as follows.

Input force: $Fin := 1$ Hence: $$SNR(f) := \frac{|Vf(f)| \cdot \left(\frac{Ra}{|Zt(f)| + Ra}\right)}{|vnt(f)|}$$

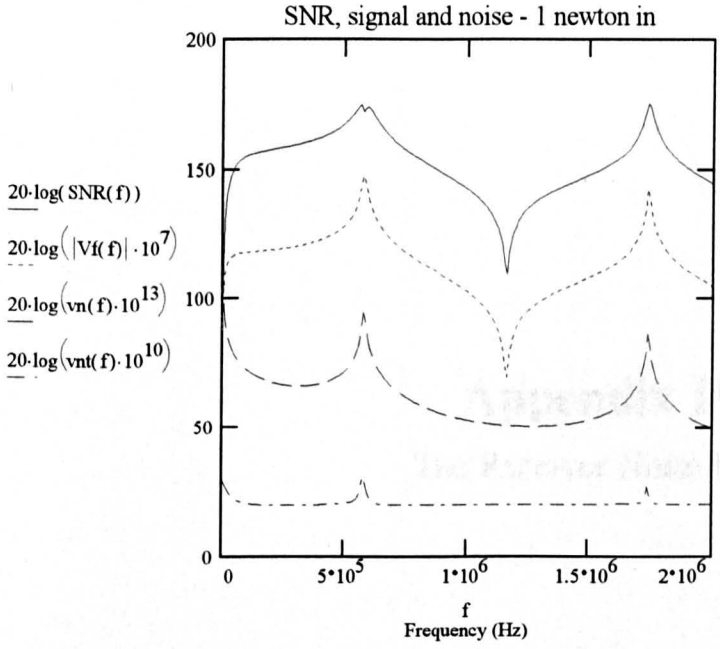

The signal to noise ratio displayed is exact for an input signal of 1N r.m.s. Multiplying factors have been used to display the shape of the signal spectrum, transducer noise spectrum and total noise spectrum in descending order on the same graph. If there is no feedback and no amplifier noise then the noise spectrum has the same shape as the signal spectrum and hence the SNR is flat w.r.t. frequency.

$20 \cdot \log(SNR(fo)) = 170.439$ Signal to noise ratio at fundamental resonance frequency

SAVE DATA TO FILE

$WRITEPRN(e\_imp\_m_{dat}) := (f \ \ |Zt(f)| \ )$

$WRITEPRN(e\_imp\_p_{dat}) := \left(f \ \ arg(Zt(f)) \cdot \frac{180}{\pi}\right)$

$WRITEPRN(Re\_imp_{dat}) := (f \ \ Re(Zt(f)) \ )$

$WRITEPRN(transfun_{dat}) := (f \ \ |Vf(f)| \ )$

$WRITEPRN(noise_{dat}) := (f \ \ |vn(f)| \ )$

$WRITEPRN(Tnoise_{dat}) := (f \ \ |vnt(f)| \ )$

$WRITEPRN(snr_{dat}) := (f \ \ |SNR(f)| \ )$

Appendix IV

The Receiver Noise Model

THE RECEIVER NOISE MODEL

This *Mathcad* document illustrates the operation of the The Receiver Noise Model (RNM). As discussed in the main text of the Ph.D. thesis, the RNM is based on an extensively modified version of the Linear Systems Model (LSM). A key component of the modified LSM is the mechanical gain equation which expresses the relative sensitivity of an open circuit transducer as a function of relative frequency, R. The entire performance of an open circuit transducer is controlled by the mechanical quality factor, Q_M.

The following input parameters are for a typical PZT-5A transducer and a ZN460 ultra low noise pre-amplifier:

$Q_M := 75$

Let the relative frequency range be:

$R := .01, .013 .. 3.5$

The relative sensitivity is given by:

$$G_0(R) := \frac{1}{j \cdot R} \cdot \left(\frac{1}{Q_M} + \frac{\pi}{2} \cdot \frac{1 + e^{-j \cdot \pi \cdot R}}{1 - e^{-j \cdot \pi \cdot R}} \right)^{-1}$$

The magnitude and the argument of this equation are plotted below for the given parameters.

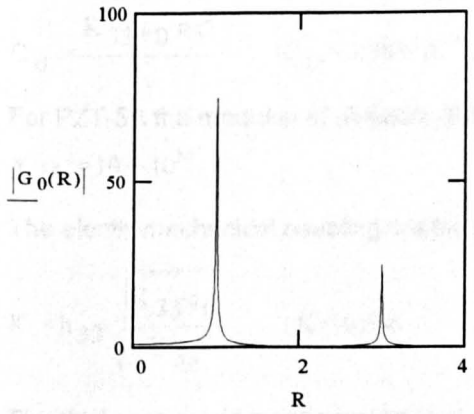

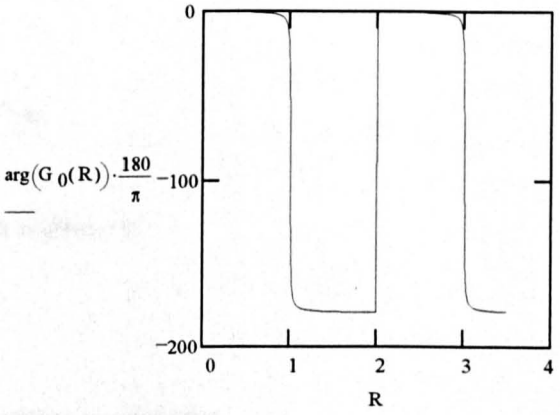

Consider a transducer with a fundamental thickness mode resonance frequency (Hz) of:

$f_n := 580 \cdot 10^3 \qquad \omega_n := 2 \cdot \pi \cdot f_n \qquad \omega_n = 3.644 \cdot 10^6$

For PZT-5A the wave velocity (ms^{-1}) is:

$c := 4350$

Hence the wave length (m) is:

$$\lambda := \frac{c}{f_n} \qquad \lambda = 7.5 \cdot 10^{-3}$$

and the thickness (m) of the transducer is:

$$\tau := \frac{\lambda}{2} \qquad \tau = 3.75 \cdot 10^{-3}$$

For PZT-5A the piezoelectric charge constant (Vm^{-1}) is:

$h_{33} := 21.5 \cdot 10^{8}$

the relative dielectric constant (constant strain) is:

$K_{33} := 830$

and the material density (kgm^{-3}) is:

$\rho := 7.75 \cdot 10^{3}$

It follows that the characteristic acoustic impedance of the material is:

$Z_{CHA} := \rho \cdot c \qquad Z_{CHA} = 3.371 \cdot 10^{7}$

Let the radius (m) of the transducer be:

$r := 15 \cdot 10^{-3}$

It follows that the transducer area is:

$A := \pi \cdot r^{2} \qquad A = 7.069 \cdot 10^{-4}$

Also, the acoustic impedance of the device is then:

$Z_{C} := A \cdot Z_{CHA} \qquad Z_{C} = 2.383 \cdot 10^{4}$

The permittivity (Fm^{-1}) of free space is:

$\varepsilon_{0} := 8.85 \cdot 10^{-12}$

The static capacitance of the transducer is:

$$C_{0} := \frac{K_{33} \cdot \varepsilon_{0} \cdot \pi \cdot r^{2}}{\tau} \qquad C_{0} = 1.385 \cdot 10^{-9}$$

For PZT-5A the modulus of elasticity (Nm^{-2}) is:

$Y_{33} := 10.6 \cdot 10^{10}$

The electromechanical coupling coefficient is given by:

$$K := h_{33} \cdot \sqrt{\frac{K_{33} \cdot \varepsilon_{0}}{Y_{33}}} \qquad K = 0.566$$

The thickness mode electromechanical coupling coefficient is:

$$k := \sqrt{\frac{K^{2}}{1 + K^{2}}} \qquad k = 0.493$$

Consider a transducer connected to a resistive load, R_L. The ZN460 pre-amplifier has an input resistance (ohms) of:

$R_{L} := 7000$

For convenience define:

$R_{2} := \omega_{n} \cdot R_{L} \cdot C_{0} \qquad R_{2} = 35.321$

The R_2 figure of merit along with the thickness mode electromechanical coupling coefficient can be used to find the equivalent Q of the electrically loaded transducer. This can be done using:

$$Q_E := \left| \left[\frac{1}{Q_M} \cdot \left(\frac{1}{j \cdot R_2} + 1 \right) - \frac{k^2}{j \cdot R_2} \right]^{-1} \right| \qquad Q_E = 67.433$$

Also, the relative sensitivity of the electrically loaded transducer is given by:

$$G(R) := \left[\frac{1}{G_0(R)} \cdot \left(\frac{1}{j \cdot R \cdot R_2} + 1 \right) - \frac{k^2}{j \cdot R \cdot R_2} \right]^{-1}$$

The magnitude of this equation is plotted below as a function of the actual frequency.

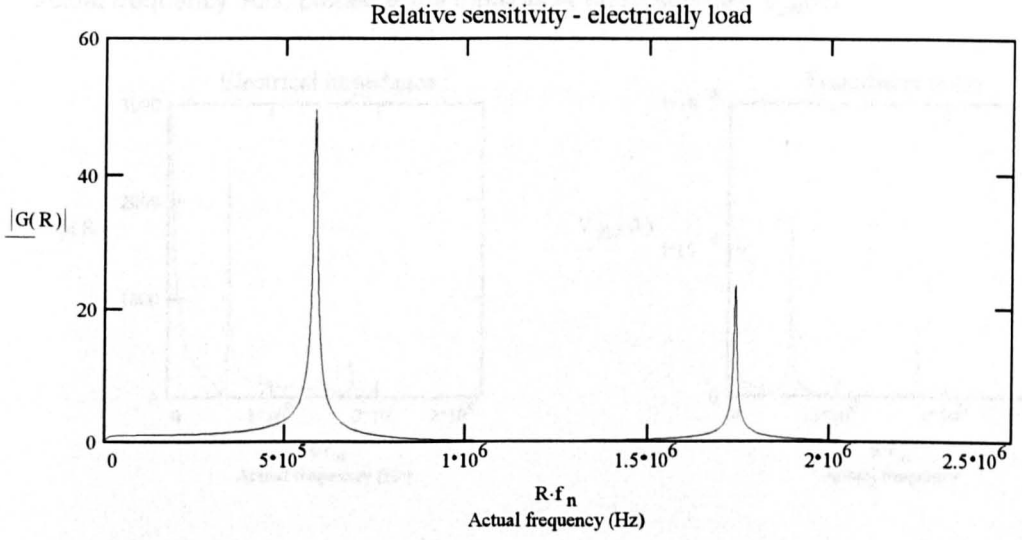

The effect of electrical loading on the transducer can be judged by comparing this graph with the previous one for $G_0(R)$. It can be seen that this particular amplifier has very little effect on the performance of the transducer. The only significant difference is that the Q of the transducer has been reduced by the following percentage:

$$\frac{Q_M - Q_E}{Q_M} \cdot 100 = 10.089$$

As a consequence of electrical loading, the bandwidth of the transducer has been increased from:

$$B_0 := \frac{f_n}{Q_M} \qquad B_0 = 7.733 \cdot 10^3$$

to:

$$B_E := \frac{f_n}{Q_E} \qquad B_E = 8.601 \cdot 10^3$$

TRANSDUCER NOISE

In order to calculate the total system noise it is necessary to know the transducer's electrical impedance. This is given by:

$$Z_E(R) := \frac{1 - k^2 \cdot G(R)}{j \cdot \omega_n \cdot R \cdot C_0}$$

Knowing Boltzmann's constant (k_B) and the absolute temperature (T_A), the corresponding electrical noise is:

$$k_B := 1.38 \cdot 10^{-23} \quad T_A := 293 \quad V_{JN}(R) := \left| \sqrt{4 \cdot k_B \cdot T_A \cdot Re(Z_E(R))} \right|$$

The magnitude of the transducer impedance (in ohms) is plotted below as a function of the actual frequency. Also plotted is the transducer noise sources, $V_{JN}(R)$.

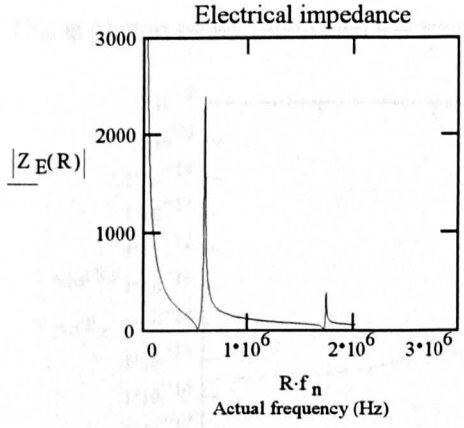

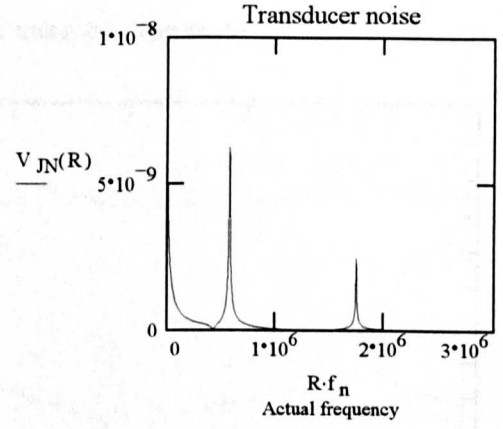

TRANSFER FUNCTION

The time taken for a sound wave to travel from one face of the transducer to the opposite face is given by:

$$T := \frac{1}{2 \cdot f_n}$$

$$T = 8.621 \cdot 10^{-7}$$

In the new model, the force to voltage transfer function is given by:

$$V_S(R) = \frac{-h_{33} \cdot T}{Z_C} \cdot G(R) \cdot F_{SM} \qquad (T_F \text{ is incorporated in } h_{33}T/Z_C)$$

Here, $V_S(R)$ is the signal voltage across the terminals of the transducer and F_{SM} is the signal force in the coupling medium.

EXTERNAL NOISE

Using the Callen and Welton theorem it is possible to calculate the amplitude of the force fluctuations in the coupling medium. In order to do this it is necessary to know the acoustic impedance (Z_1) of the coupling medium:

$Z_1 := 400 \cdot A \qquad Z_1 = 0.283$

The external noise (F_{NM}) is:

$F_{NM} := \sqrt{4 \cdot k_B \cdot T \cdot Z_1}$

The magnitude of the equivalent voltage noise can be found using the transfer function. Thus:

$$V_{NM}(R) := \left| \frac{-h_{33} \cdot T}{Z_C} \cdot G(R) \cdot F_{NM} \right|$$

This is plotted below along with the transducer noise on a log scale:

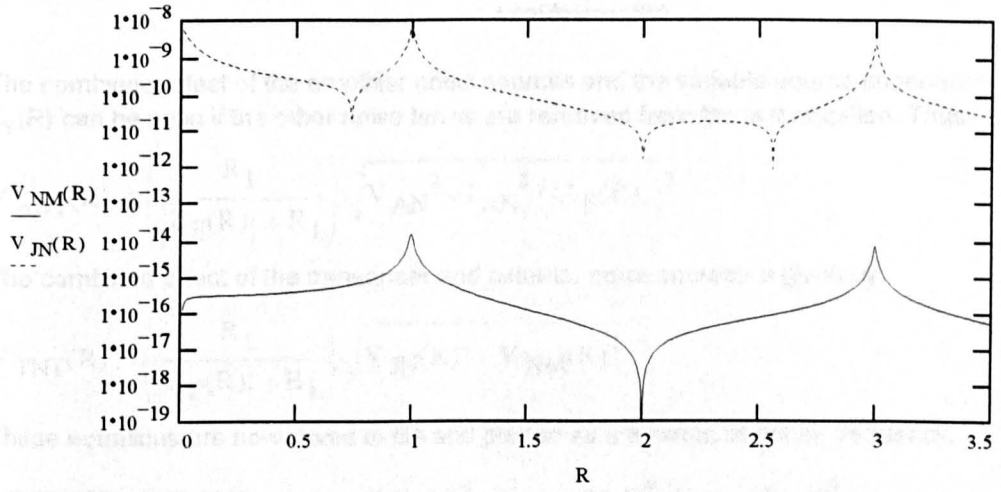

TOTAL NOISE

For the ZN460 pre-amplifier the equivalent input voltage noise spectral density (volts per root Hertz) is:

$V_{AN} := 800 \cdot 10^{-12}$

The current noise spectral density (amps per root Hertz) is:

$I_{AN} := 1 \cdot 10^{-12}$

The total receiver noise (front-end) is given by:

$$V_{RN}(R) := \left(\frac{R_L}{|Z_E(R)| + R_L} \right) \cdot \sqrt{V_{AN}^2 + I_{AN}^2 \cdot \left(|Z_E(R)| \right)^2 + V_{JN}(R)^2 + V_{NM}(R)^2}$$

This equation is now saved to file and plotted as a function of the actual frequency:

$$\text{WRITEPRN}(\text{VRN}_{\text{DAT}}) := \left(R \cdot f_n \cdot 10^{-6} \quad |V_{RN}(R)| \cdot 10^{9}\right)$$

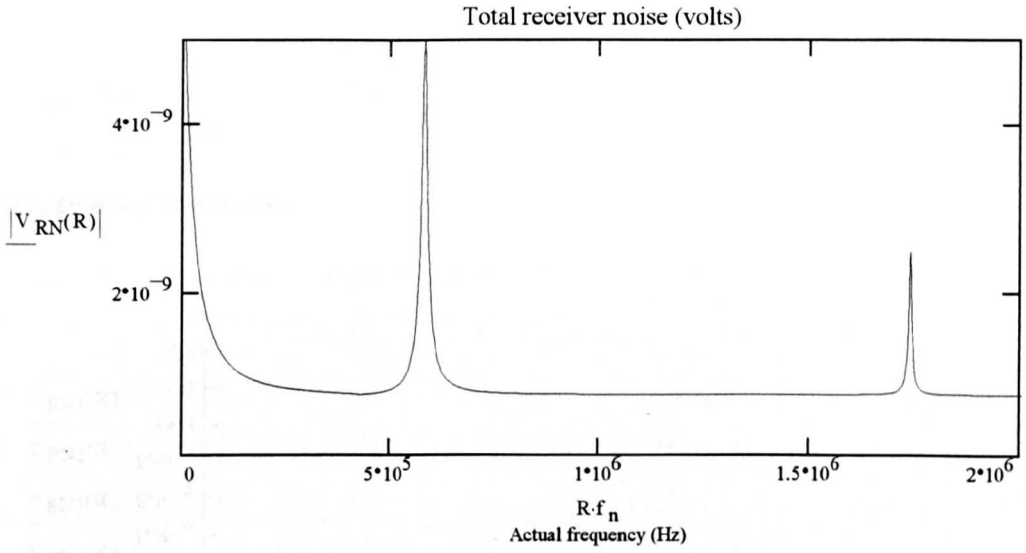

The combined effect of the amplifier noise sources and the variable source impedance $Z_E(R)$ can be seen if the other noise terms are removed from the last equation. Thus:

$$V_{ANT}(R) := \left(\frac{R_L}{|Z_E(R)| + R_L}\right) \cdot \sqrt{V_{AN}^2 + I_{AN}^2 \cdot \left(|Z_E(R)|\right)^2}$$

The combined effect of the transducer and external noise sources is given by:

$$V_{TNT}(R) := \left(\frac{R_L}{|Z_E(R)| + R_L}\right) \cdot \sqrt{V_{JN}(R)^2 + V_{NM}(R)^2}$$

These equations are now saved to file and plotted as a function of actual frequency.

$$\text{WRITEPRN}(\text{ANT\_TNT}_{\text{DAT}}) := \left(R \cdot f_n \cdot 10^{-6} \quad V_{ANT}(R) \cdot 10^{9} \quad V_{TNT}(R) \cdot 10^{9}\right)$$

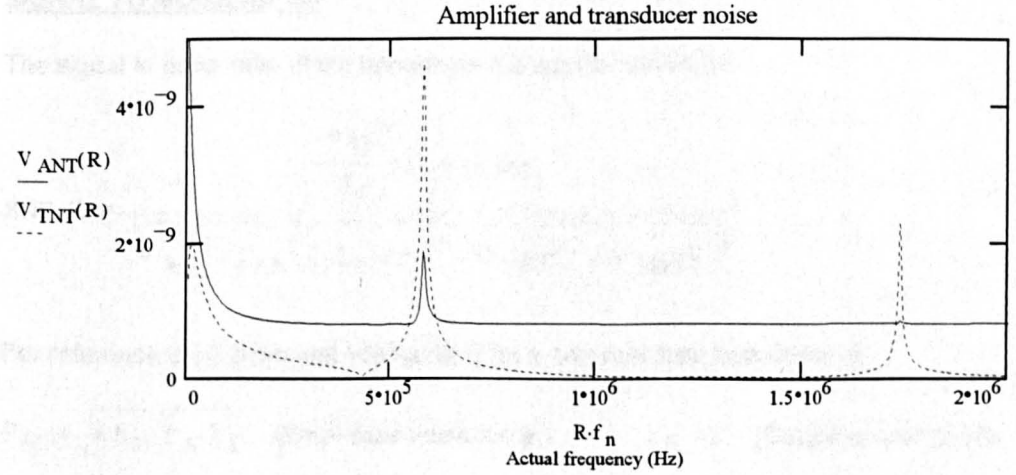

The individual noise sources as they would appear at the pre-amplifier input are:

$$V_{RN1}(R) := \left(\frac{R_L}{|Z_E(R)| + R_L}\right) \cdot V_{AN} \cdot 10^9 \qquad V_{RN2}(R) := \left(\frac{R_L}{|Z_E(R)| + R_L}\right) \cdot I_{AN} \cdot |Z_E(R)| \cdot 10^9$$

$$V_{RN3}(R) := \left(\frac{R_L}{|Z_E(R)| + R_L}\right) \cdot V_{NM}(R) \cdot 10^9 \qquad V_{RN4}(R) := \left(\frac{R_L}{|Z_E(R)| + R_L}\right) \cdot V_{JN}(R) \cdot 10^9$$

These are plotted below:

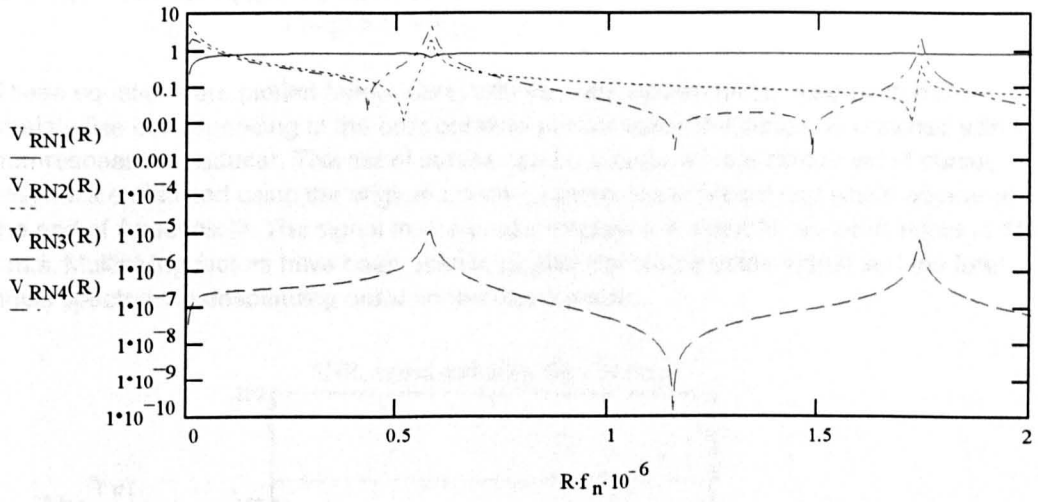

Save to file (nV and MHz):

$$\text{WRITEPRN}(\text{VRN\_X4 DAT}) := \left(R \cdot f_n \cdot 10^{-6} \quad V_{RN1}(R) \quad V_{RN2}(R) \quad V_{RN3}(R) \quad V_{RN4}(R)\right)$$

SIGNAL TO NOISE RATIO

The signal to noise ratio at the transducer's output terminals is:

$$SNR(R) = \frac{\frac{-h_{33} \cdot T}{Z_C} \cdot G(R) \cdot F_{SM}}{\sqrt{V_{AN}^2 + I_{AN}^2 \cdot \left(|Z_E(R)|\right)^2 + V_{JN}(R)^2 + V_{NM}(R)^2}}$$

For reference the Callen and Welton limit for a non-resonant transducer is:

$F_N := \sqrt{4 \cdot k_B \cdot T_A \cdot Z_C}$ (Front face noise force.) $T_F := 2$ (Coupling coefficient)

For F_{SM}=1 N the signal to noise ratio is:

$$SNR1(R) := \frac{\frac{-h_{33} \cdot T}{Z_C} \cdot G(R)}{\sqrt{V_{AN}^2 + I_{AN}^2 \cdot \left(\left|Z_E(R)\right|\right)^2 + V_{JN}(R)^2 + V_{NM}(R)^2}}$$

For F_{SM}=1 N the amplitude of the signal (volts) at the pre-amp input is:

$$V_{S1}(R) := \frac{-h_{33} \cdot T}{Z_C} \cdot G(R) \cdot \left(\frac{R_L}{\left|Z_E(R)\right| + R_L}\right)$$

These equations are plotted below along with the total system noise. Also plotted is a straight line corresponding to the best possible performance that could be obtained with a non-resonant transducer. This set of curves can be compared to a similar set of curves which were obtained using the original Linear Systems Noise Model and which appear at the end of Appendix III. The signal to noise ratio displayed is exact for an input signal of 1N r.m.s. Multiplying factors have been used to display the shape of the signal and the total noise spectrum in descending order on the same graph.

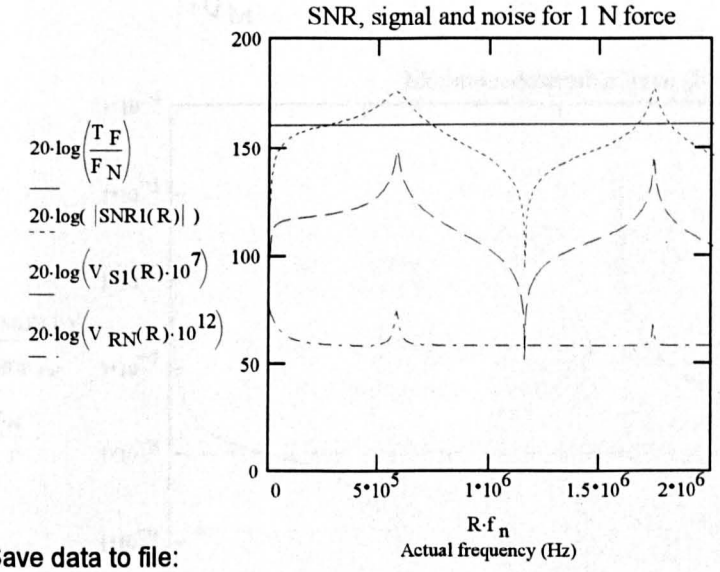

Save data to file:

$$WRITEPRN(SNR\_A\_DAT) := \left(R \cdot f_n \cdot 10^{-6} \quad 20 \cdot \log\left(\frac{T_F}{F_N}\right)\right)$$

$$WRITEPRN(SNR\_B\_DAT) := \left(R \cdot f_n \cdot 10^{-6} \quad 20 \cdot \log\left(\left|SNR1(R)\right|\right)\right)$$

$$WRITEPRN(SNR\_C\_DAT) := \left(R \cdot f_n \cdot 10^{-6} \quad 20 \cdot \log\left(V_{S1}(R) \cdot 10^7\right)\right)$$

$$WRITEPRN(SNR\_D\_DAT) := \left(R \cdot f_n \cdot 10^{-6} \quad 20 \cdot \log\left(V_{RN}(R) \cdot 10^{12}\right)\right)$$

MINIMUM DETECTABLE SIGNAL

Setting SNR(R)=1, the minimum detectable force in the coupling medium is:

$$MDF(R) := \frac{\sqrt{V_{AN}^2 + I_{AN}^2 \cdot \left(\left|Z_E(R)\right|\right)^2 + V_{JN}(R)^2 + V_{NM}(R)^2}}{\frac{-h_{33} \cdot T}{Z_C} \cdot G(R)}$$

With no amplifier noise this last equation becomes:

$$MDF_{NN}(R) := \frac{\sqrt{V_{JN}(R)^2 + V_{NM}(R)^2}}{\frac{-h_{33} \cdot T}{Z_C} \cdot G(R)}$$

Open circuit reference:

$$MDF_{OC} := \frac{\sqrt{4 \cdot k_B \cdot T_A \cdot Z_C}}{\sqrt{\pi \cdot Q_M}}$$

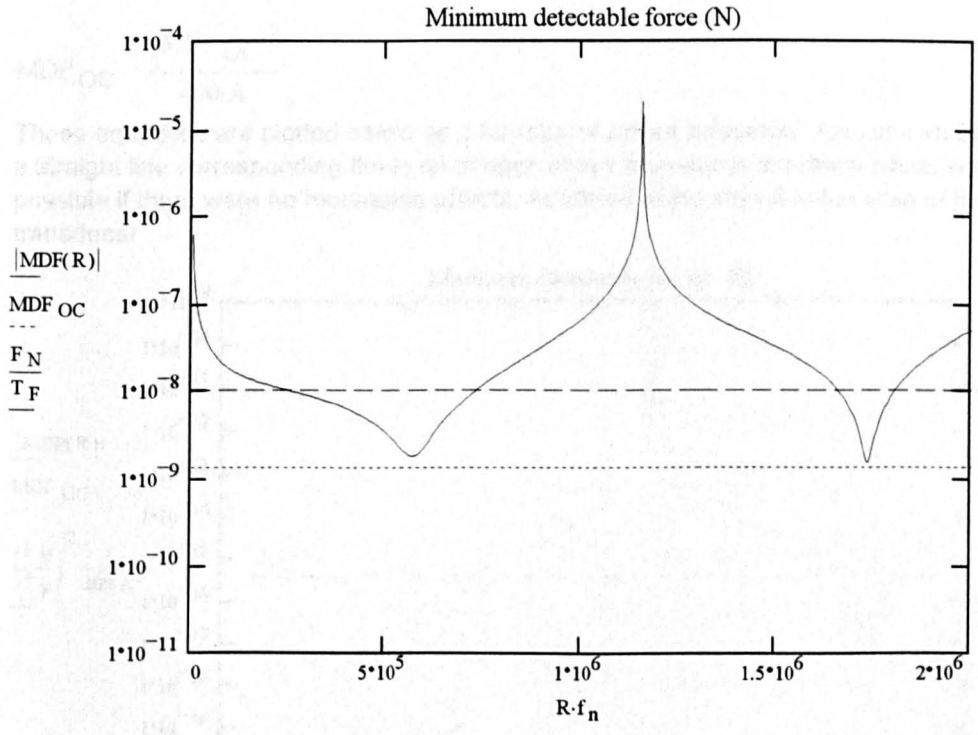

Also shown in the last graph is a straight line corresponding the level of open circuit transducer sensitivity which would be possible if there were no resonance effects. Clearly resonance results in an improvement in sensitivity and a loss of bandwidth.

Save MDF data to file:

$$\text{WRITEPRN}(\text{MDF\_A}_{\text{DAT}}) := \left(R \cdot f_n \cdot 10^{-6} \quad |\text{MDF}(R)|\right)$$

$$\text{WRITEPRN}(\text{MDF\_B}_{\text{DAT}}) := \left(R \cdot f_n \cdot 10^{-6} \quad |\text{MDF}_{\text{NN}}(R)|\right)$$

$$\text{WRITEPRN}(\text{MDF\_C}_{\text{DAT}}) := \left(R \cdot f_n \cdot 10^{-6} \quad |\text{MDF}_{\text{OC}}|\right)$$

$$\text{WRITEPRN}(\text{MDF\_D}_{\text{DAT}}) := \left(R \cdot f_n \cdot 10^{-6} \quad \frac{F_N}{T_F}\right)$$

Since the acoustic impedance of air is 400 MRayl, the minimum detectable power in the coupling medium is given by:

$$\text{MDP}(R) := \frac{(\text{MDF}(R))^2}{400 \cdot A}$$

With no amplifier noise the MDP is:

$$\text{MDP}_{\text{NN}}(R) := \frac{(\text{MDF}_{\text{NN}}(R))^2}{400 \cdot A}$$

With no amplifier noise and no electrical loading the MDP is:

$$\text{MDP}_{\text{OC}} := \frac{(\text{MDF}_{\text{OC}})^2}{400 \cdot A}$$

These equations are plotted below as a function of actual frequency. Also shown below is a straight line corresponding the level of open circuit transducer sensitivity which would be possible if there were no resonance effects. As stated at the start *A* is the area of the transducer.

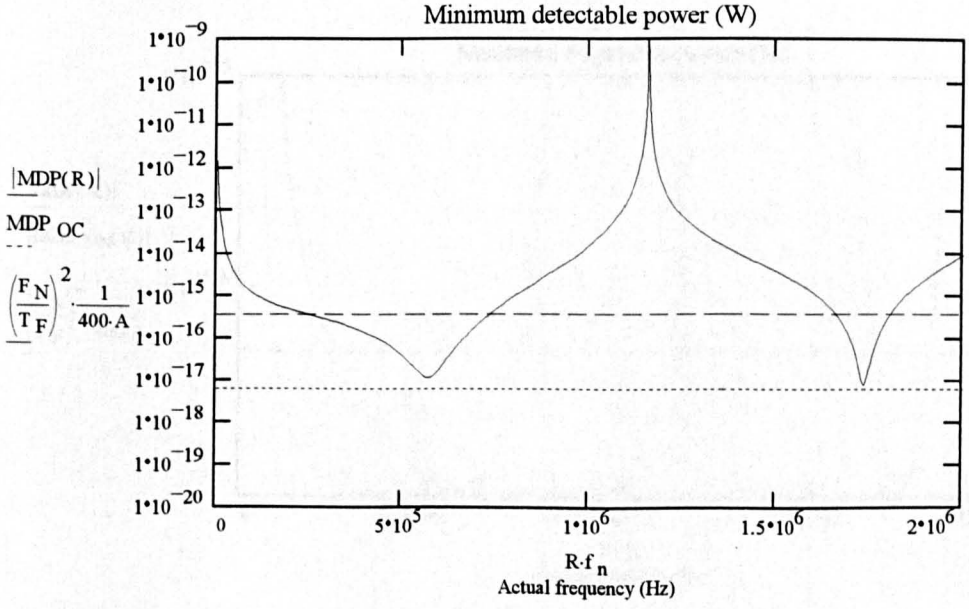

Save MDP data to file:

$$\text{WRITEPRN}(\text{MDP\_A}_{\text{DAT}}) := \left(R \cdot f_n \cdot 10^{-6} \quad |\text{MDP}(R)|\right)$$

$$\text{WRITEPRN}(\text{MDP\_B}_{\text{DAT}}) := \left(R \cdot f_n \cdot 10^{-6} \quad |\text{MDP}_{\text{NN}}(R)|\right)$$

$$\text{WRITEPRN}(\text{MDP\_C}_{\text{DAT}}) := \left(R \cdot f_n \cdot 10^{-6} \quad |\text{MDP}_{\text{OC}}|\right)$$

$$\text{WRITEPRN}(\text{MDP\_D}_{\text{DAT}}) := \left[R \cdot f_n \cdot 10^{-6} \quad \left(\frac{F_N}{T_F}\right)^2 \cdot \frac{1}{400 \cdot A}\right]$$

Detailed version of the MDF graph:

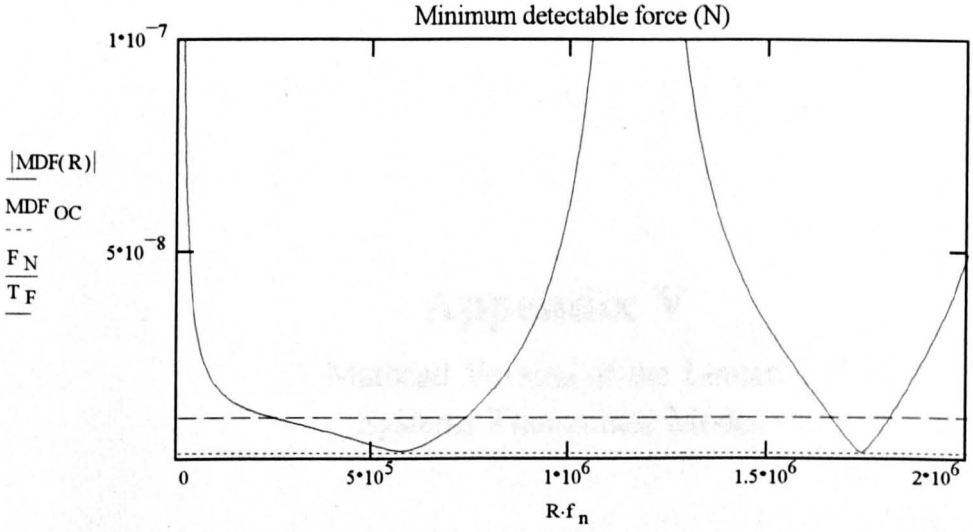

Detailed version of the MDP graph:

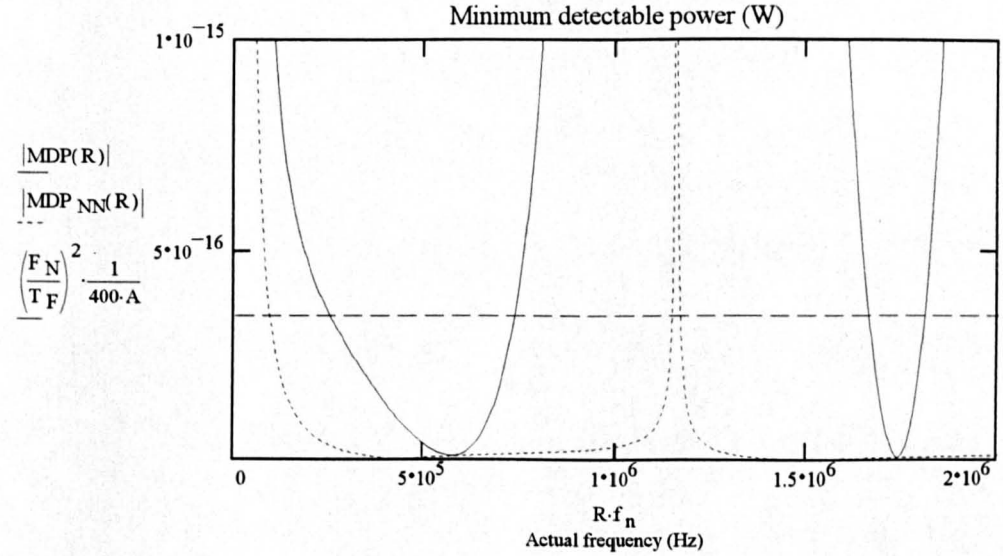

Appendix V

Mathcad Version of the Linear
Systems Transmitter Model

LINEAR SYSTEMS TRANSMITTER MODEL

The purpose of this Mathcad version of the Linear Systems Transmitter Model is to calculate the efficiency with which a piezoceramic plate transducer can convert electrical power into mechanical power. The model input parameters are as follows:

$f := 1, 2000 .. 1.5 \cdot 10^6$ — Frequency range of interest

$f_n := .650 \cdot 10^6$ — Resonant frequency of transducer

$K_{33} := 916$ — Relative dielectric constant

$\varepsilon_0 := 8.85 \cdot 10^{-12}$ — Permittivity of free space

$d := 30 \cdot 10^{-3}$ $\quad r := \frac{d}{2}$ $\quad A := \pi \cdot r^2$ — Diameter, radius, area

$N_{33} := 1880$ $\quad v := N_{33} \cdot 2$ $\quad v = 3.76 \cdot 10^3$ — Frequency constant and velocity

$t := \frac{N_{33}}{f_n}$ $\quad t = 0.00289$ — Transducer thickness

$C_0 := \frac{K_{33} \cdot \varepsilon_0 \cdot \pi \cdot r^2}{t}$ $\quad C_0 = 1.981 \cdot 10^{-9}$ — Transducer static capacitance

$h_{33} := 21.5 \cdot 10^8$ $\quad h := h_{33}$ — Piezoelectric charge constant

$\rho := 7750$ $\quad \rho \cdot v = 2.914 \cdot 10^7$ — Density, characteristic impedance

$Z_C := \rho \cdot v \cdot A$ $\quad Z_C = 2.06 \cdot 10^4$ — Impedance (mech.) of transducer

$Z_1 := 400 \cdot A$ — Impedance of front face medium

$Z_2 := 400 \cdot A$ — Impedance of front face medium

$T := \frac{1}{2 \cdot f_n}$ $\quad T = 7.692 \cdot 10^{-7}$ — Transit time from front to back face

$k := \sqrt{\frac{h^2 \cdot C_0 \cdot T}{Z_C}}$ $\quad k = 0.585$ — Electromechanical coupling coefficient

$\omega_0 := 2 \cdot \pi \cdot f_n$ $\quad \omega_0 = 4.084 \cdot 10^6$ — Mechanical resonance - angular

$\omega(f) := 2 \cdot \pi \cdot f$ — Frequency range of interest - angular

$R_F := \frac{Z_C - Z_1}{Z_C + Z_1}$ $\quad R_F = 1$ — Front face reflection coefficient (force)

$R_B := \frac{Z_C - Z_2}{Z_C + Z_2}$ $\quad R_B = 1$ — Rear face reflection coefficient (force)

$T_F := \frac{2 \cdot Z_C}{Z_C + Z_1}$ $\quad T_F = 2$ — Transmission coefficient (front face)

$T_B := \frac{2 \cdot Z_C}{Z_C + Z_2}$ $\quad T_B = 2$ — Transmission coefficient (back face)

$$A_F := \frac{2 \cdot Z_1}{Z_C + Z_1} \qquad A_F = 2.745 \cdot 10^{-5}$$ Transmission coefficient

$$k := \sqrt{\frac{h^2 \cdot C_0 \cdot T}{Z_C}} \qquad k = 0.585$$ Electromechanical coupling coefficient

$La := .02$ **(intrinsic damping factor)** Loss due to attenuation of sound

$$K_F(f) := \frac{\left(1 - e^{-j \cdot \omega(f) \cdot T - La}\right) \cdot \left(1 - R_B \cdot e^{-j \cdot \omega(f) \cdot T - La}\right)}{1 - R_F \cdot R_B \cdot e^{-j \cdot 2 \cdot \omega(f) \cdot T - 2 \cdot La}}$$ Reverberation factor (front face)

$$K_B(f) := \frac{\left(1 - e^{-j \cdot \omega(f) \cdot T - La}\right) \cdot \left(1 - R_F \cdot e^{-j \cdot \omega(f) \cdot T - La}\right)}{1 - R_F \cdot R_B \cdot e^{-j \cdot 2 \cdot \omega(f) \cdot T - 2 \cdot La}}$$ Reverberation factor (back face)

$R_S := 50$ Source impedance

$V_S := 95$ Source voltage (peak)

$$Y_i(f) := \frac{1}{\left(1 + j \cdot \omega(f) \cdot C_0 \cdot R_S\right)}$$ Forward loop parameter

$$Y_f(f) := \frac{1}{\left(1 + j \cdot \omega(f) \cdot C_0 \cdot R_S\right)}$$ Feedback parameter

Output force in the coupling medium as a function of signal voltage:

$$F(f) := \frac{-h \cdot C_0 \cdot Y_i(f) \cdot K_F(f) \cdot \frac{A_F}{2}}{1 - Y_f(f) \cdot \left(K_F(f) \cdot \frac{T_F}{2} + K_B(f) \cdot \frac{T_B}{2}\right) \cdot \frac{k^2}{j \cdot \omega(f) \cdot T}} \cdot V_S$$

Output power in the coupling medium as a function of signal voltage:

$$P(f) := \frac{F(f)^2}{Z_1}$$

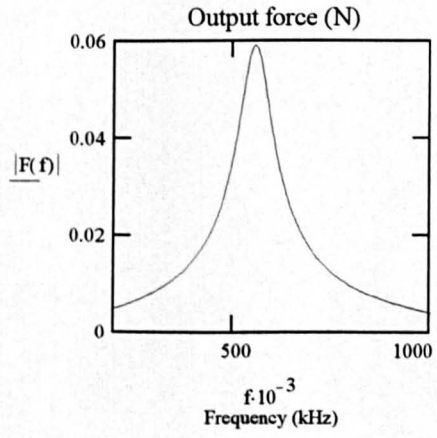

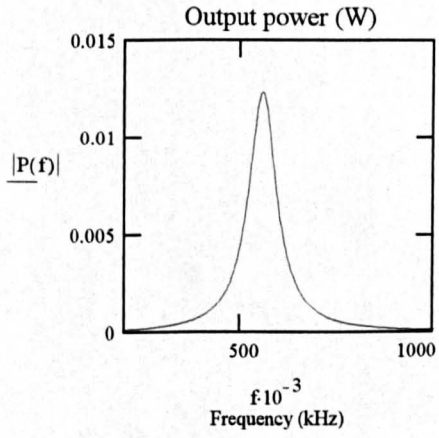

Save data to file:

$$\text{WRITEPRN}(\text{TX\_F\_DAT}) := (f \cdot 10^{-3} \quad |F(f)|)$$

$$\text{WRITEPRN}(\text{TX\_P\_DAT}) := (f \cdot 10^{-3} \quad |P(f)|)$$

Appendix VI

More Detail on Lamb Wave Equations

The purpose of this appendix is to prove the following:

$$-\lambda k^2 + \lambda\alpha^2 + 2\mu\alpha^2 \equiv \mu(k^2 + \beta^2) \tag{A6.1}$$

To do this it is necessary to use Equations (8.9), (8.10), (8.21) and (8.25). For convenience these have been reproduced here:

$$V_L = \sqrt{\frac{\lambda + 2\mu}{\rho}} \tag{A6.2}$$

$$V_S = \sqrt{\frac{\mu}{\rho}} \tag{A6.3}$$

$$\alpha = k\sqrt{1 - \frac{V^2}{V_L^2}} \tag{A6.4}$$

$$\beta = k\sqrt{1 - \frac{V^2}{V_S^2}} \tag{A6.5}$$

The left hand side of Equation (A6.1) is:

$$LHS = -\lambda k^2 + \lambda\alpha^2 + 2\mu\alpha^2 = \lambda(\alpha^2 - k^2) + 2\mu\alpha^2$$

From Equation (A6.2):

$$\lambda = V_L^2\rho - 2\mu$$

Hence:

$$LHS = (V_L^2\rho - 2\mu)(\alpha^2 - k^2) + 2\mu\alpha^2$$

Expanding:

$$LHS = V_L^2\rho\alpha^2 + 2\mu k^2 - k^2V_L^2\rho - 2\mu\alpha^2 + 2\mu\alpha^2$$

$$LHS = V_L^2\rho\alpha^2 + 2\mu k^2 - k^2V_L^2\rho$$

Substituting from Equation (A6.4):

$$LHS = V_L^2 \rho k^2 \left(1 - \frac{V}{V_L^2}\right) + 2\mu k^2 - k^2 V_L^2 \rho$$

$$LHS = 2\mu k^2 - \rho k^2 V^2$$

$$LHS = k^2(2\mu - \rho V^2)$$

The right hand side (RHS) is:

$$RHS = \mu(K^2 + \beta^2)$$

Substituting from Equation (A6.5):

$$RHS = \mu\left(k^2 + k^2 - \frac{k^2 V^2}{V_S^2}\right)$$

$$RHS = \mu k^2 \left(2 - \frac{V^2}{V_S^2}\right)$$

Substituting from Equation (A6.3):

$$RHS = \mu k^2 \left(2 - \frac{V^2 \rho}{\mu}\right)$$

$$RHS = k^2(2\mu - \rho V^2)$$

Hence:

$$LHS \equiv RHS$$

or:

$$-\lambda k^2 + \lambda \alpha^2 + 2\mu \alpha^2 \equiv \mu(k^2 + \beta^2)$$

Appendix VII

Pulser-Receiver Unit used in the High Pressure Study

Pulser-Receiver Specification

	Pulser
Maximum pulse amplitude	-220 Volts into 50 Ω -300 Volts into 250 Ω
Repetition rate	Int. 200 to 5000 Hz Ext. 0 to > 10 kHz (50 Ω damping and #1 energy setting)
Damping range	10 to 250 Ω
Rise time	< 10 nS (50 Ω damping and #1 energy setting)
Available pulse energy	15 to 94 μJ adjustable in 4 steps
Sync. signal output	> +2 V into 50 Ω, T_R = 200 nS, T_{PW} = 3 μS
Ext. trigger requirements	+5 V (15 V max.) into 50 Ω, 100 nS min. pulse width
	Receiver
Voltage gain	20 dB (X10) and 40 dB (X100) selectable by gain switch
Input impedance	500 Ω
Output impedance	50 Ω in series with 50 μF
Attenuator	0 to 68 dB in 2 dB steps
Noise	25 μV r.m.s. referred to the input (bandwidth = 35 MHz)
Bandwidths	1 kHz to 35 MHz 0.03 to 35 Mhz 0.1 to 35 MHz 0.3 to 35 MHz 1.0 to 35 MHz
Maximum output voltage	±1 V (open circuit), ±0.5 V into 50 Ω